INFORMATION TO USERS

This manuscript has been reproduced from the microfilm master. UMI films the text directly from the original or copy submitted. Thus, some thesis and dissertation copies are in typewriter face, while others may be from any type of computer printer.

The quality of this reproduction is dependent upon the quality of the copy submitted. Broken or indistinct print, colored or poor quality illustrations and photographs, print bleedthrough, substandard margins, and improper alignment can adversely affect reproduction.

In the unlikely event that the author did not send UMI a complete manuscript and there are missing pages, these will be noted. Also, if unauthorized copyright material had to be removed, a note will indicate the deletion.

Oversize materials (e.g., maps, drawings, charts) are reproduced by sectioning the original, beginning at the upper left-hand corner and continuing from left to right in equal sections with small overlaps.

Photographs included in the original manuscript have been reproduced xerographically in this copy. Higher quality 6" x 9" black and white photographic prints are available for any photographs or illustrations appearing in this copy for an additional charge. Contact UMI directly to order.

ProQuest Information and Learning
300 North Zeeb Road, Ann Arbor, MI 48106-1346 USA
800-521-0600

Université d'Ottawa · University of Ottawa

To

My Grandparents

Abstract

This thesis represents the culmination of four and half years of research into two aspects of gas phase ion chemistry. The first was the systematic study of the kinetic method to obtain the proton affinity values for compounds with various functional groups and to provide a critical evaluation of the method on the basis of the case studies. The second was concerned with the investigation of the α-cleavage mechanism and mass spectrometric characterization of immonium ions.

The systematic study of the kinetic method has been carried out by observing a wide variety of proton-bound pairs consisting of amines, nitriles and alkanols using tandem mass spectrometry. The majority of the compounds studied were homologous alkyl series. The results were obtained for other selected amines such as pyridine, allylamine, benzylamine and phenylethylamine. The proton affinities of many of these compounds are well established in the NIST database, although some needed either to be revised or to be given their first experimental values.

For the competitive dissociations of proton-bound dimers, which were studied under MI and CID conditions, the relative product yields, $[B_1H^+]/[B_2H^+]$, have been related to the proton affinities (PA) of B_1 and B_2 by the kinetic method. In its simplest form, the method assumes that there are no entropy effects and a zero reverse energy barrier for the competing dissociations.

The general effects expected from non-zero entropies of activation are described in terms of how they influence log k(rate constant) vs. E(internal energy) plots for such competing dissociations. For these homologous series such effects were observed to be minimal and the kinetic method well reproduces most of the reference PA values. However, in view of the very close agreement between the present results and many reference PA values obtained from equilibrium studies, it is possible that small reverse energy barriers (ca. 5 kJ mol^{-1}) may in some cases be identifiable by the kinetic method, in particular for t-$C_4H_9NH_2$, the homologous di-n-alkylamines and possibly larger barriers for di-sec-alkylamines. The method is quite sensitive to small discrepancies in PA and new values have been proposed for $C_6H_5CH_2NH_2$ (923 kJ mol^{-1}), $C_6H_5CH_2CH_2NH_2$ (930 kJ mol^{-1}), $(CH_3)(n\text{-}C_4H_9)NH$ (951 kJ mol^{-1}), $(i\text{-}C_4H_9)_2NH$ (969 kJ mol^{-1}) and for homologous nitriles and alkanols, namely from C_5 to C_8. The PA value for n-C_4H_9OH was revised from 789.2 to 793.7 kJ mol^{-1}.

Results have also been obtained for some bidentate species such as 1,2-, 1,3- and 1,4-diaminoethene, propane and butane, respectively. Particular attention was given to the effects of activation entropies, $\Delta S^{\neq}$, and the presence of reverse energy barriers, E_{rev}, both of which are here a significant problem for the kinetic method. It was found that for 1,2-diaminoethane there was a $\Delta S^{\neq}$ effect, particularly for collisionally activated ions. The derived PA of 949 ± 4 kJ mol^{-1} is quite close to the reference value (952 ± 4 kJ mol^{-1}). It was concluded that for 1,3-diaminopropane (reference PA = 987 ± 4 kJ mol^{-1}), the method failed due both to an activation

entropy effect and the presence of a significant reverse energy barrier. The latter was estimated to be ca. 20 kJ mol^{-1}, making ca. 967 kJ mol^{-1} the *apparent* PA resulting from the kinetic method. For 1,4-diaminobutane (reference PA = 1006 ± 4 kJ mol^{-1}), the kinetic method failed and similar difficulties arose, with an estimated reverse energy barrier of ca. 32 kJ mol^{-1}. The overall results for these three compounds were compared with a recent report on low energy collision-induced fragmentations. These results for species having a bidentate structure indicate that similar difficulties may apply to biomolecules and that PA values for such species obtained by the kinetic method may be flawed.

The kinetic method was extended to determine molecular-pair proton affinities (MPPA), which were investigated through a study of proton-bound alkanol trimers. Since these values were not available, it was necessary to establish a set of data for the reference bases prior to actual measurements.

Second part of the thesis regards the following aspects: (A) Investigation of the α-cleavage mechanism in simple amine molecular ions. α-cleavage has traditionally been regarded as an extremely simple process, in which a C-C bond is broken essentially without reverse critical energy. This view was undermined by the discovery that several ionized t-butylamines, $(CH_3)_3CNHR^{+\bullet}$, expel a methyl radical with the production of a broad, dished metastable peak. The observed kinetic energy release (KER) is substantial (11 – 21 kJ mol^{-1}) which indicates that there is a definite energy barrier towards the reverse reaction. The KER values corresponding

to the methyl loss reactions for t-butylamine, isopropylamine were remeasured, which were 10 kJ mol^{-1} (indeed close to the reported value), 0.3 kJ mol^{-1} (not in agreement with the reported result, 5 kJ mol^{-1}). The shapes of the metastable peaks are broad Gaussian instead of dish-topped for t-butylamine and Gaussian for isopropylamine. The strikingly different KER values indicate different reaction mechanisms may be involved. The α-cleavage reaction for t-butylamine suggests that an ion-neutral complex, separated from the molecular ion by a large energy barrier, was proposed as intermediate species, as confirmed by *ab initio* calculation. However, the α-cleavage reaction for isopropylamine was found to be a simple bond cleavage process. The $\Delta_f H°$ for $(CH_3)C^+NH_2$ was revised from 141 kcal mol^{-1} to 133 kcal mol^{-1} on the basis of the appearance energy measurements. (B) Mass spectrometric studies of immonium ions, $CH_3CH_2CH^+NH_2$ and $(CH_3)_2C^+NH_2$ and their oxygen analogues (oxonium ions) were made using tandem mass spectrometry. It is concluded that the immonium (or oxonium) ions interconvert freely at internal energies near their dissociation limit, on the basis of their having very closely similar fragmentation patterns and KER values but slightly different product ion abundances. The possible fragment ions' structures produced by these immonium (or oxonium) ions were assigned by observing their corresponding CID mass spectra.

Acknowledgements

I would like to thank the people who have contributed to this thesis.

Thank you Dr. Holmes for your continuous support, encouragement and guidance throughout the course of this work. I gained very much from your knowledge and your positive view of life. Your profound knowledge and wisdom are always a key to many puzzles. It is a treasure to be able to work with such an admirable and understanding professor.

Thank you Sander for all the instrumental problems you have solved. Thank you Christiane for all the works in which you were actively involved, for many valuable discussions and perceptive suggestions. Thank you Paul for your direction of calculations, providing references from CISTI. Thank you big Clem for scanning pictures. A special thank to all my colleagues: Don, Julie (enjoyable to sit aside), Richard (for being supportive), Danielle (my English tutor), little Clem (for helping me solve calculation problems), Ya-Ping, Natalia and Vladimir, Wei-Xing.

I would like to thank my family for their support, especially my grandparents who raised me and nurtured me with endless love. I will always feel indebted to you.

Thank you Prof. Liu who was a supervisor of my Master studies. I feel privileged to have experienced your guidance and love.

Contents

List of Figures

List of Tables

List of Abbreviations

AE:	Appearance energy
IE:	Ionization energy
IE_a:	Adiabatic ionization energy
IE_v:	Vertical ionization energy
EI:	Electron impact
CI:	Chemical ionization
ESA:	Electrostatic analyzer
FFR:	Field-free region
MI:	Metastable ion dissociation
CID:	Collision induced dissociation
CIDI:	Collision induced dissociative ionization
CR:	Charge reversal
CS:	Charge stripping
NR:	Neutralization-reionization
$\Delta_f H°$:	Standard heat of formation
KER:	Kinetic energy release
PA:	Proton affinity
GB:	Gas-phase basicity
MPPA:	Molecular pair proton affinity
MPGB:	Molecular pair gas-phase basicity

Chapter 1 Introduction

Gas phase ion chemistry is concerned with the production and study of gas phase ionic and neutral species. Its aims are to obtain information on the structural characteristics of species, on the reactivity of these species and on their thermochemical stability. The study of these species may be undertaken by a variety of means and mass spectrometry is one method of choice.

The technique of mass spectrometry began in J.J. Thomson's vacuum tube[1] where he studied the nature and behavior of positive rays. "I feel sure that there are many problems in chemistry which could be solved with far greater ease by this than by any other method. The method is surprisingly sensitive – more so even than that of spectrum analysis - requires an infinitesimal amount of material and does not require this to be specially purified..." His statement about the technique of mass spectrometry, even more apt in describing tandem mass spectrometry (MS/MS)--in which a mass spectrometer isolates a single ionic species, subjects to a chemical change, and observes the charged products with a second mass spectrometer, indicates that he was quite confident that mass spectrometry will serve the chemist well. He was considered to be the fatner of mass spectrometry, was also the forefather of MS/MS.

The next major development leading to the technique of MS/MS occurred in 1945 when Hipple and Condon[2] observed and explained the presence of

metastable ions in a mass spectrum. This work was the driving force that has led to MS/MS as it is practiced today. In the early 1960s, the first experiments were performed in which instruments were used in unconventional modes to study the metastable decompositions of ions. These studies were made possible by developments in two different areas. The first development was the introduction of the accelerating-voltage scan on sector instruments by Barber and Elliott.[3] The next major development was the discovery of the enhancement of magnitude and quantity of peaks in a "metastable ion" spectrum upon introduction of a collision gas into a localized region of the mass spectrometer.[4-6] In some ways, this brought mass spectrometry full circle in that a gas was deliberately introduced into a mass spectrometer to cause reactions that Thomson has observed because of the poor vacuum of his time. The fragmentation of a polyatomic ion following an energetic collision with a target gas is referred to as collision-induced dissociation (CID). Publication of the book,[7] "Metastable Ions", marked the beginning of the modern era of MS/MS, a period in which instruments would be designed expressly for MS/MS experiments. The availability of that instrumentation led to the rapid transformation and expansion of the technique from predominantly physical/organic investigations to a wide variety of new applications. Demonstrations of the utility of MS/MS in analytical applications provided continuing impetus for instrument development, including the incorporation of computers into more automated MS/MS instruments and the exploration of a diverse mix of instrument types and configurations.

MS/MS has played a particularly important role in assigning ion structures, elucidation of reaction mechanisms and obtaining thermochemical information. These data have been acquired using several approaches, including measurements of energy loss, kinetic energy release and relative fragment ion abundances. Most chemical research experiments using MS/MS fall into one of these three classes, i.e., ion structures, reaction mechanisms and thermochemistry. A summary of these applications and examples, i.e., the use of MS/MS techniques and the ion thermochemistry of the immonium ions, are given in Chapters 3 and 4.

Gas phase ion thermochemistry is of practical importance. It includes establishing the heats of formation ($\Delta_f H°$) and other thermochemical properties such as proton affinity (PA) and gas-phase basicities (GB), etc. The former can be achieved by ionization energy measurements (IE) of the molecular ions or AE measurements of fragment ions. The $\Delta_f H°$ data of organic ions in the gas phase may permit the unequivocal assignment of structure to a daughter ion, or at least to allow the number of energetically feasible daughter ion structures to be reduced to a minimum. The latter (PA and GB) can be obtained by the kinetic or equilibrium method through measuring the relative product ion abundances or with a combination of the partial pressures of the neutrals. These methods can provide the relative PA or GB values of the organic compounds. The importance of PA and GB data of molecules relies on the fact that they define the inherent properties of the parent bases, thus permitting a more refined understanding of the correlation between molecular structure and basicity, but they also show how solvents affect

the reactivity of molecules on comparison of the gas phase data with that in solution. Chapter 6 is a review of the kinetic method as a mean of determining the proton affinities of organic compounds. Chapters 7 to 9 are concerned with the systematic investigations of the kinetic method in the application of proton affinity measurement to alkylamines (Chapter 7), alkylnitriles (Chapter 8) and alkanols (Chapter 9). Chapter 5 addresses the experimental aspects with regard to this method.

The instruments used in the thesis are described in Chapter 2.

References

(1) Thomson, J. J. In *Rays of positive electricity and their applications to chemical analysis.*; Longmans: London, 1913.

(2) Hipple, J. A.; Condon, E. U. *Phys. Rev.* **1945**, *68*, 54.

(3) Barber, M.; Elliot, R. M. ASTM E-14 conference on mass spectrometry, 1964, Montreal.

(4) Haddon, W. F.; McLafferty, F. W. *J. Am. Chem. Soc.* **1968**, *90*, 4745.

(5) Jennings, K. R. *Int. J. Mass Spectrom. Ion Phys.* **1968**, *1*, 227.

(6) Rosenstock, H. M.; Melton, C. E. *J. Chem. Phys.* **1957**, *26*, 314.

(7) Cooks, R. G.; Beynon, J. H.; Caprioli, R. M.; Lester, G. R. In *Metastable ions*; Elsevier: Amsterdam, 1973.

Chapter 2 Instrumentation

2.1 Introduction

In this chapter, the components of the instruments used to complete the work presented in the thesis are described. Two instruments were used, a modified ZAB-2F mass spectrometer of BEE geometry for standard gas phase ion chemistry and the AEI-MS902 apparatus for appearance energy determinations.

2.2 The VG ZAB-2F Mass spectrometer

The VG ZAB-2F[1] mass spectrometer is a double focusing instrument of reversed geometry. Double focusing, because the beam is submitted to the focusing action of both a magnetic and an electric sector and of reverse geometry since the magnetic sector precedes the electric sector. Over the past 12 years, it has been extensively modified to allow novel experiments to be carried out. The last major modification (1992) was the addition of a third field free region and hence a second electric sector, making the instrument triple focusing. A schematic diagram of the instrument is shown in Figure 2.1. The individual components of the ZAB will be described in the following sections.

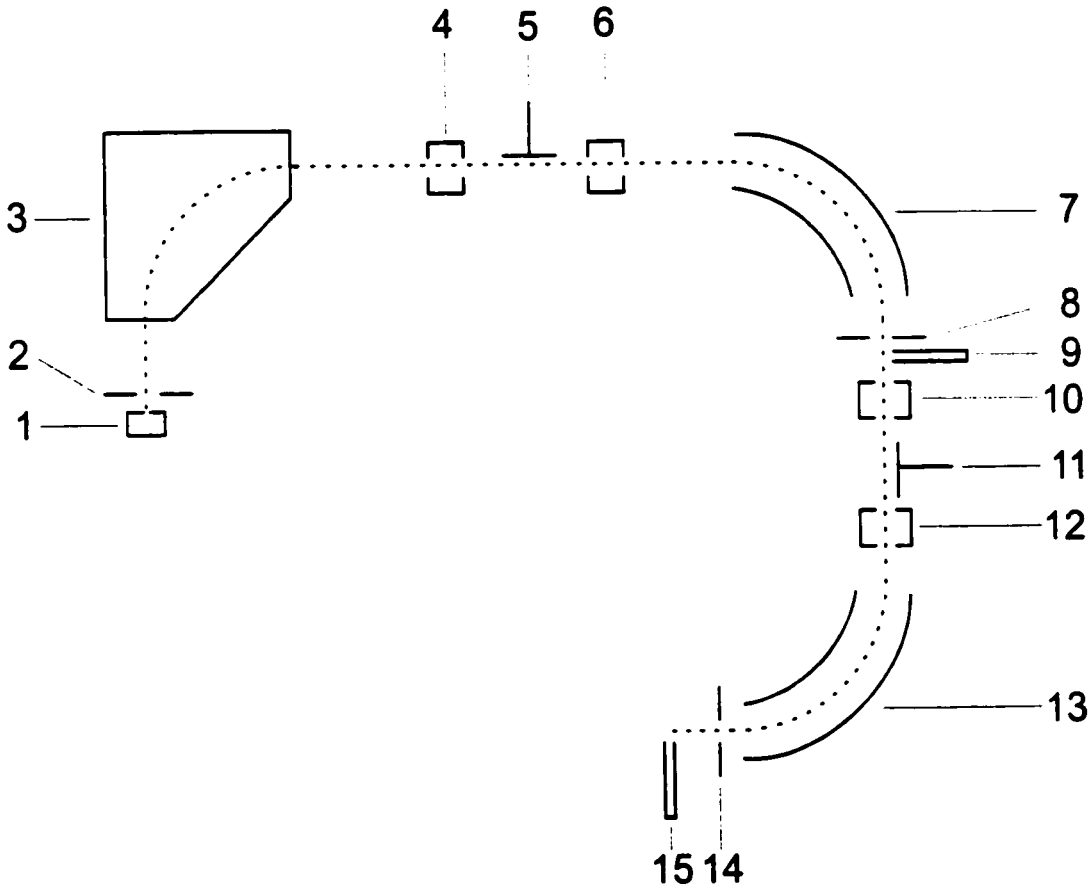

Figure 2.1 Schematic diagram of the modified VG ZAB-2F mass spectrometer 1: ion source, 2: source slit, 3: magnetic sector, 4, 6, 10, 12: collision cells, 5, 11: deflector electrodes, 7, 13-electric sectors, 8, 14: collector slits, 9,15: detectors

2.2.1 *The ion source*

The ion source, as is the rest of the interior of the mass spectrometer, is kept at a high vacuum of 10^{-8} torr. A sample can be introduced into the ion source via an appropriate inlet system at a constant rate, resulting in a stable sample pressure of $\leq 10^{-6}$ torr (see Figure 2.2).

Ionization of the sample molecules can be achieved by passing a beam of electrons emitted from a filament, through the ion source. The energy (velocity) of the electron beam can be adjusted and is usually $\cong$ 70 eV. Ionization of the sample using these electrons will follow the Franck-Condon principle, i.e., the ionization process is fast compared to a molecular vibration. Since ionization energies of molecules are usually around $\cong$ 10 eV, the molecular ions can be generated with a large amount of excess internal energy. This excess energy causes the molecular ion to decompose into fragments. These fragments, in turn, have sufficient energy to fragment further. In effect, a range of competitive and consecutive reactions can take place starting from the molecular ion.

The production and relative intensities of those fragments can be explained by the Quasi Equilibrium Theory (QET),[2] which assumes that following ionization the excess energy is distributed among all vibrational and rotational degrees of freedom of the ground state of the molecular ion in a random fashion, and that fragmentation will occur when sufficient energy is accumulated in the critical

vibrational mode(s) which leads to decomposition; i.e., the excited molecular ion has a lifetime of at least several vibrations.

All ions generated in the ion source will fall through a potential gradient (the accelerating voltage, V_{acc}, typically 8 kV) as they leave the ion source, so all ions with mass m and charge z generated inside the source will leave carrying zeV_{acc} of kinetic energy, $1/2mv^2$:

$$\frac{mv^2}{2} = zeV_{acc} \qquad 2.1$$

Hence, all ions of the same charge acquire the same kinetic energy, irrespective of their mass.

2.2.2 *Magnetic sector*

The function of a magnetic analyzer is shown in Figure 2.3. The magnetic sector is a momentum analyzer which can separate the ions according to their momentum-to-charge ratios:

$$Bze = \frac{mv}{r_B} \qquad 2.2$$

By rearranging and combining equations 2.1 and 2.2, the following relationship is obtained:

$$\frac{m}{ze} = \frac{B^2 r_B^2}{2V_{acc}} \qquad 2.3$$

where B and r_B are the magnetic field strength and radius of the trajectory. By varying B, ions of different m/z can be selected (r_B and V_{acc} are fixed).

2.2.3 *Electric sector*

The electric sector acts as an energy analyzer which can separate ions via their translational energy-to-charge ratios:

$$Eze = \frac{mv^2}{r_E} \qquad 2.4$$

where E and r_E are the electric field strength and radius of the electric sector. By combining and rearranging equations 2.1 and 2.4 the following relationship is obtained:

$$E = \frac{2V_{acc}ze}{r_E} \qquad 2.5$$

Setting E to match V_{acc} will ensure that any mass selected, source generated ions will be transmitted through the electric sector. For the ions generated in the FFR before the electric sector, scanning E will allow the fragment ions of different kinetic energy to be detected (see Figure 2.4).

2.2.4 *Field free regions*

There are three field free regions in the instrument corresponding to the region between the source and magnet (1FFR), the magnet and ESA1 (2FFR), and ESA1 and ESA2 (3FFR). In the field free regions, the ions decompose either

spontaneously or by collisional activation. One pair of collision cells is respectively placed in the 2FFR and 3FFR, namely cell 1 to cell 4. The cells 1 and 2 are 2 cm long and 10 cm apart while cells 3 and 4 are separated by 6 cm. Half-way between each pair of cells is placed a deflector electrode allowing the ions to be expelled from the trajectory with a certain potential applied on the electrode. This device enables the study of the neutral species cogenerated in the FFR.

So far, it has been assumed that an ion leaving the ion source is a stable ion; that is, it will not fragment in flight between the ion source and the detector. This is however not necessarily the case. The ions that fragment in flight are called metastable ions. Depending on the actual site of fragmentation along the flight path, some of these metastable ion fragmentations can yield detectable products. If fragmentation takes place in the magnet or ESA, the products will not be detectable as a discrete signal; they will go off track. Fragmentation between the ESA and the detector will lead to a fragment ion which will be detected the same way as the parent ion.

If fragmentation ($m_1^+ \rightarrow m_2^+ + m_3$) takes place in the 1FFR, the magnet will not transmit the product ion (m_2^+) because the m_2^+ ion only has $m_2/m_1 \bullet eV_{acc}$ kinetic energy. Using equation 2.2 or 2.3, the magnet will transmit m_2^+ as an ion with apparent mass of m_2^2/m_1.

If fragmentation takes place in the 2FFR, the kinetic energy of the parent ion m_1^+ (eV_{acc}) will be distributed among the products. In this distribution, the law of conservation of momentum has to be obeyed. The kinetic energies of the products is thus given by:

$$\frac{m_2 v_2^2}{2} = \frac{m_2}{m_1} eV_{acc} \qquad 2.6$$

$$\frac{m_3 v_3^2}{2} = \frac{m_3}{m_1} eV_{acc} \qquad 2.7$$

in which the velocity of all particles is virtually the same. In other words, the kinetic energy of the products is a mass weighted fraction of the kinetic energy of the parent ion. The electric sector will transmit the product ion m_2^+ not at eV_{acc}, but at $m_2/m_1 \bullet eV_{acc}$. Thus the mass of a product ion can be calculated from its kinetic energy measured by the electric sector. This important result enables the electric sector to function as a pseudo-mass analyzer for unimolecularly generated products, arising from a mass selected ion.

In addition to the unimolecular fragmentation as described, fragmentation can be induced by passing the ion through a collision gas, introduced in a collision cell. The electric sector can also be used as a pseudo-mass analyzer for the products of such collisional activation (CA) (or collision induced decomposition (CID)) experiments.

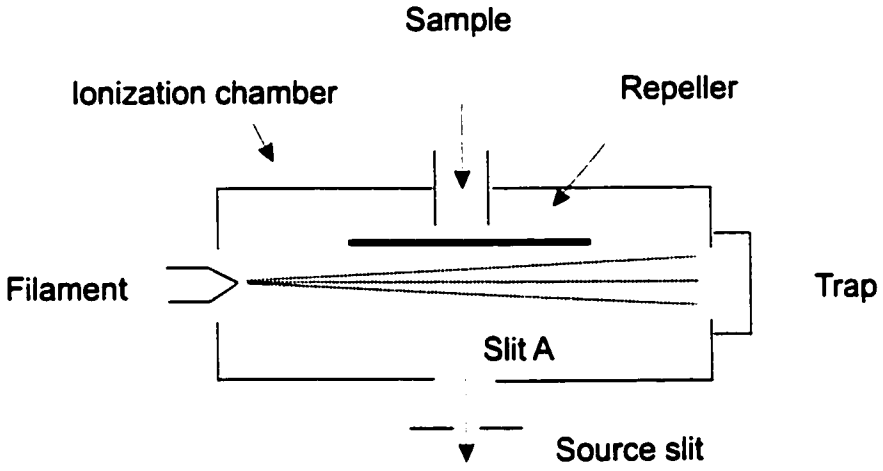

Figure 2.2 Ion source in the modified VG ZAB-2F

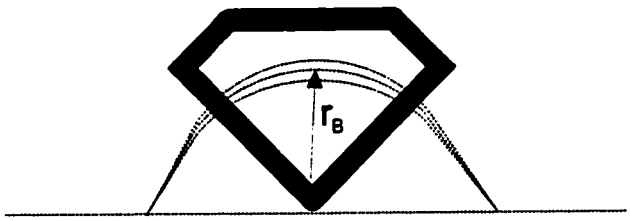

Figure 2.3 Focusing action of magnetic sector

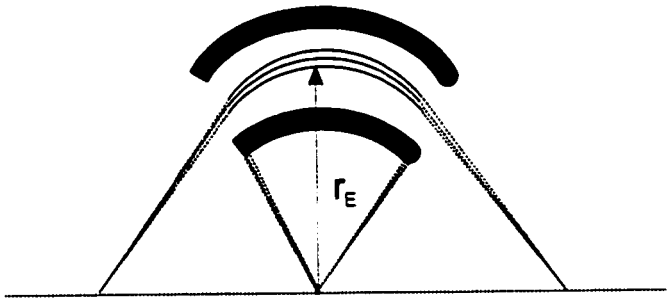

Figure 2.4 Focusing action of electric sector

2.2.5 *Detectors*

The detectors are off-axis Daly detectors, which employ a scintillator to detect secondary electrons emitted when ions strike a conversion dynode as shown in Figure 2.5. It consists of a conversion dynode onto which a high negative potential is applied (ca. 20 kV) and a photomultiplier. The positive ions are attracted towards the dynode, impinge on the central portion of the conversion dynode and secondary electrons are ejected due to the high energy collision. These electrons are then accelerated toward a CaF_2 scintillator. The scintillations produced are detected by an optically coupled photomultiplier. The detectors used in the ZAB are for positive and negative ions. Due to this flexibility, a restriction on the maximum possible potential applied to the dynode may result in mass discrimination. The ions with low translational kinetic energy, i.e. low mass fragment ions, may be discriminated against, either because they miss the conversion dynode or because the secondary electrons miss the scintillator.

2.3 *AEI-MS902 mass spectrometer*

The MS-902S is a forward geometry mass spectrometer whose configuration is that the electric sector precedes the magnetic sector (Figure 2.6). The MS-902 does not have the septum inlet system but has two inlet systems: direct insertion probe, Granville-Phillips variable molecular leak. The outstanding feature of MS-902S is that it is capable of thermochemical measurements, i.e., ionization energy (IE) and appearance energy (AE), due to the precise control of the energy of the electron beam and shorter 1FFR.

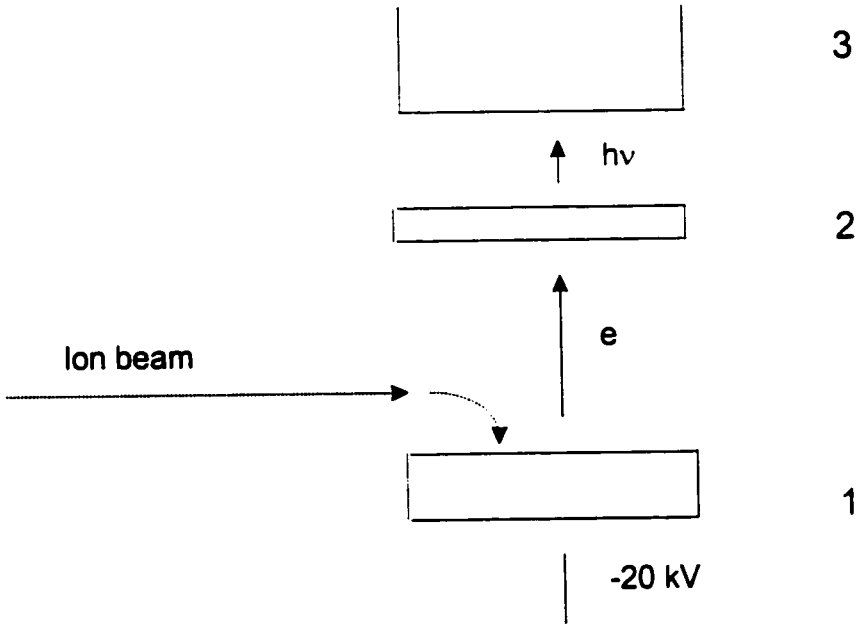

Figure 2.5 Daly detector 1: conversion dynode, 2: CaF_2 scintillator, 3: photomultiplier

Figure 2.6 Schematic diagram of the AEI-MS902S

1: ion source, 2: source slit, 3: electric sector, 4: magnetic sector, 5: collector slit, 6: detector

2.4 References

(1) Morgan, R. P.; Beynon, J. H.; Bateman, R. H.; Green, B. N. *Int. J. Mass Spectrom. Ion Phys.* **1978**, *28*, 171.

(2) Rosenstock, M. M.; Wallenstein, M. B.; Wahrhaftig, A. L.; Eyring, H. *Proc. Natl. Acad. Sci. (USA)* **1952**, *38*, 667.

Chapter 3 Mass spectrometric characterization of ions and neutrals in the gas phase

3.1 Introduction

Two main experimental methods available to assign structures of ions in the gas phase are 1) ion dissociation characteristics, including metastable ion and collision induced dissociations and 2) ion thermochemistry. The structure of the ion refers only to how the atoms are linked together and does not include more detailed information such as bond lengths and bond angles. Theoretical calculations[1] can provide such details of geometries.

Ion thermochemistry refers to the measurement of the heats of formation of ions via ionization energy and appearance energy measurements. The role of thermochemistry in ion structure determination has been reviewed by Holmes.[2] Accurate measurements (0.05 eV) are usually obtainable with photoionization mass spectrometers[3] or instruments with electron ionization sources with narrowly definable electron energy.[4] Heats of formation are almost always used in conjunction with information regarding the unimolecular chemistry of the ions. The ion dissociation characteristics are most conveniently obtained using tandem mass spectrometers with an activation method or from a study of metastable ions.

3.2 Metastable ions

3.2.1 Metastable ions

Ions in a mass spectrometer can be classified (rather arbitrarily) as stable, unstable, or metastable, depending upon where they fragment during their passage through the instrument. Stable ions are those that have lifetimes longer than the time of passage through the instrument. Unstable ions are those that fragment within the ion source, and metastable ions dissociate outside of the ion source but before detection.

Figure 3.1 shows a hypothetical potential energy diagram for ions formed in an electron impact source of a mass spectrometer. Ions with high internal energies will fragment with rate constants greater than ca. 10^6 s^{-1} and therefore do so before leaving the ion source. Ions with low internal energy (close to, or below the dissociation threshold) have rate constants smaller than ca. 10^4 s^{-1} and do not decompose during the flight time.

Metastable ions have intermediate internal energies and therefore dissociate within intermediate rate constants (ca. $10^4 - 10^6$ s^{-1}). Metastable ions typically have lifetimes of several tens of microseconds and internal energies in excess of the critical energy for the lowest energy dissociation by several tenths of an electron volt. Metastable ions therefore typically produce few product ions in their dissociative reactions, and those product ions that do form result from the lowest energy dissociation mechanisms. These dissociations are characteristic of the reacting configuration of the ion. This configuration may or may not also

characterize the structure of stable ions in the mass-selected beam used in MS/MS experiments. The role of metastable ions in ion structure assignment as well as reaction mechanism studies will be discussed in the following section.

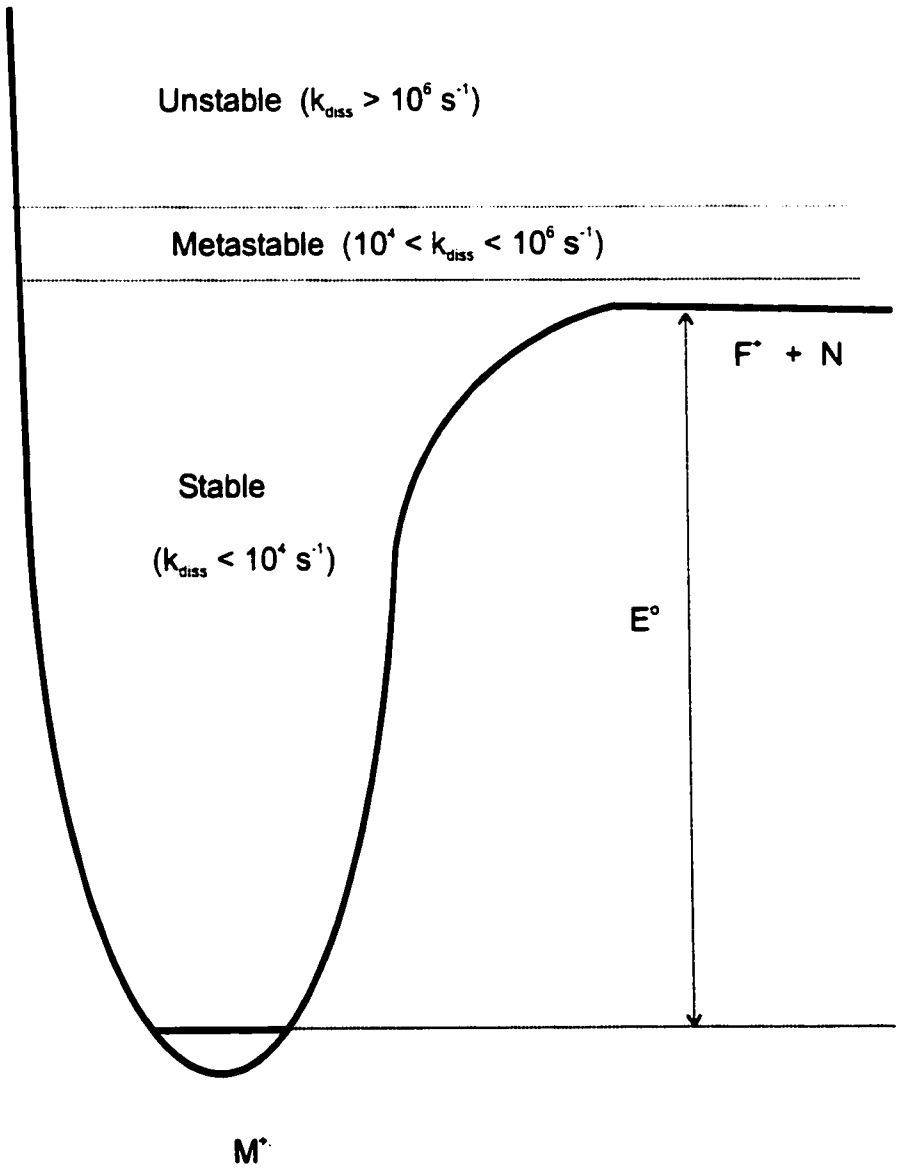

Figure 3.1 Different types of ions produced by electron impact

3.2.2 *Kinetic energy release (KER) and metastable ion peak shape*

3.2.2.1 The shape of fragment ion peaks from metastable ions

Upon decomposition part of the excess internal energy of an ion is isotropically released as kinetic energy, KER, leading to a broadening of the fragment ion beam relative to that of the undissociated ion beam. Small average KER values lead to narrow, G*aussian-shaped* peaks, whereas *flat-topped* or *dish-shaped* peaks are observed for larger KER values (see Figure 3.2). The minimum observed in the center of a dish-shaped peak results from discrimination of ions having their maximum velocity component in the collector slit direction, by the finite slit length, and is thus most pronounced for short slits and long ion paths from the point of decomposition to the collector.[5]

If the metastable peak is clearly of *composite* shape, i.e., not a simple Gaussian or dish-topped peak, but a combination of these shapes,[6] then either two transition states are involved and/or two isomeric daughter ions are generated. The number of components in a metastable peak indicates the number of transition states involved. The number of reacting configurations and daughter ion structures will be equal to or less than the number of peak components. A metastable peak of composite shape may be not very structure-characteristic.

In some cases, the reaction which gives rise to a metastable peak has an unusually large cross-section for collisional activation. In such a case, residual gas in the FFR will give rise to an apparently composite metastable peak. The

collisionally induced component is typically of Gaussian type but is generally broader than the corresponding metastable ion peak. Because translational energy of the collisionally activated ion was used in its energization, the CA component will be slightly displaced towards lower translational energy, thus producing an asymmetric composite peak.[7]

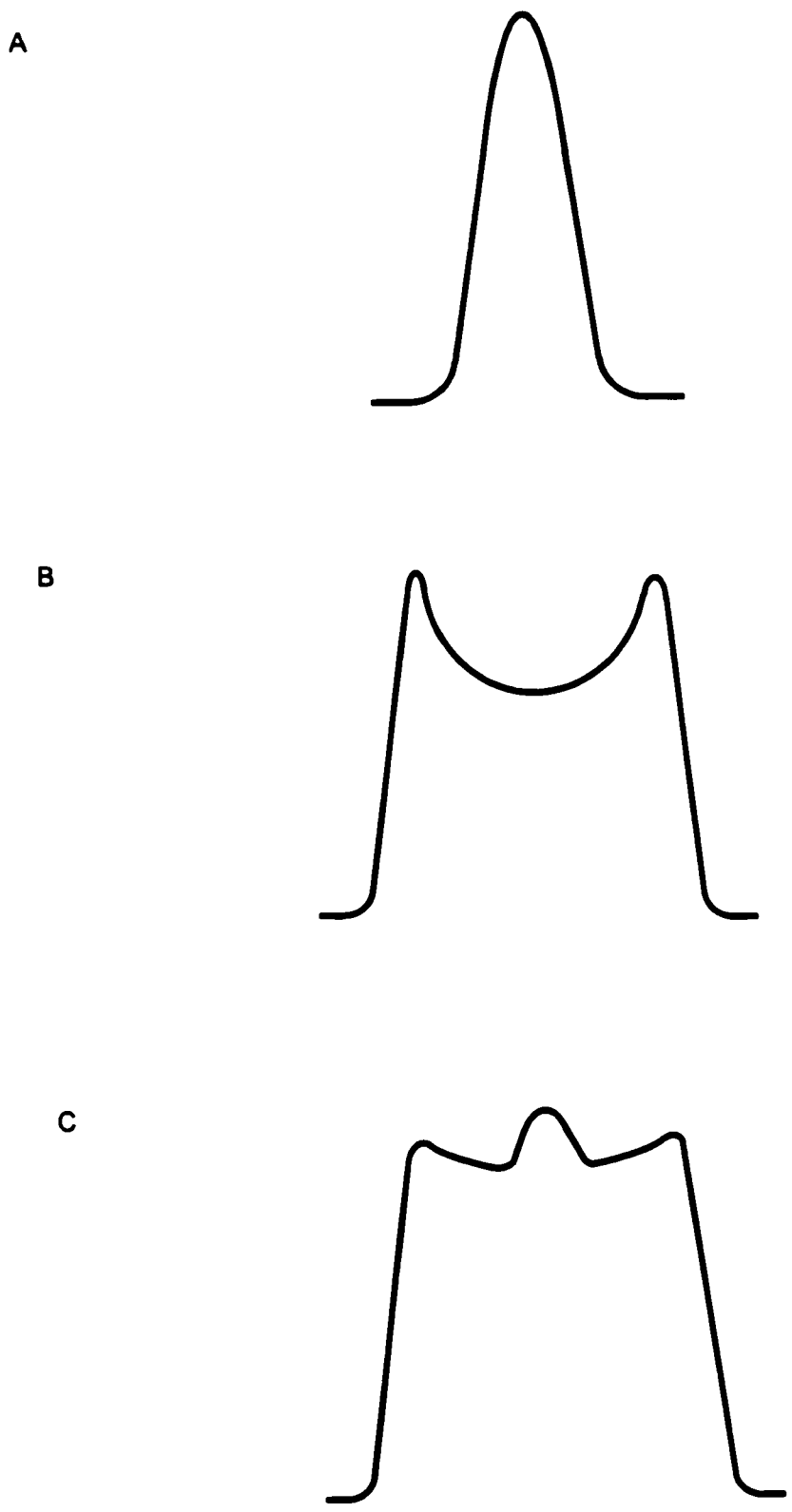

Figure 3.2 Metatable peak shapes: A) Gaussian, B) dish-topped and C) composite

3.2.2.2 Determination of kinetic energy release

Both the excess energy (ε^{*}) of the activated complex and the reverse activation energy (ε^{r}) may be released as translational energy during the metastable ion fragmentation (see Figure 3.3). The kinetic energy release (KER), which is commonly expressed as $T_{0.5}$, can be determined by measurements of the peak width at half height and calculated according to:

$$T_{0.5} = \frac{{m_1}^{+2}}{16 \cdot {m_2}^{+} \cdot m_3 \cdot V_{acc}} (W^2_{1/2(\text{fragment})} - W^2_{1/2(\text{main beam})}) \qquad 3.1$$

where ${m_1}^{+}$, ${m_2}^{+}$ and m_3 are the masses of the precursor molecule, the ionic and neutral fragments, respectively, and $w_{1/2}$ are the widths at half height of the fragment ion peak and the main ion beam, each measured in V_{acc} units.

The experiment is carried out at high energy resolution, which is obtained by narrowing down the y-slits in the instrument so that the width at half height of the fragment peaks are indicative of the kinetic energy released.

The KER associated with the fragmentation of a given metastable ion is characteristic of the stable ion (a) when there is no rearrangement, or (b) an isomeric ion structure with excess energy or (c) the reacting configuration of the ion when rearrangement occurs prior to fragmentation.[2] Therefore, this information is

very useful for distinguishing isomeric ions and elucidating reaction mechanisms (refer to the section 3.4 of the Chapter).

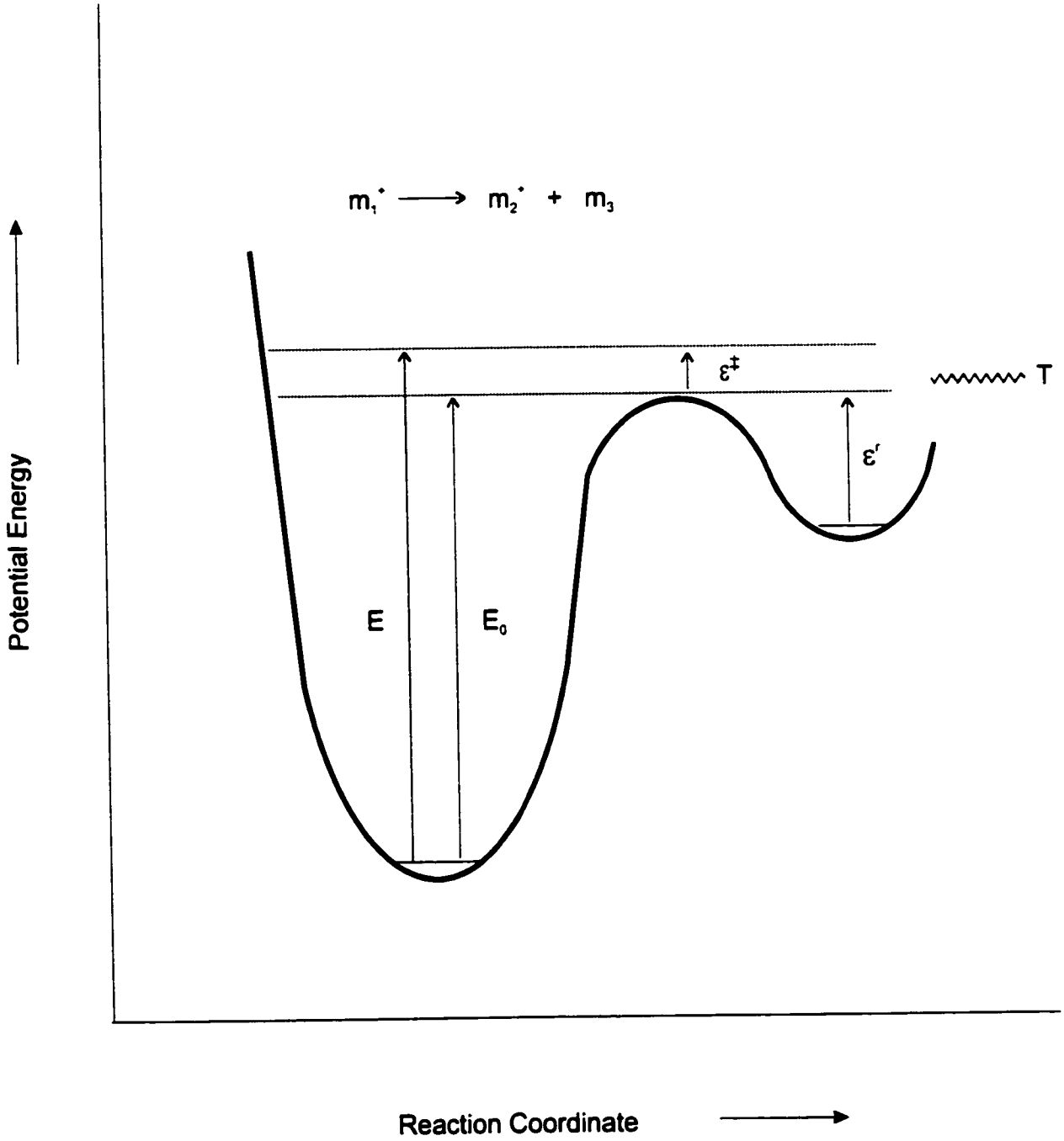

Figure 3.3 Contributions of the non-fixed energy of the activated complex and of the reverse activation energy to the observed kinetic energy release

3.3 Collision experiments

In the modern era of mass spectrometry, processes involving collisions between ions and neutral gases are key experiments for probing the structure and reactivity of ions. Collision experiments are used to excite stable mass-selected ions and thus give diagnostic structural information about the stable parent ions.

Methods of excitation for ions have been developed to increase their internal energies. Such excitation increases the absolute number of ions that dissociate and increase the likelihood for structurally diagnostic simple bond cleavage reactions. Several methods for the excitation of ions in a reaction region have been developed. The most widely used method is the collision of a high-velocity ion with a target gas. Different MS/MS instruments allow for collisional activation at ion kinetic energies of a few keV or less than 100 eV. Other methods of ion activation include interaction of the ion with an intense beam of photons, a beam of electrons, or via collision of the ion with a surface. Particular emphasis will be given to collisional activation.

3.3.1 Collision induced dissociations (CID)

When ions having a high translational energy (a few hundred eV or more) collide inelastically with neutral atoms or molecules, part of the ions' translational energy may be converted into excitation energy leading to their subsequent decomposition. The overall mechanism for collision induced dissociation at both low and high collision energy is generally accepted as proceeding in two steps.[8,9] The sequence involves collisional activation of the parent ion in the first step and unimolecular dissociation in the second step, i.e.:

$$M^+ \xrightarrow{N} M^{+*} \longrightarrow M_1^+ + M_2 \qquad 3.2$$

where M^{+*} is the activated parent ion. The overall net equation for the CID includes the mass and energy balance:

$$Q + M^+ + N = M_1^+ + M_2 + N' + T \qquad 3.3$$

where Q is the endothermicity of the collision (i.e., the amount of energy converted from the translational energy of the collision partners into internal energy of the ion), N and N' are the target molecule in its prior- and post-collision state, and T is the kinetic energy liberated in the unimolecular dissociation.

The CID mass spectrum will be different from the metastable ion mass spectrum in two major aspects: 1) the total abundance of the fragment ions will be generally increased and 2) there will be a much greater variety of fragment ions. The fragment ions thus generated will be characteristic of the structure of the mass selected ions if the precursor ions retain their structure irrespective of their internal energy. However, if some isomerization occurs following activation, the CID mass spectrum obtained will be a superposition of the dissociation characteristics of the isomeric ions.

The intensity ratios of collision-induced fragments were studied by Mclafferty et al. as a function of various parameters.[10] It was found that when the translational

energy of the impacting ions increases there is not only an increase in the yield of the collision-induced secondary fragments but also a change in the intensity ratios between these fragments. As a consequence of an increase in the mean transferred energies, the intensity of fragments having higher activation energies increases more than does that of fragments with lower activation energies. A similar increase in fragmentation processes with higher activation energy is found at high pressures of the collision gas and this is explained by the occurrence of multiple collisions. The nature of the collision gas, however, has no influence at all on the intensity ratios[10] although it does influence the yield of collision-induced fragments: as the size of the atoms or molecules decreases, the yield increases, so that helium and H_2 are particularly suitable collision gases.

The effect of ion initial internal energy on a CID mass spectrum is somewhat controversial but it is generally accepted that only the metastable reaction channels may depend on the initial internal energy distribution of the precursor molecules. All other "high critical energy" dissociation channels should be independent of the internal energy of the precursor ion and thus ion relative abundances should be independent of the initial internal energies. Consequently, identical ions generated from a variety of precursor molecules should have indistinguishable CID mass spectra, whereas isomeric ions, in general, will have distinctive CID characteristics. The effect of internal energy may be best observed when comparing CID mass spectra of both source and metastably generated ions. The two CID mass spectra will be indistinguishable if the structure of the ions is the same irrespective of their

internal energy content. However, the two CID mass spectra will be distinct when the structure of the ions is dependent upon their internal energy content.

3.3.1.1 Energy transfer in collision process

The amount of energy deposited in the ion as internal energy will vary with the "closeness" of the interaction and with the velocity and mass of the incoming ions. In 1949, Massey[11] found that the most probable amount of internal energy received by an ion upon collision (E_{mp}) can be given as:

$$E_{mp} = \frac{h}{a}\left(\frac{2eV}{m}\right)^{\frac{1}{2}} \qquad 3.4$$

where h is Planck's constant, a is the interaction distance, eV is the ion's translational energy and m is the mass of the ion. Small targets will, on average, deposit more energy into the ion than large ones because of the smaller interaction distance. Helium is by far the most common collision gas in keV collision-energy CID studies since it is the most effective for energy deposition and can minimize the processes competing with CID.

The average internal energy deposition is usually estimated to be a few eV (1-3 eV) and the distribution of internal energy deposited is wide and characterized by a high energy tail.[12] This is comparable to that of the molecular ions produced by 70 eV electron impact and thus a CID mass spectrum will resemble the normal EI mass spectrum of a molecular ion.

3.3.1.2 Target gas effect

At low collision energies (e.g., a few eV), the nature of the target gas can have a much greater effect on the appearance of the CID mass spectra than at high collision energies. This is largely due to the relatively long-lived collision complex mechanism for energy transfer. At low collision energies, a large fraction of the center-of-mass energy, $E_{c.m.}$ (A term used for description of the collision energies under low collision conditions, see the section 5.4.5 of chapter 5 for its definition), can be converted to internal energy and the mass of the target gas has a significant effect on the amount of energy transferred into the ion. However, a change in the nature of the target has different effects on high-collision-energy CID spectra due to the much shorter interaction times usually encountered at high collision energies and the much smaller fraction of a rather large $E_{c.m.}$ transferred into internal energy.

Target gas pressure effects on CID mass spectra both at high and low collision energies are best described by the Beer's law relationship:

$$\frac{I_p}{I_o} = e^{-\sigma_t \cdot L \cdot N} \qquad 3.5$$

where σ_t is the total collision cross section for all processes that lead to ion loss, in cm^2. I_p is the intensity of the transmitted parent ion and I_o is the initial intensity of the parent ion without collision gas. L is the length of the collision region, in cm. N is the

number density of the target gas, in cm^{-3}, which is proportional to the pressure. Note that equation 3.5 is only applicable for single collision conditions.

The collisions take place in the FFR of the mass spectrometer. Gas is introduced into the collision cell and the pressure of the gas is monitored at a point outside the collision cell. It is thus more convenient to rely on the amount by which the intensity of the main beam of ions is reduced due to the presence of the gas, than on the gas pressure itself. It has been shown[2] that in conditions where the main beam is reduced by 10%, 95% of the collision events are single encounters. Increasing the beam reduction to 40% generates conditions in which double and triple encounters account for 20% and 5% of the collision events, respectively. Under multiple collision conditions, higher internal energy dissociation pathways become more probable and so the structure characteristic features may often be reduced significantly or obscured. Conditions yielding single collisions are generally used.

Note that the pressure of the collision gas has no influence on the average energy deposition *per collision*. It was shown, however, that when the pressure of the collision gas is increased to a value where multiple collisions become important, the ions receive several portions of energy and therefore the average amount of energy received in the entire collision region increases.[13]

3.3.2 *Charge stripping and charge reversal*

When helium is replaced with a diatomic target gas such as oxygen, a marked increase in the amount of doubly charged ions is observed in the resulting spectrum. This process is referred to as Charge Stripping[14] (CS) and occurs when ions gain enough internal energy to expel a second electron, thus producing a doubly charged ion as described by:

$$A^+ + T \rightarrow A^{++} + T + e \qquad 3.6$$

In the resulting mass spectrum, these peaks are characteristically narrow (no KER because these ions do not originate from the fragmentation of a higher mass precursor) and appear at half their actual mass (i.e., apparent mass = m/z and for doubly charged ions z = 2).

It is also possible to induce, through collisions, processes involving the loss of two electrons. This technique is referred to as Charge Reversal[15] (CR) and allows positive ions to be generated from the corresponding negative ion precursor as described by:

$$A^- + T \rightarrow A^+ + T + 2e \qquad 3.7$$

This may allow the production of cations which otherwise may not be directly obtained, but is structure indicative only if the cation produced has the same structure as the anion precursor. Conditions for carrying out these experiments are very similar to those discussed previously for obtaining CID mass spectra.

3.3.3 *Collision induced dissociative ionization (CIDI)*

The neutral co-generated in metastable dissociations may also be investigated. The identification of these neutral species is achieved by collisional ionization. When kilovolt neutral projectiles encounter a target gas, the collision may produce an ion which contains sufficient internal energy to fragment. This technique is referred to as collision induced dissociative ionization[16] and produces a mass spectrum which can be used to characterize the structure of the neutral species co-generated in the metastable decomposition of the precursor molecule. This information is necessary if the thermochemistry of the process is to be investigated and also provides ancillary information that may prove useful when identifying the nature of the ionic species produced.

3.3.4 *Neutralization-reionization mass spectrometry (NRMS)*

In addition to the study of the neutrals co-generated in metastable dissociations, it is also possible to generate neutral species by neutralizing cations. This allows the production, and upon reionization, the characterization of molecules and radicals of unusual structure derived from the corresponding stable cation. The technique, neutralization-reionization mass spectrometry[17] consists of two sequential steps: neutralization and reionization:

step 1: neutralization: $M^{+\cdot} + N \rightarrow M + N^{+\cdot}$ 3.8

step 2: reionization: $M + R \rightarrow M^{+\cdot} + R + e$ 3.9

Neutralization occurs by an electron transfer process considered as a vertical Franck-Condon process so that if the geometries of the ion and neutral are similar, a stable neutral should be produced. If the neutral produced survives, it is then reionized by collisional activation. If the experiment is successful, the resulting mass spectrum will show a peak corresponding to the reionized species (this peak is referred to as a recovery signal) and fragment ions characteristic of the reionized species. The presence of a recovery signal indicates that the neutral produced was stable at least for a period of approximately 0.5 – 5 μs (depending on the mass of the ion and the distance between the collision cells).

3.4 Fundamental studies by using MI and CID experiments

3.4.1 Ion structure determination

Structure differentiation is normally based on the comparison of relative fragment ion abundances in the MI and CID mass spectra as well as on comparison of peak shapes corresponding to metastable dissociations. The measurement of KER from metastable ions is also useful.

The structure elucidation becomes complicated because of possible isomerization of organic ions. The relative magnitude of the energy barriers for decomposition (E_d) and isomerization (E_i) is the parameter which principally

determines if and to what extent an ion $BCAD^{+}$ rearranges to an isomeric ion $ABCD^{+}$ at a given internal energy. Figure 3.4 shows hypothetical two-dimentional energy diagrams intended to depict commonly encountered situations in ion structural studies (the energy range for metastable decomposition is indicated as a hatched area).

Figure 3.4 (A) is more complex. At $E < E_i$ no isomerization of $BCAD^{+\bullet}$ is possible while at internal energies $E_i < E < E_d$, this ion can rearrange to $ABCD^{+\bullet}$ without decomposition. However, in the absence of any mechanism for energy relaxation $BCAD^{+\bullet}$ will not rearrange completely to $ABCD^{+\bullet}$, but there will be a mixture of rapidly interconverting structures $BCAD^{+\bullet}$ and $ABCD^{+\bullet}$. The kinetic energy release (KER) is typically < 40 meV with a Gaussian metastable peak shape. The MI spectra of $BCAD^{+\bullet}$ and $ABCD^{+\bullet}$ would be expected to have similar product ion ratios for the identical reactions indicating dissociations from the same structure or mixture of structures. The CID spectra of $BCAD^{+\bullet}$ and $ABCD^{+\bullet}$ metastably generated from their respective precursors will be distinguishable indicating the distinct stable structures existing at the ionization threshold. A classic example where this is the case is the $C_4H_8^{+\bullet}$ isomers.[18,19] Each of these isomeric ions has the structure of its neutral counterpart at ionization threshold, but isomerization can readily occur with each ion at energies below the activation energy for loss of $CH_3^{\cdot}$, the lowest energy fragmentation. Therefore, in general, neither the abundances of fragment ions from metastable ions nor the KER values obtained can be regarded as characteristic of the structure of the $C_4H_8^{+\bullet}$ ion at its ionization threshold.

Figure 3.4 (B) shows the lowest threshold for decomposition of the initial ion $ABCD^{+\bullet}$ is considerably higher than the isomerization barrier, which is in turn higher than the decomposition threshold of the rearranged ion $BCAD^{+\bullet}$. All the initial ions $ABCD^{+\bullet}$ with energy of $E > E_i$ will decompose through structure $BCAD^{+\bullet}$. However, in contrast to Fig. 3.4 (A) hardly any interconverting structures $ABCD^{+\bullet} \leftrightarrow BCAD^{+\bullet}$ will be observed in this case: Once the ions $ABCD^{+\bullet}$ have overcome the isomerization barrier E_i decomposition through $BCAD^{+\bullet}$ will be much faster than rearrangement back to $ABCD^{+\bullet}$. This is the case to show that a rate-determining isomerization of structure $ABCD^{+\bullet}$ precedes a fast dissociation. It has been demonstrated that a variety of heteroatom-containing ions such as $C_2H_4O_2^{+\bullet}$,[20] $C_2H_6N^+$,[21] $C_3H_7O^+$[22-24] and $C_4H_9O^+$[25] are best represented by such a potential energy diagram. Therefore, the dissociations may not be characteristic of the structure $ABCD^{+\bullet}$. In this case, both the MI and CID mass spectra of $ABCD^{+\bullet}$ and its isomer $BCAD^{+\bullet}$ will be different. The metastable peak is usually of Gaussian shape but is broader for $ABCD^{+\bullet}$ than for $BCAD^{+\bullet}$ (also < 40 meV) reflecting the energy difference between E_i and E_d.

An excellent example of this situation was a study of the isomeric oxonium ions $CH_3CH_2O{=}CH_2^+$ and $CH_3CH{=}OCH_3^+$.[24] The MI spectrum of $CH_3CH_2O{=}CH_2^+$ shows the loss of H_2O and loss of C_2H_4, whereas the MI spectrum of $CH_3CH{=}OCH_3^+$ shows losses of H_2O, C_2H_4 and CH_2O. Furthermore, the average KER values for loss of H_2O and C_2H_4 from metastable $CH_3CH{=}OCH_3^+$ are higher than for the corresponding losses from $CH_3CH_2O{=}CH_2^+$. Both metastable ion tests

would seem to indicate that the metastable ions fragment from distinct structures. It was proposed, however, that the ion $CH_3CH=OCH_3^+$ undergoes a slow isomerization to $CH_3CH_2O=CH_2^+$ followed by rapid dissociation. The $CH_3CH=OCH_3^+$ ions with sufficient energy to isomerize have energy well in excess of that required to dissociate from $CH_3CH_2O=CH_2^+$, accounting for the differences in the fragment ion abundance ratio and average KER values. Strong evidence for this interpretation came from the measurement of the appearance energy values for the losses of H_2O, C_2H_4, and CH_2O from $CH_3CH=OCH_3^+$. These values were all higher than the corresponding values for $CH_3CH_2O=CH_2^+$. The CID spectra are clearly different from each other. The $\Delta_fH°$ of $CH_3CH=OCH_3^+$ and $CH_3CH_2O=CH_2^+$ are 151 and 150 kcal mol^{-1}, respectively.

A special case for this situation is that $BCAD^{+\bullet}$ is a distonic ion which is generally much more stable than the conventional ion $ABCD^{+\bullet}$, then the KER can be very small (< 1 meV), only a small fraction of the excess energy appears as the kinetic energy release. This is illustrated by the dissociations of $C_2H_6O^{+\bullet}$[26] and $C_3H_8O^{+\bullet}$[27] ions in which non-classical distonic ions $^\bullet CH_2CH_2OH_2^+$ and $^\bullet CH_2CH_2CH_2OH_2^+$ are the reacting configurations of their isomeric species.

In Figure 3.4 (C) ($E_i >> E_d$) no isomerization is possible at internal energies below E_i. At higher energies ($E > E_i$) isomerization is possible in principle, but in general, decomposition will be much faster than isomerization, since the density of states in the activated complex for decomposition is considerably higher than that in

the activated complex for isomerization as a result of the higher excess energy and looser transition state. The interpretation of both MI and CID spectra are generally straightforward.

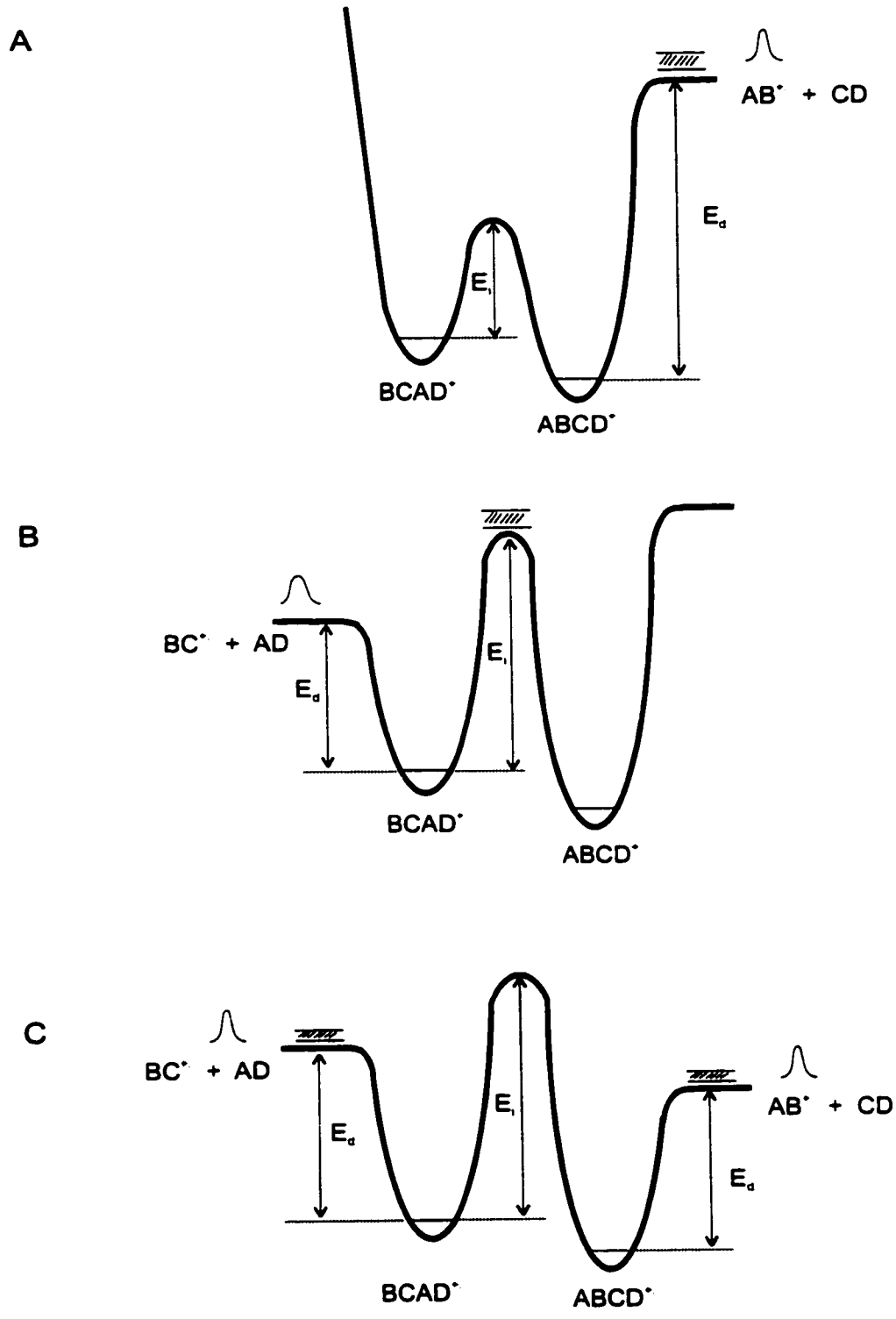

Figure 3.4 Schematic potential diagrams illustrating the parameters which influence the isomerization of organic ions

3.4.2 *Reaction mechanism*

In general, mechanisms of reactions have been indirectly established on the basis of kinetic energy release measurements, isotopic labeling and structure determination of the product ions.

The analysis of metastable peak shapes is one of the most powerful tools for the investigation of reaction mechanisms. In order to resolve fine structure in such peaks high energy resolution is required. Metastable peak shape analysis at high energy resolution led to the detection of composite metastable peaks in a large variety of reactions. Figure 3.5 shows such a composite metastable peak for HCN loss from benzaldoxime,[28] where a Gaussian-shaped peak with an average KER = 50 meV is superimposed onto a dish-shaped peak with KER = 670 meV.

If a decomposition reaction of the molecular ion leads to a composite metastable peak this may result from competing fragmentations via different transition states giving isomeric products.

For HCN loss from benzaldoxime both a four- and five-membered transition state according to Scheme I has been suggested. It should, however, be pointed out that the mere observation of a composite metastable peak does not give any information on the detailed mechanism, in particular it is not known a priori which component of the composite peak corresponds to which mechanism. In the case of the benzaldoxime, blocking of the two ortho positions by substitution with chlorine atoms led to the disappearance of the narrow component of the composite peak,

suggesting that the broad component can be assigned to the four-centered transition sate, the narrow component to the five-centered one.[28]

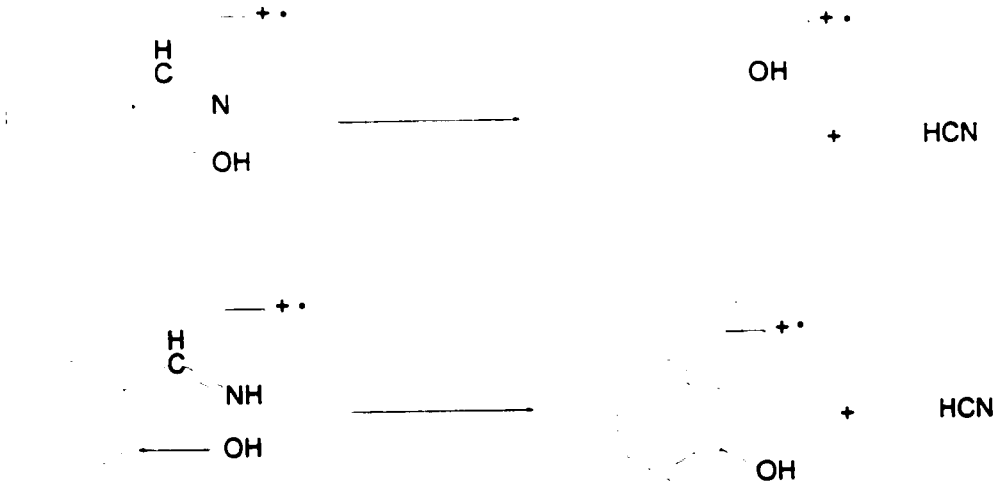

Scheme 3.1

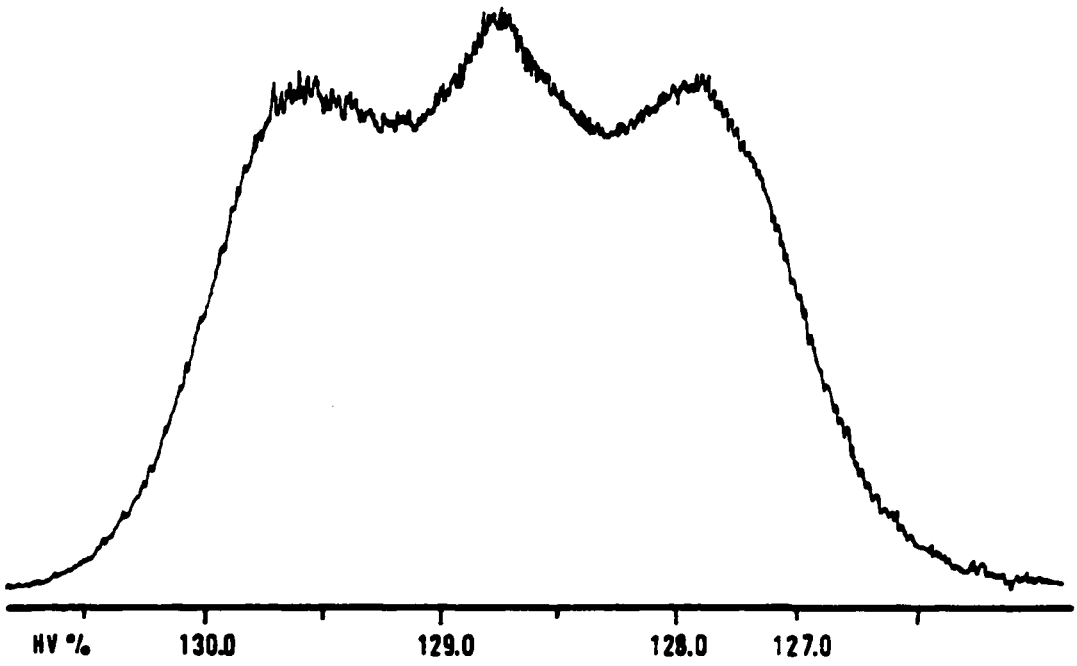

Figure 3.5 Composite metastable peak obtained for loss of HCN from benzaldoxime

Similarly composite metastable peaks led to the detection of competing four- and five-centered transition states for HCN loss from *p*-methoxy benzaldoxime-*o*-methylester[29] and HCl loss from 2,3-dichlorobutane,[30] while NO loss from substituted nitrobenzenes seems to involve three- and four-centered transition states.[31] In all these reactions the larger KER values were associated with the activated complex of smaller ring size. Thus the data available so far show that the fraction of reverse activation energy released as kinetic energy is the larger the tighter the transition state.

3.5 Thermochemistry

Complementary information to the study of ion dissociation characteristics of an ion of interest is provided by the knowledge of the heat of formation ($\Delta_f H°$) of this species. In the following sections, means by which $\Delta_f H°$ of neutrals and ions are determined, using electron impact ionization, will be described.

3.5.1 Ionization and appearance energy measurements

Ionization and Appearance Energy (IE and AE) measurements are used to obtain the $\Delta_f H°$ of an ion or neutral. Ionization energy of M is the minimum energy to produce $M^{+\bullet}$ from M.

$$M \longrightarrow M^{+\bullet} + e \qquad 3.10$$

Adiabatic (IE_a) and vertical (IE_v) ionization energies are frequently described. The latter relates to the energy difference between the ground state (electronic and vibrational) of the neutral and the point at which the value for the equilibrium internuclear spacing in the neutral molecule, r_e, cuts the potential energy surface for the ionized state, whereas the former refers to the energy difference between the ground states (electronic and vibrational) of both the neutral and ionized species. In the case where there is little or no geometry change between the neutral and the ionized species, IE_a and IE_v are the same (see Figure 3.6). IE_a is accessible in the majority of cases studied by an electron impact method. In the case where there is a big geometry change between the neutral and the ion, IE_a and IE_v are not identical and it becomes difficult to precisely determine the IE_a.

The Appearance Energy of a fragment ion (F^+) is the minimum energy needed to produce the fragment ion and neutral (N) from M:

$$M \longrightarrow F^+ + N\bullet + e \qquad 3.11$$

The Appearance Energy is also related to the activation energy that must be provided to $M^{+\cdot}$ in order to produce F^+.

The $\Delta_f H°$ of an ion or neutral is determined from the experimentally measured IE and AE. These measured quantities are related to the $\Delta_f H°$ of the species involved in the corresponding process by:

$$IE = \Delta_f H^\circ(M^{+\cdot}) - \Delta_f H^\circ(M) \qquad 3.12$$

$$AE = \Delta_f H^\circ(F^+) + \Delta_f H^\circ(N^\cdot) - \Delta_f H^\circ(M) \qquad 3.13$$

where N is the neutral species co-generated.

In order for the desired $\Delta_f H°$ to be determined accurately from IE and AE measurements, the following conditions must be met: 1) the $\Delta_f H°$ of the other species involved must be known. If no experimental data exist for the neutral molecule or radical, their $\Delta_f H°$ may be estimated using Benson's Additivity Scheme,[32] 2) the fragmentation of $M^{+\cdot}$ must have no significant kinetic shift and 3) the reverse reaction must have no significant energy barrier.

A fragmentation reaction will have a significant kinetic shift when its rate constant rises only slowly with the increase of internal energy. In this case, the AE measured will depend considerably on the time scale of the method used for the measurement.[33] Comparing the AE of F^+ produced metastably with the AE of F^+ produced in the ion source may provide some information on the presence of an important kinetic shift. The KER in a metastable dissociation may also provide information concerning the presence of either an appreciable kinetic shift or a reverse activation energy barrier. In general, if the average KER is relatively small (0 to ca. 30 meV), it is probable that the reaction involves neither a large kinetic shift nor a reverse activation energy barrier. In cases where the kinetic shift is large and/or in the presence of reverse activation energy, the measured AE must be

considered as an upper limit and the $\Delta_f H°$ value obtained for any product will consequently also be an upper limit.

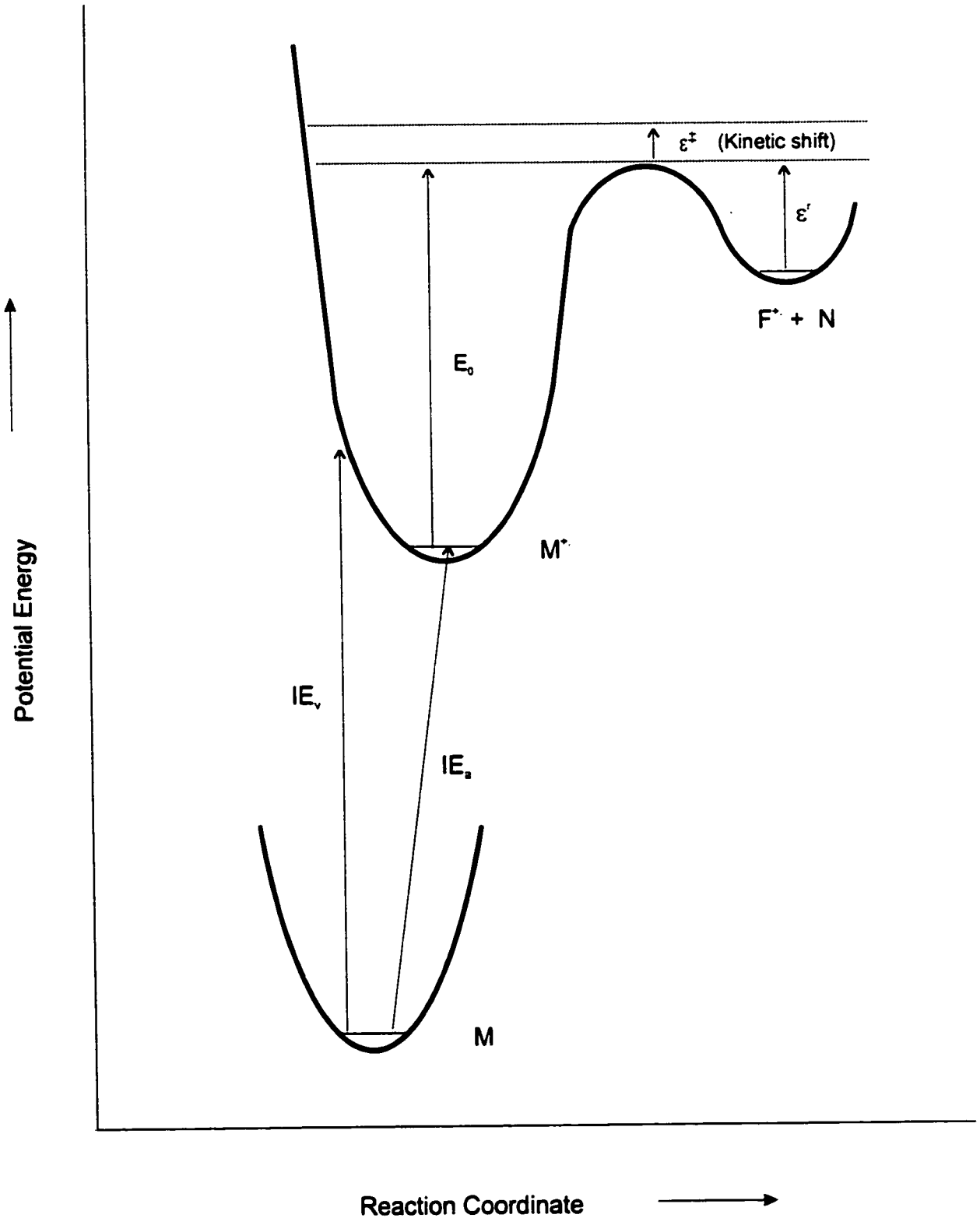

Figure 3.6 Production of $M^{+\cdot}$ and $F^{+\cdot}$ from M

3.6 Theoretical calculations

Molecular orbital (MO) calculations give valuable information which can be used to support or even precede experimental evidence. In general, three main pieces of information can be provided by MO calculations: 1) heat of formation of ions; 2) equilibrium geometries and 3) energy barriers for isomerization and fragmentation. Independent of its usefulness for ion structure elucidation the heat of formation is one of the most important properties of an ion and its theoretical determination is highly desirable. Thus computed energetic data can be directly compared with experimental values and these may in turn be used to test the accuracy of the computation if the latter are of high quality. Moreover, such MO calculations usually include various non-classical structures which the mass spectrometrist may have overlooked when discussing ion structures.

Computational methods used to calculate energetic data on gaseous organic ions consist of *ab initio* calculation and semiempirical methods. Most *ab initio* calculations which have been applied to the structures of positive ions have been on the Hartree-Fock level. It enables the determination of the structures and relative energies of the species involved in the chemical reactions. Transition structures which are not directly observable experimentally may be fully characterized and reaction potential surfaces may thus be derived and a reaction mechanism established.

This can be exemplified by the case of $CH_4O^{+\bullet}$.[1] Two distinct stable isomers, $CH_3OH^{+\bullet}$ and $^{\bullet}CH_2O^{+}H_2$, were discerned by calculation as well as by collisional activation experiments.[34-36] It was predicted by calculation that $^{\bullet}CH_2OH_2^{+}$ is a stable isomer, lying 45 kJ mol^{-1} lower in energy than $CH_3OH^{+\bullet}$. The barrier separating these two isomers (112 kJ mol^{-1} at the transition state) is sufficiently large to allow each to be separately observable. The calculated structures for these two species are shown in Figure 3.7.

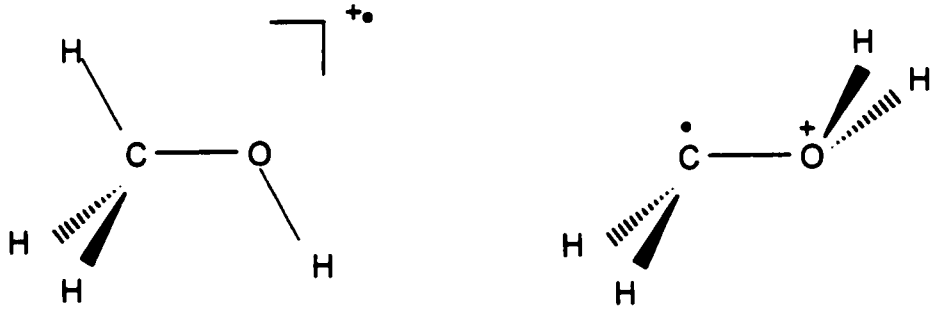

Figure 3.7 Calculated structures for $CH_4O^{+\bullet}$ ions

This theoretical prediction was confirmed by CID experiments. In these experiments, $^{\bullet}CH_2OH_2^{+}$ was generated indirectly by fragmentation of ionized ethylene glycol:

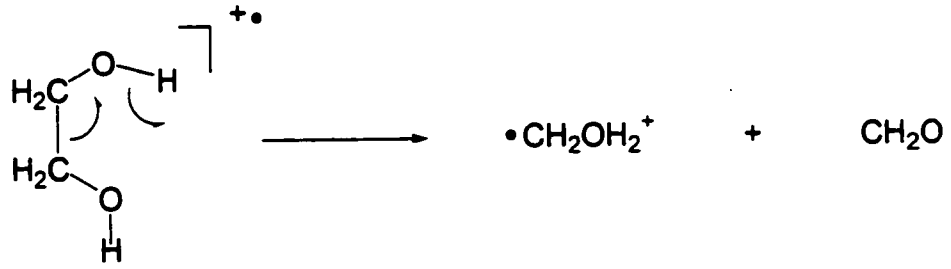

The CID mass spectrum of the $^{\bullet}CH_2OH_2^+$ formed in this manner was shown to be quite distinct from that of $CH_3OH^{+\bullet}$, generated directly from ionized methanol. The experiments also confirmed that $^{\bullet}CH_2OH_2^+$ is more stable than $CH_3OH^{+\bullet}$, finding an energy difference of 29 kJ mol^{-1},[34,35] somewhat smaller than the theoretical 45 kJ mol^{-1}.

The observation that $^{\bullet}CH_2OH_2^+$ is a stable isomer of $CH_3OH^{+\bullet}$ may be generalized to $^{\bullet}CH_2Y^+$[37-40] (Y = X (halogen), NH_2, SH, PH_2, etc) and larger systems such as $C_2H_6O^{+\bullet}$ ions. Thereafter, a new class of radical cations with separated radical and charge centers were named ylidion (adjacent radical and charge centers) or distonic ions (separated radical and charge centers).

3.7 References

(1) Radom, L.; Bouma, W. J.; Nobes, R. H.; Yates, B. F. *Pure & Appl. Chem.* **1984**, *56*, 1831-1842.

(2) Holmes, J. L. *Org. Mass Spectrom.* **1985**, *20*, 169-183.

(3) Traeger, J. C.; McLoughlin, R. G. *Int. J. Mass Spectrom. Ion Phys.* **1978**, *27*, 319.

(4) Lossing, F. P.; Traeger, J. C. *Int. J. Mass Spectrom. Ion Phys.* **1976**, *19*, 9.

(5) Williams, D. H.; Hvistendahl, G. *J. Am. Chem. Soc.* **1974**, *96*, 6755.

(6) Holmes, J. L.; Terlouw, J. K. *Org. Mass Spectrom.* **1980**, *15*, 383-397.

(7) Cooks, R. G.; Beynon, J. H.; Caprioli, R. M.; Lester, G. R. . In *Metastable ions*; Elsevier: Amsterdam, 1973.

(8) Busch, K. L.; Glish, G. L.; Mcluckey, S. A. . In *Mass spectrometry/Mass spectrometry*; VCH: New York, 1988.

(9) Douglas, D. J. *J. Phys. Chem.* **1982**, *86*, 185.

(10) Mclafferty, F. W.; Bente, P. F.; Kornfeld, R.; Tsai, S. C.; Howe, I. *J. Am. Chem. Soc.* **1973**, *95*, 2120.

(11) Massey, H. S. W. *Rep. Prog. Phys.* **1949**, *12*, 248.

(12) Vekey, K. *J. Mass Spectrom.* **1996**, *31*, 445-463.

(13) Todd, P. J.; McLafferty, F. W. *Int. J. Mass Spectrom. Ion Phys.* **1981**, *38*, 371.

(14) Cooks, R. G.; Beynon, J. H.; Ast, T. *J. Am. Chem. Soc.* **1972**, *94*, 1004.

(15) Bowie, J. H.; Blumenthal, T. *J. Am. Chem. Soc.* **1975**, *97*, 2959.

(16) Burgers, P. C.; Holmes, J. L.; Mommers, A. A.; Terlouw, J. K. *Chem. Phys. Lett.* **1983**, *102*, 1.

(17) Holmes, J. L. *Mass Spectrom. Rev.* **1989**, *8*, 513.

(18) Holmes, J. L.; Weese, G. M.; Blair, A. S.; Terlouw, J. K. *Org. Mass Spectrom.* **1977**, *12*, 424.

(19) Morgan, R. P.; Derrick, P. J. *Org. Mass Spectrom.* **1975**, *10*, 563.

(20) Levsen, K.; Schwarz, H. *J. Chem. Soc. Perkin Trans. II* **1976**, 1231.

(21) Bowen, R. D.; Williams, D. H.; Hvistendahl, G. *J. Am. Chem. Soc.* **1977**, *99*, 7509.

(22) Bowen, R. D.; Kalman, J. R.; Williams, D. H. *J. Am. Chem. Soc.* **1977**, *99*, 5481.

(23) Hvistendahl, G.; Bowen, R. D.; Williams, D. H. *J. Chem. Soc. Chem. Comm.* **1976**, 294-295.

(24) Hvistendahl, G.; Williams, D. H. *J. Am. Chem. Soc.* **1975**, *97*, 3097.

(25) Bowen, R. D.; Williams, D. H. *J. Am. Chem. Soc.* **1977**, *99*, 6822.

(26) Bouma, W. J.; Nobes, R. H.; Radom, L. *J. Am. Chem. Soc.* **1983**, *105*, 1743.

(27) Holmes, J. L.; Mommers, A. A.; Szulejko, J. E.; Terlouw, J. K. *J. Chem. Soc. Chem. Commun.* **1984**, 165.

(28) Vijfhuizen, P. C.; Heerma, W.; Dijkstra, G. *Org. Mass Spectrom.* **1975**, *10*, 919.

(29) Beynon, J. H.; Bertrand, M.; Cooks, R. G. *Org. Mass Spectrom.* **1973**, *7*, 785.

(30) Kim, K. C.; Beynon, J. H.; Cooks, R. G. *J. Chem. Phys.* **1974**, *61*, 1305.

(31) Beynon, J. H.; Bertrand, M.; Cooks, R. G. *J. Am. Chem. Soc.* **1973**, *95*, 1739.

(32) Benson, S. W. In *Thermochemical Kinetics (2nd edition)*; John Wiley & Sons: New York, 1976.

(33) Burgers, P. C.; Holmes, J. L. *Int. J. Mass Spectrom. Ion Proc.* **1984**, *58*, 15.

(34) Holmes, J. L.; Lossing, F. P.; Terlouw, J. K.; Burgers, P. C. *Can. J. Chem.* **1983**, *61*, 2305.

(35) Holmes, J. L.; Lossing, F. P.; Terlouw, J. K.; Burgers, P. C. *J. Am. Chem. Soc.* **1982**, *104*, 2931.

(36) Bouma, W. J.; MacLeod, J. K.; Radom, L. *J. Am. Chem. Soc.* **1982**, *104*, 2930.

(37) Bouma, W. J.; Yates, B. F.; Radom, L. *Chem. Phys. Lett.* **1982**, *92*, 620.

(38) Bouma, W. J.; MacLeod, J. K.; Nobes, R. H.; Radom, L. *Int. J. Mass Spectrom. Ion Phys.* **1983**, *46*, 235.

(39) Bouma, W. J.; Dawes, J. M.; Radom, L. *Org. Mass Spectrom.* **1983**, *18*, 12.

(40) Frisch, M. J.; Raghavachari, K.; Pople, J. A.; Bouma, W. J.; Radom, L. *Chem. Phys.* **1983**, *75*, 323.

Chapter 4 The application of MS/MS techniques and ion thermochemistry to the immonium ions

4.1 Introduction

Interest in the t-butylamine radical cation arose from a publication[1] which investigated the potential energy surface for the dissociation of t-butylamine radical cation using *ab initio* calculations at the UHF/3-21G level, as part of the series of compounds then under examination.[2-4] The minimum energy reaction pathway (MERP) leads to a methyl radical and an amino-isopropyl cation.

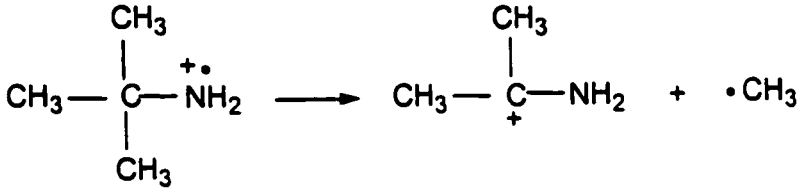

t-butylamine (m/z 73) amino-isopropyl cation (m/z 58)

According to the calculation, the molecular radical cation (the 'adiabatic' ion) is separated by a transition state (MERP, the distance between the leaving methyl C-atom and the central C-atom, = 2.01 Å) from the dissociation products. After passing over the barrier the separation fragments then pass through an ion/neutral complex at MERP = 4.2 Å before finally separating.[1]

The principal dissociation routes for simple alkylamines have been extensively studied and documented for several decades. The electron ionization (EI) mass spectra tend to be typically dominated by an abundant primary fragment ion formed by α-cleavage to give a resonance stabilized 'immonium' ion whose general formula is $C_nH_{2n+2}N^+$. This dissociation has often been considered to be 'triggered' by the lone electron situated in the singly occupied non-bonding orbital on nitrogen.

Traditionally, α-cleavage has been regarded as an extremely simple process, in which a C-C bond is broken essentially without reverse critical energy. This view was undermined by the discovery that several ionized t-butylamines, $(CH_3)_3CNHR^{+\bullet}$ [R = H, CH_3, or $(CH_3)_3C$],[5] expel a methyl radical with the production of a broad, dished metastable peak, even though the resultant products lie only 30 – 50 kJ mol^{-1} higher in energy than the reactant. The observed kinetic energy release (KER) is substantial (114 – 218 meV) which indicates that there is a definite energy barrier towards the reverse reaction.

The distinct feature for methyl loss from ionized t-butylamines shows that elimination of small radicals from the heteroatom molecules may occur in contradiction to the widely held view concerning simple bond cleavages. It was predicted by the *ab initio* calculation that the reaction mechanism involves a complex prior to its *exothermic* dissociation.

The proposal of a reverse activation energy for the α-cleavage reaction of t-butylamine casts doubt on the determination of heat of formation ($\Delta_f H°$) of the immonium ions from appearance energies (AE) for those reactions. The $\Delta_f H°$ of $(CH_3)C^+NH_2$ reported in the literature[5,6] (141 kcal mol^{-1}) may well be too high and thus needs to be revised.

The immonium ions are the products of α-cleavage in simple amines. The high stability of these ions arises from the fact that the electron-donating ability of nitrogen stabilizes the charge on the central carbon. The analogous oxonium ions have a similar but smaller stabilization effect than the immonium ions.[7] The canonical forms of the tertiary immonium ion are as follows:

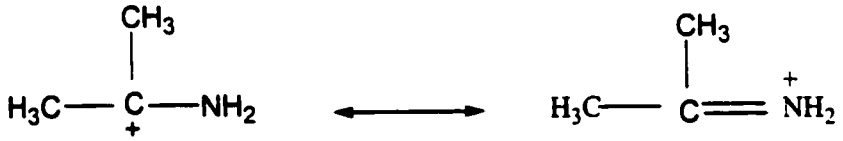

Mass spectrometric studies on the isomeric immonium ions ($C_3H_8N^+$) and the oxonium analogues ($C_3H_7O^+$) are carried out with the use of tandem sector mass spectrometer. It is concluded that the secondary and tertiary immonium (or oxonium) ions are interconverting at the internal energies near the dissociation limit on the basis of their having the same fragmentation patterns and KER value but different product ion abundances. The possible fragment ions' structures produced

by these immonium (or oxonium) ions are assigned by their corresponding CID mass spectra.

4.2 Experimental

Measurements were made on a modified VG ZAB-2F mass spectrometer and AEI-MS 902S instrument. The AE of fragment ions were determined by detecting the threshold for an ion current at the appropriate mass as the energy of the electron beam was increased by 0.2 V steps over 2 V range (MS 902S). The metastable decompositions (MI) and collision-induced dissociations (CID) were studied in the 2FFR and 3FFR of the ZAB-2F. The collision gases, i.e., He and O_2, were introduced in the FFR until 10% beam reduction was achieved. Kinetic energy release values were calculated from the peak width at half-height after correction for parent peak width. Samples were purchased from the Aldrich Chemical Co. (Milwaukee) and were of high purity.

4.3 Results and Discussion

4.3.1 α-cleavage in amine molecular ions

α-cleavage is a reaction initiated by the radical site. It arises from its strong tendency for electron pairing; the odd electron is donated to form a new bond to an adjacent atom accompanied by cleavage of another bond to that atom. It is a widely held view in mass spectrometry that simple bond cleavage reactions do not have appreciable reverse activation energies. We draw attention to α-cleavage reactions of certain amine molecular ions which give rise to broad Gaussian or narrow

Gaussian metastable peaks with an indication of the existence of an appreciable or small energy barrier towards the reverse reaction. It is suggested that different reaction mechanisms must apply.

Secondary and tertiary amines are good examples for a mechanistic investigation since there are a larger number of α-cleavage possibilities and the molecular ions do not rearrange to distonic ions by the hydrogen transfer process.

A series of t-butylamines, $(CH_3)_3CNHR^{+\bullet}$ were studied by Hammerum[5] for the methyl loss reactions. The corresponding metastable peaks are broad and dished.

$$(CH_3)_3CNHR^{+\bullet} \longrightarrow (CH_3)_2C{=}NHR^{+} + {\bullet}CH_3$$

(1) R = H	KER = 114 meV
(1) R = CH_3	KER = 166 meV
(1) R = $(CH_3)C$	KER = 218 meV

We reexamined the methyl loss process for t-butylamine and found that the KER value (105 meV) is indeed close to the reported values (114 – 218 meV) except that the shape of the metastable peak is broad Gaussian instead of a dish-topped peak. The production of $(CH_3)_2C^{+}NH_2$ is <u>insensitive</u> to collision gas in keeping with rearrangement preceding dissociation.

Methyl loss from ionized isopropylamine proceeds, however, only with very small KER, e.g. 0.3 kJ mol^{-1} (3 meV). This observation is not in agreement with the results from Hammerum[5] (KER = 5 kJ mol^{-1}). The corresponding metastable peak has a Gaussian profile. The fragmentation is very sensitive to collision gas. This indeed suggests a 'simple bond cleavage' process in which the transition state is an ion/neutral complex. The KER value corresponding to methyl loss from N-ethylisopropylamine, $(CH_3)_2CHNH^{+\bullet}C_2H_5$, is 3 kJ mol^{-1} (30 meV) with a Gaussian metastable peak shape. This fragmentation however, is insensitive to collision gas.

$$(CH_3)_2CHNH_2^{+\bullet} \longrightarrow CH_3CH{=}NH_2^{+} + \bullet CH_3$$

$$(CH_3)_2CHNH^{+\bullet}C_2H_5 \longrightarrow CH_3CH{=}NH^{+}C_2H_5 + \bullet CH_3$$

Loss of larger alkyl groups from some aliphatic amines is characterized by Gaussian metastable peaks corresponding to KER < 2 kJ mol^{-1} (typical for a simple bond cleavage) according to the measurements made by Hammerum.[5] α-cleavage loss of a larger alkyl radical from an alkylamine commonly gives rise to narrow, Gaussian-type peaks which shows that the translational energy released in the dissociation is quite small.

Amines	Radical loss	KER (meV)
1-Ethylbutylamine	C_2H_5	3
1-Methylbutylamine	C_3H_7	2
N,N-Dipropylmethylamine	C_2H_5	16
N,N-Bis(2-methylpropyl)methylamine	C_3H_7	16
N,N-Dipentylmethylamine	C_4H_9	18
N,N-Dimethyl-1-ethylpropylamine	C_2H_5	13
N,N-Dimethyl-1-propylbutylamine	C_3H_7	14

In general, α-cleavage in amine molecular ions is a not–so-simple simple cleavage. It may undergo rearrangement to an isomeric ion as a reacting configuration before fragmentation or take place as a simple bond cleavage. The former case is exemplified as methyl loss from t-butylamines. The latter is the case for methyl or large alkyl loss from isopropylamine and some aliphatic amines. The potential diagrams for the cases of t-butylamine and isopropylamine are shown in Figure 4.1.

In the case of the t-butylamine molecular ion, making the simple assumption that the methyl group departs in the plane of symmetry, treatment of the energy partitioning in terms of the direction of the transition state reaction co-ordinate predicts the release of a significant fraction of a reverse activation energy as translational energies of the products, whereas reactions in which the neutral released contains more than 4 or 5 atoms normally do not release translational

energy to any great extent during dissociation. The reverse activation energies proposed for the amine reactions would require very little reorganization within the incipient products to be dissipated.

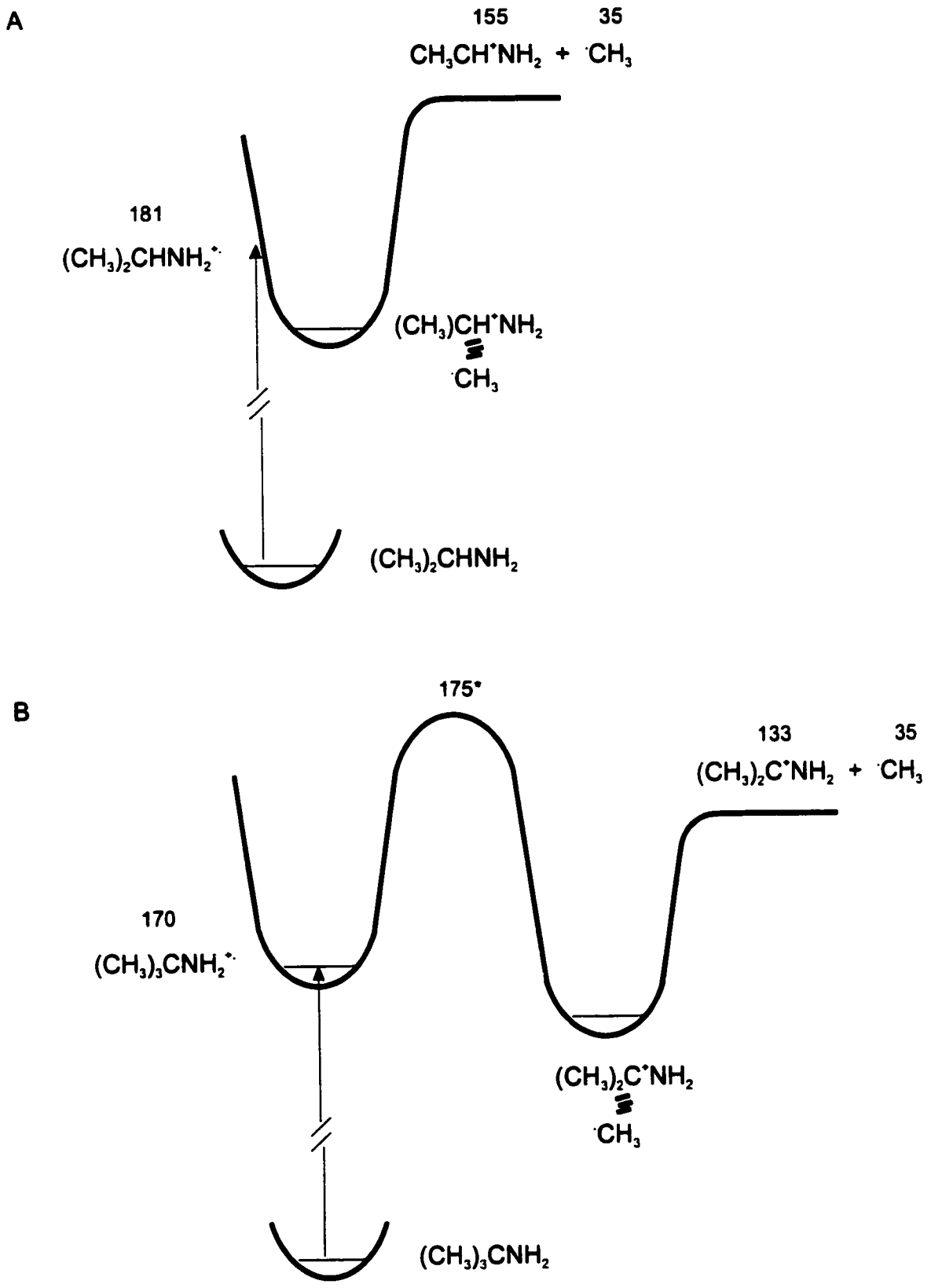

Figure 4.1 Potential energy diagrams for the dissociations of (A) s-$C_3H_7NH_2$; (B) t-$C_4H_{11}NH_2$

* from AE of $(CH_3)_2C^{\bullet}NH_2$

4.3.2 *Thermochemistry of the $(CH_3)_2C^+NH_2$*

The tertiary immonium ion, $(CH_3)_2C^+NH_2$, is the most stable of the five immonium isomers (I – V).

$(CH_3)_2C^+NH_2$	$CH_3CH_2CH^+NH_2$	$CH_3CH_2{}^+NHCH_3$	$CH_2{}^+NHCH_2CH_3$	$CH_2{}^+N(CH_3)_2$
I	II	III	IV	V

The appearance energies of $(CH_3)_2C^+NH_2$ were measured experimentally from several t-alkylamines (see Figure 4.2) in order to obtain the $\Delta_fH°$ data. The ion $(CH_3)_2C^+NH_2$ was produced metastably from the t-butylamine molecular ion. The kinetic energy release (KER) was measured to be 105 meV (10 kJ mol^{-1}) which clearly indicates the existence of an appreciable energy barrier towards the reverse reaction. The results are listed in Table 4.1.

It should be noted that the generation of $(CH_3)_2C^+NH_2$ through ethyl loss from t-amylamine is only very weakly metastable and is moderately sensitive to collision gas. The attempt to measure the KER value was just manageable which is ca. 0.1 meV, the metastable peak is almost at the same width as the main beam but becomes slightly broader in the collision process. This observation indicates that the α-cleavage reaction with a larger alkyl radical loss from simple amines may have a small or zero reverse energy barrier in keeping with the reported series of examinations of α-cleavage reactions for amines.[5] Accordingly the $\Delta_fH°$ of

$(CH_3)_2C^+NH_2$ obtained from this process (136 kcal mol^{-1}) should be more convincing than that from methyl loss of ionized t-butylamine.

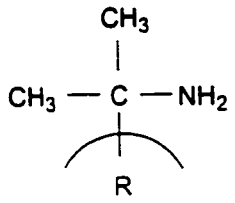

(R = CH_3, C_2H_5 and C_2H_3)

Figure 4.2 t-alkylamines to generate $(CH_3)_2C^+NH_2$ ions

The $\Delta_fH°$ of $(CH_3)_2C^+NH_2$ can be calculated from the measured AE value on the basis of the following equation.

$$AE = \Delta_fH^\circ[(CH_3)_2C^+NH_2] + \Delta_fH^\circ[R] - \Delta_fH^\circ[\text{neutral}] \qquad 4.1$$

With application of the $\Delta_fH°$ for alkyl radical and precursor molecule, the $\Delta_fH°$ for $(CH_3)_2C^+NH_2$ are obtained. The results are listed in Table 1. Note that the $\Delta_fH°$ for 1,1-dimethylallylamine is estimated to be -2.7 kcal mol^{-1} on the basis of Benson's additivity rule.[8]

$\Delta_fH°$ (1,1-dimethylallylamine) 4.2

$= 2C-(C)(H)_3 + C-(C)_2(C_d)(N)^* + C_d-(C_d)(C) + C_d-(H)_2 + N-(C)(H)_2$

$= 2(-10.2) + (-2.0)^* + 8.6 + 6.3 + 4.8$

$= -2.7 \pm 0.5$ (kcal mol^{-1})

* $C\text{-}(C)_2(C_d)(N)$ is estimated to be –2.0 kcal mol^{-1} resulting from adding 1.2 kcal mol^{-1} to the value of $C\text{-}(C)_3(N)$, -3.2 kcal mol^{-1}.

Table 4.1 Thermochemical data for $(CH_3)_2C^+NH_2$ and relevant species

Precursors	AE $(CH_3)_2C^+NH_2$ (eV)	KER $(CH_3)_2C^+NH_2$ (meV)	$\Delta_fH°^{6}$ (neutral) (kcal mol^{-1})	$\Delta_fH°^{6}$ (precursor) (kcal mol^{-1})	$\Delta_fH°_{exp}$ $(CH_3)_2C^+NH_2$ (kcal mol^{-1})
$(CH_3)_3CNH_2$ t-butylamine	8.8 ± 0.1	105	35.1	-28.7	139 ± 2
$(CH_3)_2(C_2H_5)CNH_2$ t-amylamine	8.4 ± 0.1	< 1[b]	28	-30	136 ± 2
$CH_2=CHC(CH_3)_2NH_2$ 1,1-dimethylallylamine	9.00[c] ± 0.05	-	71.5	-2.7[a]	133 ± 1

a) estimated by Benson's additivity rules
b) see text
c) Lossing's work in 1980

Therefore, the $\Delta_fH°$ of $(CH_3)_2C^+NH_2$ will be revised to be 133 kcal mol^{-1}.

4.3.3 Mass spectrometric investigation of $(CH_3)_2C^+NH_2$ and $CH_3CH_2CH^+NH_2$

4.3.3.1 EI mass spectra for the simple alkyl amines and alkanols

The Electron Impact (EI) mass spectra of t-butylamine and 3-pentanamine are both dominated by the peak at m/z 58 corresponding to alkyl radical loss (methyl or ethyl) from the molecular ions, indicating that α-bond cleavages are the

major dissociation route for these amines. The molecular ions are very weak (< 1%). The resulting tertiary and secondary immonium ions (m/z 58), $(CH_3)_2C^+NH_2$ and $CH_3CH_2CH^+NH_2$, contain the NH_2 group, distinguishing them from the other $C_3H_8N^+$ isomers by their distinct fragmentation characteristics.[9-13]

EI mass spectra of the analogous 2-methyl-2-propanol and 3-pentanol show the base peak at m/z 59 indicating that α-bond cleavages are also prevalent for the oxygen-containing species. The resultant ions are called oxonium ions. Table 4.2 shows the structures of these immonium and oxonium ions as well as their precursor molecules. Figures 4.3-4.4 show 70eV EI mass spectra of these molecules.

Table 4.2 Precursors and their main fragment ions

Precursors	$(CH_3)_3CNH_2$	$CH_3(C_2H_5)CHNH_2$	$(CH_3)_3COH$	$CH_3(C_2H_5)CHOH$
	t-butylamine	3-pentanamine	2-methyl-2-propanol	3-pentanol
Fragment ions	$(CH_3)_2C^+NH_2$	$CH_3CH_2CH^+NH_2$	$(CH_3)_2C^+OH$	$CH_3CH_2CH^+OH$
	tertiary immonium ion	secondary immonium ion	tertiary oxonium ion	secondary oxonium ion
	m/z 58	m/z 58	m/z 59	m/z 59

4.3.3.2 MI mass spectra of $(CH_3)_2C^+NH_2$ and $CH_3CH_2CH^+NH_2$

The two metastable $C_3H_8N^+$ ions exhibit three major dissociations corresponding to the losses of NH_3 (m/z 41, $C_3H_5^+$), C_2H_4(m/z 30, CH_4N^+), C_3H_4(m/z

18, NH_4^+). Loss of NH_3 is the most intense metastable reaction. The relative abundances of the peaks as well as the KER values are given in Table 4.3. Figure 4.5 shows the MI mass spectra of the $C_3H_8N^+$ ions.

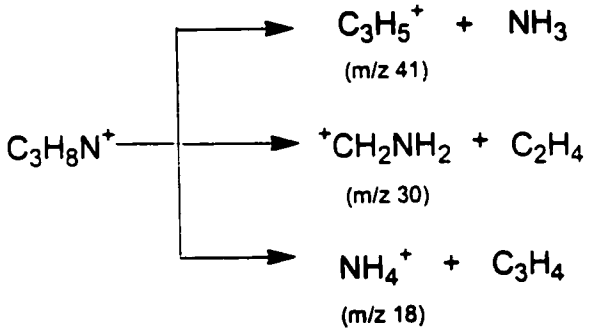

Table 4.3 Relative abundances, as % of base peak, and KER in the MI mass spectra of $(CH_3)_2C^+NH_2$ and $CH_3CH_2CH^+NH_2$ (KER in meV)

Ions (m/z 58)	Fragment ions (KER)					
	m/z 41		30		18	
	2[a]	3[a]	2	3	2	3
$(CH_3)_2C^+NH_2$	100[b]	100	5.3	8.9	6.6	18.5
	(33)		(660)		(25)	
$CH_3CH_2CH^+NH_2$	100	100	4.7	8.4	1.8	5.4
	(21.4)		(619)		(27.5)	

a) refer to 2FFR and 3FFR

b) using peak height as the criterion of peak abundance

All the fragment ion peaks are Gaussian except the one corresponding to the loss of ethylene (m/z 30), which is a dish-topped peak with a large kinetic energy release.

That the two ions show the same fragmentation pattern together with similar KER values suggests that their rearrangement to common dissociating configurations takes place in both ions at some energy between the bottom of the potential well and the dissociation limit. However, the MI mass spectra of the two isomeric ions do differ from each other by the relative intensities of the fragment ions, especially for the intensity of NH_4^+, implying that these two isomeric ions do not interconvert completely freely before dissociation.

The secondary fragment ions were characterized by transmitting them into the 3FFR where they were collisionally activated by He and O_2. The CID mass spectra of the metastably generated fragments at m/z 41 from the isomeric ions (Figures 4.11-4.12, p90-91) displayed identical dissociation characteristics suggesting that the ions formed by the two species are the same. There are two possible structures for this ion ($C_3H_5^+$, m/z 41), one is the allyl cation, $CH_2{=}CHCH_2^+$; the other is the 2-propenyl cation, $CH_3C^+{=}CH_2$. The partial CID(He) mass spectra[14] of the two types of ions are shown in Figure 4.14 (p93). It is evident that the $C_3H_5^+$ ions produced by $(CH_3)_2C^+NH_2$ and $CH_3CH_2CH^+NH_2$ ions have the allyl structure.

4.3.3.3 CID mass spectra of $(CH_3)_2C^+NH_2$ and $CH_3CH_2CH^+NH_2$

The CID mass spectra of the two $C_3H_8N^+$ ions are given in Figures 4.7-4.8 (p86-87). The relative abundances of the peaks in the CID spectra are shown in Table 4.5.

Table 4.5 Relative abundance[a], as % of base peak, in the partial CID mass spectra of $(CH_3)_2C^+NH_2$ and $CH_3CH_2CH^+NH_2$

Ions (m/z 58)	CID, He(O_2)[b] m/z										
	15	18	26	27	28	29	30	39	41	42	43
$(CH_3)_2C^+NH_2$	8.6	4.1	6.8	15.9	26.6	6.2	13.4	50.8	100	98.4	21.9
	7.1	*3.8*	*7.2*	*13.4*	*26.8*	*9.7*	*13.1*	*39*	*92.1*	*100*	*22.4*
$CH_3CH_2CH^+NH_2$	4.4	2.3	7.3	18.4	43.3	12.7	20.7	40.9	100	54.5	27.3
	5.9	*3.0*	*15.6*	*28.5*	*75.9*	*41.8*	*39.2*	*35.2*	*100*	*66.7*	*24.8*

a) using peak height as the criterion of peak abundance
b) using He and O_2 (italic) as collision gas

As in MI mass spectra, the distinction between the CID spectra of the $C_3H_8N^+$ ions lies only on the differences of relative intensities. The most obvious differences are the intensities of the m/z 42, 28 and 29 ions. For $CH_3CH_2CH^+NH_2$, it can easily eliminate a molecule of C_2H_6 (m/z 28) whereas the $(CH_3)_2C^+NH_2$ ion prefers to lose CH_4 (m/z 42). This observation is in accord with that reported in the literature. The origin of these differences may be rationalized by the following mechanism for both ions, α-cleavage accompanying loss of an H atom:[9]

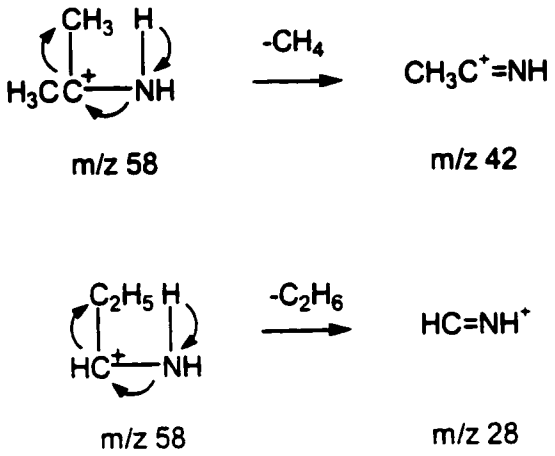

Another important feature to distinguish these two isomers is the abundance of the ion at m/z 29. This ion is favorably produced by $CH_3CH_2CH^+NH_2$. The CID mass spectrum of ion m/z 29 (Figure 4.22, p101) shows that the ions generated by the two isomers may have different structures. The low end of the spectrum from $(CH_3)_2C^+NH_2$ presents the characteristic pattern for the $C_2H_5^+$ ion which is different from that from $CH_3CH_2CH^+NH_2$, the latter suggests the ion has the structure $^{+\bullet}CHNH_2$. Moreover, Oxygen can greatly facilitate the production of the fragment ion (m/z 29) from $CH_3CH_2CH^+NH_2$. Why oxygen rather than helium favors the reaction remains unclear.

The CID mass spectra of the fragment ions at m/z 42, 43 are shown in Figures 4.20 and 4.15 (p99, 94). It is obvious that the ion at m/z 43 contains five hydrogen atoms, giving a composition, $C_2H_5N^{+\cdot}$. Again, it can be either of the two stable structural forms: $CH_2=CHNH_2^{+\cdot}$ (vinylamine) and $CH_3CH=NH^{+\cdot}$ (acetaldimine).

Vinylamine is the most stable form of the $C_2H_5N^{+\cdot}$ ions although the neutral counterpart does not exist as a stable species.[15]

Cyclobutylamine[16] is found to produce the vinylamine ion (base peak) specifically in its mass spectrum. The KER value for the metastable dissociation is 0.68 meV, which is relatively low compared to that of simple bond cleavage (typically, 10-20 meV). The $\Delta_f H°$ of $CH_2=CHX^{+\bullet}$ (X=OH and NH_2), 768 ± 5 and 838 ± 5 kJ mol^{-1}, have been obtained from the measurements of the first dissociation onsets for cyclobutanol and cyclobutylamine by the photoionization method.[16]

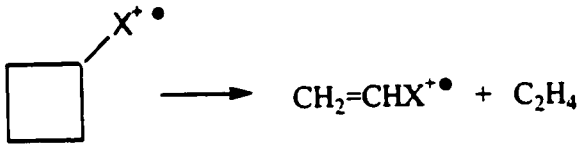

The source-generated ion at m/z 43 should exclusively represent the structure of vinylamine and its CID mass spectrum is given in Figure 4.16 (p95). It is noticed however in the metastable dissociation of the molecular ion (m/z 71), that a composite peak is found at m/z 43 at high energy resolution, with a narrow component atop a broad component. The narrow component is the major feature of the peak. This observation indicates that the metastable dissociation of the molecular ion is interfered with another process in which $C_3H_7^+$ hydrocarbon species is produced. The CID mass spectra of the two components of the peak shows the assumption is correct. The ion of $C_4H_7O^+$ (m/z 71) which has the same mass to

charge ratio can generate $C_3H_7^+$ by loss of CO. This type of ion could come from the degradation product of the sticky residue in the ion source or inlet system. Unfortunately, we cannot separate the molecular ion of cyclobutylamine from $C_4H_7O^+$ by using high mass resolution due to the very low intensities of both ions.

By comparison of the CID spectra of $C_2H_5N^{+\cdot}$ ions collisionally generated from the two $C_3H_8N^+$ ions with that from cyclobutylamine, it can be concluded that the ion with m/z 43 has the vinylamine structure.

The fact that the CID mass spectra of the two isomeric $C_3H_8N^+$ ions show so many similar dissociation characteristics confirms that they are capable of interconverting at energies below the lowest dissociation limit. The depth of the potential energy wells of the two isomeric ions, which are approximately the difference between the sum of the products' $\Delta_f H°$ for the lowest energy dissociation channel and the $\Delta_f H°$ of the ions, are of the order of 2 - 3 eV. Therefore, near the dissociation threshold the density of states are large and the two isomeric ions may interconvert and access a large number of different structures. However, that the probability of accessing different structures still exists, accounts for the dissociation characteristics not being exactly the same. The potential energy diagrams for the dissociation characteristics of the two isomeric species are depicted in Figure 3.4 (B) of Chapter 3.

4.3.3.4 Thermochemistry of the secondary fragment ions

The appearance energies for the fragment ions (m/z 41, 30, 18) were measured in the 1 FFR of the MS-902 instrument. The instrument was set to allow metastable observations in the corresponding reactions. The results were listed in Table 4.4.

Table 4.4 Experimental determinations of the appearance energies (AE) for the secondary product ions

Ions	AE (eV)	KER (meV)	$\Delta_fH°$(neutral)[6] (kcal mol^{-1})	$\Delta_fH°_{exp}$ (kcal mol^{-1})	$\Delta_fH°_{lit}$[6] (kcal mol^{-1})
$CH_2CHCH_2^+$	12.0 ± 0.1	33	-11.0	224 ± 2	226
$^+CH_2NH_2$	12.0 ± 0.1	660	12.5	200 ± 2	178

The $\Delta_fH°$ of the product ions were calculated in the same manner as the case of $(CH_3)_2C^+NH_2$ ion. The high value for $\Delta_fH°$ of $^+CH_2NH_2$ can be explained by the existence of a reverse activation energy. However the $\Delta_fH°$ of $CH_2CHCH_2^+$ is lower than the reference value, but taking into account the uncertainty of measurement then it can be considered to be the same as that for the allyl ion.

4.3.4 MI and CID mass spectra of $(CH_3)_2C^+OH$ and $CH_3CH_2CH^+OH$

In the view of the similarity with which oxygen and nitrogen atom direct mass spectral decompositions, it is interesting to see whether the oxygen-containing

analogous ions have similar dissociation characteristics to nitrogen-containing species.[17-20] The precursors used to generate the $C_3H_7O^+$ ions are presented in Table 4.1.

The two isomeric $C_3H_7O^+$ ions show the same behavior in their metastable dissociation. Note that all of the metastable peaks are Gaussian. The relative abundances as well as the KER values are listed in Table 4.6. Figure 4.6 (p85) shows the MI mass spectra of the $C_3H_7O^+$ ions. Like the $C_3H_8N^+$ isomers, both the $C_3H_7O^+$ ions show similar dissociation characteristics, the only differences are in the relative intensities of the peaks. The $C_3H_5^+$ fragment ions generated in the dissociation of $C_3H_7O^+$ isomers have allyl structure (see Figure 4.12, p91).

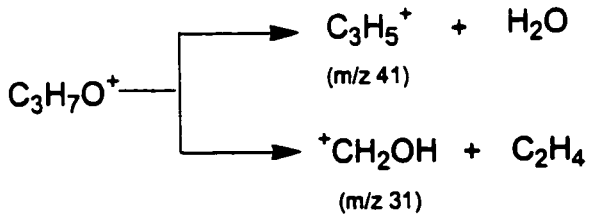

Table 4.6 Relative abundance[a], as % of base peak, and KER (in meV) in the MI mass spectra of $(CH_3)_2C^+OH$ and $CH_3CH_2CH^+OH$

ions	Fragment ions (KER)			
m/z 59	m/z 41		m/z 31	
	2[b]	3[b]	2	3
$(CH_3)_2C^+OH$	100 (22.2)	100	10.8 (14.4)	7.3
$CH_3CH_2CH^+OH$	71.8 (27.4)	54.6	100 (14.7)	100

a) using peak height as the criteria of peak abundance

b) refer to 2 FFR and 3FFR

The CID mass spectra of the two $C_3H_7O^+$ ions shown in Figures 4.9-4.10 (p88-89) seem similar despite the differences in the relative intensities of the fragment ions. The relative abundances in the CID mass spectra of $C_3H_7O^+$ species are listed in Table 4.7.

The obvious differences between the two spectra are the intensities of ions at m/z 42 and 43.[20] The structures of the secondary fragment ions at m/z 44, 43, 29 are characterized by their corresponding CID mass spectra (Figures 4.17, 4.21 and 4.23, p96, 100 and 102). The ion at m/z 44 may exist either in the form of ionized vinyl alcohol ($CH_2CHOH^{+\cdot}$) or acetaldehyde ($CH_3CHO^{+\cdot}$). The CID mass spectra of these species are shown in Figure 4.19 (p98).[21] The ion is clearly vinyl alcohol. Cyclobutanol[16] is an excellent source to produce the vinyl alcohol ion, whose CID mass spectrum of the source-generated ion at m/z 44 is shown in Figure 4.18 (p97).

Most of the fragment ions produced by the $C_3H_7O^+$ isomers are comparable to the nitrogen-containing analogues. For example, vinylalcohol (m/z 44), CH_2=$CHOH^{+\cdot}$, relates to the vinylamine (m/z 43), CH_2=$CHNH_2^{+\cdot}$; the ion of CH_3C^+=O (m/z 43) corresponds to CH_3C^+=NH (m/z 42). However, unlike the pair of $C_3H_8N^+$ ions, the $C_3H_7O^+$ species give an inverse order of abundance of CH_3C^+=O from the dissociating $(CH_3)_2C^+OH$ and $CH_3CH_2CH^+OH$ ions. The fragment ions at m/z 29

formed in the CID process are the $C_2H_5^+$ species. The key distinction between the two CID mass spectra is the ion of m/z 42 with the structure of ketene $CH_2{=}CO^{+\cdot}$, which is unique for the oxygen-containing species. The mechanism regarding the formation of this ion remains unclear.

In general, through the mass spectrometric study of two pairs of isoelectronic ions, it is found that many similar dissociation properties are possessed by the two species. The oxygen atom plays almost the same role as nitrogen in stabilization of the ion as well as the ability to orient the dissociation chemistry.

Table 4.7 Relative abundance[a], as % of base peak, in the CID mass spectra of $(CH_3)_2C^+OH$ and $CH_3CH_2CH^+OH$

ions	CID, He(O_2)[b]												
(m/z 59)	m/z 14	15	26	27	28	29	30	31	39	41	42	43	44
$(CH_3)_2C^+OH$	1.6	3.8	12	27.9	10.5	37.2	8.4	100	19.2	42.9	6.9	12.6	3.6
	2.4	*4.1*	*17.6*	*34*	*30.6*	*54.7*	*21.2*	*100*	*23.5*	*51.8*	*12.9*	*18.8*	*5.9*
$CH_3CH_2CH^+OH$	6.1	15.1	12.7	26.8	7.0	31.2	3.8	100	48.4	60.5	35.7	83.4	7.0
	5.3	*9.3*	*8.8*	*17.6*	*7.7*	*26.4*	*4.4*	*61.5*	*33*	*41.8*	*39.6*	*100*	*10*

a) using peak height as criteria of peak abundance

b) using He and O_2 (italics) as collision gas

4.4 References

(1) Parker, J. E.; Johnson, C. A. F.; Smith, M. *Proceedings of 22nd British Mass Spectrometry Society Conference, Swansea* **1996**, 57.

(2) Parker, J. E.; Beveridge, W.; Johnson, C. A. F. *Eur. Mass Spectrom.* **1995**, *1*, 229.

(3) Beveridge, W.; Hunter, J. A.; Johnson, C. A. F.; Parker, J. E. *Org. Mass Spectrom.* **1992**, *27*, 543.

(4) Beveridge, W.; Garioch, I. W.; Hunter, J. A.; Johnson, C. A. F.; Parker, J. E. *Org. Mass Spectrom.* **1991**, *26*, 416.

(5) Hammerum, S.; Derrick, P. J. *J. Chem. Soc., Chem. Commun.* **1985**, 996.

(6) Hunter, E. P. L.; Lias, S. G. *J. Phys. Chem. Ref. Data* **1998**, *27*, 413.

(7) Lossing, F. P.; Lam, Y. T.; Maccoll, A. *Can. J. Chem.* **1981**, *59*, 2228.

(8) Benson, S. W. . In *Thermochemical Kinetics (2nd edition)*; John Wiley & Sons: New York, 1976.

(9) Audier, H. E.; Millet, A.; Sozzi, G. *Org. Mass Spectrom.* **1984**, *19*, 79.

(10) Bowen, R. D.; Williams, D. H.; G.Hvistendahl; Kalman, J. R. *Org. Mass Spectrom.* **1978**, *13*, 721.

(11) Bowen, R. D.; Williams, D. H. *J. Chem. Soc. Perkin II* **1978**, 1064.

(12) Levsen, K.; McLafferty, F. W. *J. Am. Chem. Soc.* **1974**, *96*, 139.

(13) Uccella, N. A.; Howe, I.; Williams, D. H. *J. Chem. Soc. (B)* **1971**, 1933.

(14) Burgers, P. C.; Holmes, J. L.; Mommers, A. A.; Szulejko, J. E. *Org. Mass Spectrom.* **1983**, *18*, 596.

(15) Holmes, J. L.; Terlouw, J. K. *Can. J. Chem.* **1976**, *54*, 1007.

(16) Bouchoux, G.; Alcaraz, C.; Dutuit, O.; Nguyen, M. T. *Int. J. Mass Spectrom. Ion Proc.* **1994**, *137*, 93.

(17) Bowen, R. D.; Kalman, J. R.; Williams, D. H. *J. Am. Chem. Soc.* **1977**, *99*, 5481.

(18) Holmes, J. L.; Rye, R. T. B.; Terlouw, J. K. *Org. Mass Spectrom.* **1979**, *14*, 606.

(19) Hvistendahl, G.; Bowen, R. D.; Williams, D. H. *J. Chem. Soc. Chem. Comm.* **1976**, 294.

(20) McLafferty, F. W.; Sakai, I. *Org. Mass Spectrom.* **1973**, *7*, 971.

(21) Terlouw, J. K.; Wezenberg, J.; Burgers, P. C.; Holmes, J. L. *J. Chem. Soc., Chem. Commun.* **1983**, 1121.

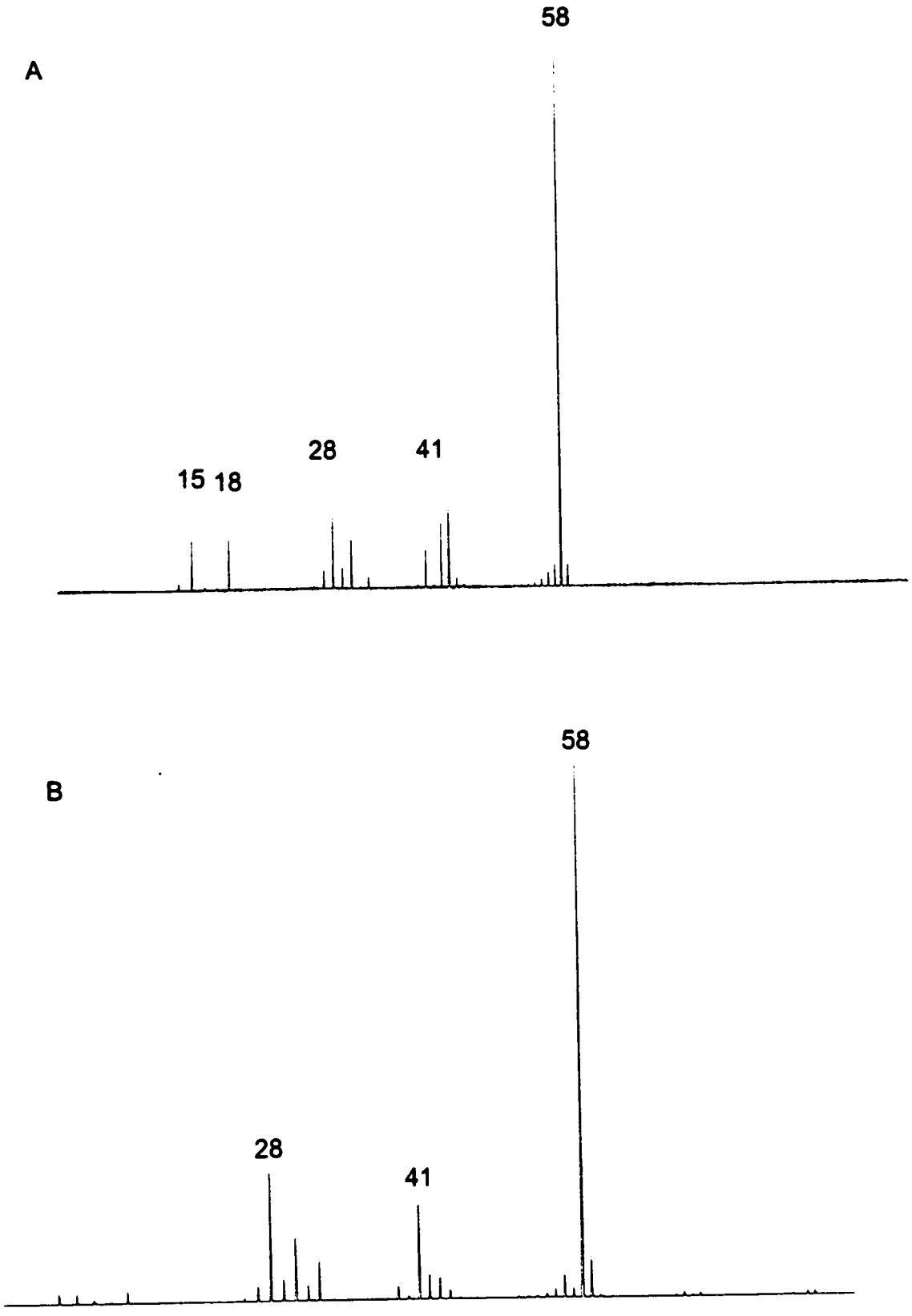

Figure 4.3 EI mass spectra of (A) t-butylamine; (B) 3-pentanamine

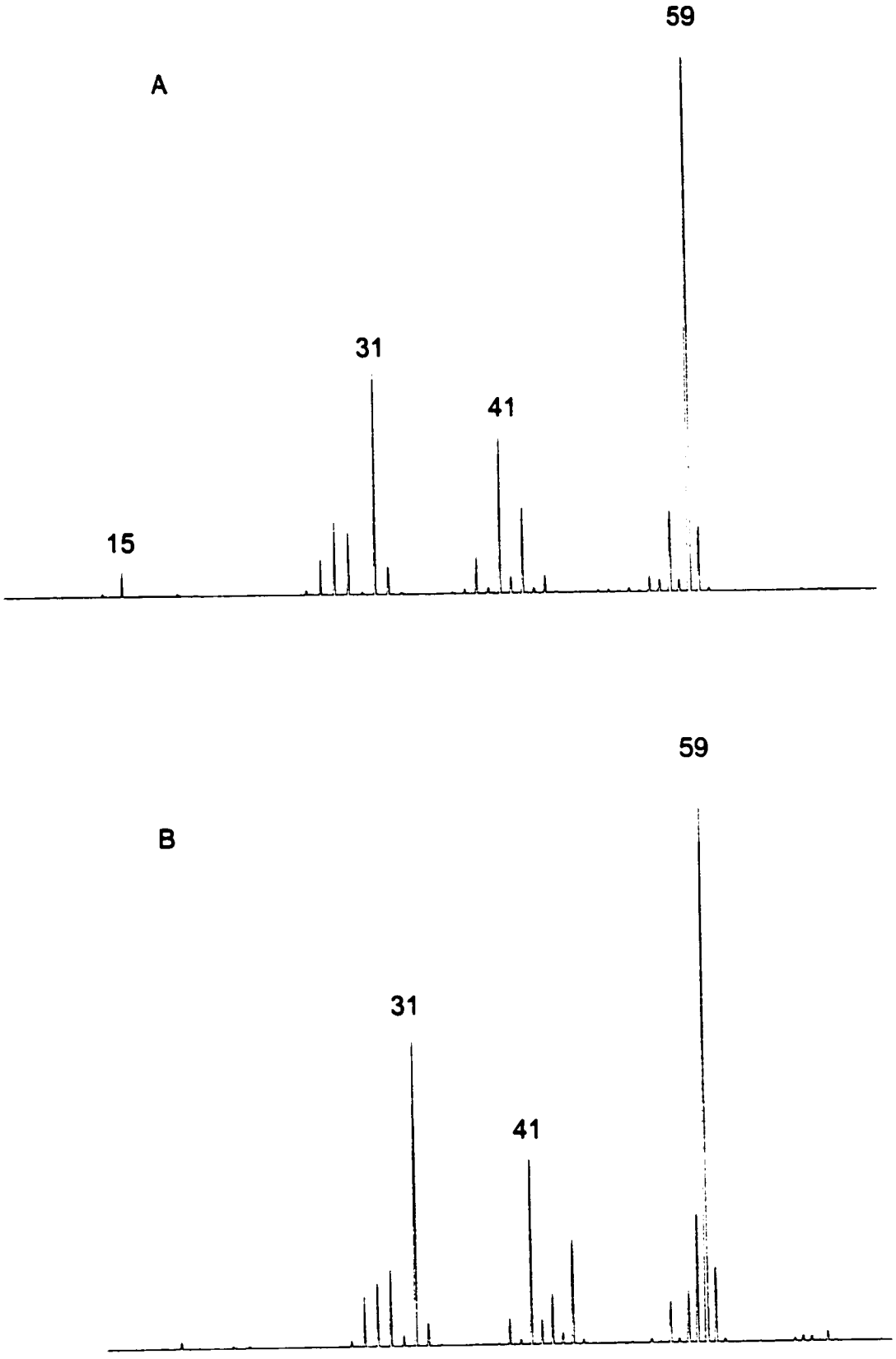

Figure 4.4 EI mass spectra of (A) 2-methyl-2-propanol; (B) 3-pentanol

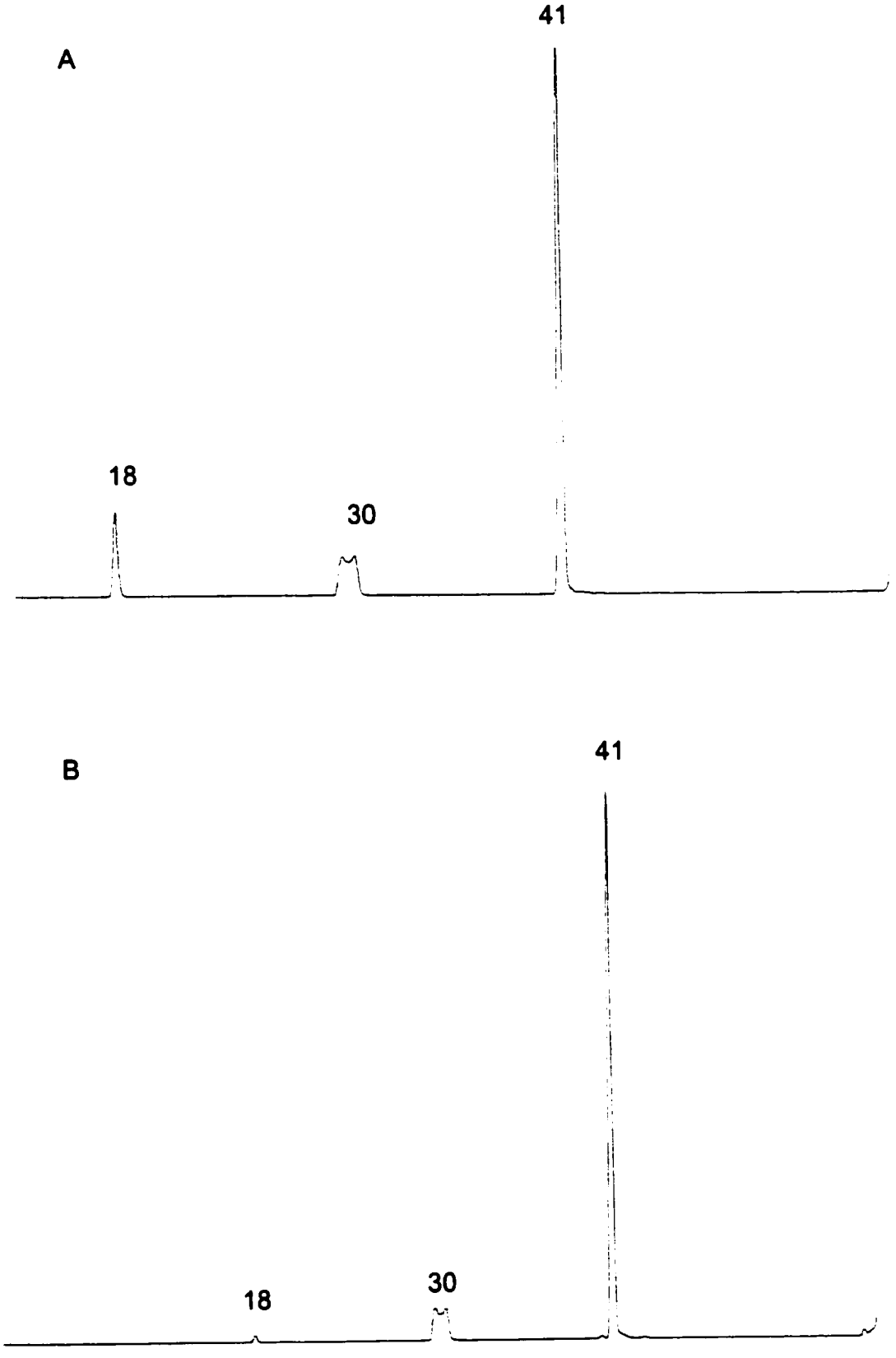

Figure 4.5 MI mass spectra of (A) $(CH_3)_2C^{\bullet}NH_2$; (B) $CH_3CH_2CH^{\bullet}NH_2$

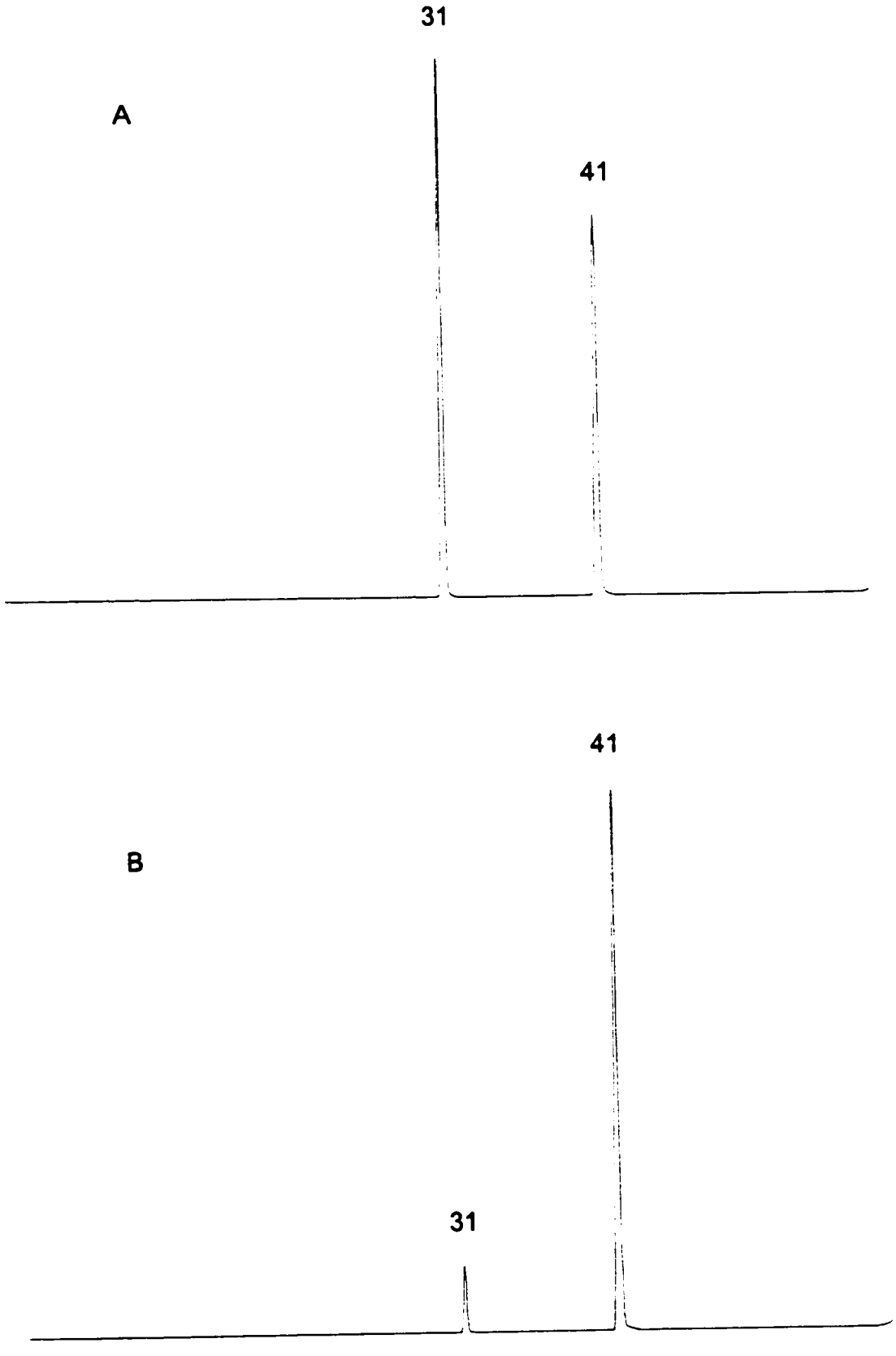

Figure 4.6 MI mass spectra of A) $(CH_3)_2C^+OH$; (B) $CH_3CH_2CH^+OH$

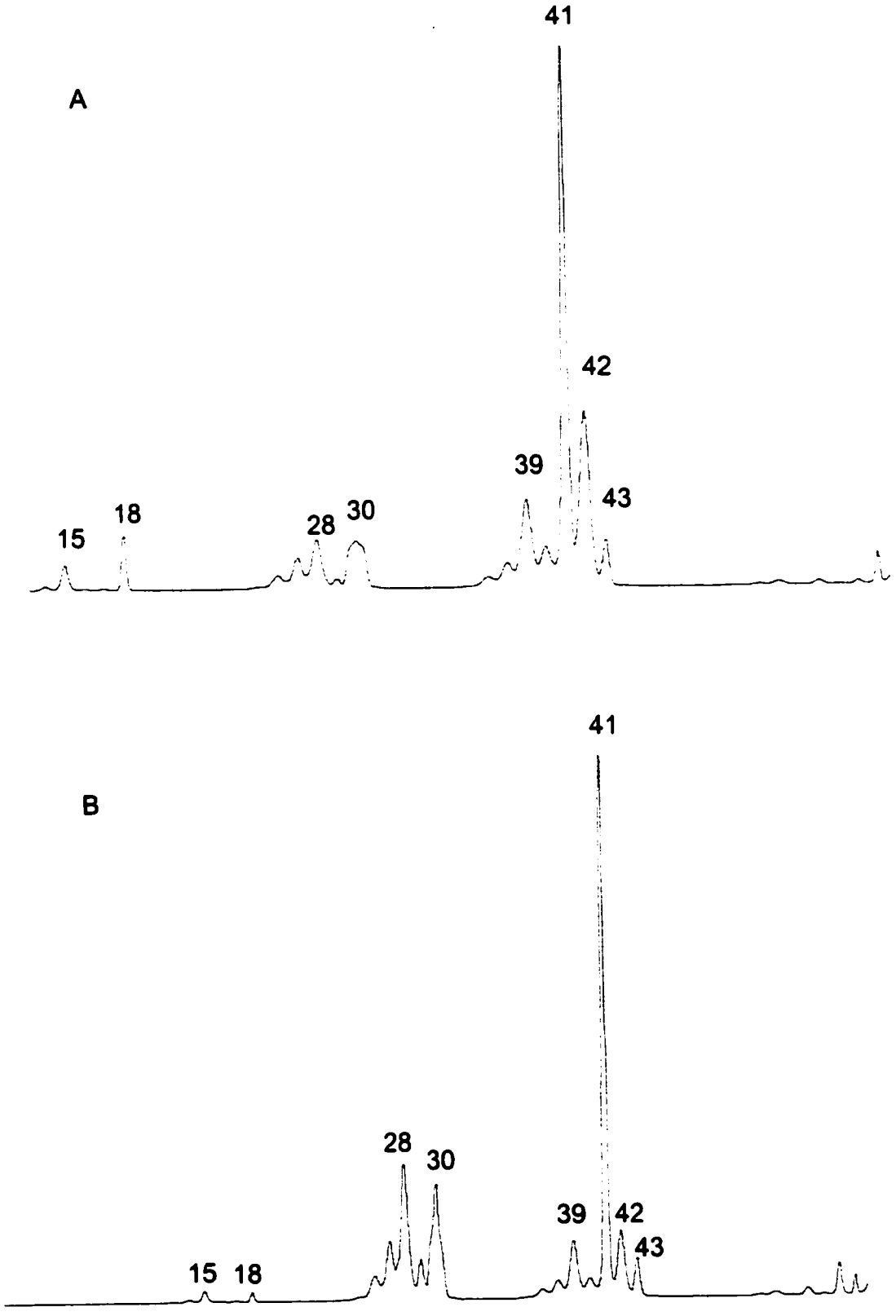

Figure 4.7 CID (He) mass spectra of A) $(CH_3)_2C^{\bullet}NH_2$; (B) $CH_3CH_2CH^{\bullet}NH_2$

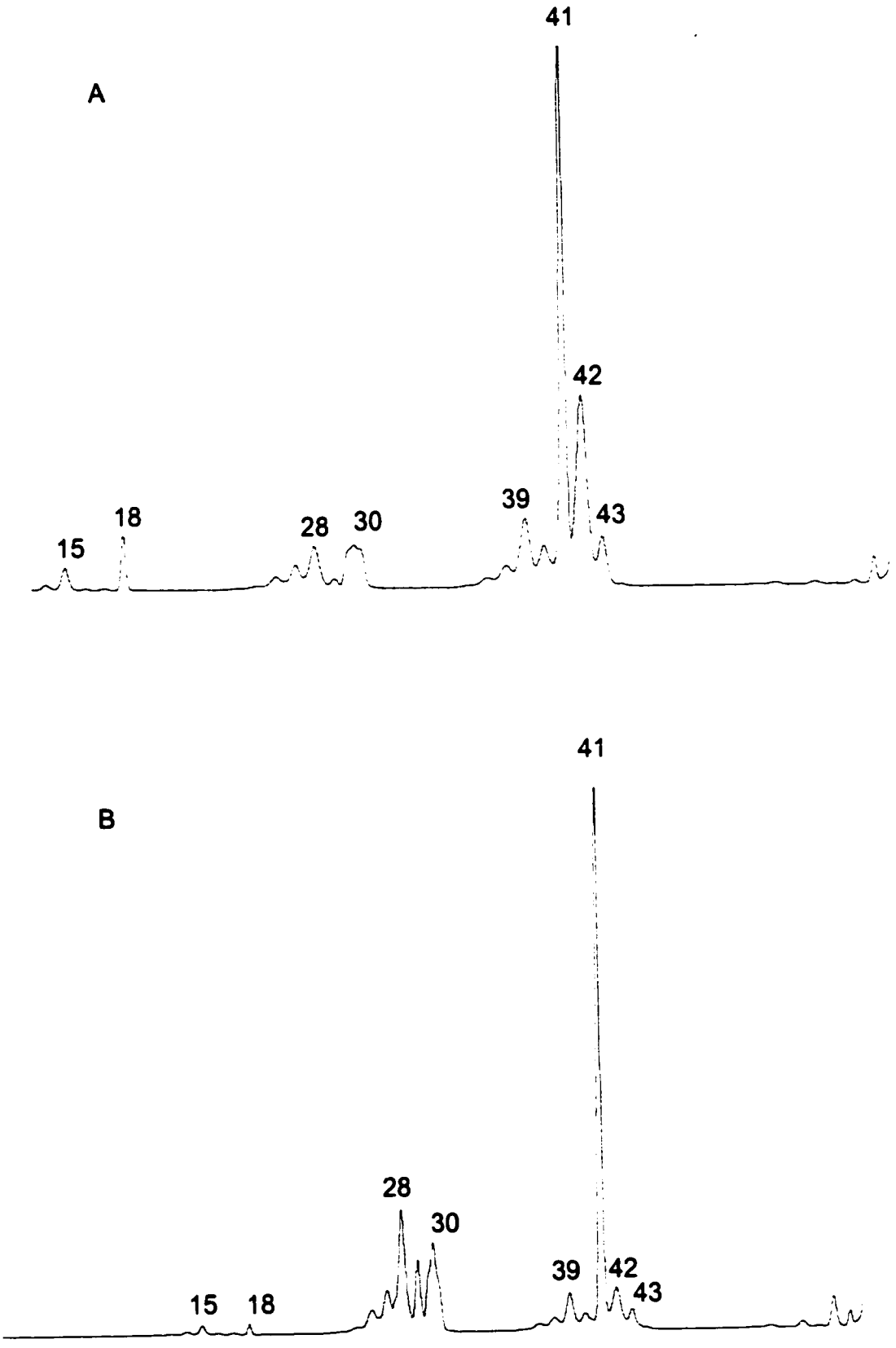

Figure 4.8 CID (O_2) mass spectra of A) $(CH_3)_2C^{\bullet}NH_2$; (B) $CH_3CH_2CH^{\bullet}NH_2$

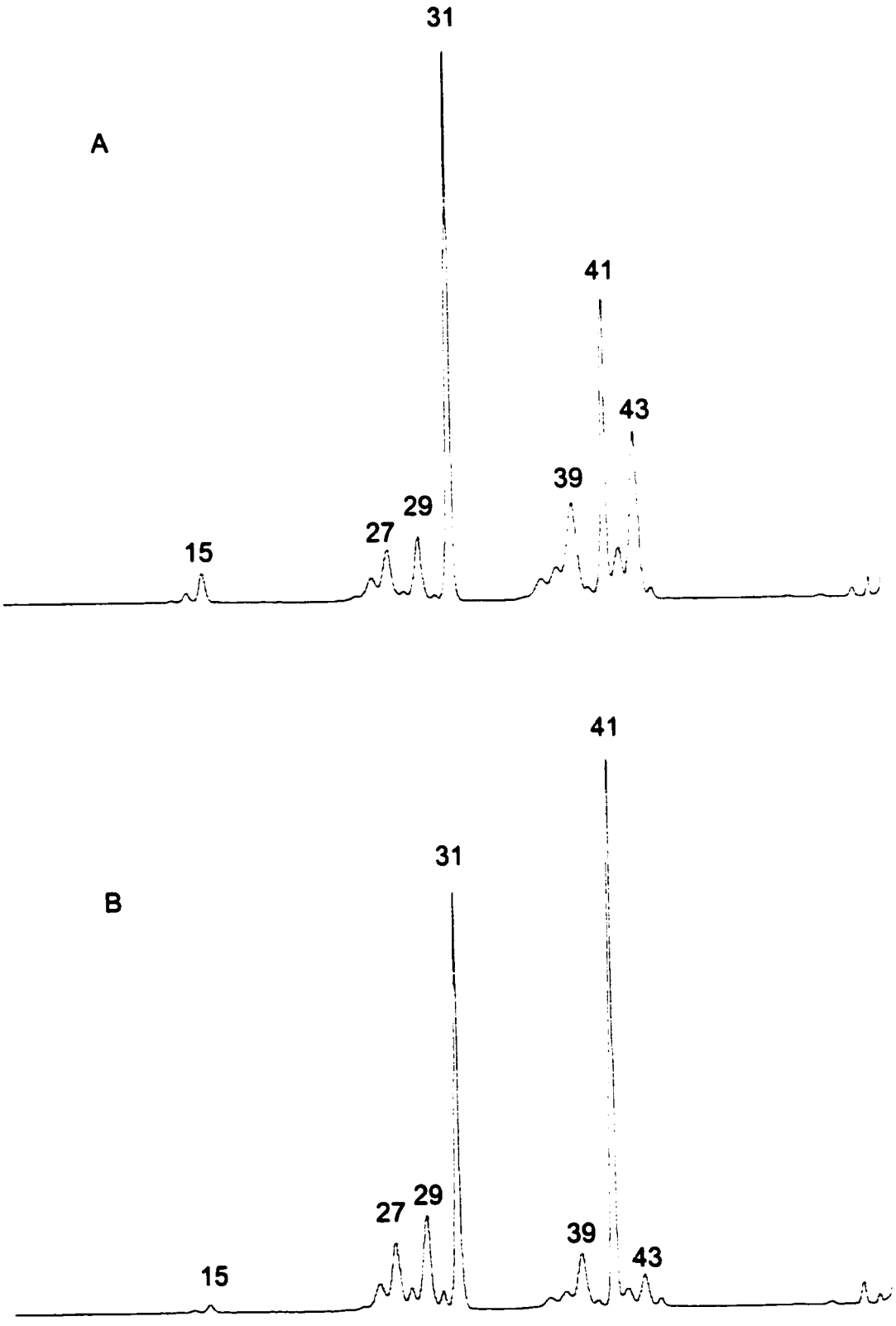

Figure 4.9 CID (He) mass spectra of A) $(CH_3)_2C^{\bullet}OH$; (B) $CH_3CH_2CH^{\bullet}OH$

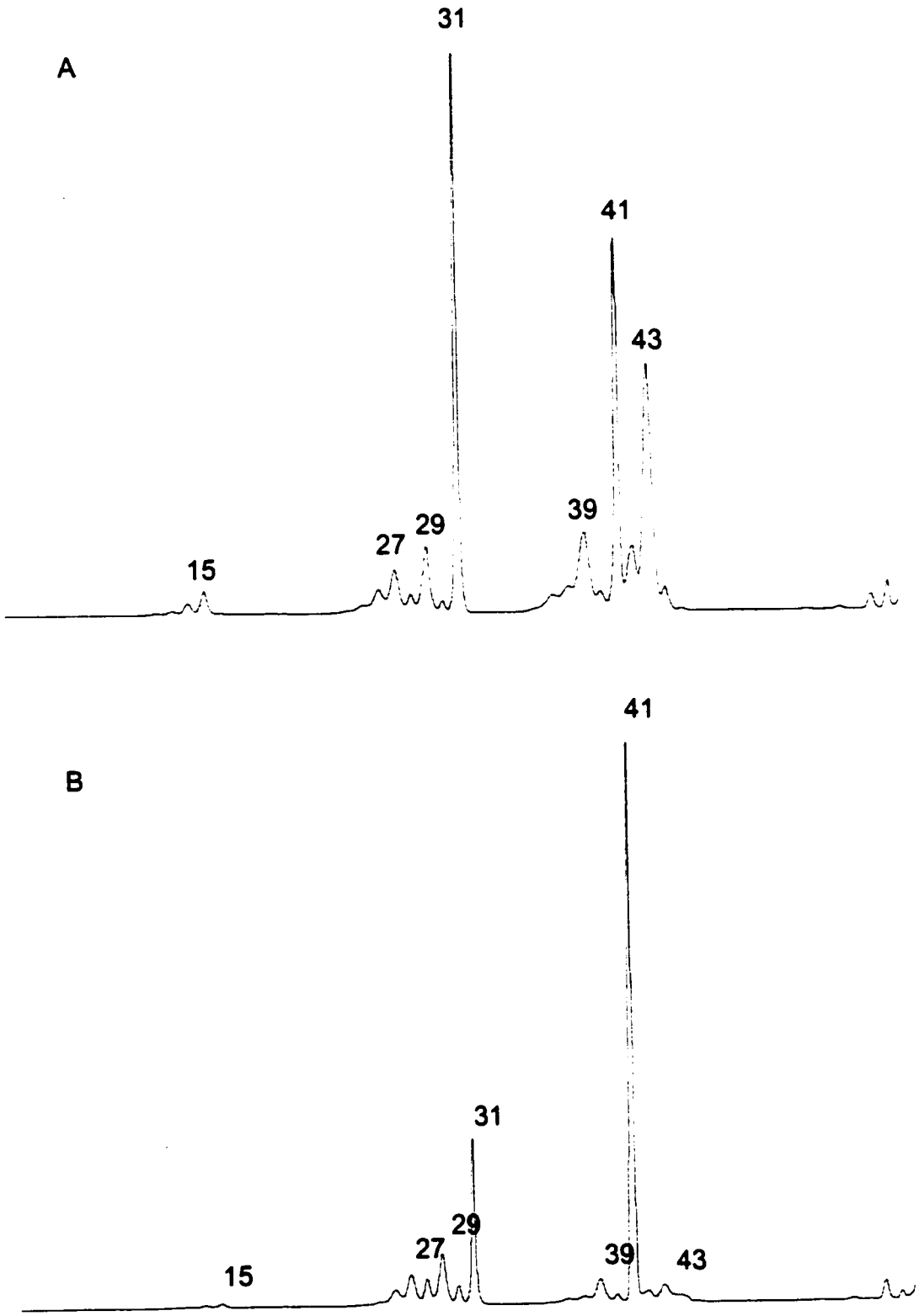

Figure 4.10 CID (O_2) mass spectra of A) $(CH_3)_2C^{\bullet}OH$; (B) $CH_3CH_2CH^{\bullet}OH$

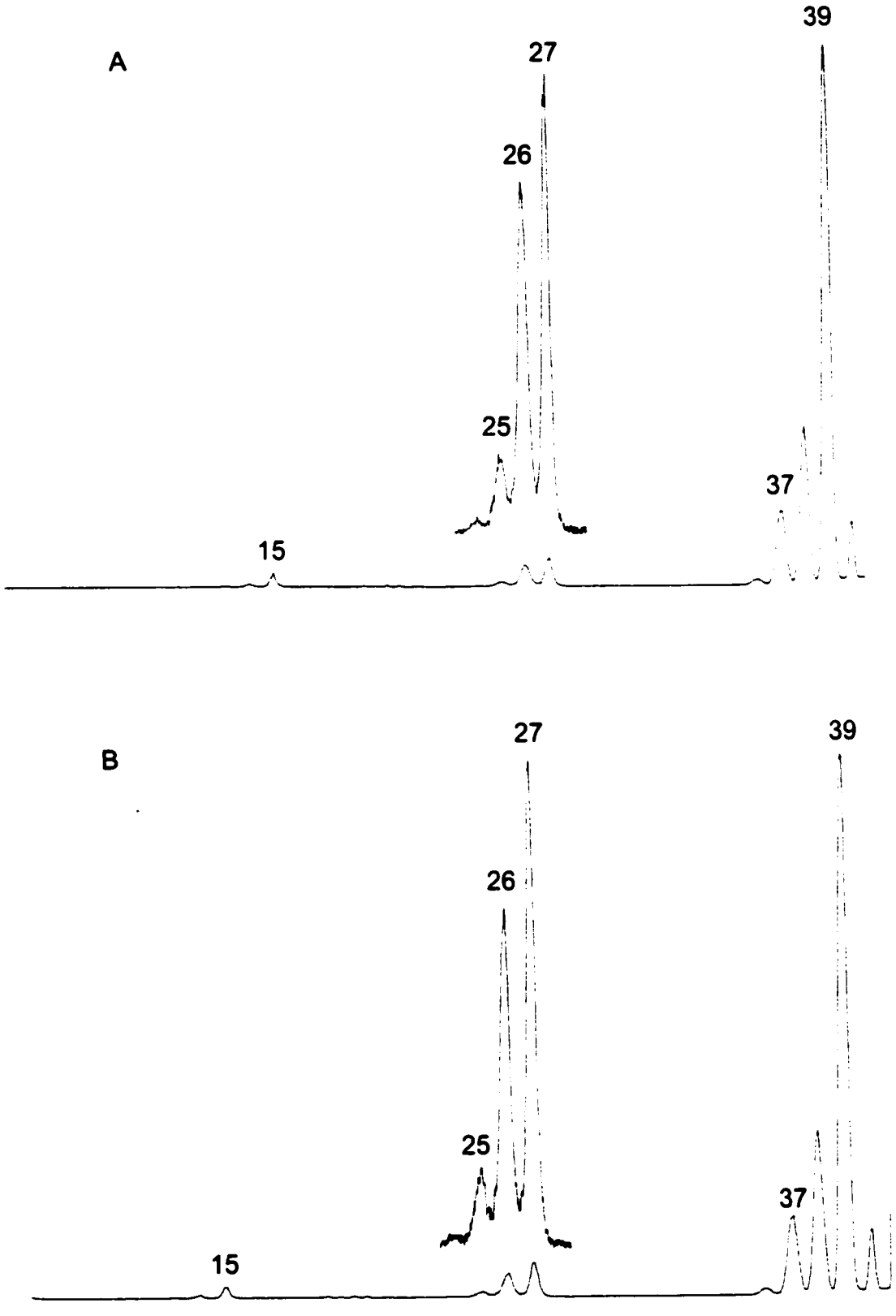

Figure 4.11 CID (He) mass spectra of m/z 41 from A) $(CH_3)_2C^{\bullet}NH_2$; (B) $CH_3CH_2CH^{\bullet}NH_2$

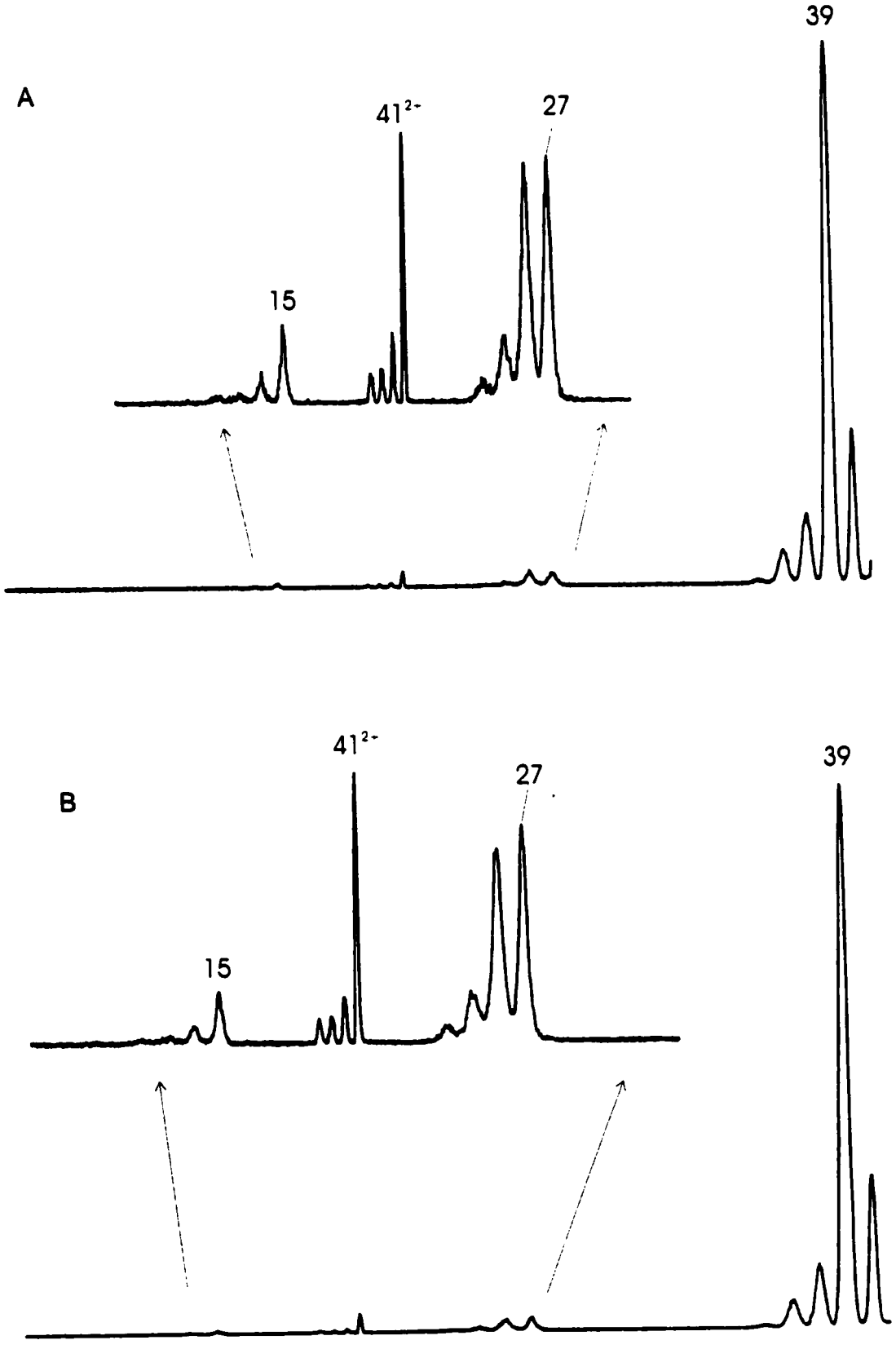

Figure 4.12 CID (O_2) mass spectra of m/z 41 from A) $(CH_3)_2C^{\bullet}NH_2$; (B) $CH_3CH_2CH^{\bullet}NH_2$

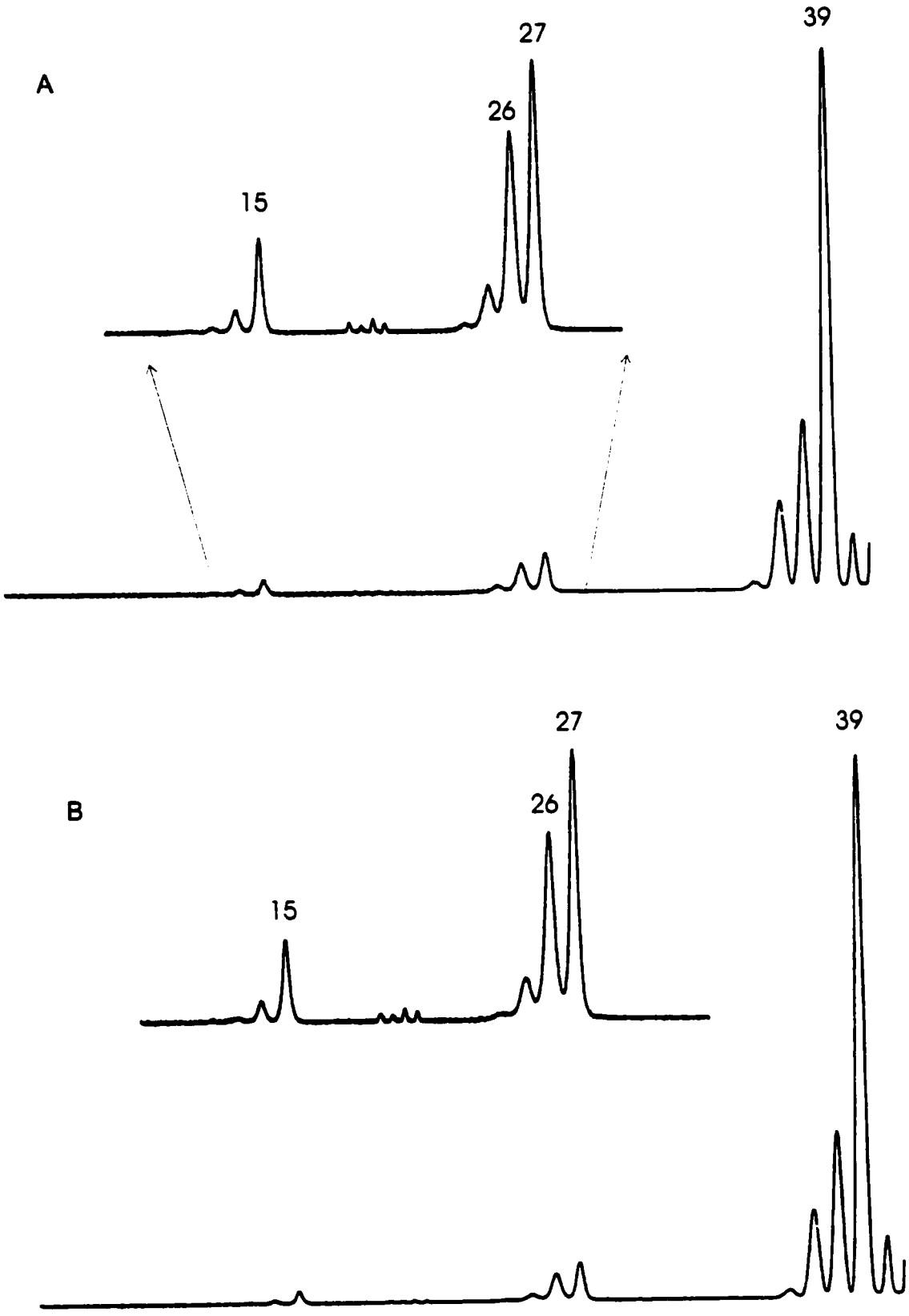

Figure 4.13 CID (He) mass spectra of m/z 41 from A) $(CH_3)_2C^{\bullet}OH$; (B) $CH_3CH_2CH^{\bullet}OH$

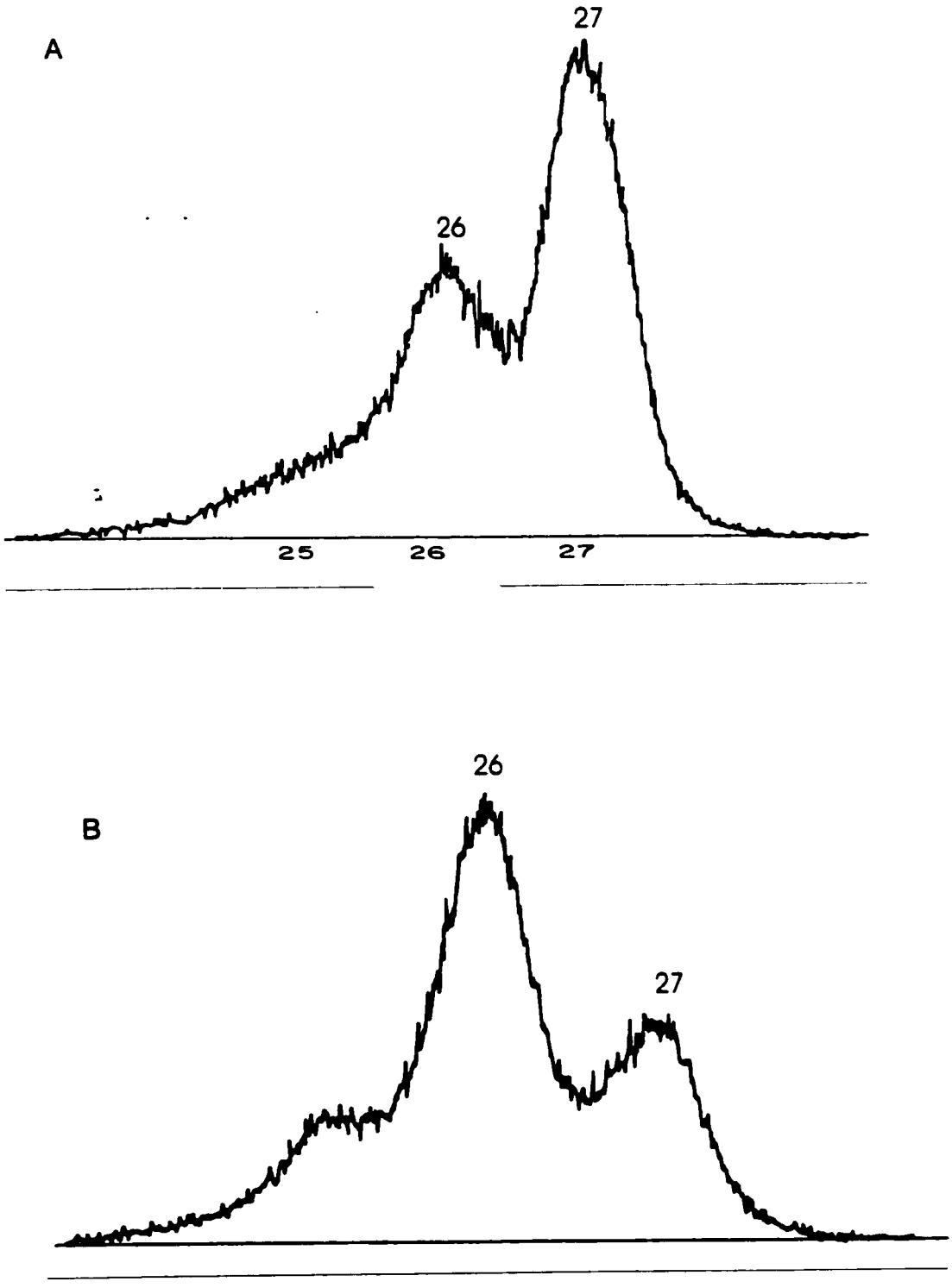

Figure 4.14 Partial CID (He) mass spectra of m/z 41 (A) $CH_2CHCH_2^{\bullet}$; (B) $CH_3C^{\bullet}CH_2$

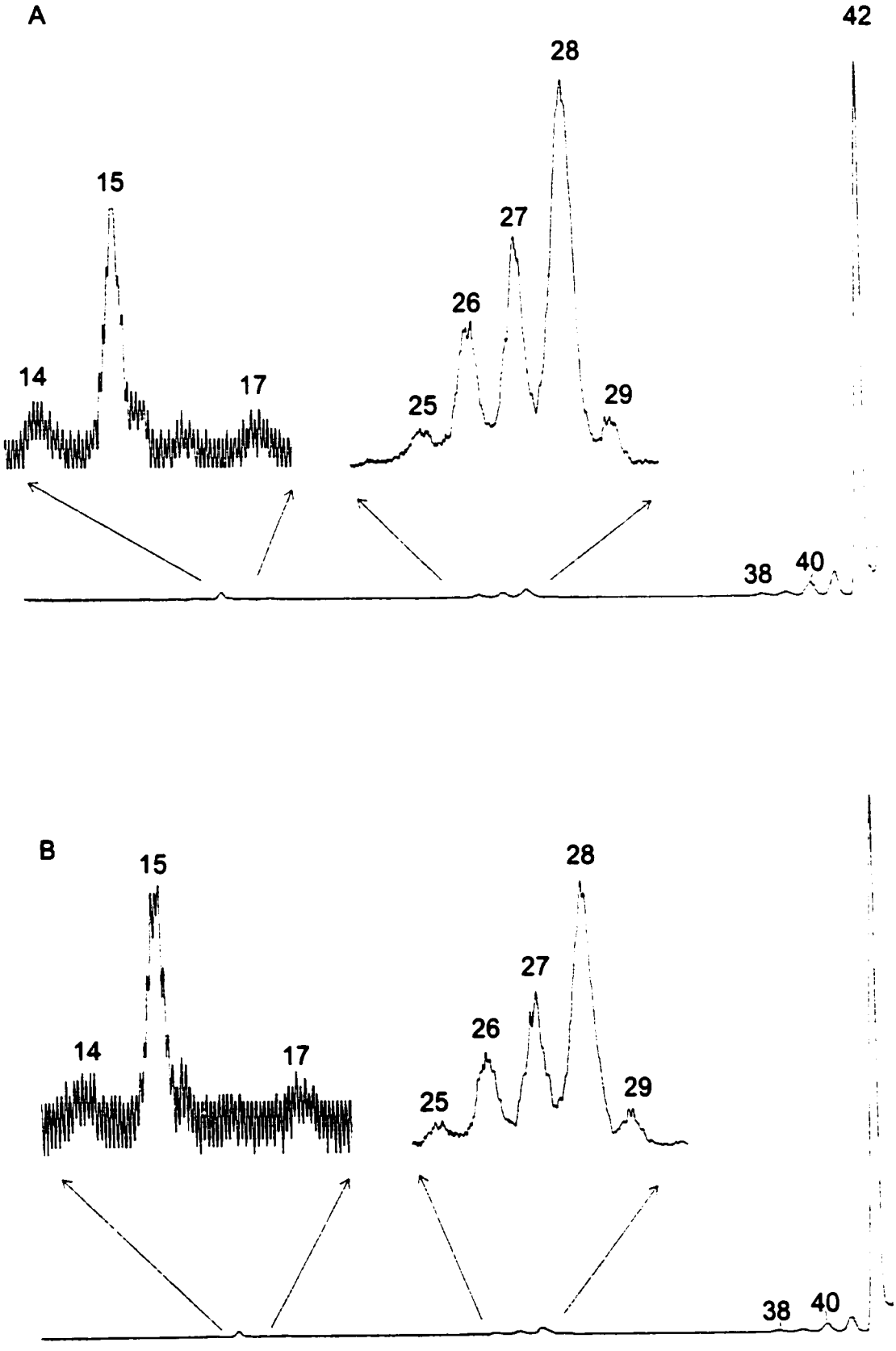

Figure 4.15 CID (He) mass spectra of m/z 43 from A) $(CH_3)_2C^{\bullet}NH_2$; (B) $CH_3CH_2CH^{\bullet}NH_2$

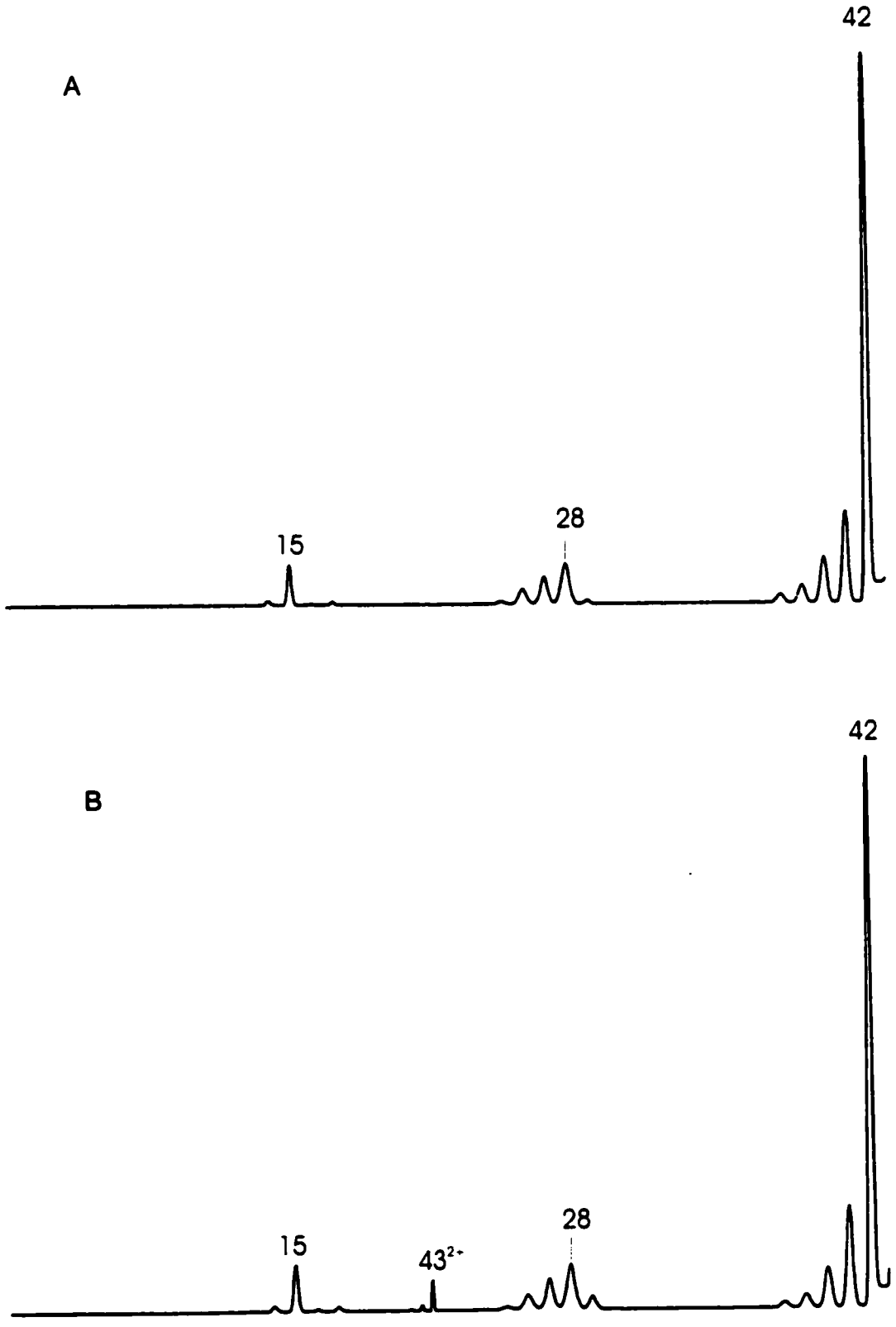

Figure 4.16 CID mass spectra of m/z 43 from cyclobutylamine (A) He; (B) O_2

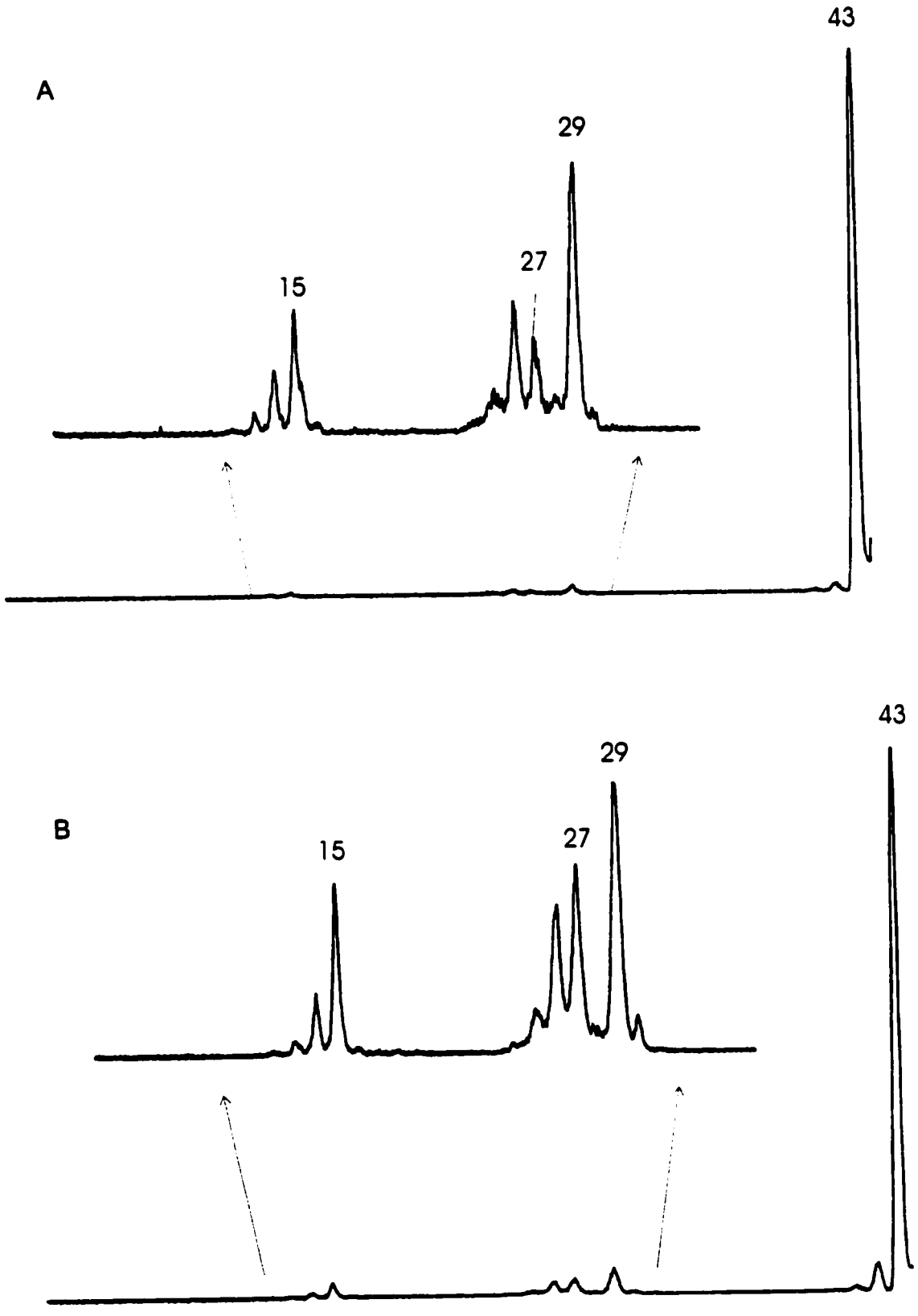

Figure 4.17 CID (He) mass spectra of m/z 44 from A) $(CH_3)_2C^{\cdot}OH$; (B) $CH_3CH_2CH^{\cdot}OH$

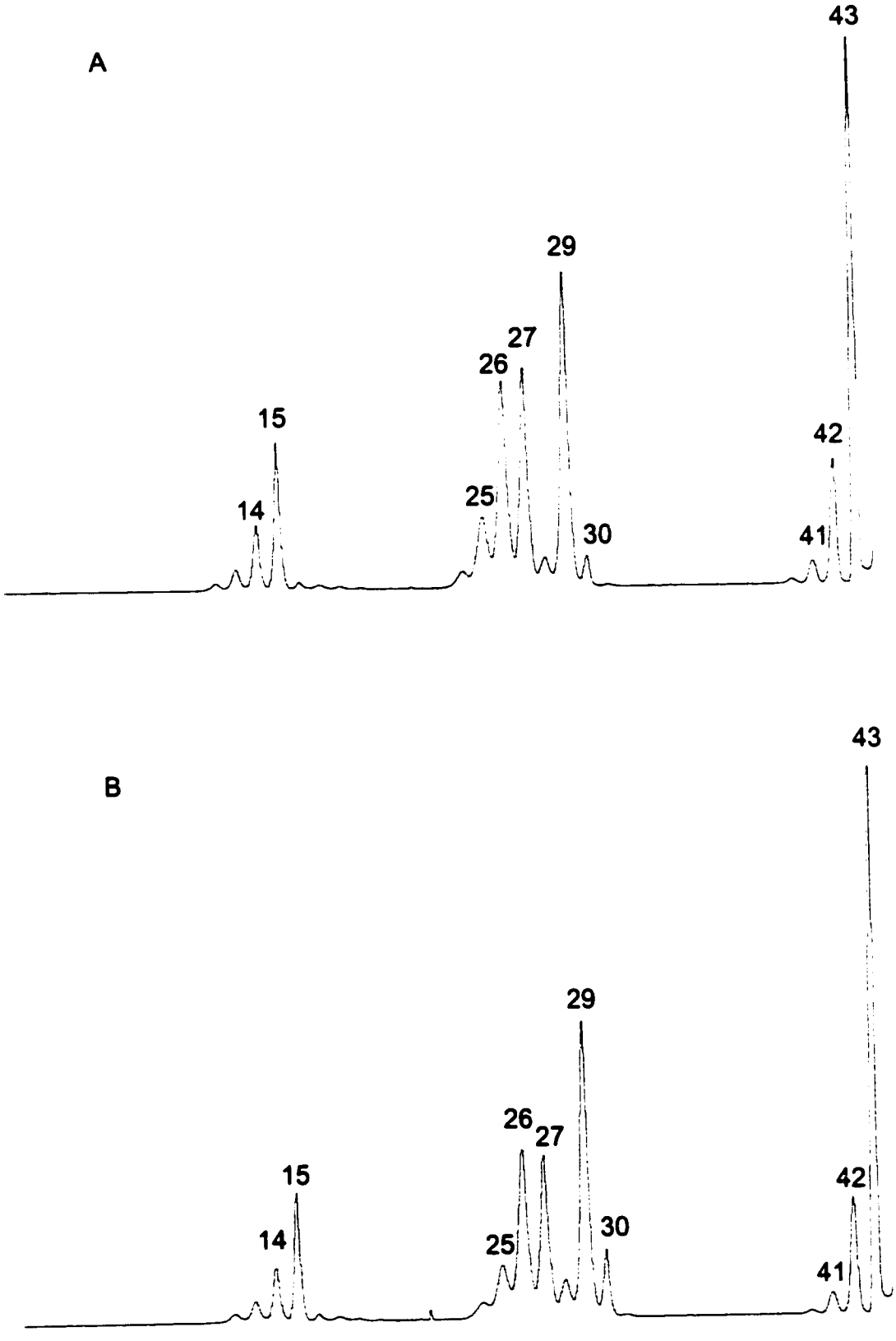

Figure 4.18 CID mass spectra of m/z 44 from cyclobutanol (A) He; (B) O_2

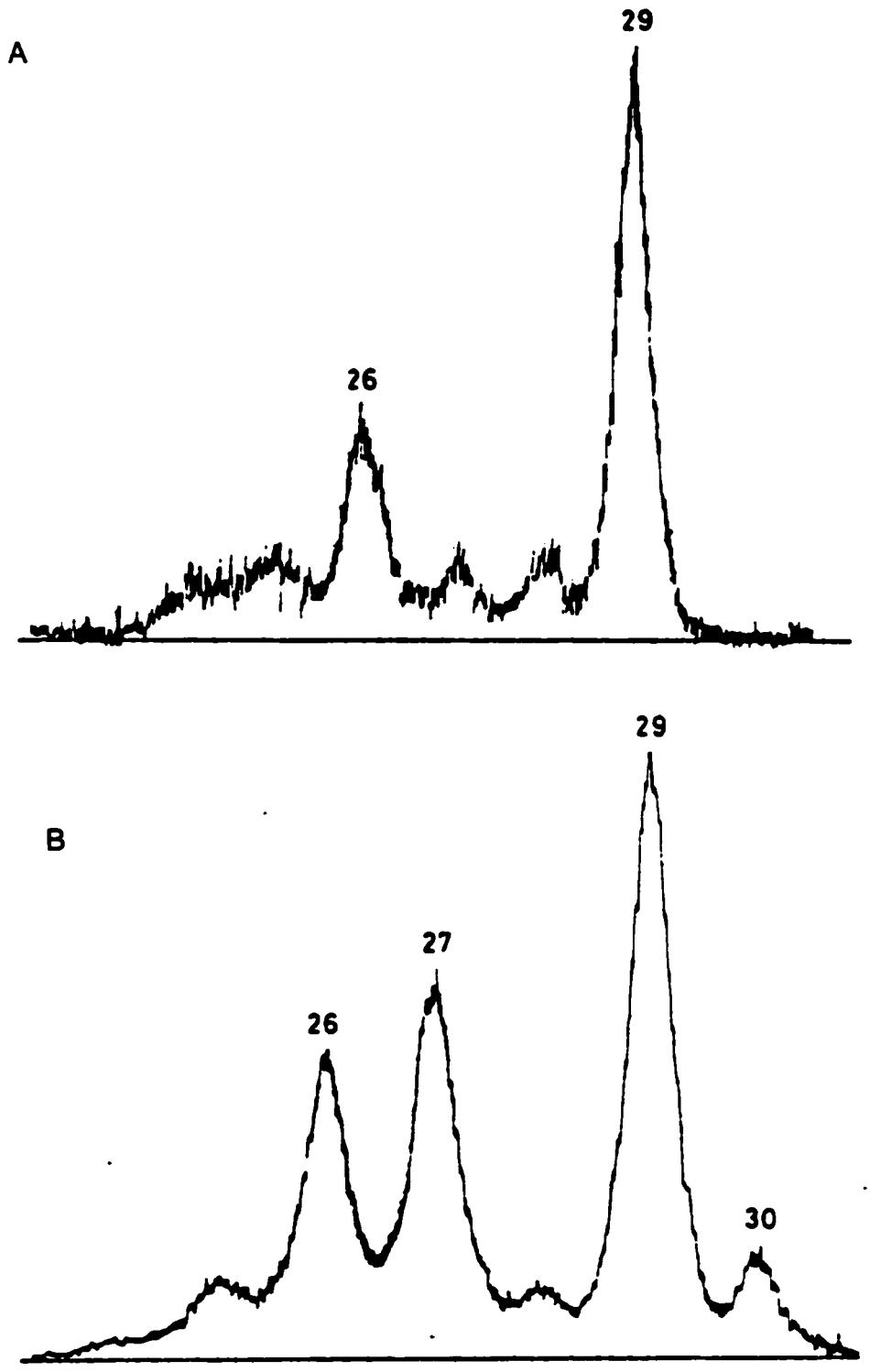

Figure 4.19 Partial CID (He) mass spectra of (A) $CH_3OH^{+\cdot}$; (B) $CH_2CHOH^{+\cdot}$

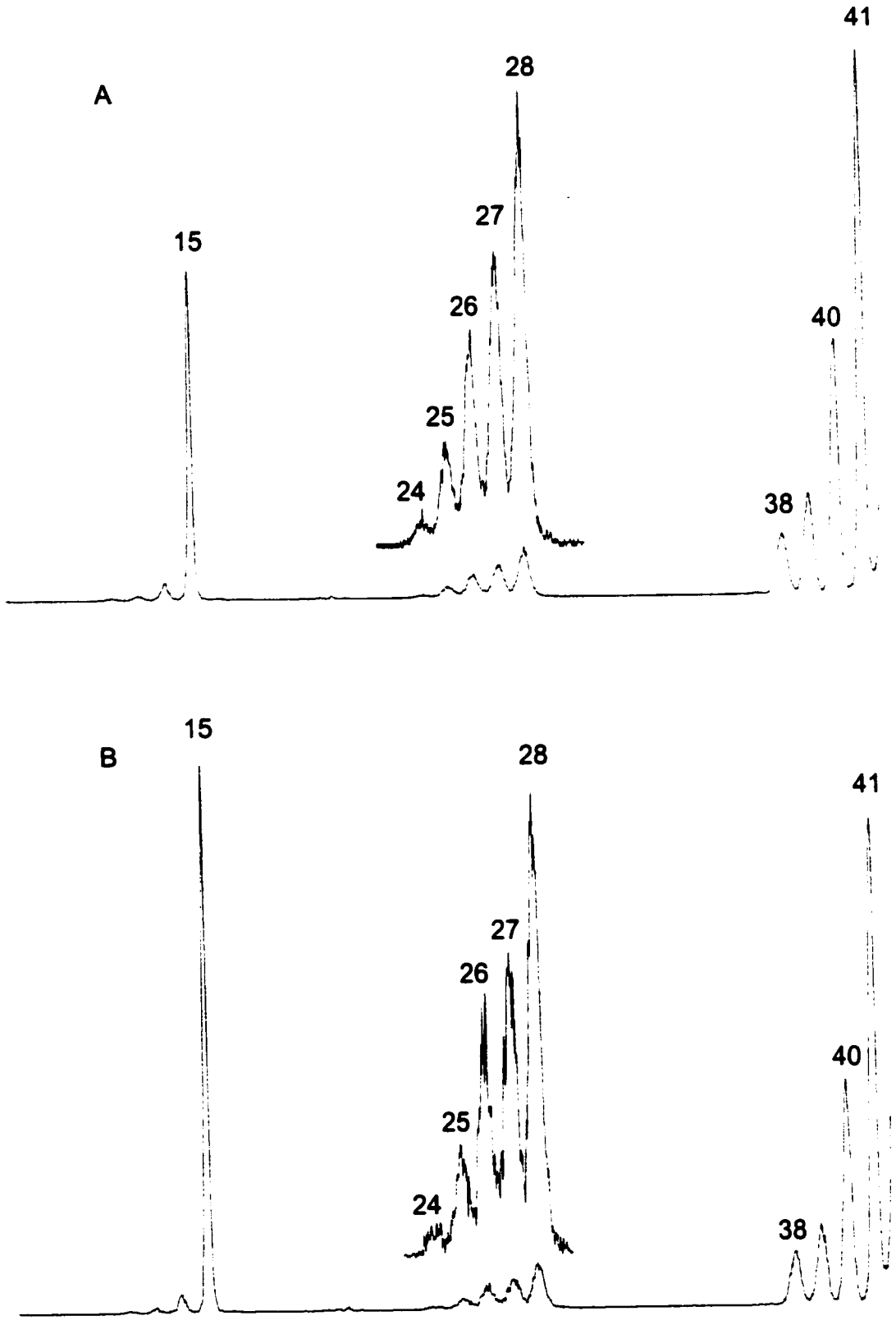

Figure 4.20 CID (He) mass spectra of m/z 42 from A) $(CH_3)_2C^{\bullet}NH_2$; (B) $CH_3CH_2CH^{\bullet}NH_2$

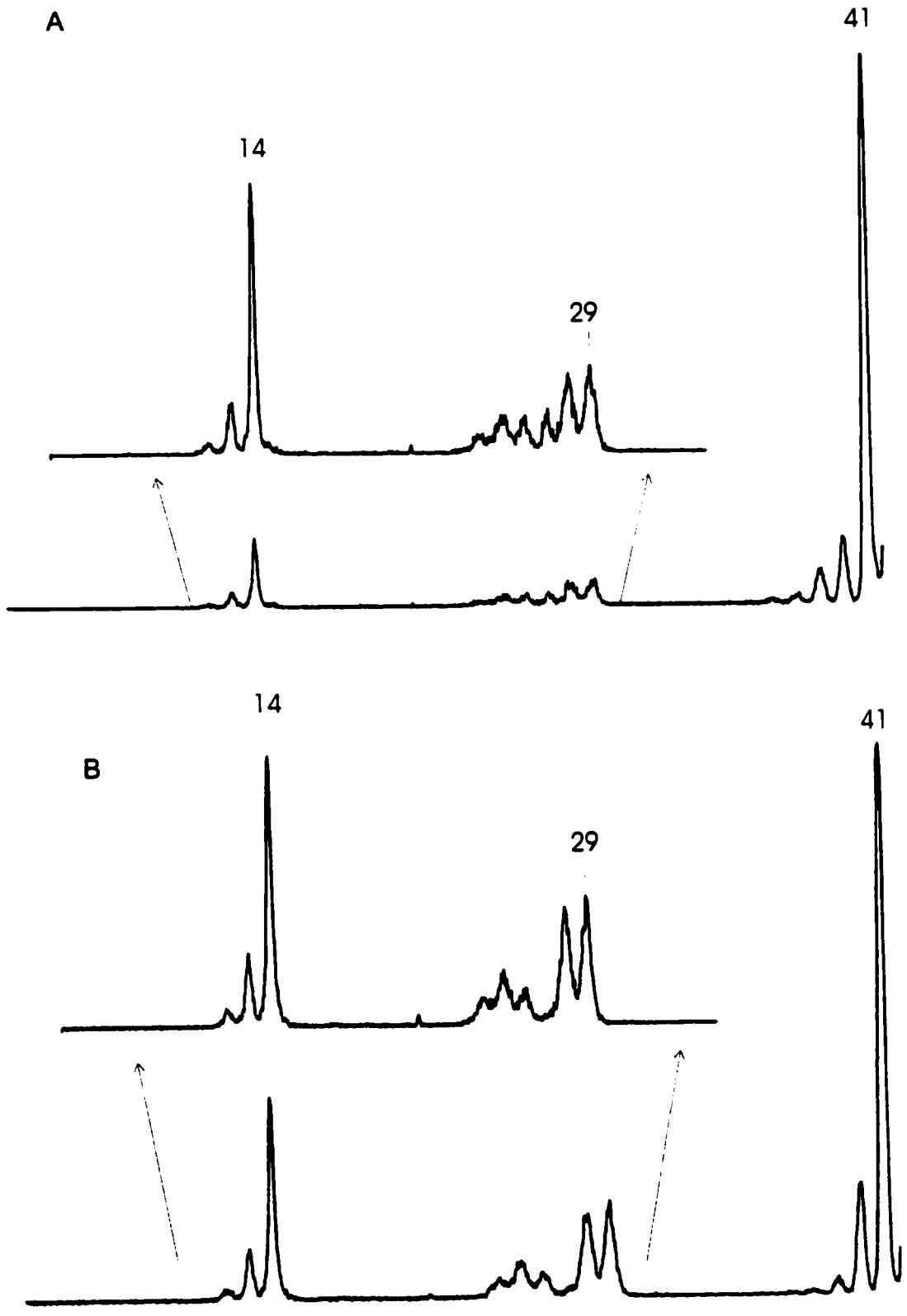

Figure 4.21 CID (He) mass spectra of m/z 43 from A) $(CH_3)_2C^{+}OH$; (B) $CH_3CH_2CH^{+}OH$

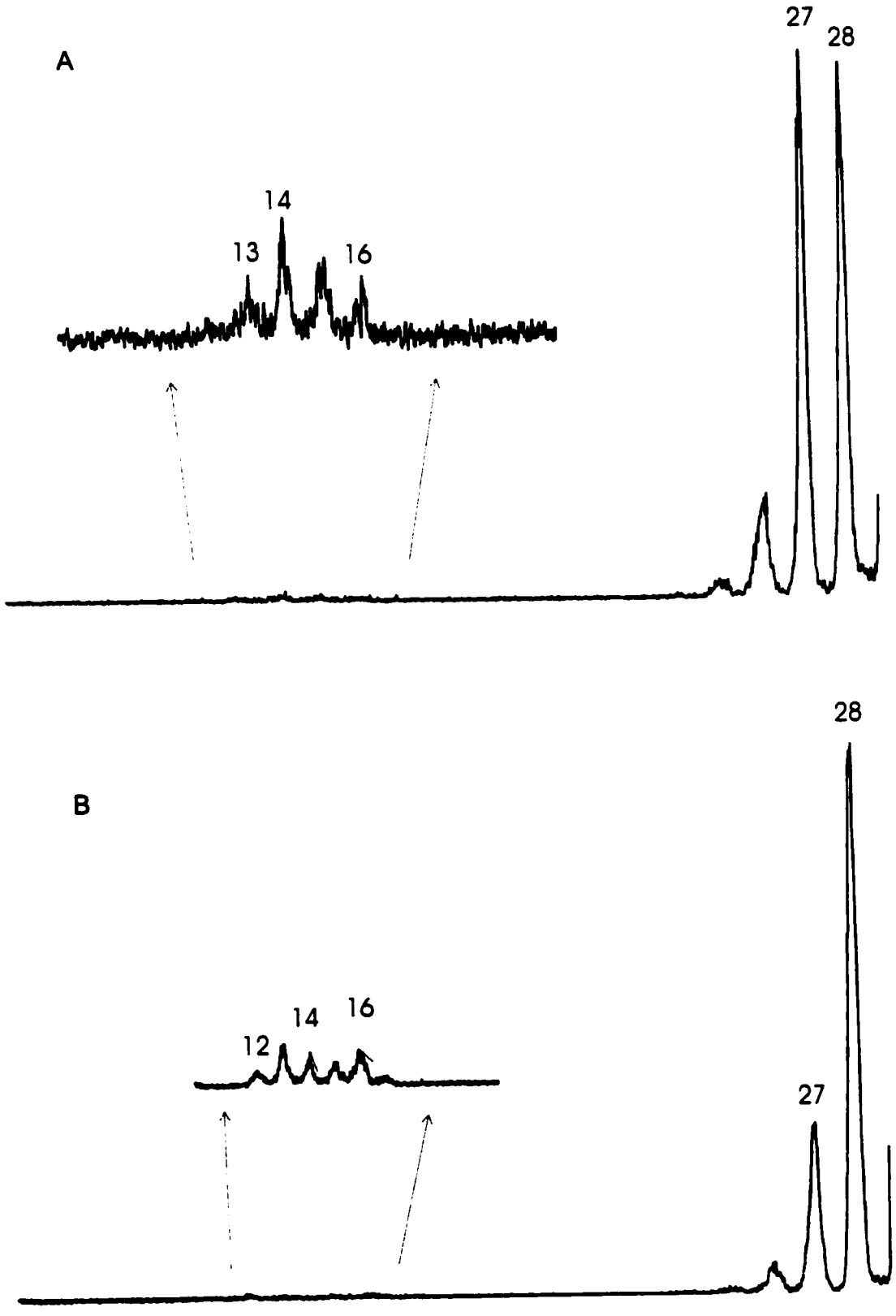

Figure 4.22 CID (He) mass spectra of m/z 29 from A) $(CH_3)_2C^+NH_2$; (B) $CH_3CH_2CH^+NH_2$

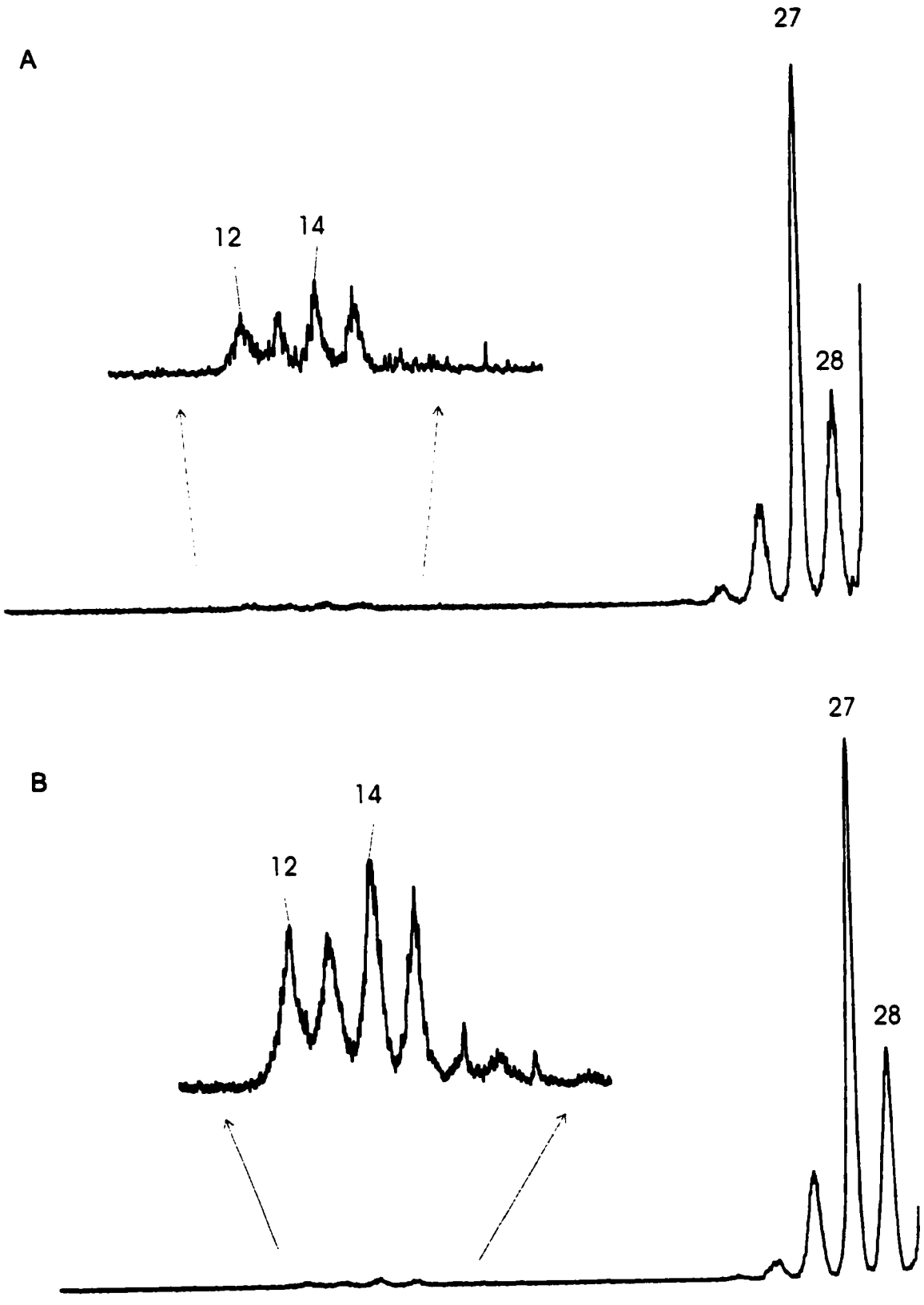

Figure 4.23 CID (He) mass spectra of m/z 29 from A) $(CH_3)_2C^{\bullet}OH$; (B) $CH_3CH_2CH^{\bullet}OH$

Chapter 5 Thermochemical determinations by the kinetic method

5.1 Introduction

Thermochemical properties have the same importance in gas-phase ion chemistry and mass spectrometry as they do in other branches of chemistry. The methods available for determining these quantities have been classified by R.R. Squires[1] as shown in Table 5.1.

Table 5.1 Methods for obtaining thermochemical data

Calorimetry	
Spectroscopy	
Theoretical calculations	
Equilibrium methods	Equilibrium constant (K) Forward and reverse rates (k_f, k_{-f})
Thermokinetic methods	Kinetic Method Bracketing Threshold analysis

Absolute methods are less applicable than the relative methods, so most data are obtained by relative experimental methods.[2-6] Among these are the important thermokinetic methods – methods in which reaction rates provide the thermochemical information. The thermokinetic methods comprise the kinetic method, the subject of this chapter, threshold measurements and the bracketing

method. Hunter and Lias[7] have used the term 'thermokinetic' in a more restricted sense to refer to a type of ion-molecule reaction bracketing experiment in which the relative efficiencies of a series of reactions are used to obtain thermodynamic data.[8] This term is used in a broader sense in Table 5.1.

This review will describe briefly the equilibrium and reaction bracketing methods and then the kinetic method will be described in detail. This includes the introduction to its theoretical basis and assumptions, a discussion of entropy effects, investigation of the physical significance of the temperature-like term, T_{eff}, and the applications of the kinetic method.

5.2 Gas-Phase Basicity and Proton Affinity

5.2.1 Definitions

Gas-phase basicity (GB) and proton affinity (PA) of molecules provide insights into molecular structure, stability and reactivity. They are defined as the negative of the free energy change ($-\Delta G$) and the enthalpy change ($-\Delta H$), respectively, for the reaction:

$$B(g) + H^+(g) \rightleftharpoons BH^+(g)$$

The two quantities are related through the expression of $\Delta G° = \Delta H° - T\Delta S_{H^+}°$ to give $PA(B) = GB(B) + T\Delta S°$, where $\Delta S° = S°(BH^+) - S°(H^+) - S°(B)$. This quantity arises from the contributions of translational, rotational and vibrational motions.

For systems in which there is no intramolecular hydrogen bonding in BH^+, the major contribution to $\Delta S°$ arises from ΔS_{trans} on protonation. From the Sackur-Tetrode equation,[9] this loss of $\Delta S°_{trans}$ on protonation gives a term $T\Delta S°_{trans}$ = -7.8 kcal mol^{-1} at 298 K. $\Delta S°_{rot}$ is thought to arise from symmetry changes of B and BH^+.

$$\Delta S°_{rot} = R\ln\left(\frac{\sigma_B}{\sigma_{BH^+}}\right) \qquad 5.1$$

where σ_B and σ_{BH+} are the rotational symmetry numbers of B and BH^+. This term usually will be very small for complex molecules but may be significant for simpler species. The $\Delta S°_{vib}$ term usually is negligible because the *vibrational* frequencies of B and BH^+ will not be greatly different and, in addition, vibrational motion makes only a small contribution to the total entropy of most molecules at 298 K.

Most references represent the entropy term for base B as the entropy of protonation ($\Delta S°_{H+}$),[7] which is defined as the entropy change between BH^+ and B. It is found that for simple molecules where there is no intramolecular hydrogen bond in the protonated form, $\Delta S°_{H+}$ are usually negligibly small (a few J mol^{-1} K^{-1}), these small values are only due to the *geometry changes* between the neutral molecules (B) and the protonated molecules (BH^+). However, for molecules with multifunctional groups, which are capable of forming an intramolecular hydrogen bond in the protonated form (BH^+), $\Delta S°_{H+}$ are usually large negative values (< -20 J mol^{-1} K^{-1}) due to *loss of rotational modes* in forming the protonated species. The magnitude of $\Delta S°_{H+}$ depends on the ring strain of the cyclic structure.

5.2.2 *Proton affinity of organic molecules*

Proton affinity seems to inversely relate to the electronegativity (EN) of the atoms in the functional groups. For example, the EN order (Pauling's scale[10]) for O, N, S is that O (3.4) > N (3.0) > S (2.6). The PA for molecules having the functional groups –OH, $-NH_2$ and –SH are generally in order of $-NH_2$ > -SH > -OH (CN ≈ SH).

5.2.2.1 Thermochemical aspects of proton affinities

Proton affinity varies with ion size in a similar manner to ionization energy (IE),[11] increasing along a homologous series and reaching an asymptote for the largest members; plots of PA vs. 1/n give excellent straight lines and these can be used to estimate PA values for missing homologues. The long-chain members do not show an abrupt leveling of PA values with chain length, instead there seems to be a small but continuous increase in PA. This may result from a coiling of the polarizable alkyl chain to bring it into closer proximity to the charged site.[12] On the basis that protonation is analogous to ionization, the significance of the slope of the line should be indicative of the extent of charge delocalization.[11] Figure 5.1(A) shows plots of PA vs. 1/n for series of RNH_2, RCN and ROH.

Methyl substitution at the proton sited atom, i.e., $-NH_2$, -OH, shows that the PA values change exponentially with the size of the molecule as a result of stabilization of BH^+. This methyl effect is large and distinctly nonadditive (Figure 5.1(B) exhibits methyl substitution effect on the N-atom of amines). In contrast, methyl substitution on the α-C shows nearly additive effects of ca. 2.5 kcal mol^{-1}.

These results may be ascribed to predominant inductive and polarization stabilizing effects of methyl on cationic BH^+.[13]

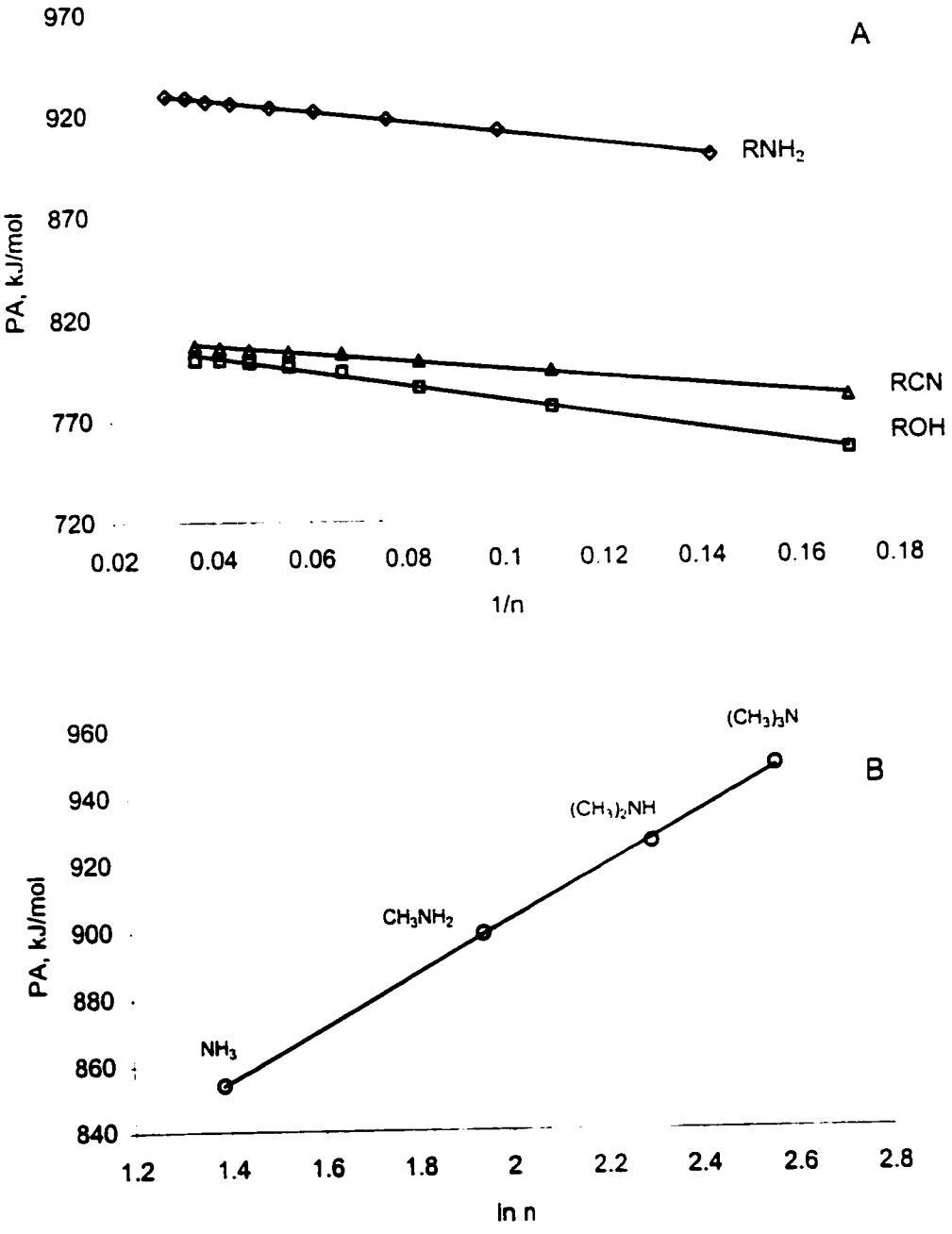

Figure 5.1 (A) Effect of size of molecules on PA;
(B) Effect of methyl subsitution at the N-atom on PA

5.2.2.2 PA for unsaturated molecules

Allyl and benzylamines show lower PAs (ca. 2.0 kcal mol^{-1} lower PA for $C_3H_5NH_2$ than n-$C_3H_7NH_2$) than saturated analogs as a result of small electron-withdrawing effects of the electronegative sp^2 hybridized carbon. Propargylamine shows a much larger electronwithdrawing effect for a *sp* hybridized carbon. Its PA is fully 7 kcal mol^{-1} lower than that of n-propylamine. We find that PA for benzylamine is 923 kJ mol^{-1}; it is likely therefore PA for cyclohexanemethylamine (927 kJ mol^{-1}) is too low.

5.2.2.3 PA for halogenated molecules

Halogenated amines, alcohols and nitriles show lower PAs as a result of electron-withdrawing inductive effects of the halogen substituent.

5.2.2.4 PA for molecules with bifunctional groups

PA of bidentate species, i.e. diamines, show much higher PA values than that of similar monodentates. These high PA values are the results of unusual stabilization of the ammonium ions by the formation of strong intramolecular hydrogen bonds as will be seen in the section on diaminoalkanes of Chapter 6. Comparisons of PAs of diamines with appropriate models, give ΔPA values that serve as an estimate of the intramolecular hydrogen bond strengths in the molecules. Even weakly basic chloro and fluoro substituents seem to be capable of such hydrogen bonding to some extent.[12]

5.3 *Methods of determining GB(B) and PA(B)*

5.3.1 Equilibrium Measurements

The equilibrium method is an excellent relative method based on the measurement of the equilibrium constants of gas phase proton transfer reactions between two bases B_1, a reference, and B_2, an unknown base, at a single temperature. The majority of PA values have been determined from such measurements.

$$B_1H^+ + B_2 \rightleftharpoons B_2H^+ + B_1$$

The equilibrium constant (K_{eq}) for the reaction is obtained from a mass spectrometric observation of the relative abundances of the ions, B_1H^+ and B_2H^+, in a mixture of compounds of B_1 and B_2 of known composition:

$$K_{eq} = \frac{I_{B_2H^+} P_{B_1}}{I_{B_1H^+} P_{B_2}} \qquad 5.2$$

where I_{B1H+} and I_{B2H+} are the intensities of B_2H^+ and B_1H^+ ions, P_{B1} and P_{B2} are the partial pressures for the neutrals B_1 and B_2. When the ratio of ions is observed under conditions such that thermodynamic equilibrium has been attained, the resulting value for K_{eq} of the reaction directly provides a value for the Gibbs free energy change of the reaction ($\Delta G°$) at temperature T.

$$-RT \ln K_{eq} = \Delta G^\circ = GB(B_1) - GB(B_2) \qquad 5.3$$

By establishing ladders of relative GBs, which include reference compounds of known basicity from independent measurements, absolute gas-phase basicities can be established.

Some data have been based on the measurements of K_{eq} over a range of temperatures. When such data are treated in the van't Hoff equation, i.e., when ln K_{eq} is plotted against T^{-1}, then values of $\Delta H°$ and $\Delta S°$, the enthalpy and entropy change of the reaction, can be derived directly from the slope and intercept of the fitted line, respectively. Note that in the van't Hoff treatment, the values of $\Delta H°$ and $\Delta S°$ are considered to be constant over the temperature range for which K_{eq} is measured.

$$\ln K_{eq} = -\frac{\Delta H^{\circ}}{RT} + \frac{\Delta S^{\circ}}{R} \qquad 5.4$$

Note that $\Delta S°$ has been found to be close to zero when B_1 and B_2 are simple bases, where there is no intramolecular hydrogen bonding in the ionic species. However, when there is the possibility of intramolecular hydrogen bonding, estimates of $\Delta S°$ become much more difficult.

The measurement of K_{eq} for gas-phase proton transfer reactions requires that the number of collisions be sufficient to thermalize all the species and to allow chemical equilibrium to be established. This objective has been accomplished by using high-pressure mass spectrometry techniques (HPMS),[14] flowing afterglow

experiments (FA)[15] or ion cyclotron resonance techniques (ICR);[16] the latter method, using ion trapping by conventional ICR or Fourier transform ion cyclotron resonance (FTICR), has the advantage that equilibrium can be attained at much lower pressures than are necessary with the other methods. HPMS has been used to measure K_{eq} for proton transfer reactions involving simple amino acids,[17] whereas GB values for a variety of amino acids have been measured using ICR techniques.[18-20]

5.3.2 Reaction Bracketing

The reaction bracketing or simply bracketing[21] is used to determine the relative gas-phase basicities (GBs) or proton affinities (PAs) simply on the basis of the occurrence or non-occurrence of a proton transfer reaction between an unknown base (B) and a few reference bases, i.e., B_1 and B_2 whose GBs are known.

$$BH^+ + B_2 \longrightarrow B_2H^+ + B$$

$$BH^+ + B_1 \not\longrightarrow \text{no proton transfer}$$

In the case shown above, GB(B) is obviously between GB(B_1) and GB(B_2). In more rigorous work, a series of references is selected and the reaction is examined in both directions or the reaction efficiency is measured. For example, the protonated amino acid or peptide ion formed by matrix-assisted laser desorption-ionization (MALDI),[22] are allowed to react with a series of reference bases in order to confirm the order of thermochemical values.

The bracketing method is most subject to error because only a few reference compounds are used and because cancellation of entropy effects is assumed. It also seems to form the basis for most criticisms of the kinetic method.

5.3.3 Kinetic Method

The "kinetic method" has been used for the estimation of thermochemical data for some 22 years and has often been reviewed.[3,23-27] The experiments for the kinetic method and their interpretation are deceptively simple but they have been steadily modified as results have accumulated which complicate the simplest approach. The best known application of the method is for the determination of proton affinity (PA) values. For these to be evaluated, proton-bound dimers, $B_1H^+B_2$, are generated and isolated in a mass spectrometer and the competing reactions 5.5 and 5.6 yielding the individual protonated monomers are examined:

$$B_1H^+B_2 \xrightarrow{k_1} B_1H^+ + B \qquad 5.5$$

$$B_1H^+B_2 \xrightarrow{k_2} B_2H^+ + B_1 \qquad 5.6$$

Upon fragmentation, the monomer having the greater proton affinity should preferentially carry the proton. The reactions are observed as metastable dissociations or induced by collisional excitation at low or high translational kinetic energies.

Canonical transition state theory (which is for species at an equilibrium thermodynamic temperature) has been applied to these systems. The rate constant, k, for a reaction is given by the statistical thermodynamics version of the Arrhenius equation:

$$\ln k = \ln \frac{Q^{\neq}}{Q} - \frac{E^{\circ}}{RT} \qquad 5.7$$

where Q and $Q^{\neq}$ are the partition functions for the reactant and the transition state respectively, E° is the activation energy, R is the ideal gas constant and T is the temperature. When there are two competing dissociations, the ratio of their respective rate constants, k_1 and k_2 is given by:

$$\ln \frac{k_1}{k_2} = \ln \frac{Q_1^{\neq}}{Q_2^{\neq}} - \frac{E_1^{\circ} - E_2^{\circ}}{RT} \qquad 5.8$$

In the kinetic method, k_1 and k_2 are replaced by the respective product ion intensities $[B_1H^+]$ and $[B_2H^+]$, and equation 5.8 is simplified to permit the evaluation of the difference in proton affinities, $E_2^{\circ} - E_1^{\circ} = PA(B_1) - PA(B_2)$:

$$\ln \frac{[B_1H^+]}{[B_2H^+]} = \frac{PA(B_1) - PA(B_2)}{RT_{eff}} \qquad 5.9$$

For equation 5.9 to apply, the most important assumption is that the proton-bound molecular pairs have internal energy distributions which can be described by an "effective temperature" term, T_{eff}. Note that in general, a system of isolated ions

generated or activated in a mass spectrometer cannot be assumed to have a Boltzmann distribution of internal energies, except where special efforts are made to generate thermal equilibria, such as in high pressure mass spectrometry.

Also, to conform with reaction rate theory, the logarithm term should represent the ratio of the fractions of ions fragmenting that have internal energies from $E_1^\circ \rightarrow \infty$ and $E_2^\circ \rightarrow \infty$, respectively. This presents a problem when studying the dissociations of metastable ions in a sector mass spectrometer, reactions which take place in well defined but narrow time frames. This has recently been discussed.[28]

A third assumption is that neither dissociation involves a reverse energy barrier. This is a priori likely when only simple bond cleavages are involved. Finally, it is assumed that there are no net entropy effects, i.e., $Q_1^{\neq} = Q_2^{\neq}$.

In order to use equation 5.9 to obtain a new proton affinity value, reference bases of known PA are required.

For a series of molecules (B_n) having a common functionality, it has generally been found that a plot of $\ln([B_nH^+]/[BH^+])$ vs. $PA(B_n)$ yields a fair straight line. Thus, from the slope of the plot, a temperature-like term, T_{eff}, has been obtained. It has been assumed that this parameter relates to the average internal energy of the ion population. If the ion population is not in thermal equilibrium with its surroundings,

such as in an ion beam experiment, or in partial thermal equilibrium, as in the case of high pressure experiments, the physical interpretation of the parameter obtained from the slope of the plot can be neither straightforward nor certain.

A useful theoretical consideration of kinetic method plots in terms of the significance of their slopes (which relate to the internal energies or "effective temperature" of the fragmenting ions) has recently been made by Erwin.[29] His model is for metastable ions and uses ion source temperature as a parameter. In our earlier study on alkanols[28] we were not able to discern any ion source temperature effect on the behavior of metastable ions.

So far, the principles and assumptions of the kinetic method have been addressed. The initial derivation of the method is the establishment of the correlation between the proton affinity (PA) and fragment ion abundances, the extensions to the method include the estimation of the relative gas-phase basicity (GB), acidity (ΔH_{acid}) and so on. (see section 5.5 of this chapter).

The kinetic method has a number of advantages. It is readily employed in commercial tandem mass spectrometers of all kinds. It gives good results for small amounts of sample; it is simple, fast, and applicable to polar and nonvolatile samples without derivatization; it is also typically sensitive to small differences in the thermochemical quantity being determined; moreover, samples in general need not be specifically purified because the isolation of the dimer cluster ion in the tandem

mass spectrometry experiment represents a form of purification. However, the method relies on certain assumptions and the results obtained are approximates to the true values. As will be seen later, these estimates are often very good ones, and superior alternative methods are not often available, especially for biological compounds.

5.4 Fundamental considerations for the kinetic method

5.4.1 Bond dissociation energy for proton-bound dimers

5.4.1.1 Bond dissociation energies for the dimers with monofunctional groups

The thermochemistry of numerous proton-bound dimers, $B_1H^+B_2$, has been investigated by Kebarle and other workers.[30] Bond dissociation energies ($\Delta H°_D$) were obtained from the temperature dependence of K_{eq} of clustering reactions:

$$B_1H^+ + B_2 \rightleftharpoons B_1H^+B_2$$

The general mode for ionic hydrogen bond is $-YH^+..Y-$, where Y are atoms of large electronegativity such as halogen, O and N. The strength of ionic hydrogen bonds results from the combination of electrostatic, polarization, exchange repulsion, charge transfer, and coupling components, of which the first two are the most significant.

In general, the ionic hydrogen bonds in the protonated dimer ions are much stronger than hydrogen bonds in neutral dimers. A linear correlation[31-33] is found between $\Delta H°_D$ and ΔPA, the difference in proton affinities between B_1 and B_2.

$$\Delta H^{\circ}_{D} = \Delta H^{\circ}_{D}(0) - b\Delta PA \ (\text{kcal mol}^{-1}) \qquad 5.10$$

where $\Delta H°_{D}(0)$ is the binding energy when $\Delta PA=0$ and b is a constant.

Meot-Ner[34] examined extensive series of dimer ions and found the relations for hydrogen bonds of the types *-NH⁺..N-* and *-OH⁺..O-*. For *-NH⁺..N-* dimers including amines and pyridines, $\Delta H°_{D}(0)$ = 23.2 ± 1.2 kcal mol^{-1} and b = 0.23. For the symmetric dimers, where $B_1 = B_2$, the correlation predicts that the binding energy should remain constant regardless of the identity of B. Note that cyanide dimers do not fit the *-NH⁺..N-* correlation because these dimers show substantially stronger binding than predicted, possibly owing to the high dipole moment of these ligands. The $\Delta H^{\circ}_{D}(0)$ for nitrile dimers are about 30 kcal mol^{-1}.[35] For *-OH⁺..O-* dimers including a large variety of alcohols, ethers, and ketones, $\Delta H^{\circ}_{D}(0)$ = 30.4 kcal mol^{-1} and b = 0.30 with ΔPA ranging from 0 to 55 kcal mol^{-1}.

A similar equation was developed by Larson and McMahon[36] for the oxygen-donor bases, $\Delta H^{\circ}_{D}(0)$ = 30.8 ± 2 kcal mol^{-1} in symmetric proton-bound dimers regardless of functional group involved or gas-phase basicity; b = 0.46. Keep this correlation in mind because it will be used to estimate molecular pair proton affinities (MPPA) in Chapter 9.

Note that the ionic hydrogen bond is one of the interactions in the ion-neutral complexes, $B_1H^{+}\cdots B_2$. If B_2 is a polar base with a high dipole moment, the ion-dipole interaction between the cation and neutral could be so strong that it becomes dominant in determining the strength of the interaction. Factors such as dipole moment of the neutral base and relative proton affinities of the components will play a key role in the determination of the strength of the interaction. In such a case, the reaction to produce the protonated base of lower proton affinity could even become energetically favored. Of course, this aspect will relate to the limitations of the kinetic method for proton affinity measurement.

5.4.1.2 Bond dissociation energies for the dimers with polyfunctional groups

The effects of the structural features of B_1 and B_2 on the ionic hydrogen bond, i.e., effects of intramolecular hydrogen bonds on clustering, will cause significant deviations from the above correlations and hence lead to substantial enhancement or weakening of the ionic hydrogen bond in the corresponding complexes.

In proton-bound α,ω–diaminoalkane and monoamine pairs, the intramolecular hydrogen bonding of the α,ω–diaminoalkanes weakens the internal hydrogen bonding (by ca. 9 kcal mol^{-1}). Evidence for this phenomenon is that the bond length for the dimers is significantly decreased when compared with that for the dimers of monoamines, as has been shown by *ab initio* calculations.[37] For example, the hydrogen bond between 1,4-diaminobutane and NH_3 is greatly weakened due to the intramolecular hydrogen bonding of protonated 1,4-

diaminobutane, the cyclic structure being a stable seven-membered ring. The bond length for the dimer is decreased from 1.5 to 1.8 Å.[37]

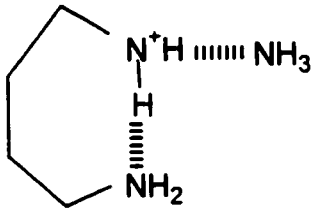

In contrast, when polyfunctional molecules complex with protonated species such as ammonium ions RNH_3^+, polydentate bonding can occur which will greatly enhance the binding of the dimers. The chelation of an ether and monoamine increases the binding energy to as high as 45 kcal mol^{-1}.[38]

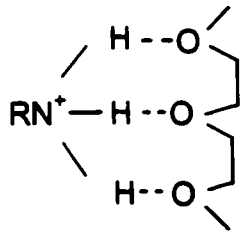

5.4.2 Entropy Effects

An important advance in the kinetic method, made by Fenselau and co-workers[39] and by Wesdemiotis and his group,[40,41] was the recognition that entropy effects were not only observable but that entropy differences could also be estimated using the kinetic method. Earlier work had sought to avoid such effects by restricting applications to cases in which the analyte and reference species were

structurally and chemically closely similar. These developments will be addressed briefly in this section.

If a series of reference compounds (B_n), structurally dissimilar from the unknown (B) but similar among themselves are used, the term $\ln(Q_n^{\neq}/Q^{\neq})$ may not be negligible.[39,41] However, plotting $\ln(k_n/k)$ vs $PA(B_n)$ may still give a straight line because $\ln(Q_n^{\neq}/Q^{\neq})$ is constant among B_n. In such a case, $\ln(Q_n^{\neq}/Q^{\neq})$ gives the difference in entropy change between the two dissociation channels.

Fenselau[39] considered $\ln(Q_n^{\neq}/Q^{\neq})$ as the difference in entropies of protonation for B_n and B, $\Delta\Delta S°_{H+} = \Delta S°_{H+}(B_n) - \Delta S°_{H+}(B)$. They studied entropy effects on protonated peptides using simple organic bases as reference compounds. A series of reference bases was chosen, the bases being structurally dissimilar to the peptide to be studied, but similar among themselves. The ratio $\ln(k_n/k)$, instead of simply providing the value $\Delta PA/RT_{eff}$, is given in the more strict treatment by equation 5.11:

$$\ln\frac{k_n}{k} = [\ln\frac{Q_n^{\neq}}{Q^{\neq}} - \frac{PA(B)}{RT_{eff}}] + \frac{PA(B_n)}{RT_{eff}} \qquad 5.11$$

Plotting $\ln(k_n/k)$ vs. $PA(B_n)$ should still give a straight-line because $\ln(Q_n^{\neq}/Q^{\neq})$ is likely to be constant among the reference bases. If it is assumed again that there is no reverse activation barrier, then $\ln(Q_n^{\neq}/Q^{\neq})$ is equal to $\Delta\Delta S_{H+}/R$.

The quantity $\Delta\Delta S_{H^+}$ can be estimated experimentally by plotting $\ln(Q_n^{\neq}/Q^{\neq}) - PA(B)/RT$ against 1/RT (the intercept and slope respectively of Figure 5.2(A)) at a variety of collision energies (Figure 5.2(B)). This plot yields a slope of -PA(B), providing a confirmation of the estimated PA(B) from the traditional plot (Figure 5.2(A)), and $\Delta\Delta S_{H^+}/R$ as an intercept. The resulting data indicate that $Q_1^{\neq}/Q_2^{\neq}$ is not unity due to differences in the entropy change for the dissociating complexes. When this methodology is applied to tri-, tetraglycines (Gly_3 and Gly_4) and 1,4-diaminobutane estimates of $\Delta\Delta S_{H^+}$ are -14.2, -10.4 and –15.6 e.u. (J mol^{-1} K^{-1}), respectively.

This approach developed by Fenselau should be applicable to any gas-phase ionic system for which an appropriate cluster ion can be generated. The significance of this method is that it provides an alternative route to the estimation of $\Delta\Delta S_{H^+}$ for a group of compounds including larger biomolecules (MW > 1000).

However, it is worthwhile to mention that the entropy term $\Delta\Delta S_{H^+}$ obtained from this method has been questioned on the grounds that T_{eff} is not a real temperature and $\Delta\Delta S_{H^+}$ is implicitly assumed to be independent of temperature.[24] Moreover, and more important is the doubtful validity of equating entropies of activation with entropies of protonation. The latter can strictly only be measured by equilibrium studies.

Wesdemiotis[41] extended the discussion about entropy effects to the measurement of alkali metal ion ($M^+ = Li^+, Na^+, K^+$) affinities of common DNA and RNA nucleobases. The competitive dissociations of metal ion-bound heterodimers were studied under both MI and CID conditions.

$$[NB + B_i]M^+ \xrightarrow{k} [NB]M^+ + B_i \qquad 5.12$$

$$[NB + B_i]M^+ \xrightarrow{k_i} [B_i]M^+ + NB \qquad 5.13$$

The nucleobases (NB) under study were guanine (G), adenine (A), cytosine (G), thymine (T) and uracil (U), which have one or more binding sites to M^+. The presence of entropy effects is inevitable in this case since some reference bases (B_i) are structurally dissimilar to the unknown (NB).

By applying transition state theory and substituting the entropy term, ln $(Q_1^{\neq}/Q_2^{\neq})$, by $\Delta\Delta S°_{M+}/R$, will lead to the complete form of the kinetic equation (equation 5.11). $\Delta\Delta S°_{M+} = \Delta S°_{M+}(NB) - \Delta S°_{M+}(B_n)$ and $\Delta H°_{M+}(NB)$ and $\Delta H°_{M+}(B_n)$ are metal ion affinities of NB and B_n.

$$\ln\frac{k}{k_n} = \ln\frac{Q^{\neq}}{Q_n^{\neq}} - \frac{E^{\circ} - E_n^{\circ}}{RT_{eff}} \qquad 5.14$$

$$= \frac{\Delta\Delta S^{\circ}_{M^+}}{R} + \frac{\Delta H^{\circ}_{M^+}(NB) - \Delta H^{\circ}_{M^+}(B_n)}{RT_{eff}}$$

It was found with the study of all three metal ions that the metal ion affinities increased in the order of U < T < A < C < G which is in the same direction as the proton affinities of the nucleobases.

Similar to proton-bound dimers, the entropy effects associated with the dissociations of metal ion-bound dimers arise from the restriction of rotational degrees of freedom in the metalated species of $[NB]M^+$ and therefore the term $\Delta\Delta S°_{M+}$ is not negligible. This point is illustrated in the dissociation of the K^+-bound dimer composing of pyridine (Py.) and adenine (A). Pyridine binds K^+ in a unidentate fashion whereas adenine complexes K^+ in a multidentate fashion (see Figure 5.3). This conformation, retained in both dimer and monomer, would freeze rotations of the amino group of adenine and in turn explain a more negative $\Delta S°_{M+}$ in the formation of AK^+ than that in the formation of PyK^+.

The method to obtain the values of $\Delta H°_{M+}(NB)$ and $\Delta\Delta S°_{M+}$ is basically the same as Fenselau's approach. The only difference is that the dissociations are observed under MI and CID conditions. The entropy term, $\Delta\Delta S°_{M+}$, is estimated by using the two T_{eff} terms extracted from these processes. The derived $\Delta\Delta S°_{M+}$ reveals insight on the structures of both $[NB + Bi]M^+$ and $[NB]M^+$.

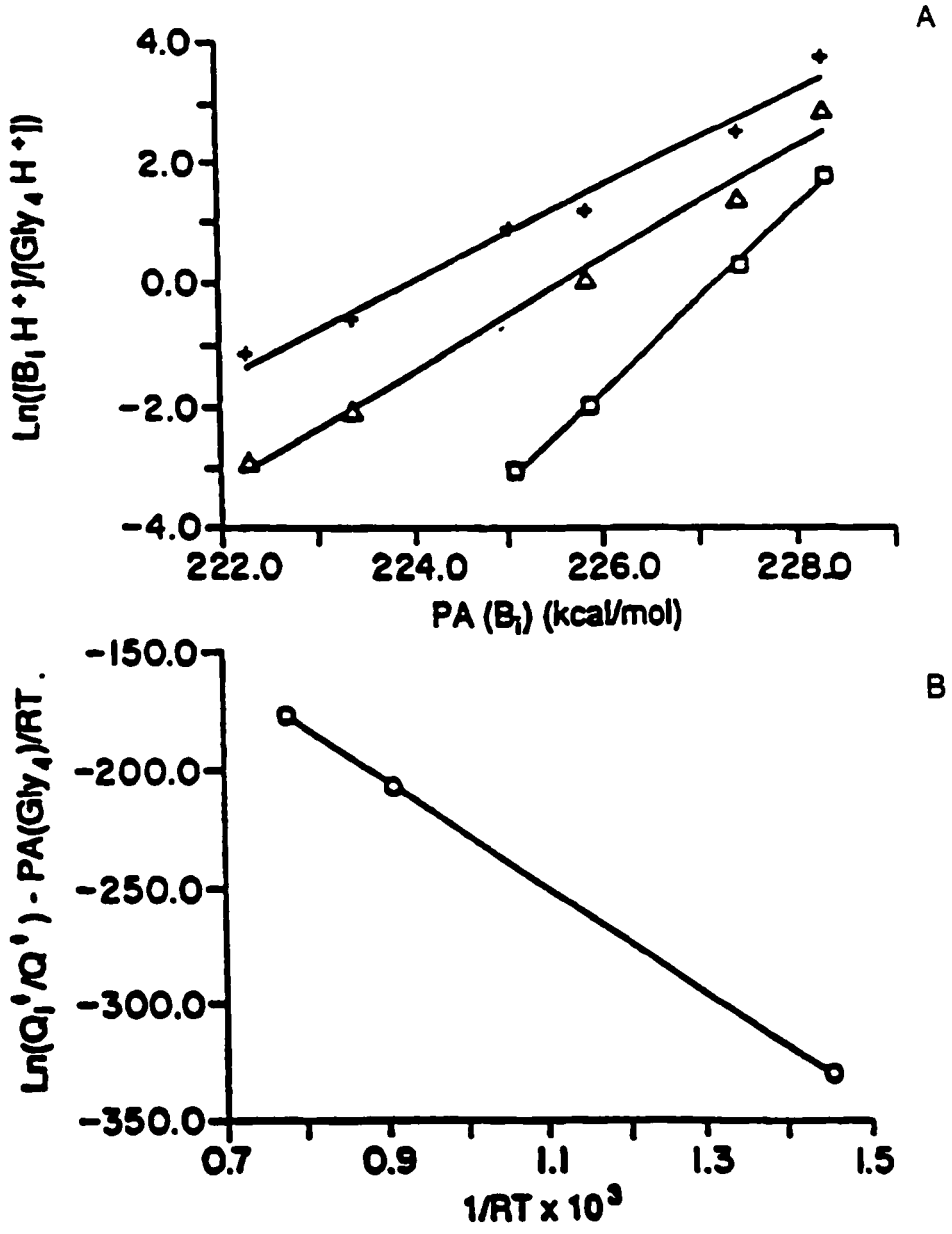

Figure 5.2 Estimation of $\Delta\Delta S_{int}$ in the dissociations of the proton-bound dimers of Gly_4 and B_i (A) Standard plot of ln k_i/k vs $PA(B_i)$; (B) ln (Q_i^*/Q^*) - $PA(B)/RT_{eff}$ vs $1/RT_{eff}$

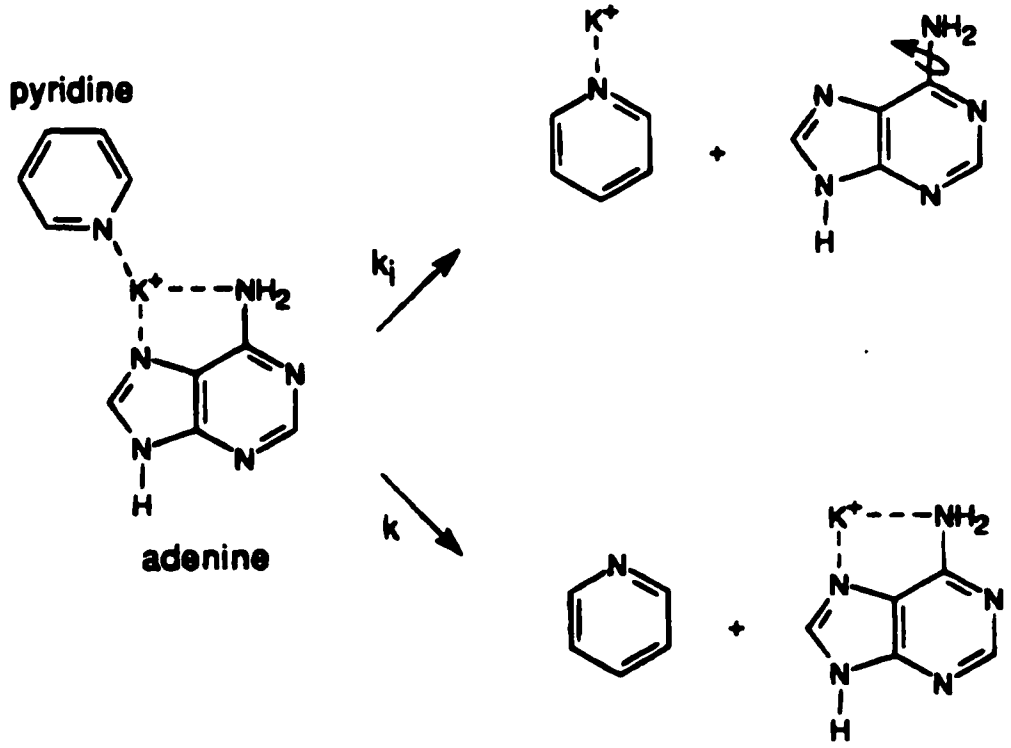

Figure 5.3 The mechanism for the competitive dissociations of [Py + A]K^+.

5.4.3 *Internal Energy Effects*

The kinetic method derivation given in equation 5.9 is based on the application of absolute rate theory, which assumes that the system is in thermal equilibrium. This is clearly not the case for the isolated ions undergoing metastable and collision-induced fragmentations. However, the temperature-like term, T_{eff}, is indeed a measure of the internal energies of the dissociating dimer ions although they are not equilibrated with the surroundings.

Drahos and Vekey[42] have provided additional and persuasive support for the view that T_{eff} is related to the internal energy of the fragmenting ion population. Importantly, they also show that it is not a thermodynamic quantity but is dependent on the properties of both the system, i.e., the activation energy of the fragmenting ions, and the experiment, i.e., the lifetime of the ions sampled.

Although it has been common practice to take T_{eff} from the slopes of ln$R$ vs. PA plots and use them to evaluate "entropies" there are serious problems with such an approach. As pointed out in the previous section, $\Delta\Delta S_{H+}$ has been incorrectly ascribed to overall entropy effects i.e., entropies of protonation,[39,41] using the T_{eff} value. The quantity T_{eff} does relate to the internal energy of the fragmenting ions but for metastable ions it can not be a temperature in the thermodynamic sense.[28] Holmes strongly proposed that the term T_{eff} is inappropriate for describing the behavior of metastable ions because of the shortcomings of MI experiments with

respect to the absolute rate theory as well as the collisionally activated ions. The MI experiment does not fulfill the two main criteria for the application of the theory.

1) The adduct ions are not completely equilibrated to the ion source temperature, ca. 420 K. We know this because at this temperature, the fraction of adduct ions that would be metastable is negligibly small. With the bond strength of proton-bound dimers of 24 - 30 kcal mol^{-1} and Arrhenius factor (A) of 10^{14} s^{-1}, only about 0.1% of the ions could be metastable at an even higher temperature of 580 K.

2) Experiments have shown that the value of R is <u>independent</u> of the fraction of mass selected ions that are metastable.[28] The latter must relate to the internal energy of the ions as a whole. This independence therefore, is <u>in spite</u> of the change in internal energy of the ions.

3) The MI experiment observes the dissociation of ions through a narrow time window and hence internal energy window, namely from $E_1°$ to $E_2°$. However, CID experiments can satisfy the second major criterion governing the application of the theory. The corresponding internal energy observation windows are from $E_1°$ or $E_2°$ to, effectively, ∞.

For the dissociations induced by collisional excitation a similar problem arises. The time frame of the CID observations is governed by the time the ions spend in the collision cell. In our apparatus this is ca. 0.2 μs and so all collisionally

activated ions which fragment from time zero (the moment of collision) to 0.2 μs, are monitored. This encompasses a rate constant range upwards from ca. 10^6 s^{-1}. The mean rate constant for the dissociation is unknown and the internal energy distribution is also unknown. This precludes the application of absolute rate theory to evaluate $\Delta S^{\neq}$, which requires $\Delta H^{\neq}$, the enthalpy of activation, the temperature, T, and a known rate constant, k. Therefore, it is suggested that the use of the term T_{eff} for analysis of both MI and CID observations be discontinued.

Furthermore, in a CID experiment using a sector mass spectrometer, the practice of employing the mixed product ion ratios in the collisional excitation with the intention of observing collision effects also appears to have no scientific basis[28] because the mixed ratios are actually the combination of the three processes, *MI* occurring in the FFR, *CID process plus a minor MI contribution* that takes place inside the collision cell, and *MI and post-CID process* which arise from the exit of the collision cell to the next analyzer. In addition, the mixed CID mass spectra will change not only with the pressures of collision gases but also on the nature of the gases since different gases have different collision cross sections.

Observation of the collision gas effects using the mixed CID ratios was well brought home in a study of Na^+ affinities to peptides by Wesdemiotis et al.[40] Three lines with different slopes corresponding to MI, CID/He and CID/Ar were generated in the plot of ln (k/k_i) vs $\Delta H°_{Na^+}(B_i)$ (see Figure 5.5). The slopes provide the effective

temperatures T_{MI}, T_{He} and T_{Ar}, respectively. However, as argued above it is highly unlikely that these T_{eff} values are meaningful.

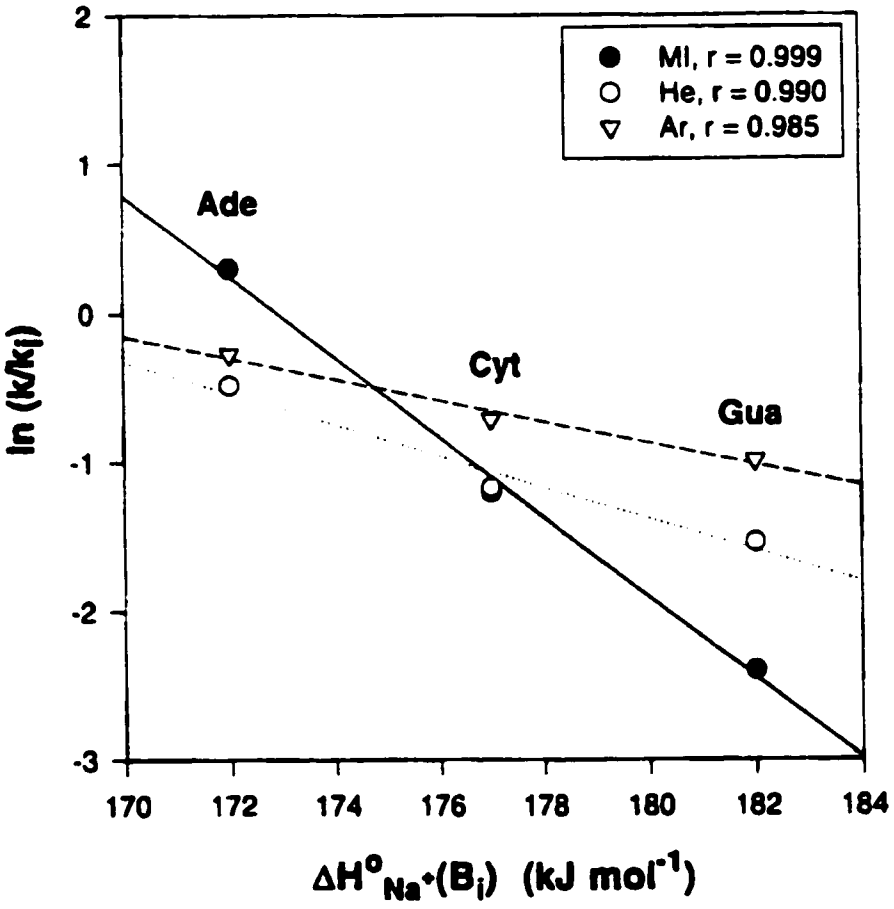

Figure 5.4 Plot of ln (k_i/k) vs $\Delta H^{B}_{Na^+}(B_i)$ for heterodimers of [AG + B_i]Na^+

Holmes pointed out in the case study of alkanols[28] that using the isolated CID ratios by applying a potential to the collision cell; for details see chapter 9, different collision gases (He, Ar, O_2, Xe) will essentially produce closely similar internal energy distributions of the dissociating proton-bound adduct ions and hence, T_{eff} obtained from the slope of the CID line will be independent of the nature and pressures of the gases (Table 5.2). The mixed CID spectra varied with both factors.

Table 5.2 Effect of target gas on the ratio $[R_1OH_2^+]/[R_2OH_2^+]$ from CID mass spectra[28]

	Target gas (pressure, mbar x 10^8)			
	He(4)	He(20)	Ar(15)	Ar(60)
	$(C_2H_5OH)H^+(n\text{-}C_3H_7OH)$			
mixed CID	5.8	3.5		4.5
isolated CID	3.3	3.3		3.2
MI		37		
	$(n\text{-}C_5H_{11}OH)H^+(n\text{-}C_6H_{13}OH)$			
Mixed CID	2.0	1.6	1.9	1.6
isolated CID	1.3	1.2	1.2	1.2
MI		2.7		

5.4.4 *Kinetic Energy Release (KER)*

The KER values for the competitive dissociations of the proton, or metal-bound dimers[23,28,41,43,44] are ca. 20 meV or less in keeping with simple bond cleavage without any appreciable reverse activation energy, as required for the kinetic method.

In principle, the reaction to form di-coordinated, protonated or metalated monomers demands a tighter transition state and could well be associated with a relatively larger KER indicating a considerable reverse activation energy than the reaction leading to mono-coordinated, protonated or metalated monomers. However, the experimental results do not support such a proposal. The KER values for the two competitive decompositions are similar (ca. 20 meV, see section 7.4.5 of Chapter 7).

5.4.5 Low Energy Collisions in the Kinetic Measurements

Magnetic and electric sector mass analyzers, but not quadrupole instruments, allow observation of the metastable fragmentation of the cluster ion. The use of the metastable ion dissociation experiment in a sector instrument with its greater dynamic range is a better choice, especially when the bases have very similar GB or PA values. At high collision energies the fragment ion abundances are greater and the differences in these abundances are smaller.

In the triple quadrupole instruments CID is the common choice for affecting dissociations, in which low energy collision conditions are usually performed. The

term "center-of-mass energies" (E_{cm}) is used to describe the collision energies in such experiments.[45] The conversion from laboratory (E_{lab}) to center-of-mass reference frame allows the energy to be normalized over a broad range of dimer ion masses, and normalization over this broad range becomes particularly important for biomolecules, where differences of more than one order of magnitude in E_{lab} and E_{cm} are common. Care must be taken to avoid mass discrimination against particular fragment ions, which can be improved by tuning the instrument and sometimes the use of single-collision conditions.[46]

$$E_{cm} = E_{lab} \frac{m}{m+M} \qquad 5.15$$

where m and M are the masses of the collision gas and the dimer ion, respectively.

5.5 *Applications*

The kinetic method has been widely used for thermochemical and structural determinations (Table 5.3) and finds increasing use for biological compounds where its advantages over alternative methods are particularly important. Below are given some representative examples of the use of the method in a variety of applications.

Table 5.3 Examples of systems to which the kinetic method is applied

Types of clusters	Applications
Proton-bound dimers	Proton affinities, gas-phase bascities and acidities
Metal ion complexes	Metal ion affinites
Cation-bound dimers	Polyatomic ion affinites
Radical cation clusters	Ionization energies
Radical anion clusters	Electron affinities
Covalently bound ions	Ionization energies
Anion-bound dimers	Heterolytic bond dissociation energies
Larger clusters (oligomers)	Molecular pair affinities, molecular triplet affinities
Biological compounds	Structures of metal complexes
	Ion structural determination

5.5.1 Gas-phase basicity (GB) and acidity (ΔG_{acid})

Applications of the kinetic method to the estimation of proton affinities of organic compounds have been important in testing the theory and developing the scope of the method. The method has been extended for determinations of GB and ΔG_{acid} of many organic compounds.[23,39,45,47-54] Experiments are performed on the mass-selected cluster ion using either spontaneous (metastable ion) dissociation or collision-induced dissociation. A plot of the logarithm of the fragment ion abundance ratio, $\ln(k_1/k_2)$, vs. an appropriate thermochemical property of the reference compounds gives a linear relationship used to estimate the thermochemical values

of unknowns. Agreement with independent literature values is normally within 2 kcal mol^{-1}.

For example, ΔG_{acid} of a number of carboxylic acids and alcohols[45] were determined by the kinetic method using a hybrid FA-triple quadrupole instrument (FA – flowing afterglow). Multiple collision energies were used to determine ΔG_{acid}. A slightly better correlation between ΔG_{acid} and $\ln(k_1/k_2)$, expressed as the logarithm of the relative fragment anion abundances, was achieved in experiments using center-of-mass energies.

5.5.2 Electron affinity (EA)

Compounds such as aromatic hydrocarbons yield negatively charged molecular clusters which fragment when activated to yield the individual radical anions:

$$M_1 \bullet\bullet e \bullet\bullet M_2 \xrightarrow{k_1} M_1^{\bullet -} + M_2 \qquad 5.16$$

$$M_1 \bullet\bullet e \bullet\bullet M_2 \xrightarrow{k_2} M_2^{\bullet -} + M_1 \qquad 5.17$$

These clusters therefore behave analogously to proton-bound dimers, and the fragmenting structure can be represented as an "electron-bound dimer". Hence, as with other enthalpic quantities, the fragment ion abundance ratio is related to the difference in electron affinity ΔEA by:

$$\ln \frac{[M_1^{\bullet -}]}{[M_2^{\bullet -}]} \approx \frac{\Delta EA}{RT} \qquad 5.18$$

For example, the dimeric radical anion of pyrene and anthracene (m/z 380), generated by electron-capture desorption chemical ionization,[55] fragments only to intact anthracene and pyrene molecular radical anions, respectively. The relative fragment ion abundances indicate that pyrene has a higher EA, assuming that the entropy changes for the competitive channels are equal. Using various PAHs of known EA as reference compounds, EA of the unknown PAHs can be estimated.

5.5.3 Metal ion affinities ($\Delta H°_{M+}$)

Metal ion affinities are important in chemical systems that model catalysts, and in biological systems, making intrinsic (i.e., gas-phase) affinity values of increasing interest.[56-61] For example, Ca^{2+} cation affinities of peptides have been reported,[59] and the metal ion affinities of amino acids show significant differences in order (and in magnitude) when compared to the corresponding proton affinities.[57] The observed differences are likely to be the result of different binding sites for protons and metal ions. For example, the relative Cu^+ cation affinities of the 20 common amino acids are substantially different from the corresponding proton affinities. Cysteine has a high ΔH_{Cu+} but a low PA; the reverse is true for proline: this is because Cu^+, a soft acid, forms particularly stable bonds with amino acids containing soft donor groups such as the SH of cysteine.

5.5.4 Ionization energy (IE)

Ionization energies have been determined by electron impact, photoionization, photoelectron spectroscopy, photoion-photoelectron coincidence, and charge exchange. The kinetic method provides a simple procedure for IE determination, using cluster ions which are positively charged. (cf. negative ion clusters used for EA determination). Fragmentation of the mass selected dimeric radical cation gives the individual molecular radical cations, $M_1^{+\bullet}$ and $M_2^{+\bullet}$. The relative rates of fragmentation are related to the ionization energy difference by:

$$M_1M_2^{+\bullet} \xrightarrow{k_1} M_1^{+\bullet} + M_2 \qquad 5.19$$

$$M_1M_2^{+\bullet} \xrightarrow{k_2} M_2^{+\bullet} + M_1 \qquad 5.20$$

$$\ln\frac{[M_1^{+\bullet}]}{[M_2^{+\bullet}]} \approx \frac{-\Delta IE}{RT} \qquad 5.21$$

where the negative sign indicates that higher ion abundances correspond to the lower IE values and where the assumptions correspond to those made for the analogous expressions. The method has been tested for halobenzenes, PAHs, and anilines.[62,63] The method will work, provided that the structures of M_1 and M_2 in the dimers of $[M_1M_2]^{+\bullet}$ are known.

5.5.5 *Molecular pair and molecular triplet affinities*

Trimers and tetramers can be used to study molecular pair and molecular triplet affinities, respectively. These thermochemical quantities represent the strength of multiple ligand binding to an ion. For example, reactions between mass-selected Fe^+ and neutral pyridines in a pentaquadrupole mass spectrometer have been used to generate Fe^+-bound pyridine trimers and tetramers. Dissociation is by ligand loss and the relative abundances of the several products provide thermochemical information. The relative molecular pair and molecular triplet Fe^+ affinities of pyridine, respectively, defined as $-\Delta H$ for the typical reactions shown above are accessible by examining the competitive dissociations of $ABFe^+$ and $ABCFe^+$.[64]

Dissociation of Fe^+-bound trimers containing two different pyridine molecules,[64] abbreviated as A and B, occurs as 5.22 and 5.23. The cluster ion A_2Fe^+B may fragment to A_2Fe^+ or to $ABFe^+$. The rate constant corresponding to loss of B is indicated as k_1 and that corresponding to loss of A is indicated as k_2. If the kinetic method treatment applies, then one gets equation 5.24, where the molecular pair Fe^+ affinity, MPFeA of dimers A_2 and AB, are defined as $-\Delta H$ of the respective reactions $A + A + Fe^+ \rightarrow A_2Fe^+$ and $A + B + Fe^+ \rightarrow ABFe^+$:

$$A_2Fe^+B \xrightarrow{k_1} A_2Fe^+ + B \qquad 5.22$$

$$A_2Fe^+B \xrightarrow{k_2} ABFe^+ + A \qquad 5.23$$

$$\ln \frac{k_1}{k_2} = \ln \frac{[A_2Fe]^+}{[ABFe]^+ / 2} = \frac{MPFeA(A_2) - MPFeA(AB)}{RT_{eff}} \qquad 5.24$$

5.5.6 *Ion structure determination*

Thermochemical properties vary for structural isomers, and this allows the kinetic method to be used for the characterization of products of gas-phase reactions.[65] In a representative study, ion/molecule gas-phase reactions were used to generate benzene radical anions ($C_6H_4^-$) from the *o*-, *m*- and *p*-bis-(trimethylsilyl)-substituted benzenes. The isomeric benzene radical anions were reacted with carbon dioxide and then with nitric oxide to generate the putative nitrobenzoate anions, which were characterized by collision-induced dissociation of proton-bound dimers formed with a reference anion, difluoroacetate. Comparison of the relative fragment ion abundance ratios of the authentic nitrobenzoate anions with those of the putative nitrobenzoate ions confirmed that these products were indeed generated in the above ion/molecule reactions.[65]

5.5.7 *Structures of metal complexes of biological molecules*

The kinetic method can be used to determine $\Delta\Delta S$ values by making measurements at two different internal energies. This measurement of relative entropy changes in the competitive dissociation of cluster ions has been used to deduce the binding mechanism of metalated nucleobases.[41] In these experiments, heterodimers of nucleobases bound by alkali metal ions were allowed to undergo low-energy (metastable ion) and high-energy collision-induced dissociation. The

$\Delta\Delta S$ value for the two competitive dissociations of the K^+-bound dimer of pyridine and adenine was found to be +6.9 J mol^{-1} K^{-1}. This entropy difference is in contrast to $\Delta\Delta S$ values near zero in several other cases and it suggests that the adenine amino substituent is involved in auxiliary bonding to K^+. Guanine and cytosine bind similarly to adenine, but thymine and uracil do not because they lack the appropriate geometry to allow chelation with K^+. However, the problem that these represent transition state rather than product entropy differences, remains.

5.6 Summary of the kinetic method

The kinetic method is extremely sensitive to small differences in the thermochemical quantities since they appear in the exponent of the rate expression. Although there are complications in some systems such as multifunctional systems where the nature of the binding in the cluster ion is not known, the results of almost all the reliable kinetic determinations are within 2 kcal mol^{-1} of the values made by more reliable alternative methods. Bearing in mind that the kinetic method is strictly a relative method and hence its precision depends on the accuracy of the reference values used. Steps to minimize errors involved in the kinetic measurements are taken by using a series of reference compounds instead of one reference.

5.7 References

(1) Squires, R. R. 44th ASMS Conference, 1996, Portland, OR.

(2) Berkowitz, J.; Ellison, G. B.; Gutman, D. *J. Phys. Chem.* **1994**, *98*, 2744.

(3) Harrison, A. G. *Mass Spectrom. Rev.* **1997**, *16*, 201.

(4) Lias, S. G.; Bartmess, J. E.; Liebman, J. F.; Holmes, J. L.; Levin, R. D.; Mallard, W. G. *J. Phys. Chem. Ref. Data* **1988**, *17*, 1.

(5) McMillen, D. F.; Golden, D. M. *Annu. Rev. Phys. Chem.* **1982**, *33*, 493.

(6) Simoes, J. A. M.; Beauchamp, J. L. *Chem. Rev.* **1990**, *90*, 629.

(7) Hunter, E. P. L.; Lias, S. G. *J. Phys. Chem. Ref. Data* **1998**, *27*, 413.

(8) Salpin, J. Y.; Leblanc, D.; Bouchoux, G. *Int. J. Mass Spectrom. Ion Processes* **1996**, *153*, 37.

(9) Levin, I. R. *Physical Chemistry; McGraw - Hill: New York* **1978**, 717.

(10) Atkins, P. W. . In *Physical chemistry (4th ed.)*; W.H. Freeman and Company: New York, 1990.

(11) Aubry, C.; Holmes, J. L. *Int. J. Mass Spectrom., in press* **2000**.

(12) Aue, D. H.; Bowers, M. T. Stabilities of positive ions from equilibrium gas-phase basicity measurements. In *Gas-phase ion chemistry*; Bowers, M. T., Ed.; Academic press: New York, 1979; Vol. 2.

(13) Henderson, W. G.; Taagepera, M.; Holtz, D.; R.T. McIver, J.; Beauchamp, J. L.; Taft, R. W. *J. Am. Chem. Soc.* **1972**, *94*, 4728.

(14) Kebarle, P. *Techniques for the study of Ion-molecule reactions, J.M. Farrar, W.H. Saunders, Jr., Eds.; John Wiley & Sons: New York* **1988**.

(15) Schiff, H. I.; Bohme, D. K. *Int. J. Mass Spectrom. Ion Phys.* **1975**, *16*, 167.

(16) Aue, D. H.; Webb, H. M.; Bowers, M. T. *J. Am. Chem. Soc.* **1976**, *98*, 311.

(17) Meot-Ner, M.; Hunter, E. P.; Field, F. H. *J. Am. Chem. Soc.* **1979**, *101*, 686.

(18) Locke, M. J.; Hunter, R. L.; R.T. McIver, J. *J. Am. Chem. Soc.* **1979**, *101*, 272.

(19) Locke, M. J. *Ph.D Thesis, University o f California* **1981**.

(20) Locke, M. J.; R.T. McIver, J. *J. Am. Chem. Soc.* **1983**, *105*, 4226.

(21) Munson, M. S. B.; Field, F. H. *J. Am. Chem. Soc.* **1966**, *87*, 3294.

(22) Gorman, G. S.; Amster, I. J. *Org. Mass Spectrom.* **1993**, *28*, 1602.

(23) Cooks, R. G.; Patrick, J. S.; Kotaho, T.; Mcluckey, S. A. *Mass Spectrom. Rev.* **1994**, *13*, 287.

(24) Armentrout, P. B. *J. Mass Spectrom.* **1999**, *34*, 74-78.

(25) Cooks, R. G.; Koskinen, J. T.; Thomas, P. D. *J. Mass Spectrom.* **1999**, *34*, 85.

(26) Cooks, R. G.; Wong, P. S. H. *Acc. Chem. Res.* **1998**, *31*, 379.

(27) Vekey, K. *J. Mass Spectrom.* **1996**, *31*, 445.

(28) Holmes, J. L.; Aubry, C.; Mayer, P. M. *J. Phys. Chem. A* **1999**, *103*, 705.

(29) Erwin, K. M. *Int. J. Mass Spectrom.* **2000**, *195/196*, 271.

(30) Kebarle, P. *Annu. Rev. Phys. Chem.* **1977**, *28*, 445.

(31) Merlet, P.; Peyerimhoff, S. D.; Buenker, R. J. *J. Am. Chem. Soc.* **1972**, *99*, 8301.

(32) Lau, Y. K.; Nishizawa, K.; Tse, A.; Brown, R. S.; Kebarle, P. *J. Am. Chem. Soc.* **1981**, *103*, 6291.

(33) Davidson, W. R.; Sunner, J.; Kebarle, P. *J. Am. Chem. Soc.* **1979**, *101*.

(34) Meot-Ner, M. *J. Am. Chem. Soc.* **1984**, *106*, 1257.

(35) Meot-Ner, M. *J. Am. Chem. Soc.* **1978**, *100*, 4694.

(36) Larson, J. W.; McMahon, T. B. *J. Am. Chem. Soc.* **1982**, *104*, 6255.

(37) Wang, Z.; Chu, I. K.; Rodriquez, C. F.; Hopkinson, A. C.; Siu, K. W. M. *J. Phys. Chem. A* **1999**, *103*, 8700.

(38) Meot-Ner, M. *31th ASMS conference, Boston, MA* **1983**.

(39) Cheng, X. H.; Wu, Z. C.; Fenselau, C. *J. Am. Chem. Soc.* **1993**, *115*, 4844.

(40) Cerda, B. A.; Hoyau, S.; Ohanessian, G.; Wesdemiotis, C. *J. Am. Chem. Soc.* **1998**, *120*, 2437.

(41) Cerda, B. A.; Wedesmiotis, C. *J. Am. Chem. Soc.* **1996**, *118*, 11884.

(42) Drahos, L.; Vekey, K. *J. Mass Spectrom.* **1999**, *34*, 79.

(43) Cao, J.; Holmes, J. L. *Euro. Mass Spectrom.* **1999**, *5*, 19.

(44) Cao, J.; Holmes, J. L. *Int. J. Mass Spectrom.* **2000**, *195/196*, 525.

(45) Graul, S. T.; Schnute, M. E.; Squires, R. R. *Int. J. Mass Spectrom. Ion Proc.* **1990**, *96*, 181.

(46) Wright, L. G.; McLuckey, S. A.; Cooks, R. G.; Wood, K. V. *Int. J. Mass Spectrom. Ion Proc.* **1982**, *42*, 115.

(47) Gal, J. F.; Herreros, M.; Maria, P. C.; Murrell, J.; Todd, J. F. J. *Rapid Commun. Mass Spectrom.* **1996**, *10*, 242.

(48) Cooks, R. G.; Kruger, T. L. *J. Am. Chem. Soc.* **1977**, *99*, 1279.

(49) Haas, M. J.; Harrison, A. G. *Int. J. Mass Spectrom. Ion Proc.* **1993**, *124*, 115.

(50) Klots, C. E. *J. Phys. Chem. A* **1997**, *101*, 5378.

(51) Majumdar, T. K.; Clairet, F.; Tabet, J. C.; Cooks, R. G. *J. Am. Chem. Soc.* **1992**, *114*, 2897.

(52) McLuckey, S. A.; Cameron, D.; Cooks, R. G. *J. Am. Chem. Soc.* **1981**, *103*, 1313.

(53) Cacae, F.; Petris, G. d.; Pepi, F.; Angelelli, F. *Proc. Natl. Acad. Sci. USA* **1995**, *92*, 8635.

(54) Chen, G.; Kasthurikrishnsn, N.; Cooks, R. G. *Int. J. Mass Spectrom. Ion Proc.* **1995**, *151*, 69.

(55) Chen, G.; Cooks, R. G. *J. Mass Spectrom.* **1995**, *30*, 1167.

(56) Bojesen, G.; Breindahl, T.; Andersen, A. N. *Org. Mass Spectrom.* **1993**, *28*, 1448.

(57) Cerda, B. A.; Wesdemiotis, C. *J. Am. Chem. Soc.* **1995**, *117*, 9734.

(58) Chen, L. Z.; Miller, J. M. *J. Organomet. Chem.* **1993**, *448*, 225.

(59) Nemirovskiy, O. V.; Ramanathan, R.; Gross, M. L. *J. Am. Soc. Mass Spectrom.* **1997**, *8*, 809.

(60) Schwarz, J.; Wesendrup, R.; Schroder; Schwarz, H. *Chem. Ber.* **1996**, *129*, 1463.

(61) Wong, P. S. H.; Ma, S.; Wang, F.; Cooks, R. G. *J. Organomet. Chem.* **1997**, *539*, 131.

(62) Chen, G.; Cooks, R. G. *J. Mass Spectrom.* **1997**, *31*, 333.

(63) Wong, P. S. H.; Ma, S.; Cooks, R. G. *Anal. Chem.* **1996**, *68*, 4254.

(64) Ma, S.; Wong, P.; Yang, S. S.; Cooks, R. G. *J. Am. Chem. Soc.* **1996**, *118*, 6010.

(65) Wenthold, P. G.; Hu, J.; Squires, R. R. *J. Am. Chem. Soc.* **1996**, *118*, 11865.

Chapter 6 Experimental aspects of the kinetic method

6.1 Specific features in the collision-induced dissociations (CID)

It is worthwhile to review the important time-frames in the modified VG ZAB-2F instrument[1] before specific features of CID experiments are addressed.

The singly charged ions generated in the ion source and then accelerated by a voltage of 8 kV will have kinetic energy of 8 keV. The velocity of these ions will vary with their masses. Higher mass ions will have lower velocity, and vice versa. Ions with m/z ca. 185, which represents a mean value for the proton-bound dimers described in this thesis, will fly through the instrument in a time of the order of 40 μs. The time-scale of the events taking place in such an instrument are summarized in Table 6.1. These values are subject to small changes with the settings of the instrument. The distribution of rate constants which shows the fraction of the ions dissociating (dn/n_0) by a first-order process as a function of the rate constants is given as Figure 6.1.

Metastable ion dissociation in the second FFR takes place anywhere between the entrance and exit of the FFR. The ions entering this region are approximately 10 μs old, the time spent in this region is about 10 μs. The corresponding rate constant range is $10^3 - 10^6$ s^{-1} with tailing at the lower rate constant end. The ions' internal energy range corresponding to the two competitive reactions in the metastable time frame is namely from ($E_1° - E_2°$). The fraction of

ions fragmenting in this time-frame is small, usually less than 20% of the total ion flux in these experiments involving proton-bound pairs.

Collision-induced dissociation occurs following excitation from collisions between the ions of keV kinetic energy and a virtually stationary neutral target gas. During this process, part of the translational energy of the ions is converted into internal energy. The time scale of such observations begins at the moment of collisional excitation (t=0) until they leave the FFR (0 - 5 μs). Since the majority of the fast reactions ($k > 10^6$ s^{-1}) take place *inside* the collision cell, the rate constant range is wide (10^6 - 10^{13} s^{-1}). Accordingly, the internal energy range is much greater, namely from $E_1°$ and $E_2°$ to, effectively, ∞. Note that this process is convoluted with minor MI dissociations which can be corrected for.

The post-CID process refers to ions collisionally excited in the cell, but which dissociate as a result of this excitation in the rest of the FFR. A relatively small fraction of the total ion dissociations take place in this time frame (0.2 - 5 μs). The rate constant range is intermediate between the above two processes (10^4 - 10^8 s^{-1}). Figure 6.2 summarizes all of the three processes.

It is commonly accepted that the $[B_1H^+]/[B_2H^+]$ ratios from CID experiments can be measured from the peak heights in the CID mass spectra. Unless steps are otherwise taken, the peaks recorded in these CID mass spectra are a combination of the three processes (MI, isolated CID and post-CID). It is worthwhile to emphasize that the practice of using these mixed CID mass spectra to generate

$\ln[(B_1H^+)/(B_2H^+)]$ data does not have a sound scientific basis since the mixed CID ratios show an apparent dependence on both the pressure of collision gas and the nature of the gas.[2]

Table 6.1 Time-scale of events in the modified ZAB-2F mass spectrometer (ions at m/z 185, acceleration voltage 8 kV)

Events	Time (s)
Ionization (electron impact)	10^{-14} - 10^{-16}
Vibration (chemistry begins)	10^{-14} - 10^{-12}
Rotation	10^{-8}
Ions leave source	10^{-6}
Ions reach 2 FFR	10^{-5}
Ions leave 2 FFR	19×10^{-6}
Time spent in 2 FFR	9×10^{-6}
Ions reach collision cell (2FFR)	16.5×10^{-6}
Ions leave collision cell (2FFR)	16.7×10^{-6}
Ions traverse collision cell	0.2×10^{-6}
Collision excitation	10^{-15} - 10^{-14}
Ions reach collector (second ESA)	40×10^{-6}

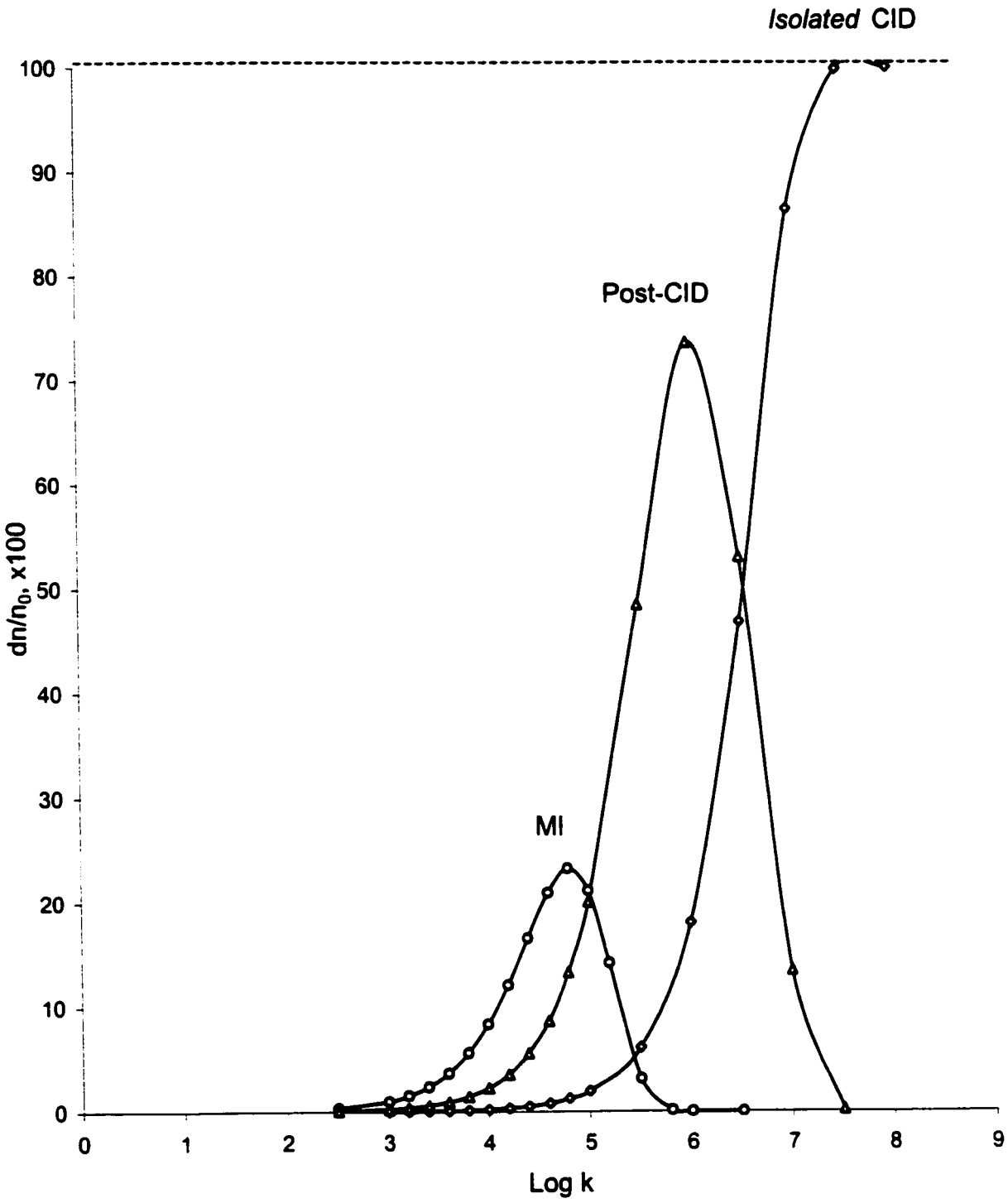

Figure 6.1 Rate constant distributions of the three processes in the 2FFR (o - MI; △- Post-CID; ◊- *Isolated* CID)

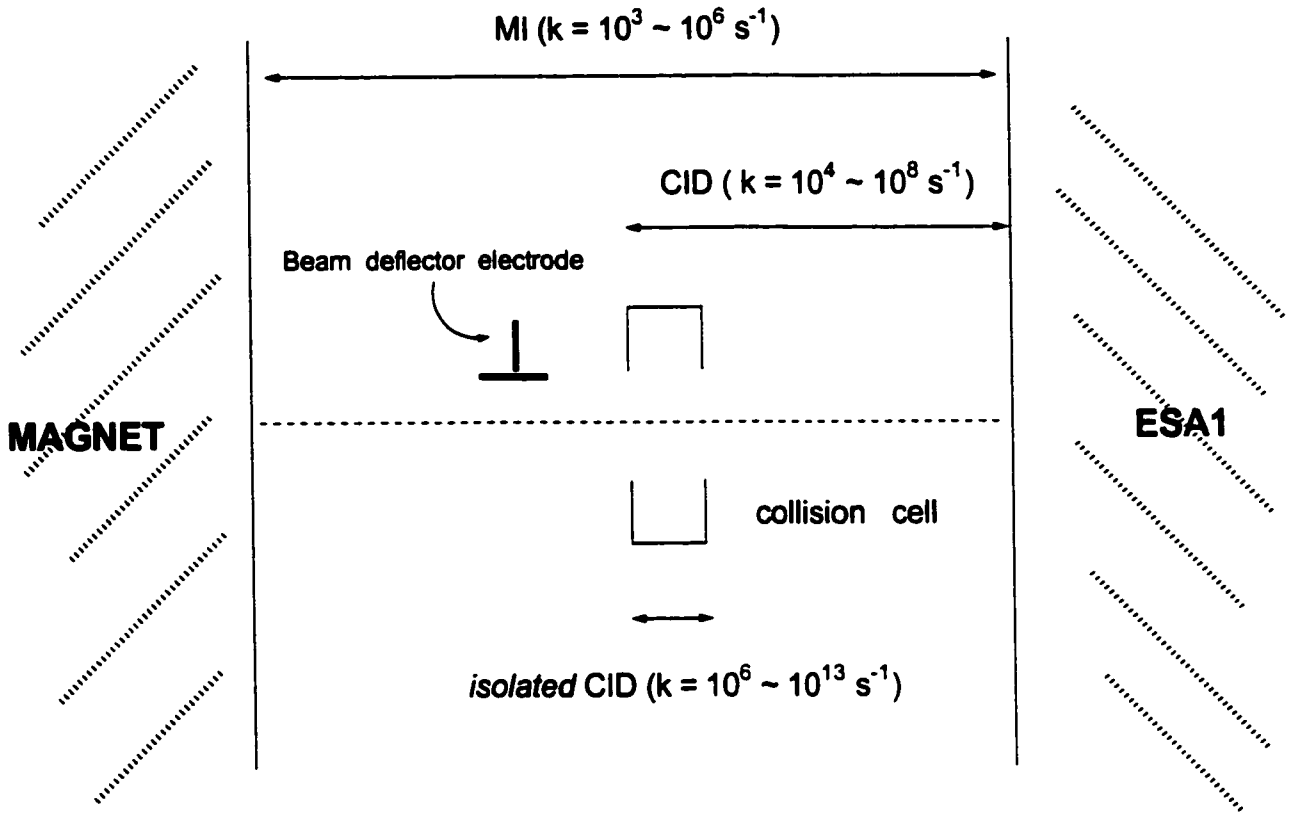

Figure 6.2 Three processes in the 2FFR of the modified ZAB-2F

The practice of applying a potential to the collision cell to separate the MI and CID processes is very useful because it is clearly essential to separate these phenomena before applying physicochemical arguments to the results. Dissociations in the charged collision cell now produce fragment ion peaks displaced from their normal position and will contain only a minimal contribution from MI products, provided that the length of the cell is much less than that of the FFR (ca. 3% in our apparatus). These displaced CID mass spectra, corrected for the minor MI contribution, yield $[B_1H^+]/[B_2H^+]$ data (*isolated* CID ratios) which have been shown to be independent of the nature of the target gases (He, O_2, Ar and Xe) as well as their pressures.[3-6]

If a positive potential, V, is applied to the collision cell, the incoming ions will be decelerated towards the cell, and accelerated upon exiting the cell. The resultant kinetic energy (KE) of the fragment ions generated inside the cell will be higher than those produced in the FFR (KE'). The corresponding ion peaks will move towards higher kinetic energy by a certain amount. For example,

$$\text{ion (m/z 100)} \longrightarrow \text{ion (m/z 70) + neutral}$$

$$KE(m/z\,70) = \frac{70}{100}(V_{acc} - V) + V \quad (eV) \qquad 6.1$$

$$KE'(m/z\,70) = \frac{70}{100} x V_{acc} \quad (eV) \qquad 6.2$$

V_{acc} is the acceleration voltage, normally set at 8000V. The displacement of ion m/z 70 is (100-70)/100•V.

Note that presence of the electric charge on the cell will have no effect on the fragment ions produced in the FFR (either prior to or after the collision cell), the kinetic energies of these ions will not be affected thereby. Therefore, by measuring the peak heights of the displaced peaks, *isolated* CID ratios will be obtained.

6.11 Problems arising from the practice of applying potential to the cell

Care must be taken to ensure that neither the sign or the magnitude of the voltage applied to the collision cell had any significant effect on the relative peak abundances. Examples show that there can be significant mass discrimination (i.e. a lower multiplier response) against lower mass fragment ions when a large negative potential (more than -500 V) is applied.

However, discrimination against lower mass fragment ions only became apparent when the mass ratio of AH^+/AH^+B fell below 0.33. Thus for metastable AH^+B ions the low recording abundance of the AH^+ fragment would lead to too high a ratio for BH^+/AH^+. Applying a positive charge (+500 V) to the cell did not affect the relative abundances of the fragment ions.

In the present experiments this situation did not arise. Note for example that Figure 7.5 was produced stepwise, with AH^+B comprising close homologues.

6.2 *Formation of the proton-bound dimers*

The proton-bound dimers were generated under CI conditions in the ion source by self-protonation of the monomers. High pressure is the key factor for the dimer ion yield as well as the ratio measurements. Compounds of high or medium volatility work well in this method. Biomolecules which in general are not volatile, are difficult to treat unless a different sample introduction system such as electrospray or a specially designed ion source is used, e.g., high-pressure pulsed ion source mass spectrometer. It was also found in the present work that for some less volatile compounds, the addition of methanol helps produce the adduct ions. Ion source temperature has only a small effect on the yield of the dimers.

6.3 *Experimental errors in the measured proton affinities; simple amines*

The $[B_1H^+]/[B_2H^+]$ ratios, *R* values, were reproducible to within 20% and so the *lnR* uncertainty was only ca ± 0.2. This is illustrated in the Figure 6.3 where the range of *R* values is very large so that as many as four stepwise R value determinations were required, leading to four times the above *lnR* uncertainty. It is also indicated in the figure that the uncertainties in *lnR* do not significantly affect the position of the cross-over point of MI and CID lines. The uncertainty in the final PA value was estimated to be no worse than ± 4 kJ mol^{-1} with consideration of the uncertainty of the NIST values (mostly less than ± 3 kJ mol^{-1}).[7]

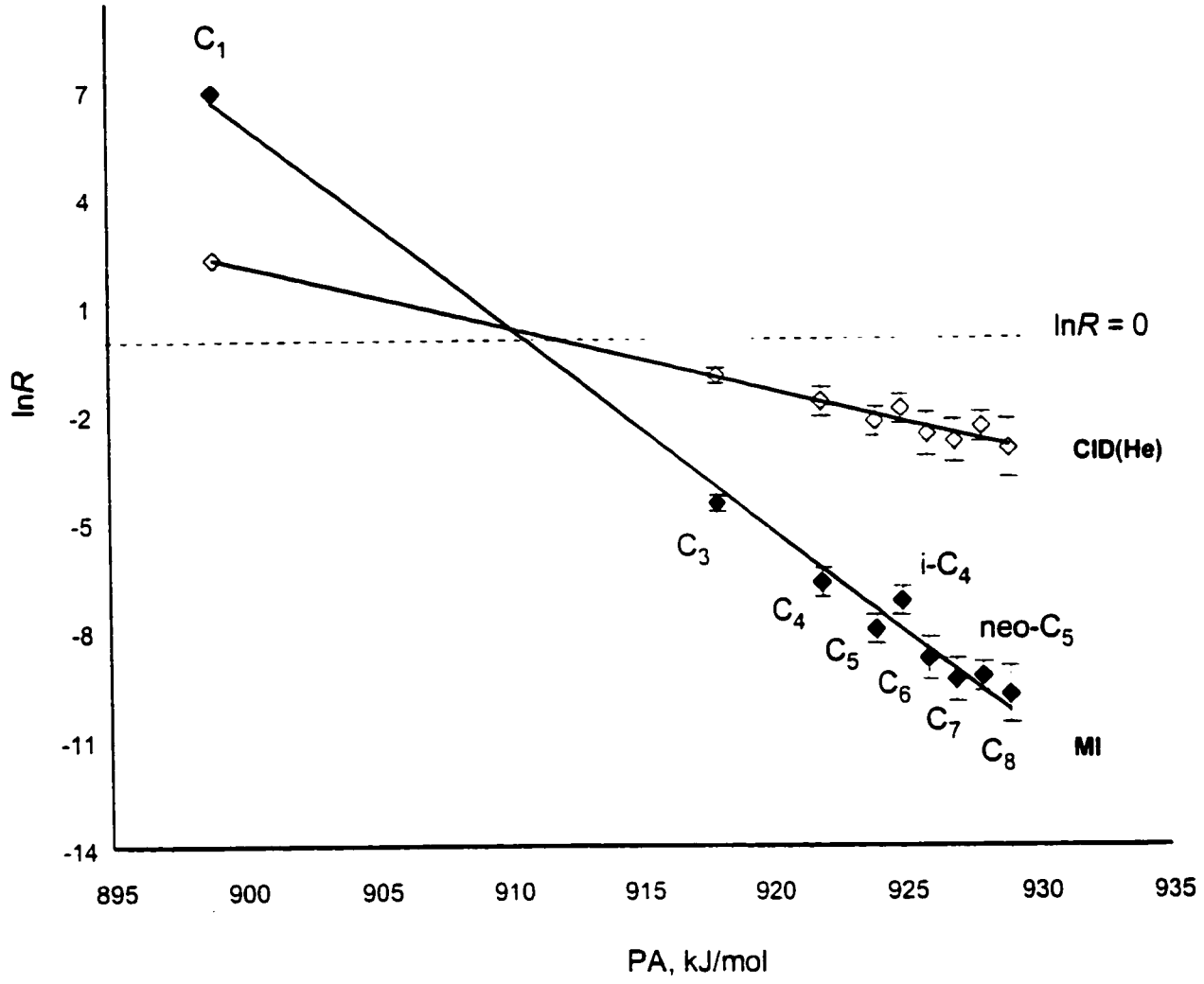

Figure 6.3 ln R vs PA values of n-alkylamines

(I - indicate the errors involved in the measured ratios)

6.4 References

(1) Holmes, J. L. *Org. Mass Spectrom.* **1985**, *20*, 169.

(2) Cerda, B. A.; Hoyau, S.; Ohanessian, G.; Wesdemiotis, C. *J. Am. Chem. Soc.* **1998**, *120*, 2437.

(3) Cao, J.; Holmes, J. L. *Euro. Mass Spectrom.* **1999**, *5*, 19.

(4) Cao, J.; Holmes, J. L. *Int. J. Mass Spectrom.* **2000**, *195/196*, 525.

(5) Cao, J.; Aubry, C.; Holmes, J. L. *J. Phys. Chem. A* **2000**, *104*, 10045.

(6) Holmes, J. L.; Aubry, C.; Mayer, P. M. *J. Phys. Chem. A* **1999**, *103*, 705.

(7) Hunter, E. P. L.; Lias, S. G. *J. Phys. Chem. Ref. Data* **1998**, *27*, 413.

Chapter 7 The proton affinities of simple amines. A test case for the kinetic method

7.1 Introduction

The kinetic method is a now well established technique for determining thermochemical properties such as proton affinities (PA) and gas-phase basicities (GB) and acidities ($\Delta G°_{acid}$). To date, with few exceptions, the kinetic method has been used to relate a known thermochemical datum (or data) with unknown values, most commonly for proton affinities, where the need for PA values for biomolecules has provided a strong incentive. The lack of systematic studies to examine the kinetic method was well brought home by the three recent "commentary" articles in which the method was critically appraised but without any new data being presented.[1-3]

The systematic study of the method for proton affinity measurement has been carried out through a variety of proton-bound pairs of amino compounds with formula R_1NH_2, R_1R_2NH, where R_1 and R_2 are chiefly alkyl groups C_1 to C_9. The results are extended and examined further to α,ω-diaminoalkanes and other selected amines. The proton affinities of most of these amines are well established in the NIST database[4] although some need either to be revised or to be given for new values.

Both metastable and collision-induced dissociations of the proton-bound amine dimers were studied. Particular attention has been given to considering activation entropy effects and the problem of reverse activation energy barriers.

7.2 Experimental

The proton-bound dimers were generated under chemical ionization conditions in the ion source of our modified triple sector (BEE) VG ZAB-2F mass spectrometer by self-protonation. The metastable and collision-induced dissociations of the mass selected proton-bound dimers were studied in the 2FFR of the instrument.

The target gas was He (unless otherwise stated). The observed He pressure required to reduce the mass selected ion flux by ca. 10% (i.e., single collision conditions) was ca. 8×10^{-8} mbar and was used in all these experiments.

Peak heights from the individual scans were used to measure the relative abundances of the fragment ions, the apparatus being set in low energy resolution mode. To separate the CID peaks from MI peaks, a potential of +500V was applied to the collision cell (cell 2), shifting the former to higher translational energies. Care was taken to ensure that neither the sign nor the magnitude of the voltage applied to the collision cell had any significant effect on the relative peak abundances. The CID peak heights were corrected for the small MI contribution.[5-8] Kinetic energy release values were measured by established methods.[9]

The ion source pressure was measured externally using an ion gauge. The ion source temperature was normally maintained at 423 ± 5 K and the inlet system was kept at a similar temperature. Compounds of research grade were purchased from Aldrich Chemical Co (Milwaukee, WI) and used without further purification.

Calculation of the log k vs. internal energy (E) curves were done using the standard RRKM expression, $k(E) = \sigma N^{\neq}/h\rho$ (no rotation effects considered), employing the sums and densities of states calculated via the direct count algorithm of Beyer and Swinehart.[10] The model compound used to generate the curves was the proton-bound dimer of methylamine and ethylamine, and the vibrational frequencies were from *ab initio* calculations. Transition state frequencies were taken as the dimer frequencies and the lowest five were scaled by a scaling factor to achieve a desired $\Delta S^{\neq}$. For $\Delta S^{\neq} < 0$, scale factors >1 were used and for $\Delta S^{\neq} > 0$, scale factors < 1 were used. Results of *ab initio* and RRKM calculations for the proton-bound dimer of methylamine and ethylamine are shown in Appendix II.

7.3 Unimolecular reaction dynamics

A unimolecular reaction is defined as any system that evolves in time as a result of some prior stimulus or excitation step. Thus, both dissociation and isomerization are examples of unimolecular processes. An unimolecular reaction, A → products, is written as:

$$-\frac{d[A]}{dt} = k[A] \qquad 7.1$$

when integrated, equation 7.1 gives rise to the time dependence of the concentration of A(t):

$$[A] = [A_0]e^{-kt} \qquad 7.2$$

where k is the unimolecular rate constant (s^{-1}) and $[A_0]$ is the concentration of species A at time, t = 0.

The connection between k(T), often called the canonical rate constant, and k(E), the microcanonical rate constant, involves averaging k(E) over the energy distribution:

$$k(T) = \int_{E^o}^{\infty} \rho(E, T)k(E)d(E) \qquad 7.3$$

where E° is the activation energy and ρ(E,T) is the distribution of internal energies at a given temperature, T. In many applications the quantity of interest is k(T) because most natural systems can be described adequately by a thermal distribution characterized a given temperature. However, there are many systems that show the importance of studying k(E) as well as ρ(E,T) rather than k(T) - the theory can be tested adequately only by comparing the measured and calculated k(E).

7.3.1 RRKM theory

The earlier version of RRKM used the classical approximation of the absolute rate theory (the oscillators are not quantized, also called RRK theory):

$$k(E) = \nu(1-\frac{E^o}{E})^{s-1} \qquad 7.4$$

where s is the number of oscillators in the molecules (sometimes also called the number of 'degrees of freedom') and E is the internal energy of the precursor ion, E° is the activation energy for the reaction, ν is frequency factor, representing the ratio of the product of vibrational frequencies in the reactants and in the transition state. Note that ν relates to the 'tightness' of the transition state: the tighter a transition state, the lower is the frequency factor.

A better description of unimolecular reactions is the RRKM (developed by Rice, Rampsperger, Kassel and Marcus) or the Quasi-Equilibrium Theory (QET, developed by Wahrhaftig, Rosenstock and coworkers). These theories take into account the quantized nature of vibrations and rotations. It is the RRKM/QET formulation which is the starting point for modern statistical theories.

$$k(E) = \frac{\sigma G^*(E-E^o)}{h\,\rho(E)} \qquad 7.5$$

where σ is the reaction symmetry factor, $G^*(E-E^o)$ is the sum of the vibrational states from 0 to E-E° in the transition state, $\rho(E)$ is the density of vibrational states at the energy E and h is Planck's constant. For simplicity, the role of rotations is not included in the equation.

The RRKM theory predicts that the rate k(E) increases exponentially with the internal energy E. The evaluation of the RRKM equation requires a knowledge of the activation energy, E°, the n vibrational frequencies of the molecule and the n-1 vibrational frequencies of the transition state. All or part of these parameters can be treated as adjustable when fitting experimentally determined rate constants.

The 2n-1 vibrational frequencies of the molecule and the transition state are not completely independent parameters. This is more evident in the canonical, thermodynamic version of transition state theory in which the rate constant is expressed in terms of entropy of activation ($\Delta S^{\neq}$) and enthalpy of activation ($\Delta H^{\neq}$):

$$k(T) = \frac{k_B T}{h} e^{\frac{\Delta S^{\neq}}{R}} e^{-\frac{\Delta H^{\neq}}{RT}} \qquad 7.6$$

$\Delta S^{\neq}$ is evaluated in terms of the vibrational frequencies of the reactant and the transition state.

The entropy of activation ($\Delta S^{\neq}$), as determined from the canonical partition function, provides a quantitative measure of the degree of "tightness" or "looseness" of the transition state.

$$\Delta S^{\neq} = k_B \ln \frac{Q^{\neq}}{Q} + \frac{U^{\neq} - U}{T} = k_B \ln \frac{\Pi q_i^{\neq}}{\Pi q^{\neq}} + \frac{U^{\neq} - U}{T} \qquad 7.7$$

where Q's are the total partition functions, q_i's are the molecular vibrational and rotational partition functions, and *U*'s are the thermodynamic internal energies at the temperature T, at which $\Delta S^{\neq}$ is to be calculated. Tight and loose TS can then be simply defined as follows:

$\Delta S^{\neq} > 0$ Loose TS 7.8

$\Delta S^{\neq} < 0$ Tight TS

The effect on the slopes of the k(E) curves for the dissociation of the bromobenzene ion with various assumed $\Delta S^{\neq}$ from positive to negative, based on the frequencies in Table 7.1, and activation energies are shown in Figure 7.1.[11] It is evident that two parameters can generate a whole family of k(E) curves. Thus, if neither E° nor the transition state structure is known, any set of data can be fitted by RRKM theory. The lower the TS frequencies, the steeper the slope. However, if either E° or if the frequencies are known from calculations, then the RRKM equation reduces to a one parameter model in which either the magnitude of the rate or the slope can be adjusted, but not both.

The frequencies along with their corresponding activation energies were arbitrarily chosen so that the curves would pass through a common point on the graph. The experimentally obtained rates are consistent with an E° of 2.76 eV and a $\Delta S^{\neq}$ of 8.3 cal mol^{-1} K^{-1}.[12,13] Clearly from a given data set in which k(E) has been measured over some energy range, it is possible to extract both the $\Delta S^{\neq}$ and E°.

The RRKM theory not only provides a simple and quantitative means for distinguishing loose and tight transition states but it also provides a means for comparing the microcanonical rate data with canonical data in which $\Delta S^{\neq}$ is extracted directly from the TST analysis of the data. The usual temperatures at which $\Delta S^{\neq}$ are reported are 600 and 1000 K because these are in the range of the usual thermal data.

Table 7.1 The vibrational frequencies used for k(E) curves of Figure 7.1

Molecular ion	3054(5), 1518(4), 1292(2), 1053(8), 821(3), 654(3), 460(1), 409(1), 315(1), 254(1), 181(1)
TS	3054(5), 1518(4), 1292(2), 1053(8), 821(3), 654(3), Y(5)
where Y(5) is	650, 450, 332, 245, 160, 115, 92 and 40 cm^{-1} for curves 1 through 8

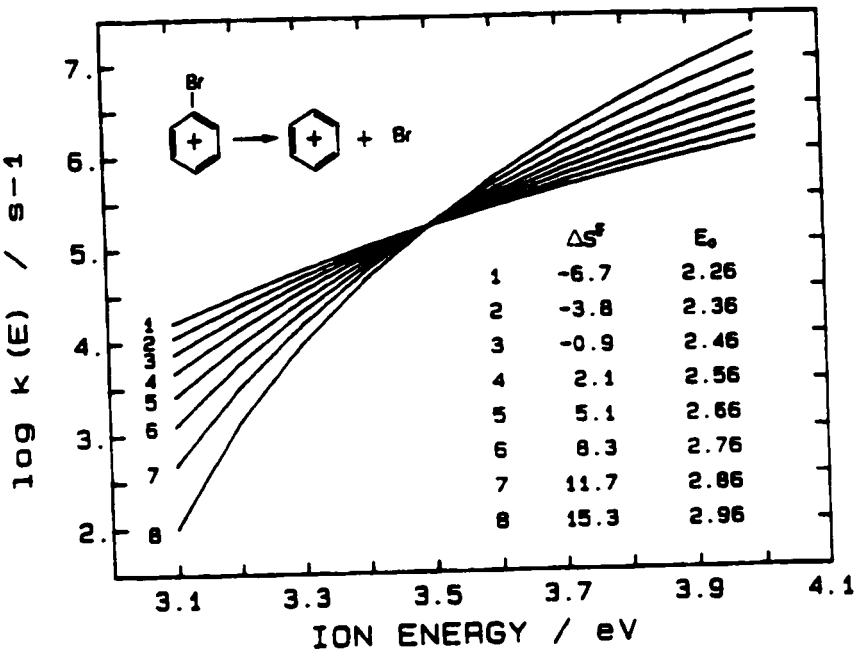

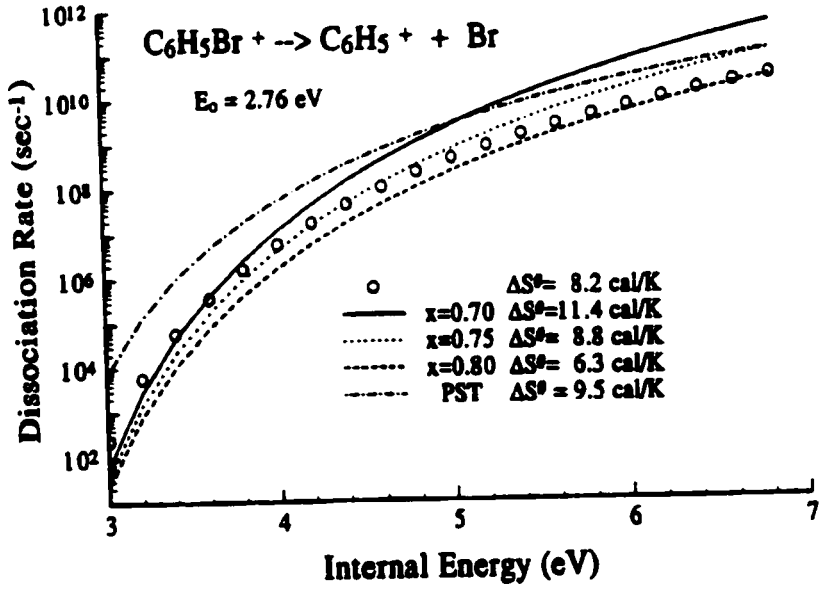

Figure 7.1 (A) Calculated k(E) curves for the bromobenzene ion dissociation in which the vibrational frequencies and the activation energies are varied, thereby providing k(E) curves with different slopes; (B) Calculated k(E) curves for bromobenzene ion. The open circles are obtained by lowering the last five vibrational frequencies to 115 cm^{-1} in the transition state. The PST(phase space theory) rate constant had the lowest two frequencies replaced by free rotors, while in the other three lines all transition state frequencies were multiplied by the indicated factor.[10]

7.3.2 Application of the RRKM theory to the dissociations of proton-bound dimers

For an homologous series of molecules, B_n, joined in pairs by a proton, it is reasonable to propose that the log k vs. E curves for the species' dissociation into the two protonated monomers will be essentially parallel to each other, separated by the difference in their proton affinities. This applies when $\Delta(\Delta S^{\neq}) = 0$, a common assumption when homologous series are being investigated. For the kinetic method to be used to measure the proton affinity of an untested homologue, B_1, there are still some more assumptions which need to be considered.

1. That the internal energy distributions of $B_1H^+B_n$ ions dissociating as metastable ions are the same, irrespective of the species, B_1 and B_n. This appears to be a reasonable assumption provided that the distribution of the relevant internal energies is a simple exponential function.[5]

2. That the same criterion (but of course, a different internal energy distribution) applies to $B_1H^+B_n$ ions activated by high translational energy collisions. Note that the criterion of essentially parallel log k vs. E curves does not rule out the possibility that the entropies of activation, $\Delta S^{\neq}$, are non-zero, but only requires that the entropies of activation for dissociating $B_1H^+B_n$ ions be *the same* i.e., $\Delta(\Delta S^{\neq}) = 0$.

3. That the competing dissociations have no reverse energy barrier. This is a reasonable assumption, especially when the dissociation can be viewed as a

simple bond cleavage. If however, the reverse reaction required a considerable geometry change in either reactant, this assumption may no longer apply. It has been customary to measure the kinetic energy releases associated with each reaction channel. Typically for metastable $B_1H^+B_n$ ions the $T_{0.5}$ values have been 15-25 meV,[6-8,14] a range believed to be compatible with the cleavage of a simple covalent bond. Note however that this argument may be incorrect; if the bond is largely electrostatic in character and the transition state has no well defined reaction coordinate (e.g., the $[CH_2CH_2OH_2]^{+\bullet}$ ion dissociation by loss of H_2O[15,16]) then the kinetic energy release can be very small indeed, < 1meV. If such a metastable ion had a large internal energy content, by for example being accessed via an energy barrier, a larger kinetic energy release would result.

In the ensuing discussion, assumptions 1-3 will initially be taken as correct, but will be modified as and when necessary.

Figures 7.2 (A) and (B) illustrate, as an example, the effect of activation entropy on the curvature of calculated log k vs. E curves for two competing dissociations with an activation energy difference of 7 kJ mol^{-1}. If both dissociations have negligible entropies of activation (Figure 7.2 (A)) their log k vs. E curves are essentially parallel within the MI rate constant range which is from ca. $10^3 - 10^6$ s^{-1}. Note however that they do tend slowly to converge at high internal energies. In Figure 7.2(B), the greater curvature of the lower energy dissociation channel's plot arises from the transition state for this dissociation being *tighter* than that for the

reaction of higher energy, (i.e., $\Delta\Delta S^{\neq}$, the activation entropy difference between the lower and higher energy channels, is negative. This convention is used throughout this work). The curves cross and this intersection in the example shown is at the upper end of the metastable ion time window. Note that the smaller the activation energy difference between the two competing dissociations (in the present case the difference in PA), the more susceptible the system becomes to such entropy effects (i.e., the more likely the curves will cross). If however the transition state for the higher energy process is *looser* than that for the other dissociation channel (Figure 7.2 (C)), then the curves will diverge. Experimentally, this should result in a CID ratio being greater than the MI ratio.

To illustrate and confirm the effect of very different log k vs. E curves for competing reactions a completely independent and well studied system was selected. The ionized butylbenzene dissociations were recorded in the MI and CID regimes:

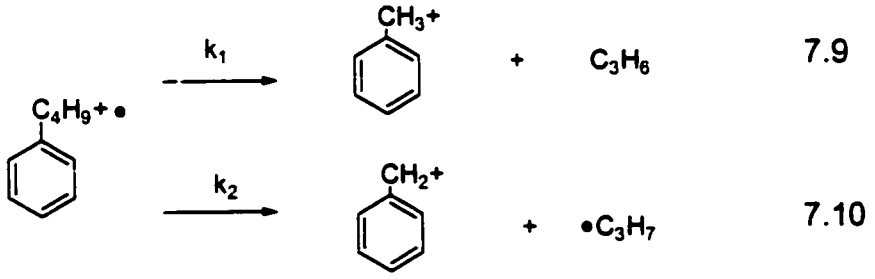

From results of Baer et al.,[17] it is known that for this system the log k vs. E curves for reactions 7.9 and 7.10 cross at $k \approx 10^{7.5}$ s^{-1} with the activation energy

difference $E_2° - E_1° \cong 60$ kJ mol^{-1} and $\Delta S_2^{\neq} - \Delta S_1^{\neq} \cong 44$ J mol^{-1} K^{-1} (see Figure 7.3). The MI ratio (k_1/k_2) was 82 and this inverted, becoming 0.46, in the CID. The CID result was obtained using He, O_2 and Xe as target gases and the ratio was target gas independent, as has been found for all our recent kinetic method studies.[5-8] Target gas densities were the same for each gas and the pressures were well below single collision conditions. Corrections for other collision-induced dissociations were minimal at such pressures.

Consider the absolute rate theory representation of the kinetic method, given by the equation

$$\ln\frac{k}{k_n} = \ln\frac{Q^{\neq}}{Q_n^{\neq}} + \frac{[PA(B) - PA(B_n)]}{RT_{eff}} \qquad 7.11$$

$$= \ln R = \ln\frac{Q^{\neq}}{Q_n^{\neq}} + \frac{\Delta PA}{RT_{eff}}$$

where ΔPA is the difference between the proton affinity of the unknown, B, and the standards B_n. If there is no net difference in entropy of activation, $Q^{\neq} = Q_n^{\neq}$, then

$$\ln R = \frac{\Delta PA}{RT_{eff}} \qquad 7.12$$

If for all MI dissociations the internal energies of the various fragmenting $B_1H^+B_n$ ions are the same, then a plot of ln*R* vs. PA(B_n) will produce a straight line. With the same proviso for collision-induced dissociations a second straight line (of different slope) will be generated. These lines should intersect at ln*R* = 0 and give

PA(B) at that point. If $\Delta\Delta S^{\neq}$ is not zero, then the intercept of each line on the ln*R* = 0 axis occurs at an *apparent gas phase basicity* value. These in turn are internal energy dependent (because a term "$T\Delta\Delta S$" is involved) and the intercept values will not therefore be identical for MI and CID plots. The lines will then cross above or below the ln*R* = 0 axis. Above, if the $\Delta S^{\neq}$ for B is greater than zero and below if $\Delta S^{\neq}$ is less than zero, relative to any activation entropy for the standards, B_n. Figure 7.4 illustrates these three situations just mentioned. The point at which the lines cross gives the PA for the base under investigation.

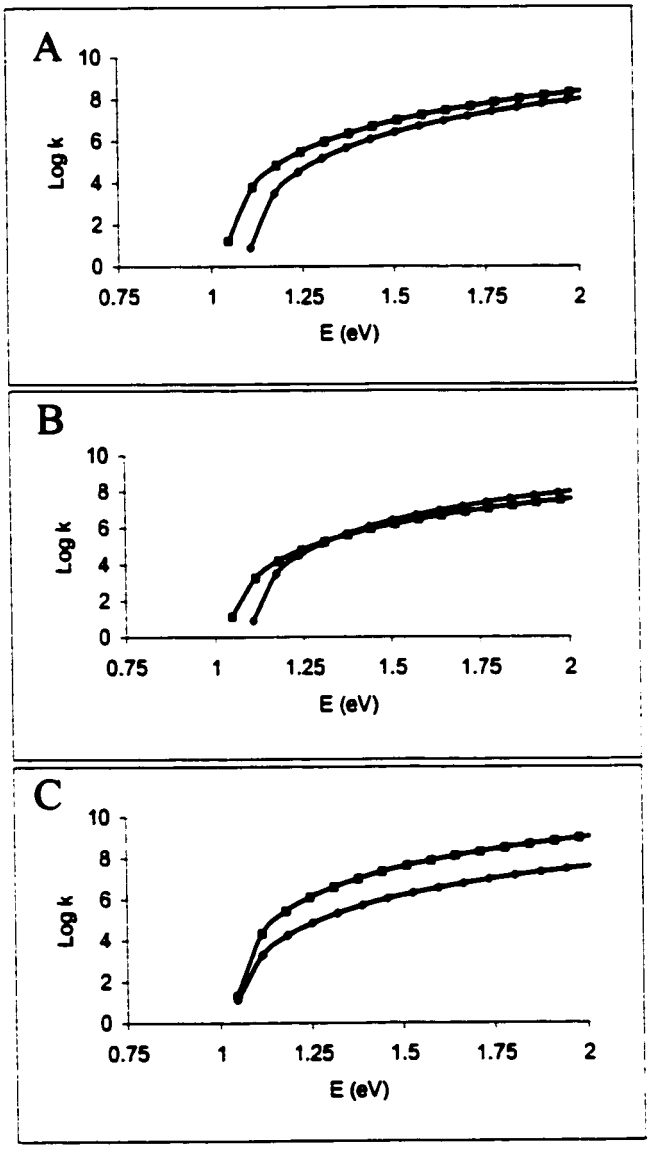

Figure 7.2 Log k vs. E curves for two competing dissociations of the proton bound dimers (A) $\Delta\Delta S^{\neq} \cong 0$ and $\Delta PA = 7$ kJ mol^{-1}; (B) $\Delta\Delta S^{\neq} =$ -16 J mol^{-1} K^{-1} and $\Delta PA = 7$ kJ mol^{-1}; (C) $\Delta\Delta S^{\neq} =$ +30 J mol^{-1} K^{-1} and $\Delta PA = 7$ kJ mol^{-1}

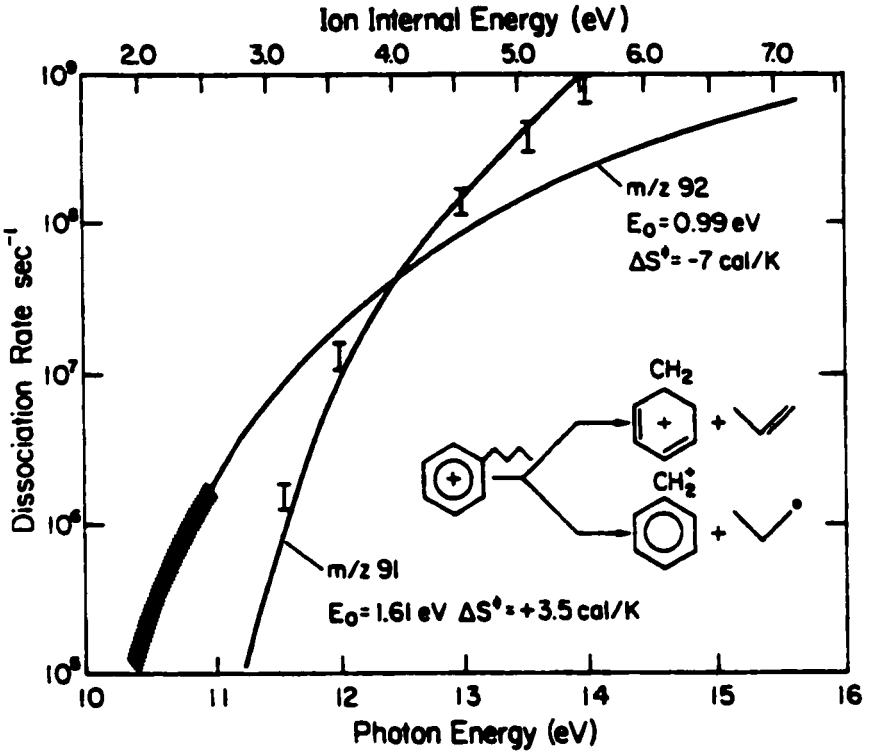

Figure 7.3 Rates for the production of m/z 92 and 91 in the dissociations of ionized butylbenzene. The results are generated from both experiment marked with hatched region or vertical lines with error bars and RRKM calculations (solid lines)[17]

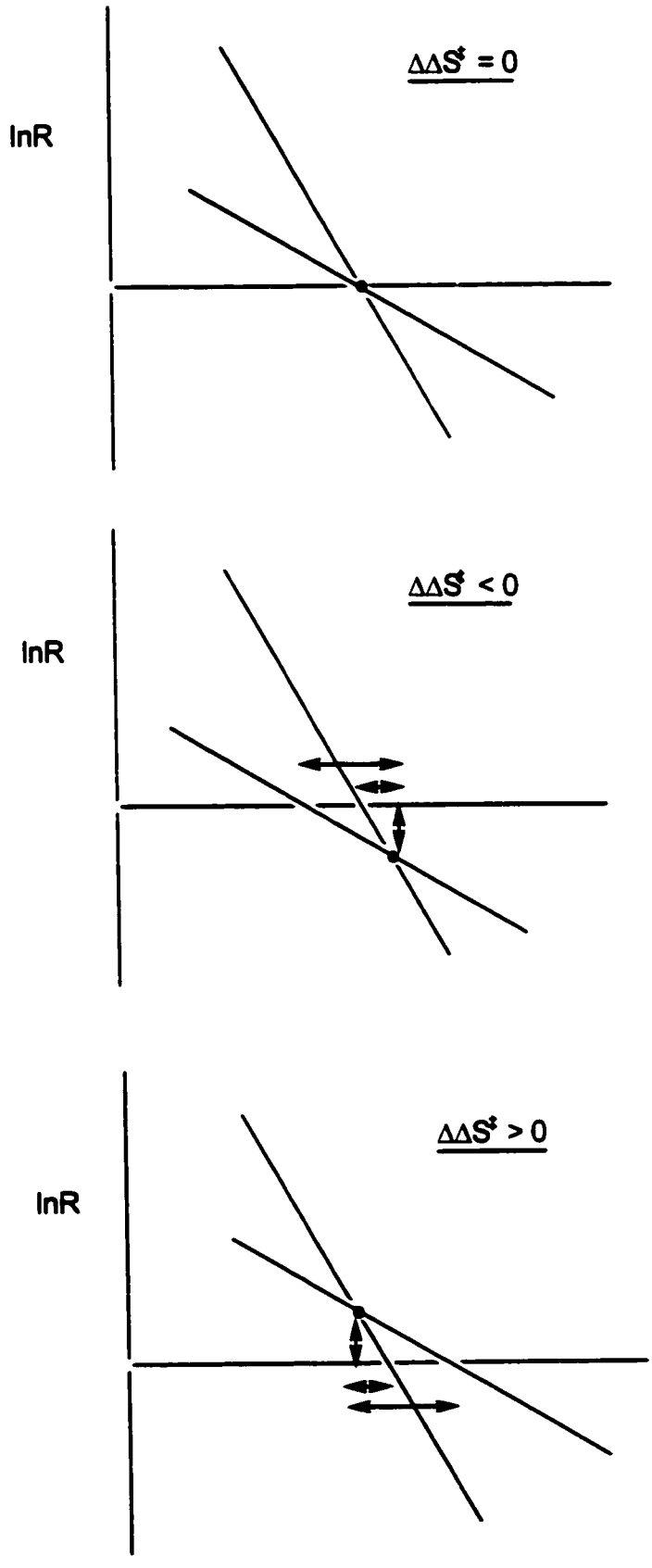

Figure 7.4 Graphical approaches to derive PA for the unknown

7.4 Results and discussion

7.4.1 Dissociation characteristics of proton-bound dimer of amines

The MI and CID mass spectra of the proton-bound dimer ions were both dominated by the production of the two protonated monomers; other fragment ion abundances were negligibly small.

Three other observations must now be discussed. The fraction of the adduct ion flux that dissociated in the FFR was dependent on the measured ion source pressure, but ln*R* was essentially independent thereon. For the proton-bound dimer of n-$C_4H_9NH_2$ and n-$C_3H_7NH_2$, the flux of adduct ion increased by a factor of ca. 800 over the ion source pressure range 10^{-5} to 10^{-4} mb, and the degree of dissociation dropped from 12% at the lower pressure (10^{-5} mb) to 3% at the higher pressure (10^{-4} mb). Thus, a greater proportion of the cluster ions are being "cooled" at higher ion source pressures (i.e., their internal energy distribution is shifted toward lower internal energy). However, the ratio of [n-$C_4H_9NH_3^+$]/[n-$C_3H_7NH_3^+$] remained in the range of 9 ± 2. The value of R was also unchanged within the same experimental reproducibility by altering the ion source temperature from 320 to 550 K (Table 7.2). The same effect was observed for the isolated CID ratios.

Table 7.2 Ion source temperature effect on the product ion ratio of the proton-bound dimer of n-$C_5H_{11}NH_2$ and n-$C_4H_9NH_2$

T(°C)	50	100	120	150	200	230	250	280
ln*R* (MI)[a]				9 ± 2				
ln*R* (CID)[b]				2 ± 0.2				

a) R=[n-$C_5H_{11}NH_3^+$]/[s-$C_3H_7NH_3^+$]

b) Helium as collision gas, +500 V on the collision cell in 2FFR

It is apparent therefore that the internal energy distribution of the adduct ions, which was clearly dependent on ion source pressure and temperature, has little or no effect on the metastable and collision- induced dissociations. The internal energy segments to observe MI and CID dissociations are $E_1° - E_2°$ and from $E_1°$ and $E_2°$ to ∞, $E_1°$ and $E_2°$ are the activation energies for the dissociations. By changing an experimental parameter, e.g., ion source pressure or temperature, it is not possible to significantly alter the ratio of adduct ion fragmentations expressed as the relative areas under the corresponding energy segments, but only the fractions of the total number of ions that could fragment in the corresponding time-frames. Thus, the ratio of the fragment ion abundances is independent of the adduct ion internal energy distribution in these experiments.

Collision gas effects including the nature of target gas as well as its pressure were studied by examining the *isolated* CID ratios of the proton-bound dimer of n-$C_4H_9NH_2$ and n-$C_3H_7NH_2$. It is commonly known that internal energies of the

dissociating ions are greatly increased with introduction of the collision gas and they are proportional to the pressure of the gases. For example, the degree of dissociation was ca. 8% at pressure of $4x10^{-8}$ mb and ca. 25% at pressure of $1x10^{-7}$ mb (He). As a comparison, the fraction of dissociation for the MI process was ca. 3%. Note that all of the observations were made under the same ion source pressure of 10^{-4} mb.

The isolated CID ratio was independent of both the nature of the collision gases and their pressures. For example, the *isolated* CID ratio, 2.0 ± 0.2, was insensitive to collision gas (He) pressures from $2x10^{-8}$ mb to $1x10^{-6}$ mb, showing that the small fraction of multiple collisions at the higher pressure did not effect the results. The same ratio was observed for other collision gases (O_2, Ar, Xe). However, the mixed CID ratio was variable with either of the two (see Table 7.3). Note that different collision gases do not produce significantly different internal energy distributions of the ions under the same collision conditions (i.e., single collision conditions) because a similar fraction of ions that dissociate are observed irrespective of the fact that they have different collision cross sections.

Table 7.3 Observation of collision gas effect for the pair of $n\text{-}C_4H_9NH_2$ and $n\text{-}C_3H_7NH_2$

				He			
$P(x10^8, mb)$	2	4	6	9	15	40	100
R_{iso}[a]	2.1	2.0	2.0	2.0	2.0	1.9	1.8
R_{mix}[b]	8	5.2	4.1	3.4	3.1	2.6	2.3
				O_2			
$P(x10^8, mb)$	5	12	40	200			
R_{iso}	2.0	2.0	2.0	1.9			
R_{mix}	6.9	4.8	3.4	2.6			
				Ar			
$P(x10^8, mb)$	6	25	60	500			
R_{iso}	2.0	2.0	2.0	1.8			
R_{mix}	6.3	4	3	2.2			
				Xe			
$P(x10^8, mb)$	20	50	130	800	1500		
R_{iso}	1.9	1.9	1.9	1.8	1.7		
R_{mix}	6.2	3.4	2.4	2.3	2.2		

a) $R_{iso} = [n\text{-}C_4H_9NH_3^+]/[n\text{-}C_3H_7NH_3^+]$ with +500 V on the collision cell in 2FFR

b) $R_{mix} = [n\text{-}C_4H_9NH_3^+]/[n\text{-}C_3H_7NH_3^+]$ without charges on the cell

7.4.2 Alkylamines

In Figure 7.5 the $\ln(B_1H^+/B_nH^+)$ values are plotted with $C_2H_5NH_2$ as the unknown using NIST[4] data and our reported results[7] for PA values of the partner amines. Table 7.4 lists all the values relevant to this study. Note that the data in Table 7.4 are from the NIST database and are derived from equilibrium measurements, unless indicated otherwise. The uncertainty in the NIST values is quite small and rarely exceeds ± 3 kJ mol^{-1}. The reversal of the NIST values for n-$C_6H_{13}NH_2$ and n-$C_7H_{15}NH_2$ is certainly incorrect and in figures where these are required, our revised PA values[7] will be used.

In keeping with the requirement that $\ln(Q_1^*/Q_n^*)$ is zero, the line for the metastable ion results crosses that for the CID observations very near to $\ln R = 0$, and gives a PA of 910 kJ mol^{-1}, within experimental error the same as the reference value for $C_2H_5NH_2$, 912 ± 2 kJ mol^{-1}.[4]

Entropies of protonation[4] are closely similar for primary amines and so the above result is perhaps not unexpected, although it should strongly be emphasized that this being a kinetic method, *transition state* rather than product entropies must apply to the observations.

The kinetic energy release accompanying the metastable ion dissociation of the proton bound amines was typically ca 15 meV, as obtained from the half height

width of the energy resolved peak. For collisionally excited ions KER was ca 30 meV, in keeping with these ions' having a higher energy content.

Table 7.5 Kinetic energy release (KER) values of metastable and collisionally activated $(n\text{-}C_4H_9NH_2)H^+(n\text{-}C_3H_7NH_2)$

Proton-bound dimer	KER (meV)					
	MI		*Isolated* CID		Mixed CID	
	m/z 60	74	60	74	60	74
$C_4H_9NH_3^+..C_3H_7NH_2$	14	15.3	32.1	27.3	30.8	24.0

It was reported[7] that for t-butylamine, there was an *inversion* of ln*R* values for MI and CID observations when the PA of the reference n-alkylamine became close to but less than the PA of $t\text{-}C_4H_9NH_2$, 934 ± 3 kJ mol^{-1} (derived from equilibrium studies[18]). This inversion was *not* reproducible and careful repeat experiments produced the results shown in Figure 7.6. The lines cross close to ln*R* = 0, eliminating the possibility of an entropy of activation; the derived PA value for t-butylamine, 930 kJ mol^{-1}, is slightly but significantly lower than the reference value. Note that for a value of 934 kJ mol^{-1} to be obtained in the present experiment, either all the reference PA values have to be too low by 4 kJ mol^{-1} (e.g. moving the MI line bodily to the right) or some of the reference PA values have to be in error beyond the NIST quoted limits. This seems unlikely given the close fit of the data to a line.

Before leaving the t-$C_4H_9NH_2$ result, the effect of a reverse energy barrier in lowering the PA obtained by the kinetic method cannot be ignored. There are fifteen values quoted in reference 4 for this PA, all in close agreement. To force the result in Figure 7.6 to give a cross-over at 934 kJ mol^{-1}, all the reference PA values for C_5 to C_9 would have to be too low by up to 4 kJ mol^{-1}. We feel that this is unlikely and we propose that the above low value arises from a small reverse energy barrier, (E_{rev}). Note that the KER for the formation of protonated t-butylamine is *not* significantly larger than that of n-alkylamine and so does not sensitively probe a small reverse energy barrier for the corresponding reaction. The existence of a reverse energy barrier can make the measured ratios not a reflection of the true PA difference (ΔPA), but the energy difference between the two transition states instead ($\Delta E°$). Figure 7.7 presents the potential diagram for the dissociations of the proton-bound dimer, one of which has a reverse energy barrier. This problem will also arise later with the observation on diaminoalkanes.

An additional evidence to support the proposal that a small reverse energy barrier towards the reaction to form protonated t-$C_4H_9NH_2$ is that the reaction 7.13 involves a large E_{rev} (KER ≅ 10 kJ mol^{-1}) indicating a large, energy demanding geometry change. Therefore, it is quite reasonable that a similar but smaller E_{rev} (ca. 4 kJ mol^{-1}) could well apply to the reaction of $(CH_3)_3CNH_3^+ \rightarrow (CH_3)_3CNH_2 + H^+$.

$$(CH_3)CNH_2^{+\bullet} \longrightarrow (CH_3)_2C^+NH_2 + \bullet CH_3 \qquad 7.13$$

Note that the above graphical approach is not radically different from that adopted by Fenselau et al.[19] who however evaluated a quasi temperature term (T_{eff}) from the slopes of such plots. The absolute magnitude of the entropy of activation cannot be evaluated without a knowledge of the internal energies of the fragmenting ions. We have already indicated doubts as to the application of equilibrium thermodynamics to such systems, particularly with regard to metastable dissociations where T_{eff} was shown to not correspond to a thermodynamic temperature.[5]

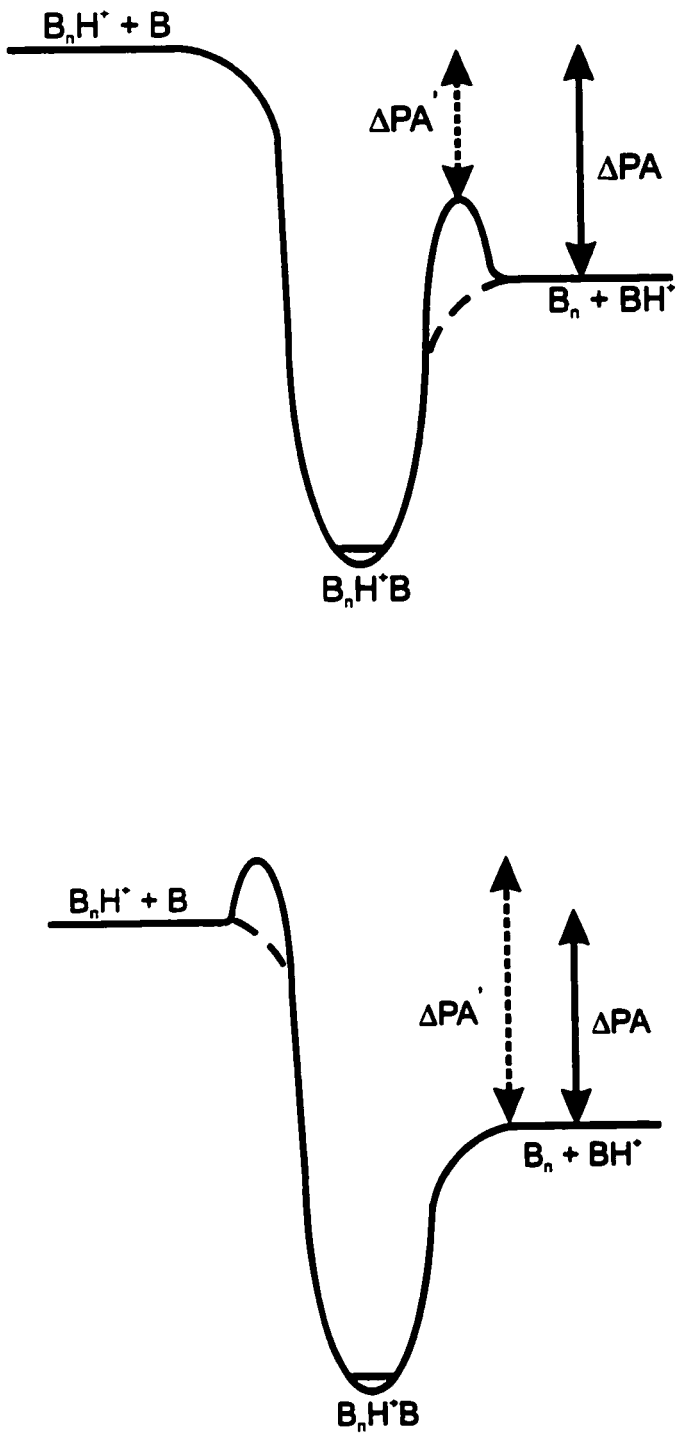

Figure 7.7 Potential diagram for the competing dissociations of proton-bound dimers, one of which has a reverse energy barrier (E_{rev})

A similar result was obtained for s-propylamine as an unknown (Figure 7.8). The cross-over point was at ln$R$ = 0 and the PA thereat, 922 kJ mol^{-1}, is within experimental error the same as that given in the reference data (Table 7.4).

It was useful to extend and replot the data obtained earlier for benzylamine,[7] where the NIST value appeared to be too low by at least 10 kJ mol^{-1}. Figure 7.9 shows the analogous graph for benzylamine vs. a series of n-alkylamines. The MI and CID lines cross close to ln$R$ = 0, giving a PA value for benzylamine of 924 kJ mol^{-1} and indicating moreover that there is apparently no significant *net* entropy of activation effect for this phenyl substituted amine. It is noteworthy that the gas phase basicity values given in the NIST tables are 879.3, 879.3 and 891.8 kJ mol^{-1}; the first two provide the listed PA value, 913 kJ mol^{-1}, whereas the latter gives a PA of 926 kJ mol^{-1} in good agreement with the present result. Also shown in Figure 7.9 are the ln$R$ values when t-butylamine was used as an additional standard. The data points are displaced from the n-alkylamine MI and CID lines by the difference between the reference and the new (cross-over) PA values, providing support to the suggested E_{rev} for t-$C_4H_9NH_2$.

7.4.3 Other selected amines

When averaged ln$R$ values are used, allylamine and pyridine appear to fit the plots for primary amines shown in the Figure 7.10 very well; the aromatic amines, benzylamine and 2-phenylethylamine, are less satisfactory.[7] If these molecules are to fit the line for n-alkylamines then the PA values for benzylamine needs

considerable revision upwards, from 913 kJ mol^{-1} to ca. 924 kJ mol^{-1}; 2-phenylethylamine may be too high, but only by ca 5 kJ mol^{-1}. The proposed PA value for benzylamine is in good agreement with the one obtained in the Figure 7.9.

Figure 7.10 was constructed as such that the anchor point for s-ions, s-$C_3H_7NH_2$ was measured against n-$C_4H_9NH_2$ and the others were measured relative to s-$C_3H_7NH_2$. Similarly, t-$C_4H_9NH_2$ was measured relative to n-$C_3H_7NH_2$. Note that beginning with s-C_4, the ln*R* values for sec-sec proton bound pairs are larger than for the corresponding s-n proton bound pairs, and t-n pairs behave likewise. This may arise from the proposed small reverse energy barriers for the generation of protonated s- and t-species. However, this effect can be canceled out when pairing s-s, t-t.

7.4.4 Dialkylamines

The kinetic method plots for dialkylamines having established PA values[4] are shown in Figure 7.11, the reference data are in Table 7.4, with new (estimated) values for $(C_5H_{11})_2NH$, $(C_6H_{13})_2NH$ and (CH_3)(n-C_6H_{13})NH derived from ln*R* results. Results for $(CH_3)(C_4H_9)NH$ are shown in Figure 7.12. The MI and CID lines intersect at ln*R* = 0, giving a PA value of 951 ± 4 kJ mol^{-1} for $(CH_3)(C_4H_9)NH$. Also shown in Figure 7.11 are the results for (s-$C_3H_7)_2NH$ and (s-$C_4H_9)_2NH$. The ln*R* values for these di-sec-alkylamines, relative to other di-n-alkylamines, are not well compatible with their NIST PA values, 972 ± 2 and 981 kJ mol^{-1} respectively, which appear to be too high. These di-sec-alkylamines were measured as unknowns vs. di-n-

alkylamines and the results are shown in Figure 7.13. The cross-over points are close to ln$R$ = 0 and are at 968 and 976 kJ mol^{-1} respectively, both below the reference PA values. An entropy effect alone would have given a cross-over point significantly below or above ln$R$ = 0 but at the reference PA value. These results mirror that for t-$C_4H_9NH_2$ and we again suggest that for these compounds too, E_{rev} is not zero but ca. 4-5 kJ mol^{-1}.

It is worth noting that the effect of ion size on the proton affinities of the di-n-alkylamines in which both substituents increase by a CH_2 group produce a smooth asymptotic curve, Figure 7.14. Also included in this Figure are $(C_5H_{11})_2NH$ and $(C_6H_{13})_2NH$ and these PA values are shown in Figure 7.11. That these values fall on the PA vs. size curve indicates that they are certainly reasonable.

Intermediate species with mixed alkyl groups have PA values which depend on the nature of the substituents rather than the size of the ion as a whole. This is also illustrated in Figure 7.14. Thus for example, single substitution in $(CH_3)_2NH$ has very close to the same effect as alkyl group change in CH_3NH_2, but double substitution has less than twice the effect e.g. $CH_3NH_2 \rightarrow C_2H_5NH_2$, ΔPA = 13 kJ mol^{-1}; $(CH_3)_2NH \rightarrow (C_2H_5)_2NH$, ΔPA = 23 kJ mol^{-1} (see Table 7.4). Now we must consider the s-C_3H_7 and s-C_4H_9 species. From the NIST data, $CH_3NH_2 \rightarrow$ s-$C_3H_7NH_2$, ΔPA = 25 kJ mol^{-1}; $CH_3NH_2 \rightarrow$ s-$C_4H_9NH_2$, ΔPA = 31 kJ mol^{-1} and $(CH_3)_2NH \rightarrow (s\text{-}C_3H_7)_2NH$, ΔPA = 42 kJ mol^{-1}; $(CH_3)_2NH \rightarrow (s\text{-}C_4H_9)_2NH$, ΔPA = 51 kJ mol^{-1}, a remarkably consistent series of changes. This consistency is lost if the

cross-over values are used. This circumstantial result lends some support to the proposed E_{rev} effect.

Finally, to search for any activation entropy effects (or reverse energy barrier), selected di-n-alkylamines, as unknowns, were run with a series of n-alkylamines. The difference in PA values is not too great for $(CH_3)_2NH$, but for the higher homologues chosen, $(n\text{-}Pr)_2NH$ and $(n\text{-}Bu)_2NH$, only CID observations could be made (MI ratios would exceed 10,000 and so be subject to collisional activation by residual gas in the FFR). The results are shown in Figure 7.15.

For $(CH_3)_2NH$, the cross over point is close to $\ln R = 0$ giving a PA $(CH_3)_2NH$ = 926 kJ mol^{-1}. At the reference value for $(CH_3)_2NH$, 930 kJ mol^{-1},[4] nonylamine and t-butylamine are significantly favored as the proton carrier. Note that the above cross-over PA value for t-butylamine, 930 kJ mol^{-1}, is shown in Figure 7.6 and is very close to the line, consistent again with the above arguments.

Is the lower PA observed here for $(CH_3)_2NH$ due to an entropy of activation or a small reverse energy barrier for the dissociation in which the dialkylamine retains the proton? The former is unlikely; a $\Delta S^{\neq}$ acting against $(CH_3)_2NH$ would lead to a cross over point *below* the x-axis at PA = 930 kJ mol^{-1}. The wealth and narrow range of data[4] for the PA $(CH_3)_2NH$ again leads us to suggest that for this dialkylamine and its homologues a small E_{rev} effects the kinetic method observations.

For $(n\text{-}Pr)_2NH$ the *extrapolated* CID line intersects the PA axis at the reference value for this amine. The $(n\text{-}Bu)_2NH$ line crosses the axis at 964 kJ mol^{-1}, reasonably close to the NIST value, 968 kJ mol^{-1},[4] considering the long extrapolation involved, a clear identification of an E_{rev} for these species cannot be confirmed.

Thus for all the n-alkyl and di-n-alkyl amines studied here, there are *no* clear effects in their "kinetic method" behavior which can be ascribed to activation entropies. There appears in some cases to be a small reverse energy barrier as considered above.

7.4.5 α, ω - diaminoalkanes

In a recent study by Siu et al.,[20] low translational energy collision-induced dissociations of α,ω-diaminoethane through pentane were described. In that work, three or four di-alkylamines were used as standards. For the ln*R* vs. PA (standard) plots, the slope was related to an apparent temperature. However, the "apparent PA" (where the ln*R* vs. PA (reference molecule) line crossed the x-axis) was plotted against the translational energy of the ions, which typically was varied from ca. 0.6 to 2.5 eV. The intercept at zero volts was proposed to give the true PA value for the di-aminoalkane. Calculations were also presented, using density functional theory, to describe the energies and equilibrium geometries of the protonated diamines and their adducts with some simple di-alkylamines. The above approach sidestepped the problem of using the apparent temperature in the determination of the PA. They

did however report that when an apparent temperature was extracted from the data and the method of Fenselau et al.[19] was applied, the resulting PA values were always higher than those derived from the apparent PA vs. ion energy graphs.

7.4.5.1 1,2-diaminoethane

The reference PA for this molecule, 952 ± 3 kJ mol^{-1},[4] is sufficiently low that both n-alkyl and di-n-alkyl amines can be used as standards. The results for MI and CID experiments are shown in Figure 7.16. The crossover point is not on the x-axis and the PA thereat, 949 kJ mol^{-1}, is close to the reference value. For collision-induced dissociations there appears to be a significant $\Delta S^{\neq}$ effect, acting against the diamino compound and giving an apparent $\Delta G^{\neq}$ of 935 kJ mol^{-1}.

Note too the inversion from positive to negative of ln*R* for $(CH_3)(C_2H_5)NH$ and for $(C_2H_5)_2NH$, whose PA is the same as that of 1,2-diaminoethane, both ln*R* values are negative. Note also that the t-butylamine PA of 930 kJ mol^{-1} appears again to be justifiable. If our E_{rev} argument for the di-n-alkylamines is also correct, then the heavy lines in Figure 7.16 should be moved 4 kJ mol^{-1} to the left. The cross-over point moves to 945 kJ mol^{-1} and the intercepts to 941.5 and 931 kJ mol^{-1} for MI and CID observations, respectively. The $\Delta S^{\neq}$ effect is unchanged but the cross-over PA, 945 kJ mol^{-1}, is now 7 kJ mol^{-1} below the NIST value.[4]

Also shown in Figure 7.16 are data from the work of Siu et al.[20] (open circles); these results were for the lowest translational energy for this

diaminoalkane, 0.8 eV. As with their corresponding data at 1.5 and 2.0 eV translational energy, the three points are poorly colinear. The three intercepts for the three energies were 940, 940 and 938 kJ mol^{-1}, respectively. Their extrapolated PA value was 942 kJ mol^{-1}, and their calculated value was 959 kJ mol^{-1}. It is curious that their ln*R* values are close to our results for high translational energy collisions, implying that the internal energies of the CID ions from the two experimental methods were similar. This however does not hold for the larger diaminoalkanes described below.

The new results here are in keeping with the calculations of Siu et al.[20] In protonated 1,2-diaminoethane, the ion is only weakly bidentate, with a long $-NH_3^+ \cdots H_2N-$ bond, 1.87 Å (supplementary data, Siu et al.[20]). From the data presented for protonated 1,4-diaminobutane, coordination with an amino substrate lengthens the above bond from 1.54 to 1.76 Å, relaxing the bidentate structure. Considering the reverse reaction for the 1,2 compound, $R_2NH + H_3N^+CH_2CH_2NH_2$, a small activation energy may be required to allow the dialkylamine to achieve the optimum distance from the $-NH_3^+$ group. For the forward reaction, it is clear that the activation entropy for the looser transition state leading to $R_2NH_2^+ + H_2NCH_2CH_2NH_2$ will be greater than that for the proton remaining with the diamine.

7.4.5.2 1,3-diaminopropane

In the same study Siu and coworkers[20] reported a PA for this compound of 971 kJ mol^{-1}, the translational energy range used was 0.6 to 2.0 eV. The NIST PA

value for this molecule is 987 ± 2 kJ mol^{-1}.[4] Their calculated value was again higher, 992 kJ mol^{-1}.

A problem which arises in the above study concerns the PA of di-isobutylamine, whose PA should (by analogy with the monoamines) be greater than that of di-n-butylamine. The NIST values are 958 and 968 kJ mol^{-1},[4] respectively. Accordingly we have measured the ln*R* values for di-isobutylamine against other di-alkylamines (Figure 7.17) and the derived PA, 969 ± 4 kJ mol^{-1} shows that the NIST value is indeed too low by ca. 11 kJ mol^{-1} (see also Figure 7.11 and Table 7.4). Moreover, this properly reflects the difference between the corresponding simple alkylamines. Replotting Siu's data using the revised PA value for di-isobutylamine gives better lines and an extrapolated PA (by their method) of 975 kJ mol^{-1}.

Our results for 1,3-diaminopropane are shown in Figure 7.18. Only di-alkylamines could be used as standards and MI measurements were restricted to only four reference compounds. Note that all standard molecules having PA > 955 kJ mol^{-1} preferentially retain the proton in CID experiments. The crossover point is at 971 kJ mol^{-1}, well below the reference value, and although their data do not fall close to our line (see Figure 7.18) this value is the same as that found by Siu et al.[20]

The new results differ from those for the diaminoethane in that there is a large $\Delta S^{\neq}$ effect, for CID ions amounting to a $\Delta G^{\neq}$ 31 kJ mol^{-1} below the reference PA; the crossover point, 971 kJ mol^{-1}, is also low by 16 kJ mol^{-1}.

We propose that these results show the presence of both an activation entropy and a reverse activation energy barrier of about 20 kJ mol^{-1}, including the E_{rev} for dialkylamine. The above calculations of Siu et al. show an appreciably shorter —NH_3^+•••NH_2— bond in the protonated 1,3 compound than in the 1,2 analog; 1.65 vs. 1.87 Å respectively, but not as short as for the 1,4 diamine (1.54 Å). Therefore an energy barrier for the reverse reaction is indeed a reasonable proposal.

An additional experiment was performed to seek support for the suggestion that a reverse energy barrier was involved in the 1,3-diaminopropane fragmentations. The kinetic energy release values, KER, for the Gaussian product ion peaks (from the MI and CID mass spectra) for the competing dissociations of $(C_2H_5)_2NH$•••H^+•••$(NH_2CH_2)_2$, (m/z 134 → m/z 61; m/z 134 → m/z 74) and the corresponding observations for $(C_4H_9)_2NH$•••H^+•••$H_2N(CH_2)_3NH_2$ (m/z 214 → m/z 75; m/z 214 → m/z 130) were measured. The MI fragmentations gave KER values of 14, 13, 18 and 14 meV and the corresponding CID KER results were 39, 30, 28, and 32 meV, respectively. The failure of this test does not however negate the proposal; the partitioning of a significant fraction of the (quite small) excess energy in the transition state into translational degrees of freedom of the products may not be occurring here.

7.4.5.3 1,4-diaminobutane

The kinetic method graph for this compound with dialkylamines as the partner molecules is shown as Figure 7.19. The MI and CID lines cross below ln$R$ = 0 and the PA thereat, 978 kJ mol^{-1}, is far from the reference PA for this diamine, 1006 ± 1 kJ mol^{-1}. The lowest translational energy CID data of Siu et al.[20] are also shown; they are not colinear. We propose that much larger $\Delta S^{\neq}$ and E_{rev} effects are operative, the latter may be as great as 32 kJ mol^{-1}.

As found in 1,2- and 1,3- analogues, the KER values for the metastable and collision-induced dissociations of $(C_5H_{11})_2NH{\bullet\bullet\bullet}H^+{\bullet\bullet\bullet}NH_2(CH_2)_4NH_2$, m/z 246 → m/z 89; m/z 246 → m/z 158, were measured. The MI fragmentations gave KER values of 19, 19 meV and the corresponding CID KER results were 23, 39 meV, respectively. Again failure to observe the presumably appreciable E_{rev} in the corresponding dissociation.

The results from these last three compounds illustrate the chief weaknesses of the kinetic method, which clearly does produce reliable results but only when entropies of activation and reverse energy barriers are negligible (as exemplified by the homologous compounds described here). Note that a cross-over point at ln$R$ = 0 is *not* a guarantee that the PA thereat is correct. The effect of a reverse energy barrier, which in principle could give too high as well as too low an observed PA, cannot be discounted. That these difficulties arose for molecules having two proton binding groups in fairly close proximity gives cause for alarm as to how these

problems will apply to simple biomolecules such as amino-acids, where carbonyl and amino groups are both present.

7.5 References

(1) Armentrout, P. B. *J. Mass Spectrom.* **1999**, *34*, 74.

(2) Cooks, R. G.; Koskinen, J. T.; Thomas, P. D. *J. Mass Spectrom.* **1999**, *34*, 85.

(3) Drahos, L.; Vekey, K. *J. Mass Spectrom.* **1999**, *34*, 79.

(4) Hunter, E. P. L.; Lias, S. G. *J. Phys. Chem. Ref. Data* **1998**, *27*, 413.

(5) Holmes, J. L.; Aubry, C.; Mayer, P. M. *J. Phys. Chem. A* **1999**, *103*, 705.

(6) Cao, J.; Aubry, C.; Holmes, J. L. *J. Phys. Chem., in press* **2000**.

(7) Cao, J.; Holmes, J. L. *Int. J. Mass Spectrom.* **2000**, *195/196*, 525.

(8) Cao, J.; Holmes, J. L. *Euro. Mass Spectrom.* **1999**, *5*, 19.

(9) Holmes, J. L.; Terlouw, J. K. *Org. Mass Spectrom.* **1980**, *15*, 383.

(10) Baer, T.; Hase, W. L. *Unimolecular Reaction Dynamics, Oxford University Press, New York* **1996**.

(11) Baer, T.; Booze, J. A.; Weitzel, K. M. . In *Vacuum ultraviolet photoionization and photodissociation of molecules and clusters*; Ng, C. Y., Ed.; World scientific: Singapore, 1991; pp 259.

(12) Rosenstock, H. M.; Stockbauer, R.; Parr, A. C. *J. Chem. Phys.* **1980**, *73*, 773.

(13) Baer, T.; Kury, R. *Chem. Phys. Lett.* **1982**, *92*, 659.

(14) Cerda, B. A.; Wedesmiotis, C. *J. Am. Chem. Soc.* **1996**, *118*, 11884.

(15) Terlouw, J. K.; Heerma, W.; Dijkstra, G. *Org. Mass Spectrom.* **1981**, *16*, 326.

(16) Ruttink, P. J. A. *J. Phys. Chem.* **1987**, *91*, 703.

(17) Baer, T.; Dutuit, O.; Mestdagh, H.; Rolando, C. *J. Phys. Chem.* **1988**, *92*, 5674.

(18) Szulejko, J. E.; McMahon, T. B. *J.Am. Chem. Soc.* **1993**, *115*, 7839.

(19) Cheng, X. H.; Wu, Z. C.; Fenselau, C. *J. Am. Chem. Soc.* **1993**, *115*, 4844.

(20) Wang, Z.; Chu, I. K.; Rodriquez, C. F.; Hopkinson, A. C.; Siu, K. W. M. *J. Phys. Chem. A* **1999**, *103*, 8700.

Table 7.4 Proton affinity values from the NIST database and kinetic measurements from this thesis

Compounds	PA (kJ mol^{-1}) NIST'98[a]	Compounds	PA (kJ mol^{-1}) NIST'98[a]	Compounds	PA (kJ mol^{-1}) NIST'98[a]
CH_3NH_2	899 ± 2	s-$C_6H_{13}NH_2$	936± 4[b]	$NH(i\text{-}Bu)_2$	958 969 ± 4[c]
$C_2H_5NH_2$	912 ± 2	n-$C_7H_{15}NH_2$	923 927± 4[b]	$NH(s\text{-}Bu)_2$	981 (976 ± 4[c])
n-$C_3H_7NH_2$	918 ± 2	n-$C_8H_{17}NH_2$	929	$NH(Pe)_2$	971 ± 4[b]
s-$C_3H_7NH_2$	924 ± 2	n-$C_9H_{19}NH_2$	930 ± 4[b]	$NH(Hex)_2$	973 ± 4[b]
n-$C_4H_9NH_2$	922 ± 2	$NH(Me)_2$	930 ± 2 926 ± 4[c]	$NH_2(CH_2)_2NH_2$	952 ± 2 (950 ± 4[c])
i-$C_4H_9NH_2$	925 ± 5	NH(Me)(Et)	942 ± 2	$NH_2(CH_2)_3NH_2$	987 ± 2 (971 ± 4[c])
s-$C_4H_9NH_2$	930 ± 2	NH(Me)(n-Pr)	950 ± 4[c]	$NH_2(CH_2)_4NH_2$	1006 ± 2 (979 ± 4[c])
t-$C_4H_9NH_2$	934 ± 3 (930 ± 4[b])	NH(Me)(n-Bu)	952 ± 4[c]	C_5H_5N	930 ± 2
n-$C_5H_{11}NH_2$	924 ± 2	NH(Me)(n-Hex)	955 ± 4[c]	$C_6H_5CH_2NH_2$	913 923 ± 4[c]
neo-$C_5H_{11}NH_2$	928 ± 2	$NH(Et)_2$	952 ± 4	$C_6H_5CH_2CH_2NH_2$	936 930 ± 4[b]
s-$C_5H_{11}NH_2$	933 ± 4[c]	$NH(n\text{-}Pr)_2$	962 ± 3	CH_2=$CHCH_2NH_2$	910 ± 2
t-$C_5H_{11}NH_2$	938 ± 4	$NH(s\text{-}Pr)_2$	972 ± 2 (968 ± 4[c])		
n-$C_6H_{13}NH_2$	928 ± 2 926 ± 4[b]	$NH(n\text{-}Bu)_2$	968 ± 2		

a) The uncertainty given for the PA is the spread of the values given in the NIST tables unless otherwise indicated. Where no uncertainty is given, NIST quotes only one value; b) Measured from their position on the ln*R* vs. PA lines; c) Measured from the crossover points (see text). Values in parenthesis should not be quoted as new PA values because of the possible involvement of the reverse energy barrier, see text for discussion.

Table 7.6 Product ion ratios for metastable and collision-induced dissociations of the proton-bound dimers of n-alkylamines

		C_1	C_2	n-C_3	n-C_5	n-C_7
R: MI (CID)	C_2	1000* (8.2)				
$InR^{\#}$: MI (CID)		6.9 (2.1)				
R: MI (CID)	n-C_3		91 (2.7)			
$InR^{\#}$: MI (CID)			4.5 (1)			
R: MI (CID)	n-C_4			9 (2)		
$InR^{\#}$: MI (CID)				6.7 (1.7)		
R: MI (CID)	i-C_4			14.7 (2.5)		
$InR^{\#}$: MI (CID)				7.2 (1.9)		
R: MI (CID)	n-C_5			33.5 (3.5)		
$InR^{\#}$: MI (CID)				8 (2.2)		
R: MI (CID)	neo-C_5			126 (4.2)		
$InR^{\#}$: MI (CID)				9.3 (2.4)		
R: MI (CID)	n-C_6			68 (4.9)	2.2 (1.4)	
$InR^{\#}$: MI (CID)				8.7 (2.6)	8.8 (2.6)	
R: MI (CID)	n-C_7			115 (5.8)	4 (1.7)	
$InR^{\#}$: MI (CID)				9.2 (2.8)	9.4 (2.8)	
R: MI (CID)	n-C_8					1.4 (1.2)
$InR^{\#}$: MI (CID)						9.8 (2.9)
R: MI (CID)	n-C_9					2.3 (1.2)
$InR^{\#}$: MI (CID)						10.2 (2.9)

R: the ratios for the compounds listed in the columns to those in the rows

$R^{\#}$: ratios normalized to $[C_2H_5NH_3^+]$

Table 7.7 Product ion ratios for metastable and collision-induced dissociations of the proton-bound dimer of s-, t-alkylamines and other selected amines

		n-C_2	n-C_3	n-C_4	n-C_5	n-C_6	n-C_7	n-C_8	n-C_9	s-C_3	s-C_4	s-C_5	t-C_4	
R: MI (CID)	s-C_3			1.3* (1.1)	2.6^{-1} (1.7^{-1})	5.3^{-1} (2^{-1})	9.3^{-1} (2.6^{-1})	24^{-1} (3.7^{-1})	36.6^{-1} (4.5^{-1})					
R: MI (CID)	s-C_4		300 (5.6)		5.8 (1.5)	2.4 (1.1)	1.3 (1.2)			32* (2.9)				
R: MI (CID)	s-C_5					8.8 (2.4)	6.2 (2.2)				5.6* (1.9)			
R: MI (CID)	s-C_6				50.5 (4.5)		14.4 (2.6)	9.2 (2.1)	4.9 (1.9)			3.2* (1.3)		
R: MI (CID)	t-C_4		2321* (7)		42 (3)	14 (2.2)	6.4 (1.7)	3.2 (1.6)	1.9 (1.3)					
R: MI (CID)	t-C_5												20.9* (2.9)	
R: MI (CID)			18.3 (1.8)	2.5 (1.2)	1.5^{-1} (1.3^{-1})	3.1^{-1}* (1.8^{-1})	4.9^{-1}* (2.1^{-1})						59^{-1}* (3.3^{-1})	
R: MI (CID)							7.5* (1.5)		3* (1.1)					56* (2.4)
R: MI (CID)		2.6^{-1}* (1)		1285^{-1}* (5.5^{-1})										
R: MI (CID)					14.7* (3.3)		2.1* (2.1)							16.8 (5.2)

R: the ratios for the compounds listed in the columns to those in the rows

Table 7.8 Product ion ratios for metastable and collision-induced dissociations for the proton-bound dimers of dialkylamines

		$NH(Me)_2$	NH(Me)(Et)	NH(Me)(n-Pr)	$NH(Et)_2$	$NH(n\text{-}Pr)_2$	$NH(s\text{-}Pr)_2$	$NH(n\text{-}Bu)_2$	$NH(n\text{-}Pe)_2$	$NH(n\text{-}Hex)_2$
R: MI (CID)	NH(Me)(Et)	1719 (6.4)								
R: MI (CID)	NH(Me)(n-Pr)		28 (2.5)			2584^{-1} (5.9^{-1})		- (11^{-1})		
R: MI (CID)	NH(Me)(n-Bu)		205 (4.3)	5.5 (1.9)	1.9^{-1} (1^{-1})	403^{-1} (6.2^{-1})		- (10^{-1})		
R: MI (CID)	NH(Me)(n-Hex)				3.8 (1.6)					
R: MI (CID)	NH(Et)(n-Bu)				94 (4)					
R: MI (CID)	$NH(Et)_2$		702 (5.1)							
R: MI (CID)	$NH(n\text{-}Pr)_2$				254 (4.7)				80^{-1} (5.3^{-1})	392^{-1} (5.9^{-1})
R: MI (CID)	$NH(s\text{-}Pr)_2$				1512 (9.4)			1.4 (1.2)	5.2^{-1} (1.6^{-1})	
R: MI (CID)	$NH(n\text{-}Bu)_2$		- (23)		3064 (9.2)	15 (2.6)			4.9^{-1} (1.8^{-1})	19^{-1} (2.6^{-1})
R: MI (CID)	$NH(i\text{-}Bu)_2$				5247 (9.8)	32.5 (3.1)	1.1 (1)		3.4^{-1} (1.6^{-1})	12.4^{-1} (2.4^{-1})
R: MI (CID)	$NH(s\text{-}Bu)_2$				- (14)	895 (9.1)			18.5 (2.7)	4 (1.9)
R: MI (CID)	$NH(n\text{-}Hex)_2$								2.8 (1.4)	

R: the ratios for the compounds listed in the columns to those in the rows

Table 7.9 Product ion ratios for metastable and collision-induced dissociations for the proton-bound dimers of dialkylamines and n-alkylamines

		n-C_3	n-C_4	n-C_5	n-C_6	n-C_7	n-C_8	n-C_9	t-C_4	⬡
R: MI (CID)	$NH(Me)_2$	135 (4.4)	18 (3.1)	3.5 (2)	1.4 (1.3)	2^{-1} (1.1^{-1})	5.5^{-1} (1.2^{-1})	8^{-1} (1.3^{-1})	12.6^{-1} (1.6^{-1})	2.2^{-1} (1.8^{-1})
R: MI (CID)	$NH(n\text{-}Pr)_2$	(28)	(21)	(20)		(16)	(12.5)	(11)		
R: MI (CID)	$NH(n\text{-}Bu)_2$	(54)	(36)	(34)	(32)	(24)		(13)		

R: the ratios for the compounds listed in the columns to those in the rows

Table 7.10 Product ion ratios for metastable and collision-induced dissociations of the proton-bound dimers for α,ω-diaminoalkanes and dialkylamines

		$NH(Me)_2$	NH(Me)(Et)	$NH(Et)_2$	$NH(n\text{-}Pr)_2$	$NH(i\text{-}Pr)_2$	$NH(n\text{-}Bu)_2$	$NH(n\text{-}Pe)_2$	$NH(n\text{-}Hex)_2$	$NH(i\text{-}Bu)_2$	$NH(s\text{-}Bu)_2$	NH(Me)(n-Bu)	NH(Me)(n-Hex)	NH(Et)(Bu)
R: MI (CID)	1,2-diaminoethane	1852 (2.1)	5.6 (2^{-1})	40 (9^{-1})	3884 (21^{-1})		- (36^{-1})	- (54^{-1})						
lnR: MI (CID)		7.5 (0.7)	1.7 (-0.7)	-3.7 (-2.2)	-8.3 (-3)		- (-3.6)	- (-4)						
R: MI (CID)	1,3-diaminopropane			- (1.4)	51 (2.2^{-1})	2 (9^{-1})	1.1 (5.9^{-1})	10 (12.5^{-1})	88 (15^{-1})		50 (18^{-1})	- (1.34)	- (1)	99 (1.8^{-1})
lnR: MI (CID)				- (0.34)	3.9 (-0.8)	0.7 (-2.2)	0.09 (-1.8)	-2.3 (-2.5)	-4.5 (-2.7)		-3.9 (-2.9)	- (0.29)	- (0)	4.6 (-0.6)
R: MI (CID)	1,4-diaminobutane			- (2.9)	- (1.4)		455 (1.5^{-1})	86 (2.9^{-1})	10 (3.7^{-1})	260 (1.6^{-1})	30 (4.4^{-1})			
lnR: MI (CID)				- (1.1)	- (0.3)		6.1 (-0.4)	4.4 (-1.1)	2.3 (-1.3)	5.6 (-0.5)	3.4 (-1.5)			

		$n\text{-}C_3$	$n\text{-}C_4$	$n\text{-}C_5$	$n\text{-}C_7$	$n\text{-}C_9$	$t\text{-}C_4$
R: MI (CID)	1,2-diaminoethane	(4.4)	(3.7)	(2.8)	(2.2)	(1.7)	(2)
lnR: MI (CID)		(1.5)	(1.3)	(1)	(0.8)	(0.5)	(0.7)

R: the ratios for the compounds listed vertically to those in the row

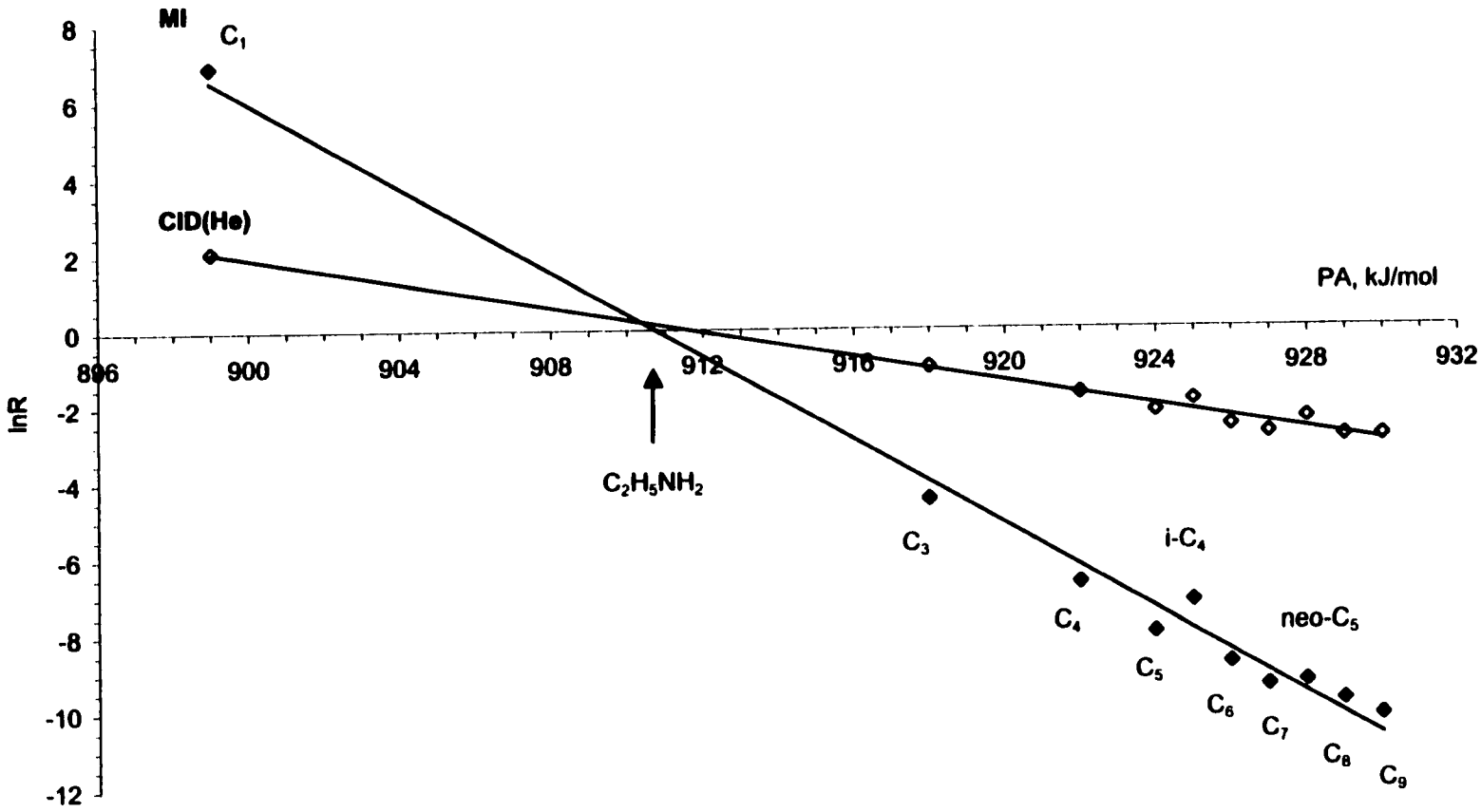

Figure 7.5 Plot of $\ln[C_2H_5NH_3^+]/[B_nH^+]$ as a function of PA values, where B_n are a series of n-alkylamines

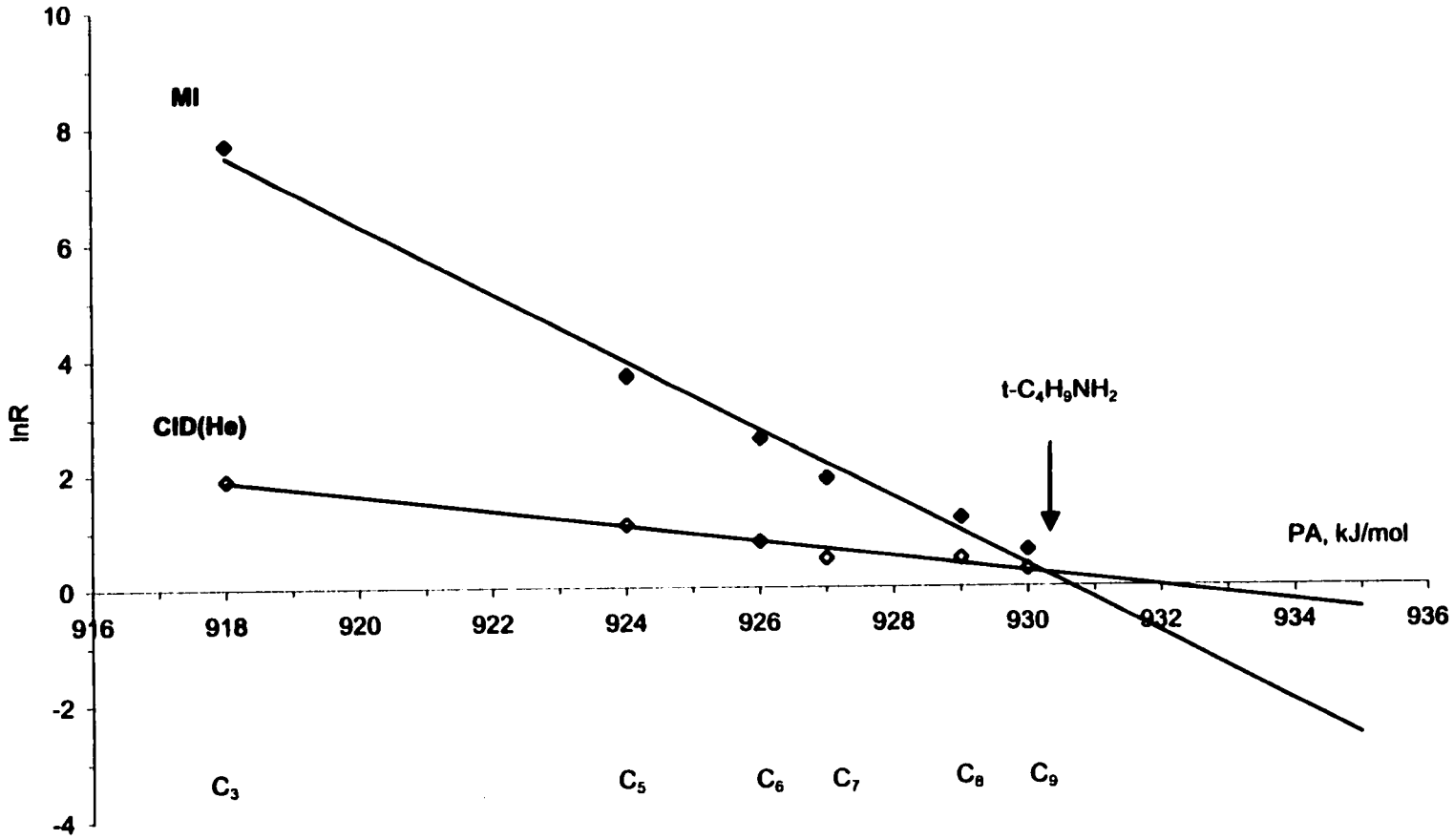

Figure 7.6 Plot of $\ln[t\text{-}C_4H_9NH_3^+]/[B_nH^+]$ as a function of PA values, where B_n are a series of n-alkylamines

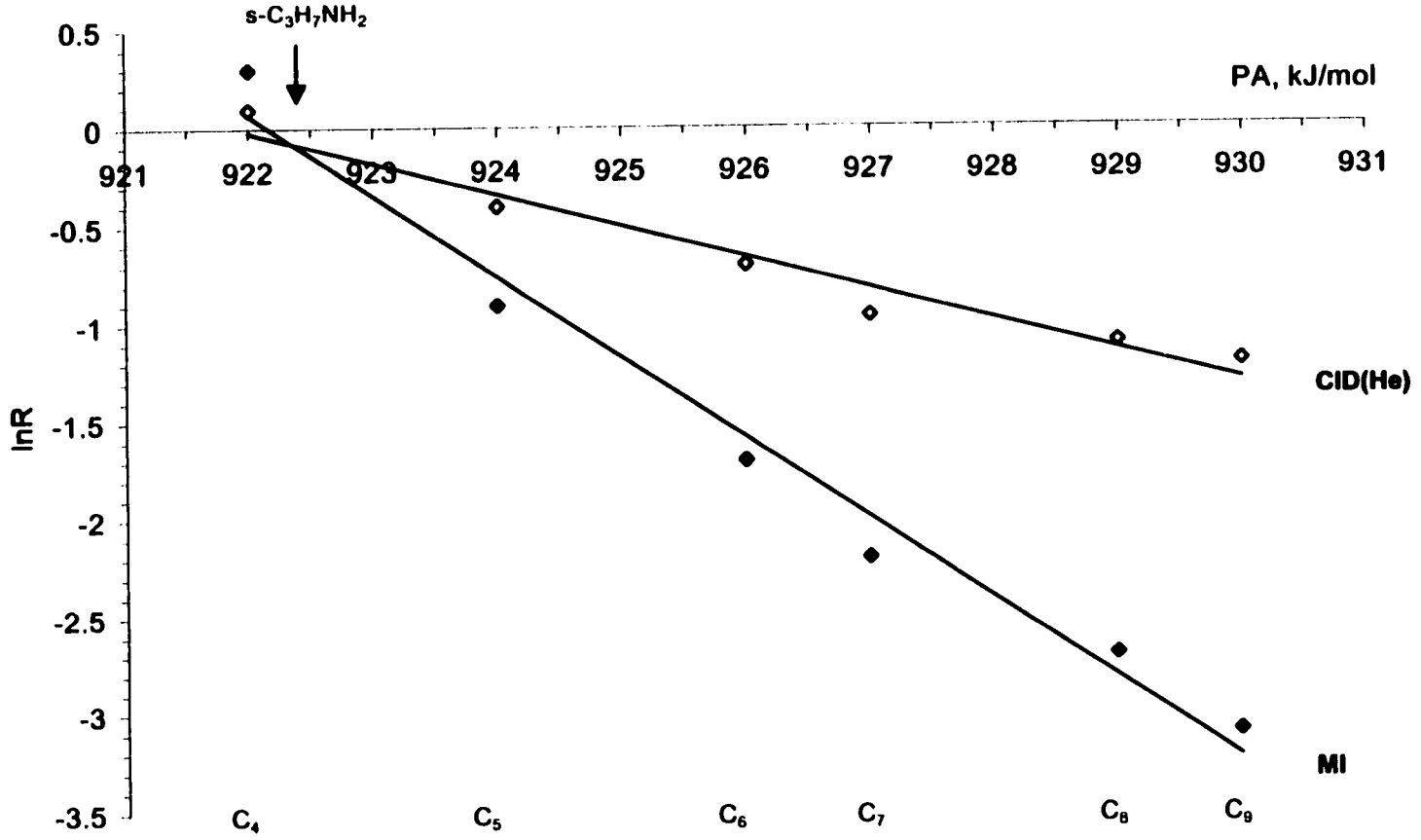

Figure 7.8 Plot of $\ln[s\text{-}C_3H_7NH_3^+]/[B_nH^+]$ as a function of PA values, where B_n are a series of n-alkylamines

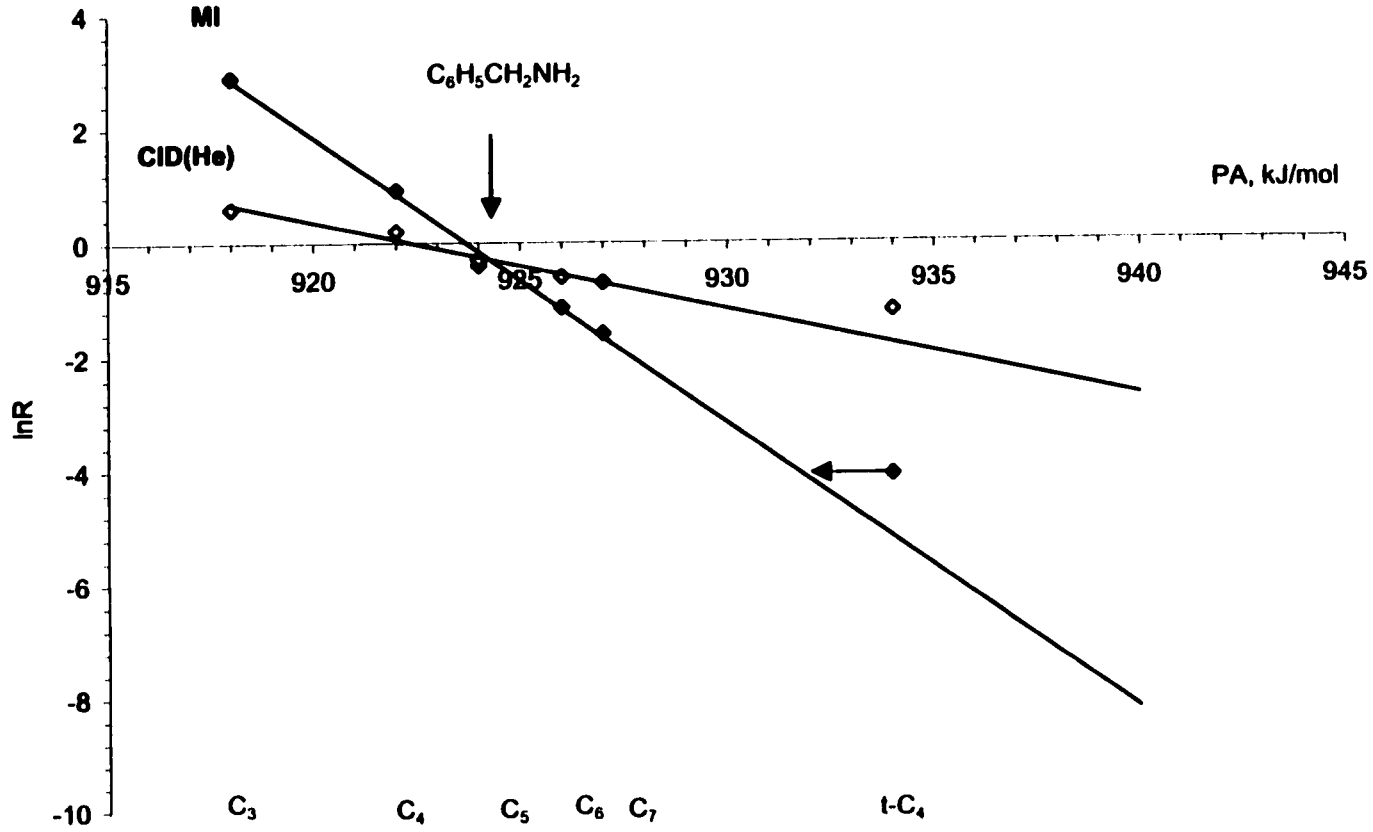

Figure 7.9 Plot of $\ln[C_6H_5CH_2NH_3^+]/[B_nH^+]$ as a function of PA values, where B_n are a series of n-alkylamines

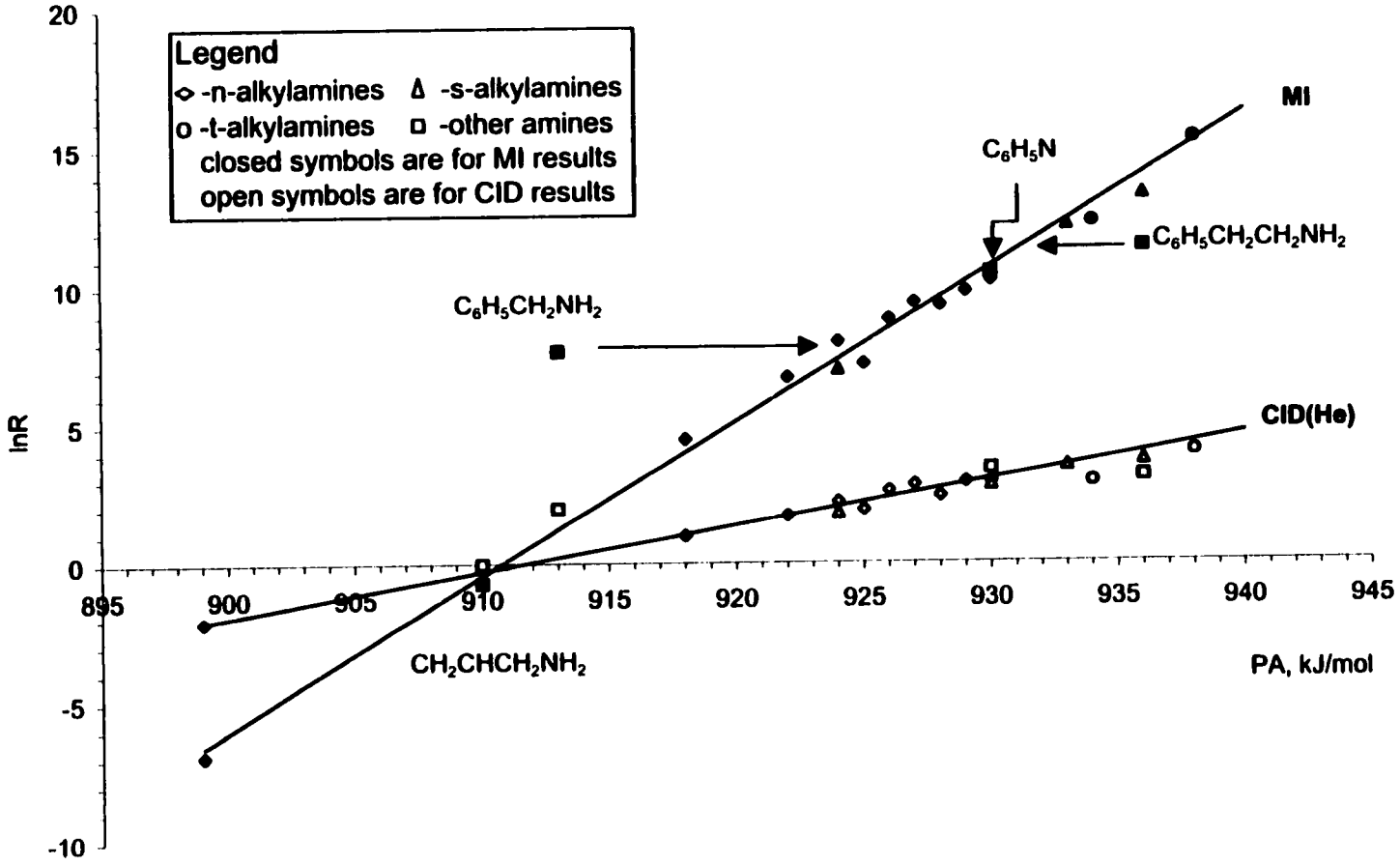

Figure 7.10 Plot of $\ln[B_nH^+]/[C_2H_5NH_3^+]$ as a function of PA values, where B_n are a series of primary amines

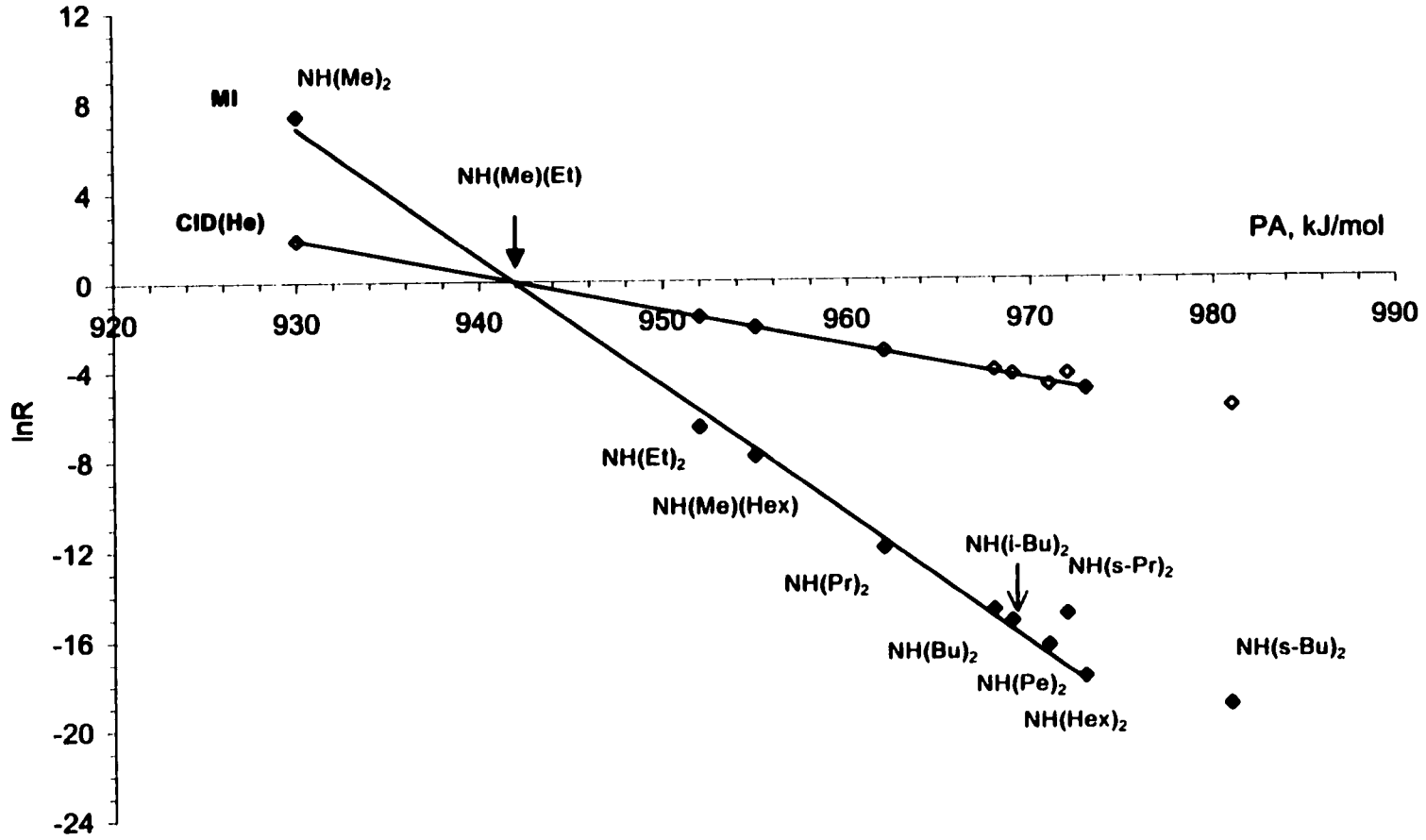

Figure 7.11 Plot of $\ln(CH_3)(C_2H_5)NH_2^+]/[B_nH^+]$ as a function of PA values, where B_n are a series of dialkylamines

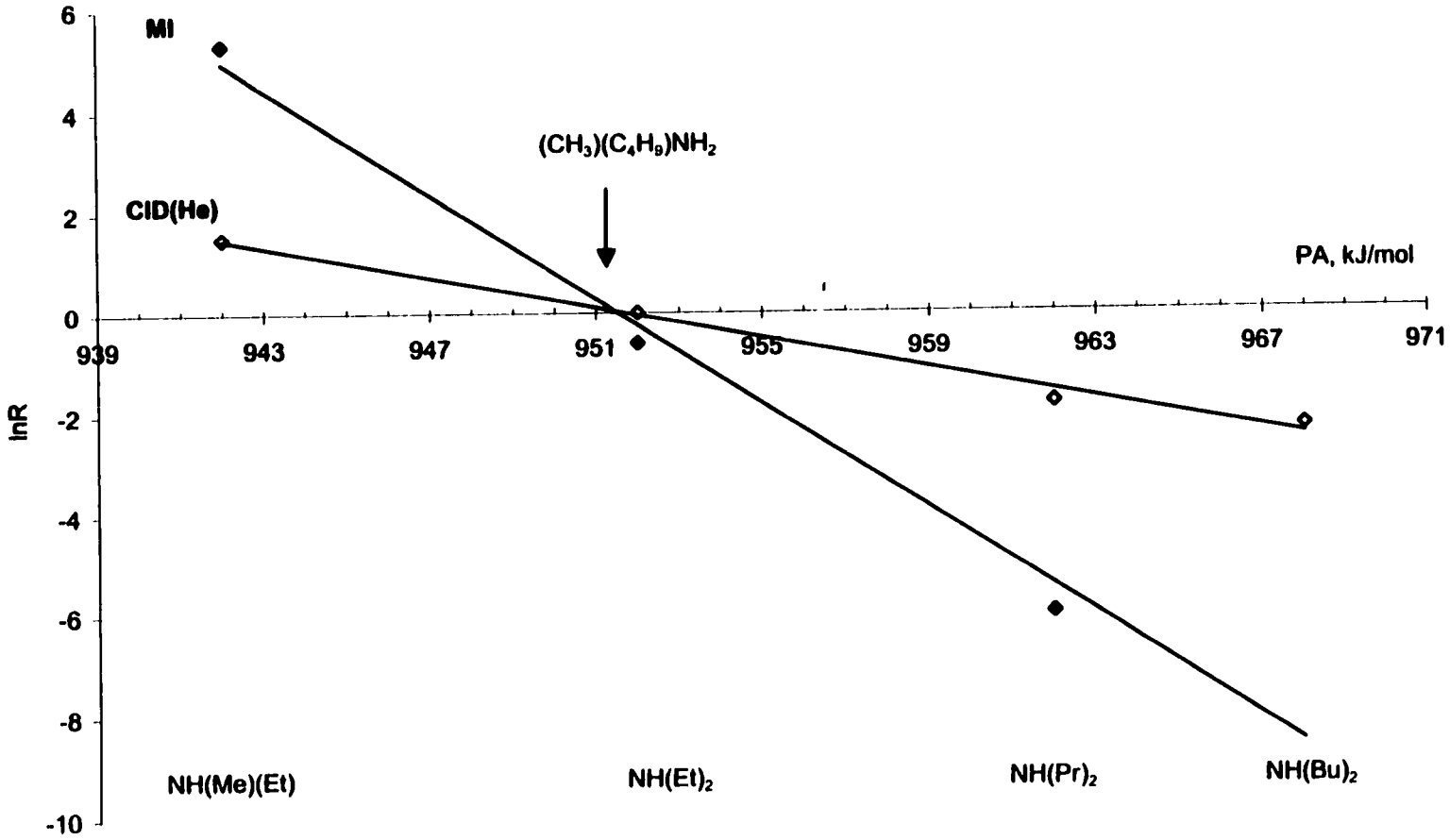

Figure 7.12 Plot of $\ln(CH_3)(C_4H_9)NH_2^+]/[B_nH^+]$ as a function of PA values, where B_n are a series of dialkylamines

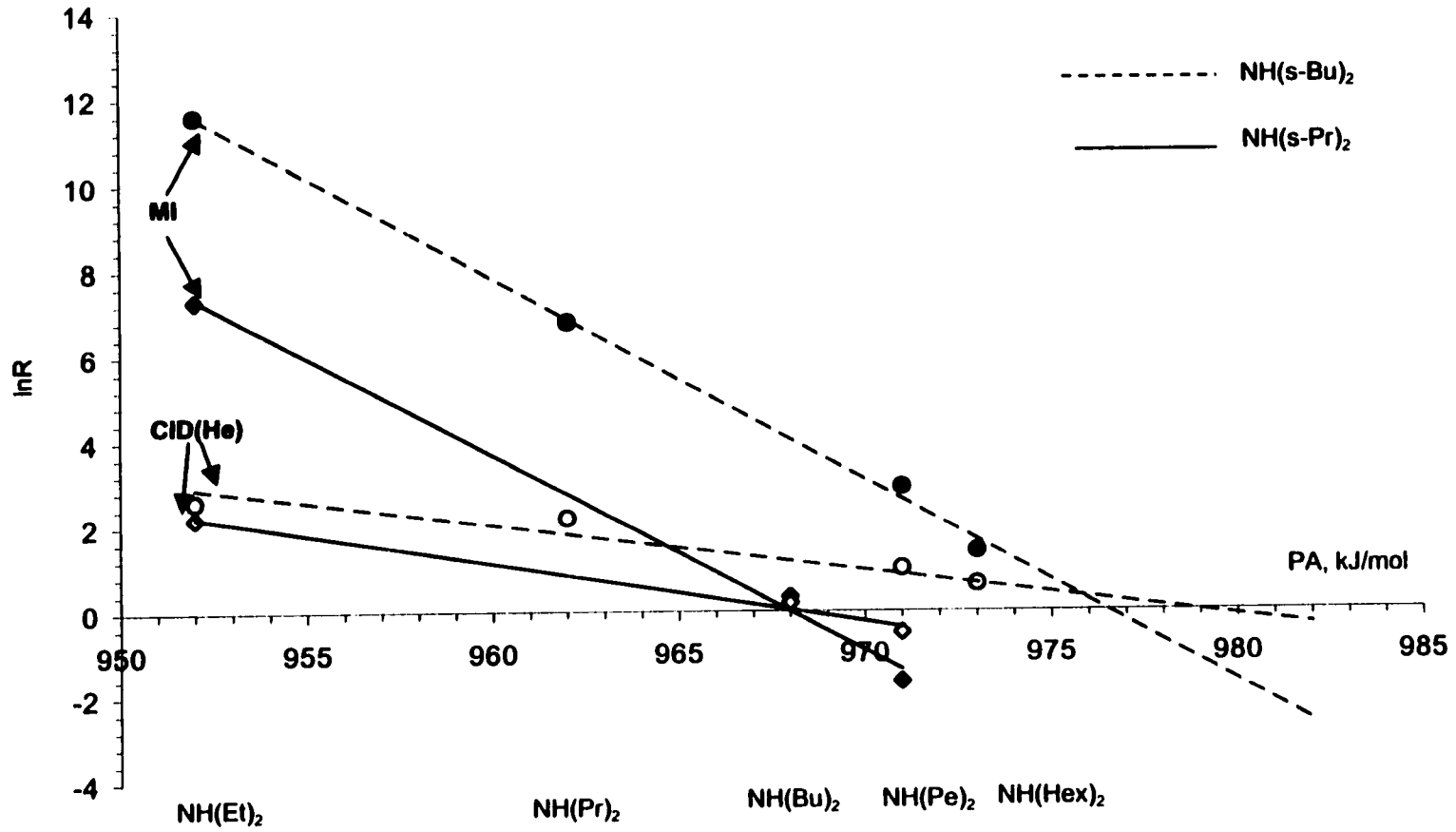

Figure 7.13 Plots of $\ln[(s\text{-}C_3H_7)_2NH_2^+]/[B_nH^+]$ and $\ln[(s\text{-}C_4H_9)_2NH_2^+]/[B_nH^+]$ as a function of PA values, where B_n are a series of dialkylamines

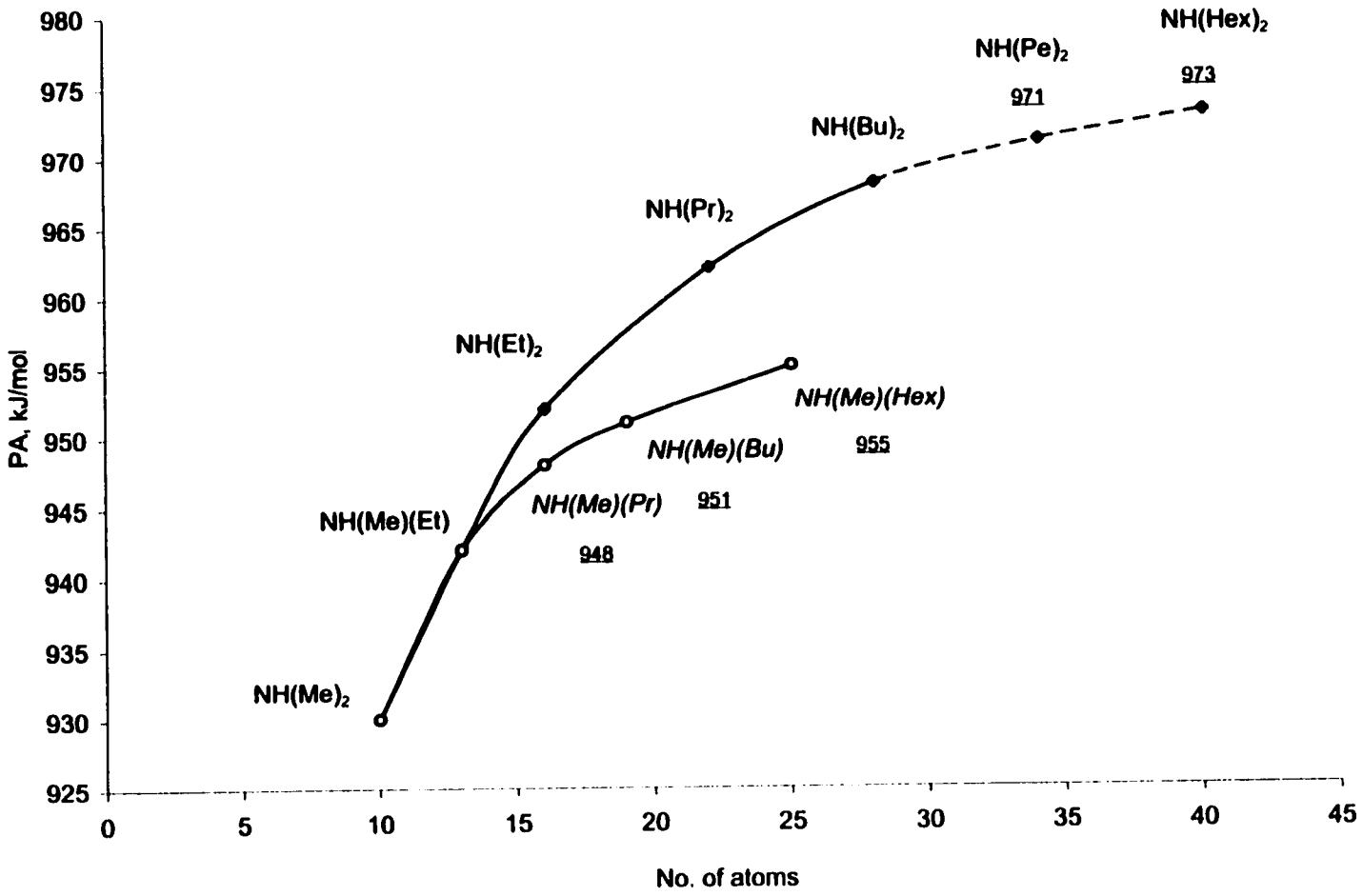

Figure 7.14 PA values of dialkylamines as a function of size; new PA valus are underlined

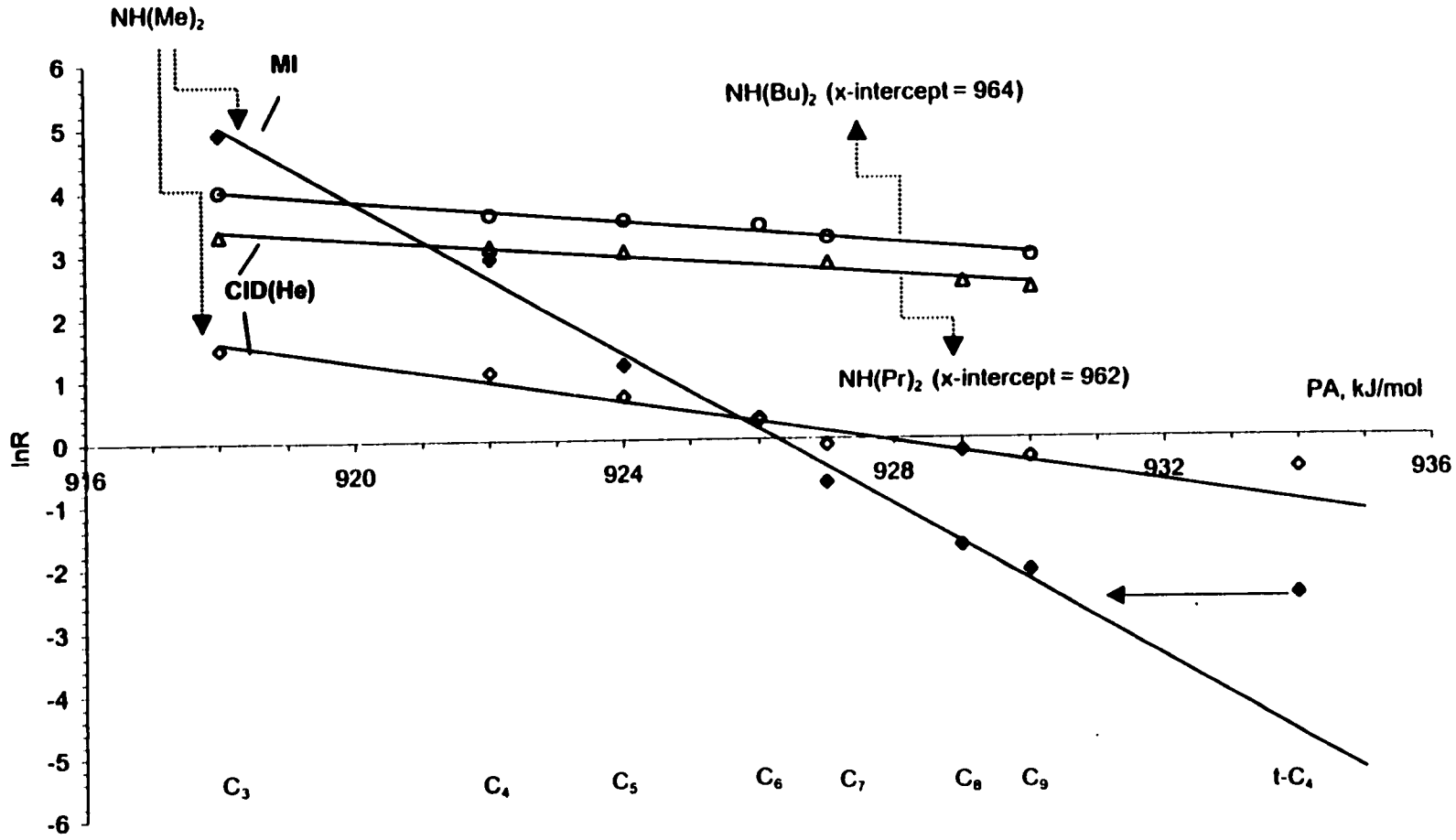

Figure 7.15 Plots of $\ln[(CH_3)_2NH_2^+]/[B_nH^+]$, $\ln[(n\text{-}C_3H_7)_2NH_2^+]/[B_nH^+]$ and $\ln[(n\text{-}C_4H_9)_2NH_2^+]/[B_nH^+]$ as a function of PA values, where B_n are a series of n-alkylamines

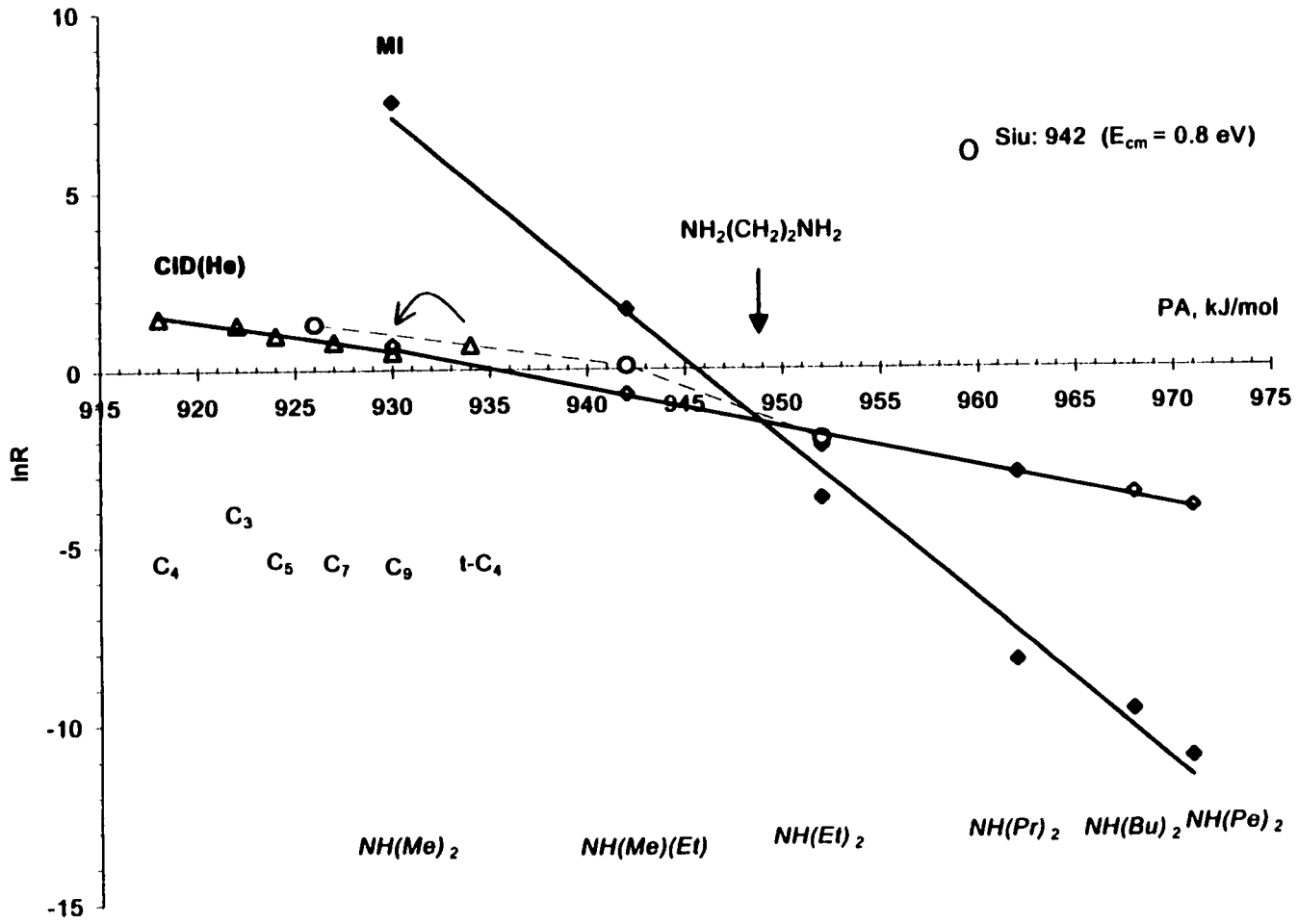

Figure 7.16 Plots of $\ln[NH_2(CH_2)_2NH_3^+]/[B_nH^+]$ as a function of PA values, where B_n are series of n-alkylamines and dialkylamines

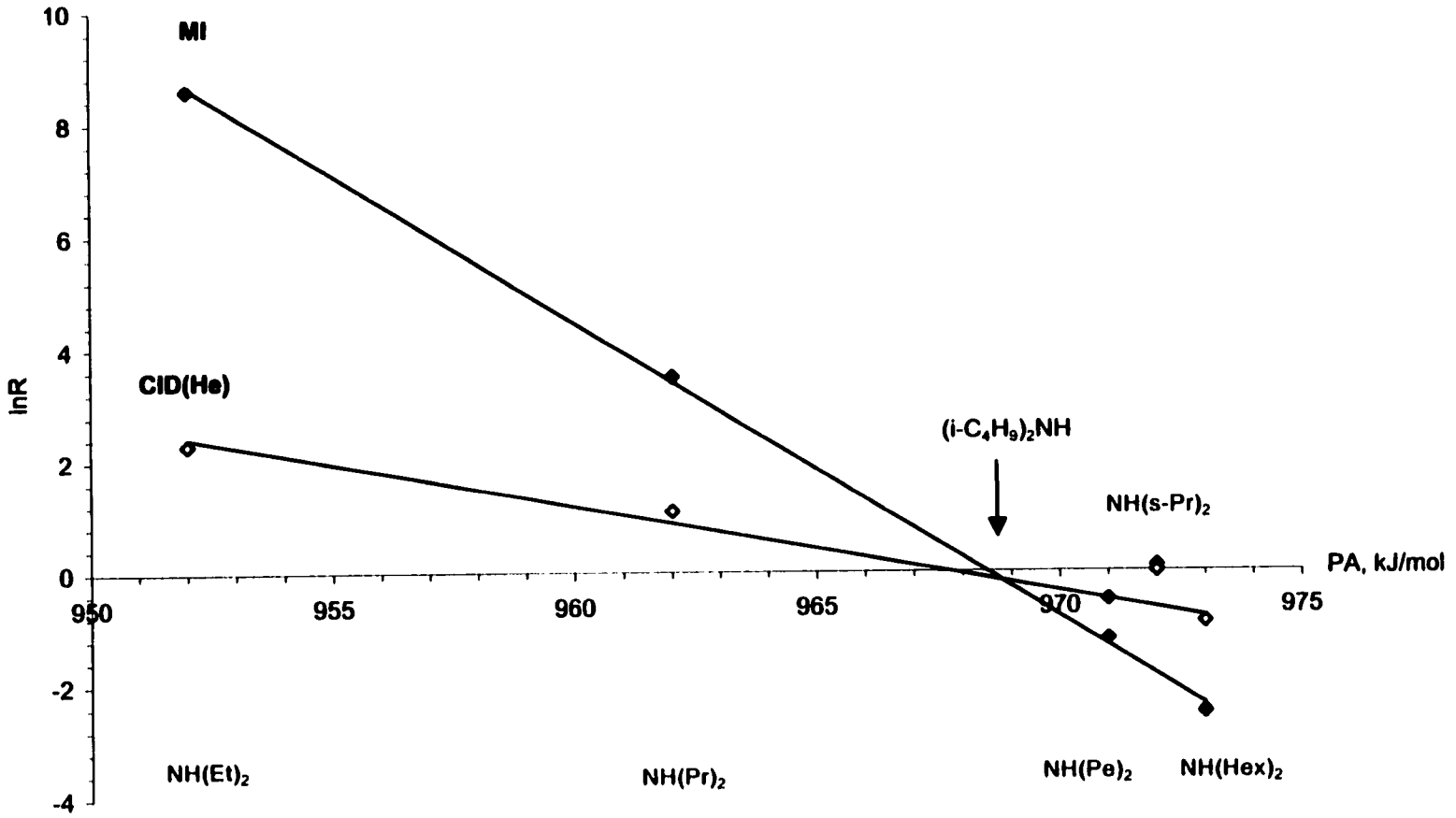

Figure 7.17 Plot of $\ln[(i\text{-}C_4H_9)_2NH_2^+]/[B_nH^+]$ as a function of PA values, where B_n are a series of dialkylamines

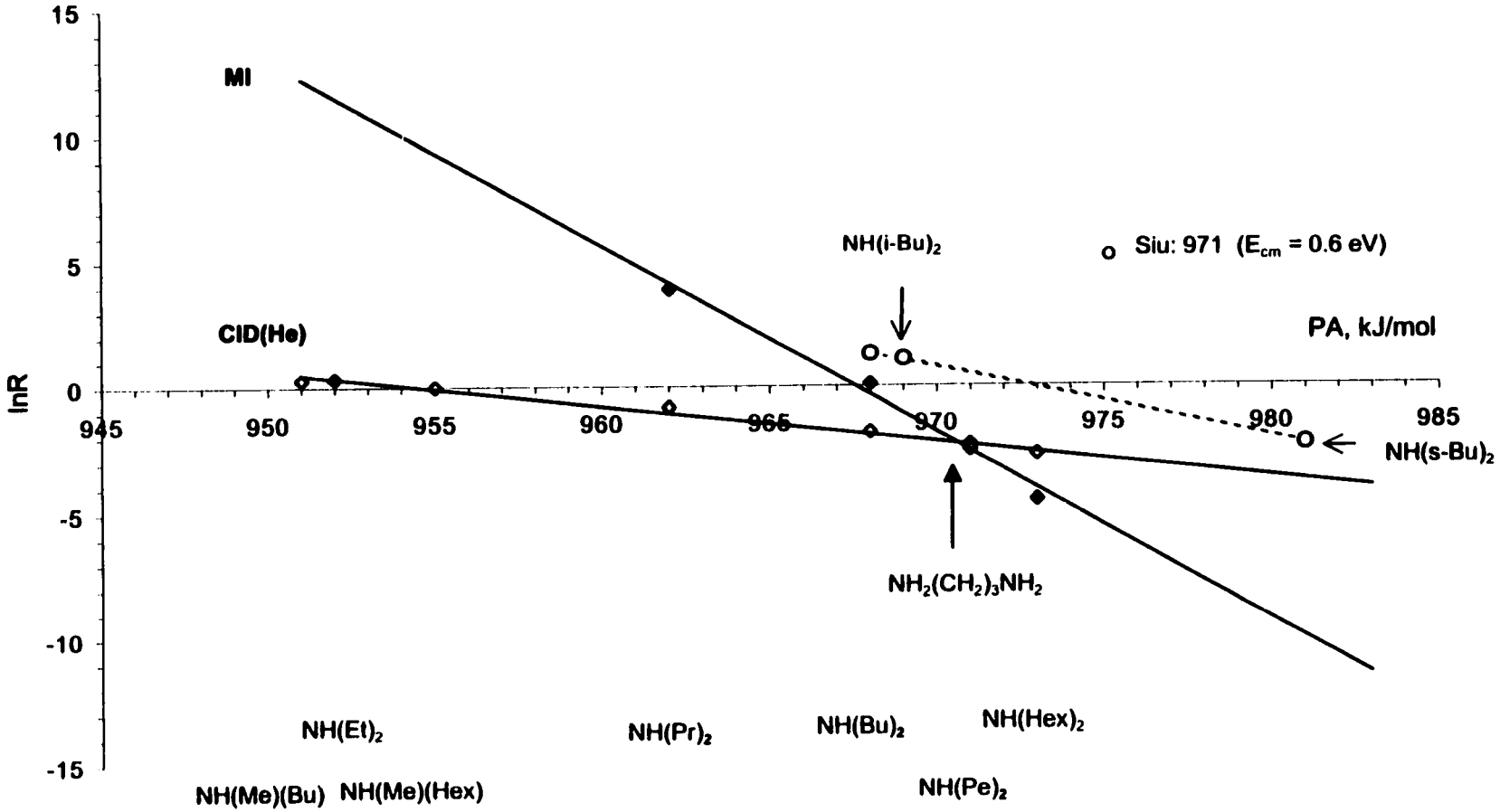

Figure 7.18 Plot of $\ln[NH_2(CH_2)_3NH_3^+]/[B_nH^+]$ as a function of PA values, where B_n are dialkylamines

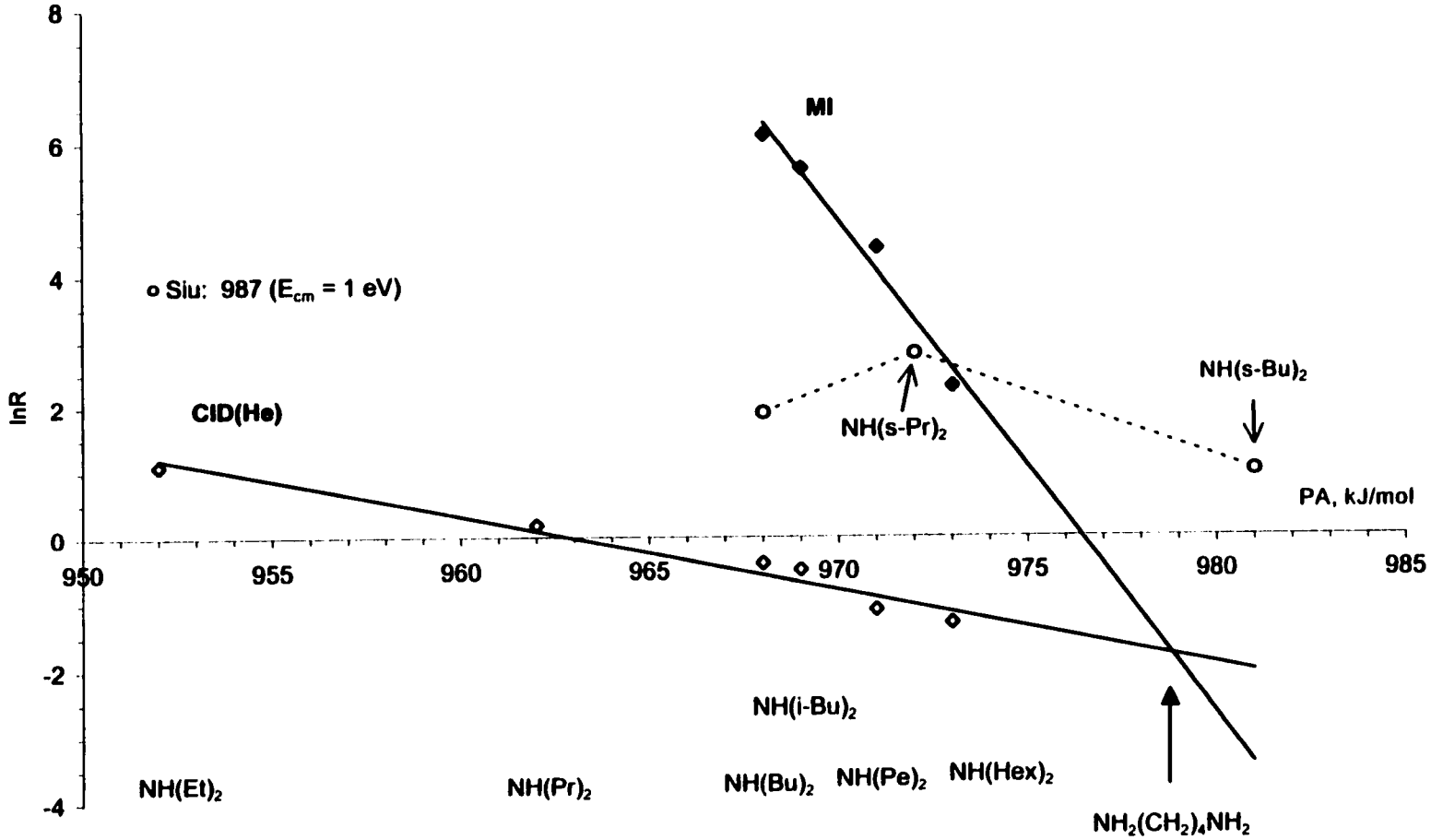

Figure 7.19 Plot of ln[$NH_2(CH_2)_4NH_3^+$]/[B_nH^+] as a function of PA values, where B_n are a series of dialkylamines

Chapter 8 Determining the proton affinities of nitriles by the kinetic method

8.1 Introduction

The kinetic method was used to determine the proton affinities of homologous alkyl nitriles from CH_3CN to n-$C_8H_{17}CN$. The available PA values for these nitriles are only for five members of the series, i.e., CH_3CN, C_2H_5CN, n-C_3H_7CN, i-C_3H_7CN and n-C_4H_9CN.

The recent experiments by McMahon et al[1] provided PA values for CH_3CN, C_2H_5CN, n-C_3H_7CN, and i-C_3H_7CN measured by the equilibrium method using high pressure mass spectrometry with a sector mass spectrometer. In the same report, the kinetic method was applied to these bases using metastable ion abundances to investigate the relationship between ion source temperature and the 'effective temperature', derived from the plot of ln $[B_1H^+]/[B_2H^+]$ vs. gas-phase basicities of the nitriles. The 'effective temperature' was found to be related to the measured ion source temperature but in an unexpected inverse ratio.

Meanwhile, the term 'effective temperature' has been addressed in a recent study in this laboratory[2] in which metastable and collision-induced dissociation experiments were performed using a sector instrument. On the basis of the experimental results, it was concluded that the 'effective temperature' is not likely to

have any physico-chemical significance and that the kinetic method is no better than a semi-empirical approach.

Despite the problems of the physico-chemical interpretation of results, the kinetic method appears generally to be satisfactory for measuring thermochemical properties. In this chapter, the method was used for the determination of the PA values for homologous alkyl nitriles, using the results of McMahon[1] and other literature data as reference values. Both metastable and collision-induced dissociations of proton-bound nitrile cluster ions were studied.

It has been shown[2] that it is necessary to correct $[B_1H^+]/[B_2H^+]$ ratios measured in collision-induced dissociations for contributions from metastable ion fragmentations. This is achieved by using an electrostatically charged collision cell, effectively separating the two types of dissociations in an ion kinetic energy spectrum. When such corrections were fully applied, the $[B_1H^+]/[B_2H^+]$ ratios for proton-bound primary alkanol pairs were found to be independent of target gas pressure (provided multiple collisions were not involved) and also of the target gas itself.[2] Many studies using sector mass spectrometers reported in the literature do not take such corrections into account. Indeed, without corrections, $[B_1H^+]/[B_2H^+]$ ratios can appear to be significantly dependent on the nature of the target gas. The CID results were remeasured by applying a positive potential to the collision cell since the 'mass discrimination' will result in incorrect ratios.

The purpose of the present work was to try to repeat the McMahon results[1] using a sector mass spectrometer, to compare MI and CID processes, and also to estimate PA values for other homologous nitriles.

8.2 Results and discussions

8.2.1 Metastable ion and collision-induced dissociation experiments

The MI and CID mass spectra of the proton-bound dimer ions showed that both spectra are dominated by production of the two protonated monomers; other fragment ion abundances were negligibly small. The MI and CID lines cross very near to ln$R$ = 0 and give a PA of 781 kJ mol^{-1}, within experimental error the same as the reference value for CH_3CN, 780.4 kJ mol^{-1}.[3] The fact that the cross over point is close to ln$R$ = 0 axis is in keeping with the requirement that $\ln(Q_1^*/Q_n^*)$ is zero.

As has been found for alkanol proton-bound pairs[2] and also for amines,[4,5] the $[B_1H^+]/[B_2H^+]$ ratios were independent of ion source pressure for both MI and CID processes. The ratios from CID experiments were always smaller that those from MI results alone. This is compatible with a much greater internal energy range being observed for the former dissociating ions, where the observational time-frame is from the collision (time zero) to the ions' exit from the field-free region (μs). The narrow internal energy range sampled in the MI experiment has been discussed in detail elsewhere.[2]

At low ion source pressures (ca. $1x10^{-5}$ mb) as much as 10% of the $[B_1HB_2]^+$ ion flux was metastable, whereas at high source pressures (ca. $1x10^{-4}$ mb) the fraction was 2% or less. Within these limits the product ion ratio was therefore independent of the fragmenting ions' internal energy. The same effect has been observed for protonated alkanol pairs[2] and amines,[4,5] with no change in $[B_1H^+]/[B_2H^+]$ from > 20% to < 1% dissociation of the adduct ion.

The kinetic energy releases for the metastable ion fragmentations were, as expected, smaller than those for the CID dissociations. For example, for the $(C_2H_5CN)H^+(n\text{-}C_4H_9CN)$ pair KER values for the production of $C_2H_5CNH^+$ were 20 meV (MI) and 56 meV (isolated CID) and for $n\text{-}C_4H_9CNH^+$ were 22 meV and 40 meV, respectively.

The results are presented in Table 8.1 and are shown in graphical form in Figure 8.1. The values were obtained in a ladder fashion, pairing the following nitriles to produce the results shown in the Table, C_2H_5CN/CH_3CN, $n\text{-}C_3H_7CN/C_2H_5CN$, $i\text{-}C_3H_7CN/C_2H_5CN$, $n\text{-}C_4H_9CN/C_2H_5CN$, $i\text{-}C_4H_9CN/C_2H_5CN$, $n\text{-}C_5H_{11}CN/n\text{-}C_4H_9CN$, $n\text{-}C_5H_{11}CN/C_2H_5CN$, $n\text{-}C_6H_{13}CN/n\text{-}C_5H_{11}CN$, $n\text{-}C_6H_{13}CN/n\text{-}C_4H_9CN$, $n\text{-}C_6H_{13}CN/n\text{-}C_3H_7CN$, $n\text{-}C_7H_{15}CN/n\text{-}C_6H_{13}CN$, $n\text{-}C_8H_{17}CN/n\text{-}C_7H_{15}CN$.

The reference PA values used are the average of those reported by McMahon[1] and the selected values in the NIST compilation.[3] Using the above reference data, new PA values derived from MI and CID measurements for five

nitriles are given in Table 8.2. Also shown in Figure 8.1 are the abundance ratios from the results of McMahon.[1] The adduct ions in McMahon's ion source were in thermal equilibrium with their surroundings. At the quoted ion source temperatures, ranging from ca. 300 to 580 K, only ions at the highest temperatures should have been discernibly metastable. The [$RCNH^+NCR$] bond strength[6] is ca. 125 kJ mol^{-1} and with an Arrhenius *A* factor of 10^{14} s^{-1}, only about 0.4% of the ions at 580 K could be metastable. In view of the good fit of their data on Figure 8.1, it seems highly likely that the dissociations observed by them resulted only from CID processes. Thus the ratios from their MI observations were actually the results of residual collisions in the FFR and they, of course, were subject to change with the background pressure in the FFR.

A temperature dependence test was performed using the proton-bound pair of n-C_4H_9CN and C_2H_5CN over the range of 323 to 523 °C by using the ZAB mass spectrometer. It was found that the ratio, [n-$C_4H_9CNH^+$]/[$C_2H_5CNH^+$], was constant at 87.3 ± 5.0. Therefore, there was *no* correlation between T_{eff} and ion source temperature.

As pointed out previously,[2] the quantity T_{eff} does relate to the internal energy of the fragmenting ions but for metastable ions it is clearly not a temperature in the thermodynamic sense. A similar problem arises from the collisionally activated ions. The term 'effective temperature' does not apply to the behavior of both metastable and collisionally excited ions. If indeed, the slopes of any of these lines cannot

legitimately be quantitatively related to a real temperature then secondary estimates, such as attempts to identify entropy effects cannot properly be made.[7,8] Moreover, the entropy term, $\Delta(\Delta S^{\neq})$, derived by taking the slope (T_{eff}) and intercept of the ln*R* vs. PA plot has been so far incorrectly ascribed to relative entropies of protonation.

With regard to the CID experiment, it is highly recommended that a positive charge be applied to the collision cell in order to preclude the possible discrimination against the low product ions. The problem of less secure PA values for the higher homologues obtained in the CID experiment vanishes because of utilization of such practice. The extreme example for this case is the proton-bound dimer of n-$C_5H_{11}CN$ and C_2H_5CN, the CID branching ratio drops from 46.5, which is anomalous for the whole series, to 6.3 with switching the polarity of the potential applied to the collision cell from negative to positive. The kinetic energy for the low fragment ($C_2H_5CNH^+$) is 2928 eV which is low enough to suffer from discrimination against the low fragment ion.

An interesting phenomenon observed in the experiment is that the dissociation leading to protonated CH_3CN is extremely sensitive to collision gas and thus the ratio of $[C_2H_5CNH^+]/[CH_3CNH^+]$ becomes variable because of the residual background in the FFR. The shape of the metastable peak appears composite with a Gaussian peak atop a broad base. With the introduction of the collision gas, it becomes Gaussian (see Figure 8.2). The ratio was then measured by extracting

height from the top component of the composite peak for protonated acetonitrile relative to the that for protonated propanenitrile.

Several gases (Ar, Xe, O_2) other than He were used in the CID experiments in order to investigate target gas effects.[9] Table 8.3 shows that the corrected CID ratio for the [n-C_4H_9CN-H^+-C_2H_5CN] ion pair is almost independent of both the target gas and its pressure. For He, essentially single collision conditions exist up to ca. 10^{-7} mb and to ca. $3x10^{-7}$ mb for the other gases. Under multiple collision conditions ($1x10^{-6}$ mb He corresponds to more than 50% beam reduction), the mixed CID ratios became unreliable owing to secondary fragmentations. In general, target gas effects are indeed very small when full corrections are made for metastable ion contributions.

In summary, the kinetic method allowed the measurement of PA values of a series of homologous nitriles. The proton affinity values from metastable and collision-induced dissociation are in good agreement only when care is taken to avoid possible discrimination effects.

8.3 Future work

In the light of the successful application of the kinetic method to the simple alkyl nitriles, a continuing interest will be the PA values for substituted nitriles such as halogenated nitriles. For the halogenated nitriles, only $ClCH_2CN$ has a PA value in the NIST database. A recent paper by Wenthold[10] determined the proton affinities

of bromo- and iodoacetonitriles using a flowing afterglow-triple quadrupole apparatus. The branching ratios for dissociation of proton-bound dimers were measured for collision energies ranging from ca 2 to 5 eV (center-of-mass energy). Analysis of the CID branching ratios over the collision energy range gave PA values for these two species of 179.8 and 182.9 ± 1.6 kcal mol^{-1}, respectively. Irrespective of the method used to obtain these values, the uncertainty of assigning T_{eff} (ca. ± 40%) can result in errors of ca. 1 kcal mol^{-1} for the ultimate PA data. The reliability of these values for bromo- and iodoacetonitriles could usefully be confirmed by carrying out metastable and isolated CID experiments in a sector mass spectrometer.

8.4 References

(1) Norrman, K.; McMahon, T. B. *Int. J. Mass Spectrom.* **1998**, *176*, 87.

(2) Holmes, J. L.; Aubry, C.; Mayer, P. M. *J. Phys. Chem. A* **1999**, *103*, 705.

(3) Hunter, E. P. L.; Lias, S. G. *J. Phys. Chem. Ref. Data* **1998**, *27*, 413.

(4) Cao, J.; Holmes, J. L. *Int. J. Mass Spectrom.* **2000**, *195/196*, 525.

(5) Cao, J.; Aubry, C.; Holmes, J. L. *J. Phys. Chem., in press* **2000**.

(6) Meot-Ner, M. *J. Am. Chem. Soc.* **1984**, *106*, 1257.

(7) Cheng, X. H.; Wu, Z. C.; Fenselau, C. *J. Am. Chem. Soc.* **1993**, *115*, 4844.

(8) Cerda, B. A.; Wedesmiotis, C. *J. Am. Chem. Soc.* **1996**, *118*, 11884.

(9) Holmes, J. L.; Terlouw, J. K. *Org. Mass Spectrom.* **1980**, *15*, 383.

(10) Wenthold, P. G. *J. Am. Soc. Mass Spectrom.* **2000**, *11*, 601.

Table 8.1 $[B_nH^+]/[CH_3CNH^+]$ ratios (R) in the metastable ion (MI) and collision induced dissociations (CID) of proton-bound nitrile cluster ions

		C_1	C_2	n-C_3	n-C_4	n-C_5	n-C_6	n-C_7
R: MI (CID)	C_2	697 (5.5)						
In $R^{\#}$: MI (CID)		6.5 (1.7)						
R: MI (CID)	n-C_3		18.4 (3.0)					
In $R^{\#}$: MI (CID)			9.5 (2.8)					
R: MI (CID)	i-C_3		102 (4.5)					
In $R^{\#}$: MI (CID)			11.2 (3.2)					
R: MI (CID)	n-C_4		87.3 (4.5)					
In $R^{\#}$: MI (CID)			11.0 (3.2)					
R: MI (CID)	i-C_4		154 (5.5)					
In $R^{\#}$: MI (CID)			11.6 (3.4)					
R: MI (CID)	n-C_5		244 (6.3)		2.4 (1.4)			
In $R^{\#}$: MI (CID)			12.0 (3.5)		11.9 (3.6)			
R: MI (CID)	n-C_6			20.6 (3.1)	4.3 (1.9)	1.8 (1.3)		
In $R^{\#}$: MI (CID)				12.5 (3.8)	12.5 (3.8)	12.5 (3.8)		
R: MI (CID)	n-C_7						1.7 (1.1)	
In $R^{\#}$: MI (CID)							13.0 (3.9)	
R: MI (CID)	n-C_8							1.5 (1.1)
In $R^{\#}$: MI (CID)								13.4 (4.0)

R: the ratios for the compounds listed vertically to those in the row

$R^{\#}$: ratios normalized to $[CH_3CNH^+]$

Table 8.2 New PA and reference PA data for the nitriles

	PA[a] (from NIST)	PA[b] (from McMahon)	PA (from this work)
CH_3CN	779.2	781.6	780.4[c]
C_2H_5CN	794.1	794.5	794.3[c]
n-C_3H_7CN	798.4	799.1	798.7[c]
i-C_3H_7CN	803.6	804.2	803.9[c]
n-C_4H_9CN	802.4		802.7[c]
i-C_4H_9CN			803.4[d]
n-$C_5H_{11}CN$			804.4[d]
n-$C_6H_{13}CN$			805.4[d]
n-$C_7H_{15}CN$			806.2[d]
n-$C_8H_{17}CN$			806.8[d]

(a) NIST compilation (1998)[3]

(b) McMahon's data[1]

(c) average PA values from McMahon[1] and NIST[3]

(d) new PA values from Figure 8.1

Table 8.3 Target gas effect on the dissociation of the proton-bound dimer of n-C_4H_9CN and C_2H_5CN

P	He						O_2				Ar		Xe	
$X10^6$ mb	2	5	8	15	50	100	10	20	40	200	25	50	15	80
R_{iso}	5.1	4.5	4.5	4.5	4.5	4.1	4.4	4.1	4.1	3.9	4.3	4.3	4.0	3.9
R_{mix}	35	18	12	10	7	6	19	12	9	6	13	10	34	12

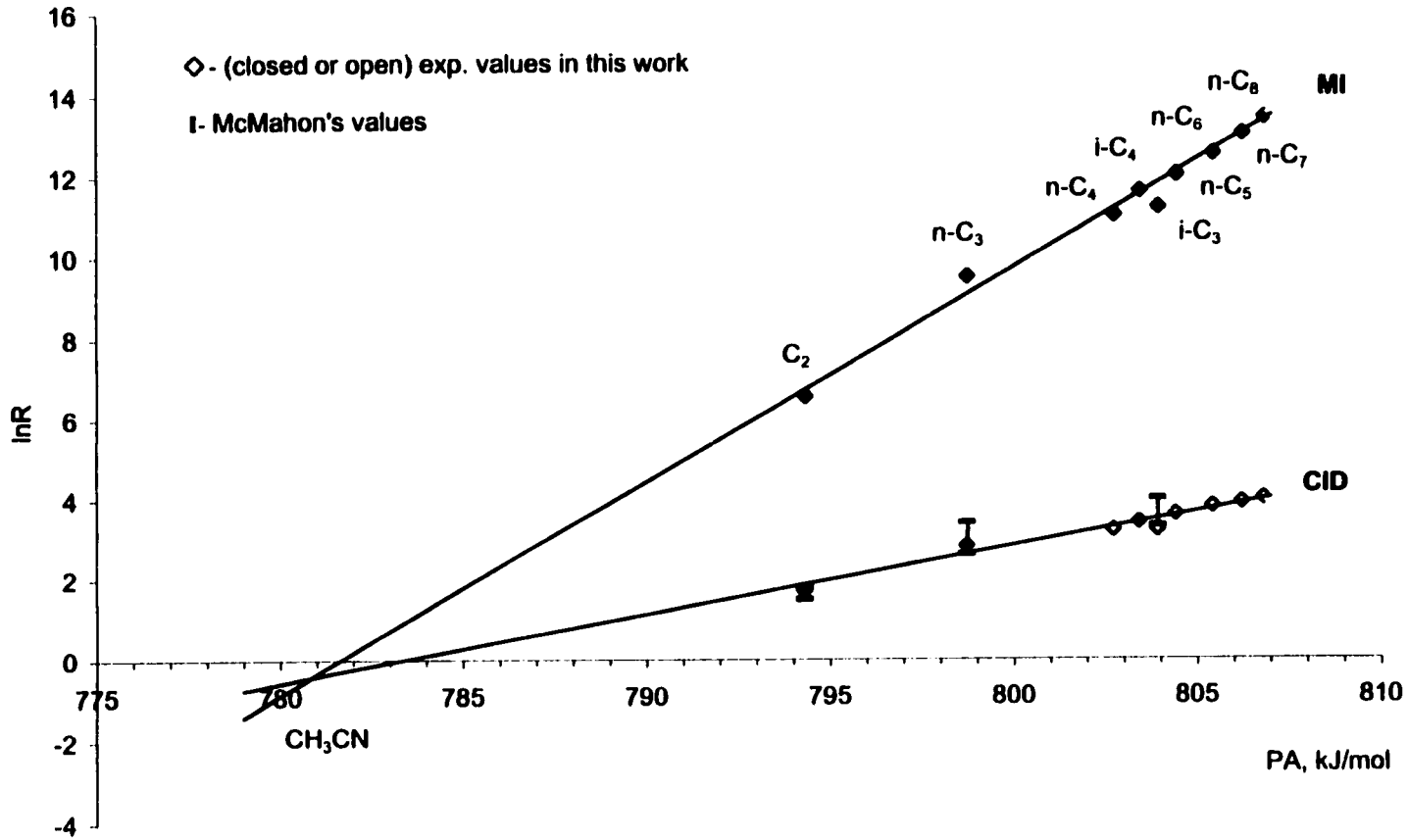

Figure 8.1 Plot of $\ln[B_nH^+]/[CH_3CNH^+]$ as a function of PA values, where B_n are a series of homologous nitriles

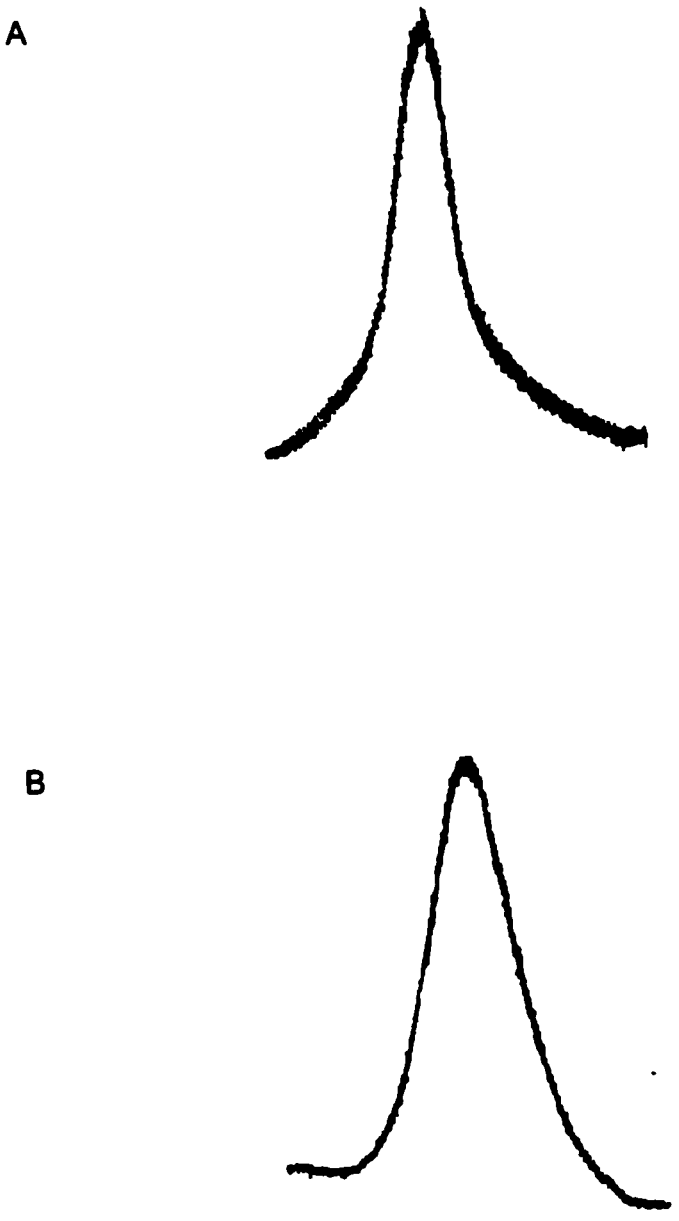

Figure 8.2 (A) Composite metastable peak in the dissociation of $C_2H_5CNH^{\bullet}..CH_3CN$ into $CH_3CNH^{\bullet}$ in which a Gaussian peak atop a broad base; (B) A Gaussian peak with a small introduction of collision gas (He)

Chapter 9 Gas-phase molecular and molecular pair proton affinities of alkanols

9.1 Introduction

The kinetic method was used to evaluate proton affinity values for alkanols.[1] The proton affinity value for n-butanol was revised from 789.2[2] to 793.7 kJ mol^{-1}, and new PA values were estimated for n-pentanol (796 kJ mol^{-1}), n-Hexanol (799 kJ mol^{-1}), n-Heptanol (800 kJ mol^{-1}) and n-Octanol (800 kJ mol^{-1}).

In this Chapter it is described how the kinetic method was extended for determining molecular-pair basicity (MPGB) and proton affinity (MPPA) values, which were investigated through a study of proton-bound alkanol trimers. Since molecular-pair proton affinity and basicity values were not available, it was necessary to establish a set of data for the reference bases prior to actual measurements.

The competitive dissociations of proton-bound trimers, i.e. three independent units bound together by a single proton, were studied under MI and CID conditions in order to determine the relative MPPA values. Simple n-alkanols were selected as monomer units and used as a test case for the studies of biomolecules.[3]

The proton-bound trimers containing two different simple alkanol molecules, abbreviated as A and B, showed that their competitive fragmentations (9.1 and 9.2)

leading to proton-bound dimers, A_2H^+ and ABH^+, were dominant processes in both MI and CID regimes. Further dissociations do occur to a minor extent and therefore, in order to estimate the rate constant ratio, k_1/k_2, it was necessary to "add back" the abundances of secondary fragments to the abundances of the parent dimers.

$$A_2BH^+ \xrightarrow{k_1} A_2H^+ + B \qquad 9.1$$

$$A_2BH^+ \xrightarrow{k_2} ABH^+ + A \qquad 9.2$$

If the kinetic method is applied to such reactions, then using the same assumptions as those for proton-bound dimers, equations 9.3 and 9.4 can be obtained. Since the kinetic method is based on the assumption that entropy effects are negligible, it is best used for pairs of homologous compounds having similar size and functional groups.

$$\ln\frac{k_1}{k_2} = \ln\frac{[A_2H^+]}{[ABH^+]/2} = \ln\frac{Q_1^{\neq}}{Q_2^{\neq}} + \frac{MPPA(A_2) - MPPA(AB)}{RT_{eff}} \qquad 9.3$$

$$= \frac{MPPA(A_2) - MPPA(AB)}{RT_{eff}} \qquad 9.4$$

The molecular pair proton affinity (MPPA), is defined as the negative of the enthalpy change on addition of the two molecules to a proton (reactions 9.5 and 9.6):

$$A + B + H^+ \longrightarrow ABH^+ \qquad 9.5$$

$$A + A + H^+ \longrightarrow A_2H^+ \qquad 9.6$$

$$MPPA(AB) = \Delta_fH^o(A) + \Delta_fH^o(B) + \Delta_fH^o(H^+) - \Delta_fH^o(ABH^+) \qquad 9.7$$

$$MPPA(A_2) = 2\Delta_fH^o(A) + \Delta_fH^o(H^+) - \Delta_fH^o(A_2H^+) \qquad 9.8$$

The factor of 2 in equation 9.3 is because the possibility for loss of A is twice that for loss of B. T_{eff} is the effective temperature of the activated trimer AB_2H^+.

The objectives of this study are to set up MPPA values for the molecular pairs and use them to derive the MPPA value of an unknown and thus get an overall picture for the dissociations of larger proton-bound adduct ions. The significance of such an investigation is that such cluster ion studies help to bridge the gap between the gas and condensed phases and in probing the details of molecular interactions.

9.2 Results and Discussion

9.2.1 Proton-bound dimers

Preliminary experiments[1] with a wide range of primary, secondary and tertiary alkanols showed that for the latter two classes of compounds the MI mass spectra for $(R_1OH)H^+(R_2OH)$ were often dominated by processes other than the dissociation to $R_1OH_2^+$ and $R_2OH_2^+$ (mainly olefin eliminations). The primary alkanols are not so disposed and the competing reactions provided the major

signals in the MI mass spectra. However, the MI mass spectra of the higher homologues also showed a weak (<10%) water loss signal. Figure 9.1 shows the MI and CID mass spectra of the proton-bound dimer of $(C_2H_5OH)H^+(n\text{-}C_3H_7OH)$.

Ratios relative to $C_2H_5OH_2^+$ are given in Table 9.1 and the corresponding plot of ln*R* vs. PAs is shown in Figure 9.2. The PA values for $n\text{-}C_3H_7OH$ and $i\text{-}C_4H_9OH$ are provided by the NIST database[2] and the revised and new PA values for $n\text{-}C_4H_9OH$, $n\text{-}C_5H_{11}OH$, $n\text{-}C_6H_{13}OH$, $n\text{-}C_7H_{15}OH$ and $n\text{-}C_8H_{17}OH$ are derived from the plot. The cross-over point of MI and CID lines gives the PA value for C_2H_5OH, 775 kJ mol^{-1}, in good agreement with the NIST value,[2] 776.4 kJ mol^{-1}.

Table 9.1 Results for proton-bound dimers of alkanols

		C_2	n-C_3	n-C_4	n-C_6
R: MI CID	n-C_3	34 (3.2)			
$lnR^{\#}$: MI (CID)		3.5 (1.2)			
R: MI CID	n-C_4		8.4 (2.2)		
$lnR^{\#}$: MI (CID)			5.6 (2)		
R: MI CID	i-C_4		11 (2.2)		
$lnR^{\#}$: MI (CID)			5.9 (2)		
R: MI CID	n-C_5				2.2^{-1} (1.3^{-1})
$lnR^{\#}$: MI (CID)					6.9 (2.6)
R: MI CID	n-C_6			8 (2.6)	
$lnR^{\#}$: MI (CID)				7.7 (2.9)	
R: MI CID	n-C_7				1.2 (1)
$lnR^{\#}$: MI (CID)					7.9 (2.9)
R: MI CID	n-C_8				1.3 (1.1)
$lnR^{\#}$: MI (CID)					8 (3)

R: ratios for the compounds in the columns to those in the rows

$R^{\#}$: ratios normalized relative to $[C_2H_5OH_2^+]$

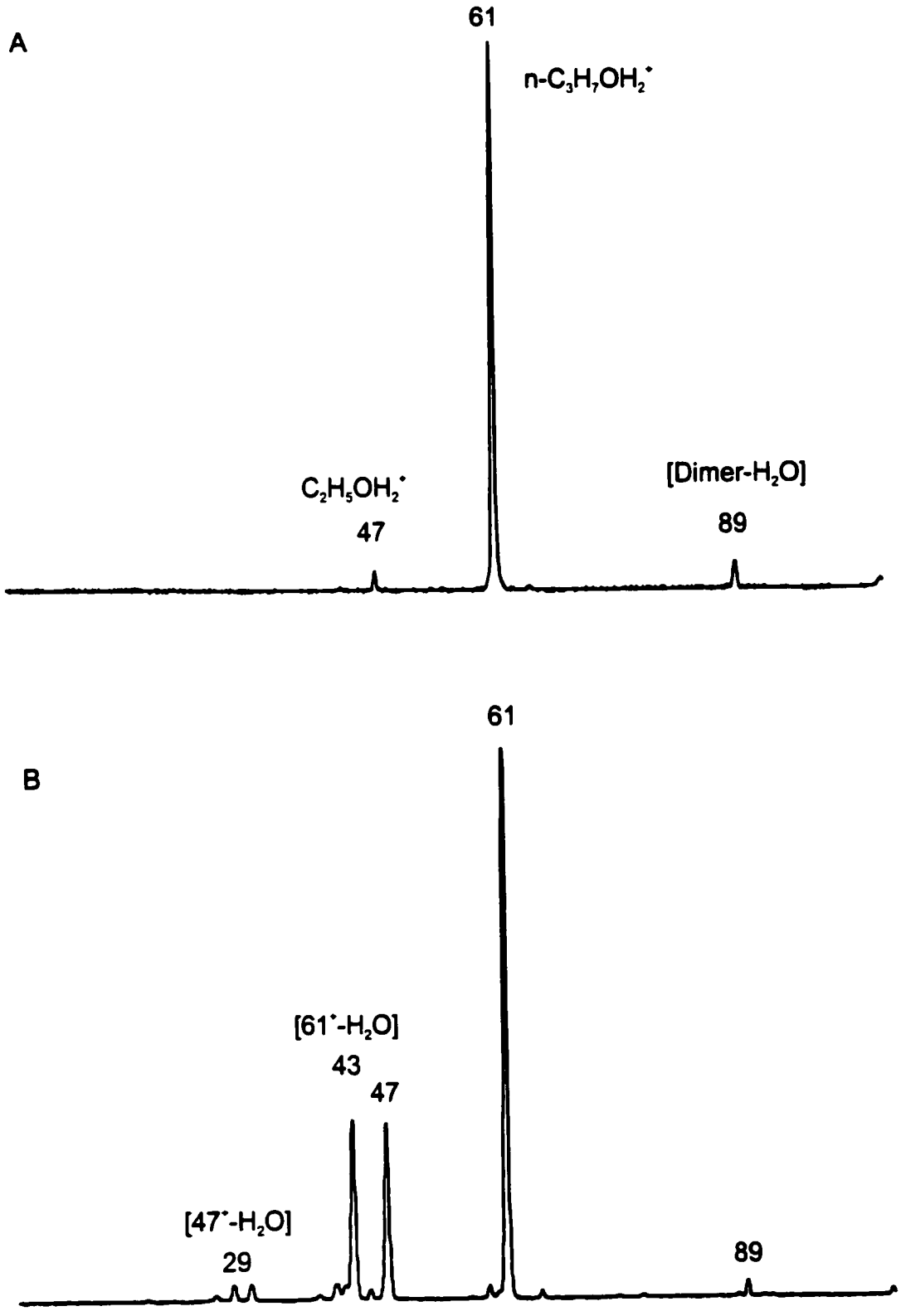

Figure 9.1 (A) MI mass spectrum and (B) CID mass spectrum of $(C_2H_5OH)H^+(n\text{-}C_3H_7OH)$

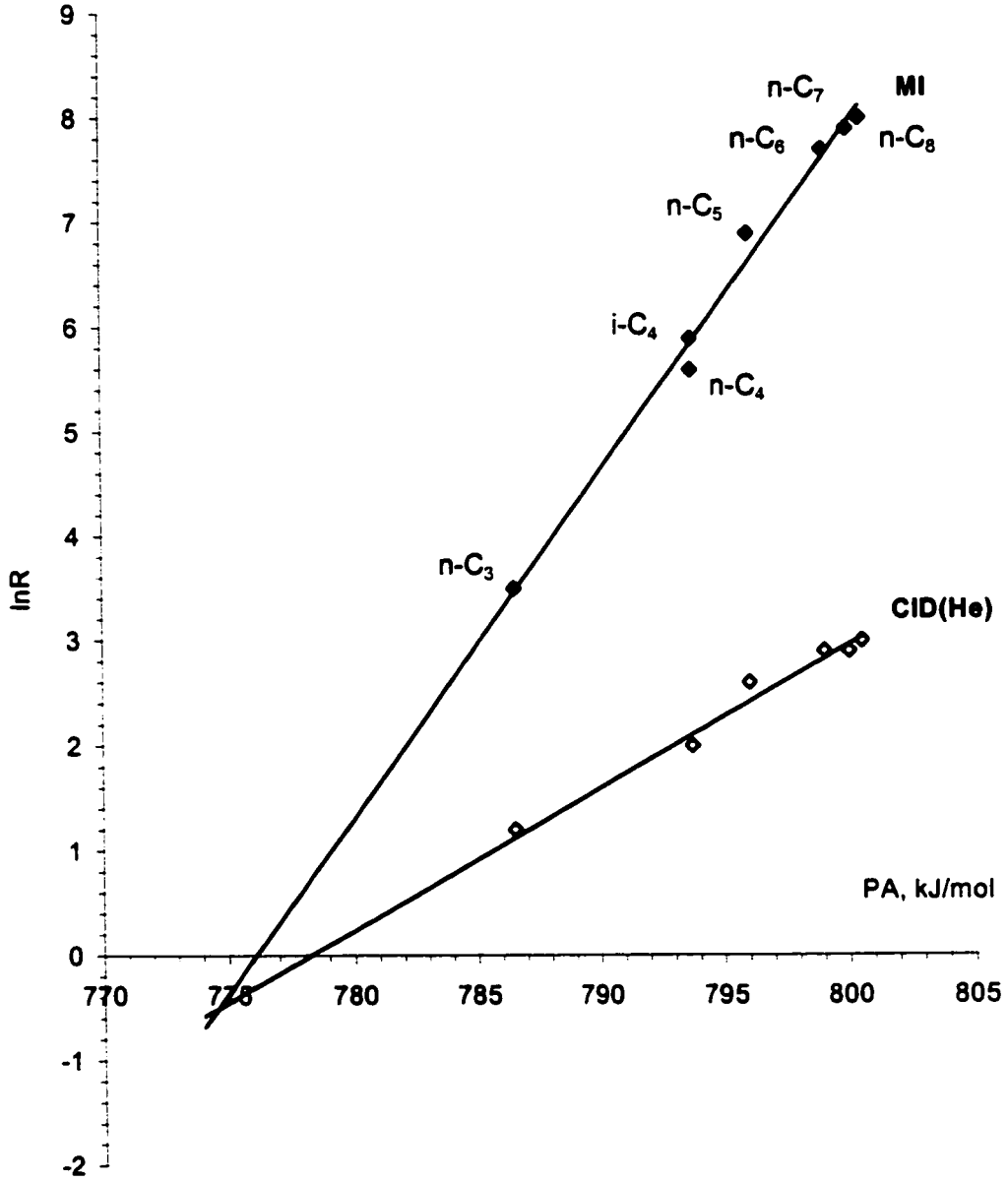

Figure 9.2 Plot of $\ln[B_nH^+]/[C_2H_5OH_2^+]$ as a function of PA values, where B_n are a series of alkanols

9.2.2 *Proton-bound trimers*

The MI and CID mass spectra of proton-bound trimers of n-alkanols were both dominated by the production of proton-bound dimers; secondary fragmentations only occur to a small extent in the CID experiments, and were taken into account when measuring the ratios. Figure 9.3 shows the MI and CID mass spectra of the proton-bound trimer of $(C_2H_5OH)_2H^+$(n-C_3H_7OH).

For a series of A_2BH^+ ions having a common functionality, then the ratios of $\ln[A_2H^+]/[AB]$, $\ln R$, relate linearly with the $[MPPA(A_2) - MPPA(AB)]/RT_{eff}$ with the same assumptions as those for the proton-bound dimers. The plot of $\ln R$ vs. MPPA of a series of reference pairs gives a straight line with a slope of $1/RT_{eff}$. If the measurements were made in both MI and CID conditions, then the cross-over point of the MI and CID lines should give the MPPA of the unknown. However, the measurements are not complete without MPPA values for the reference bases.

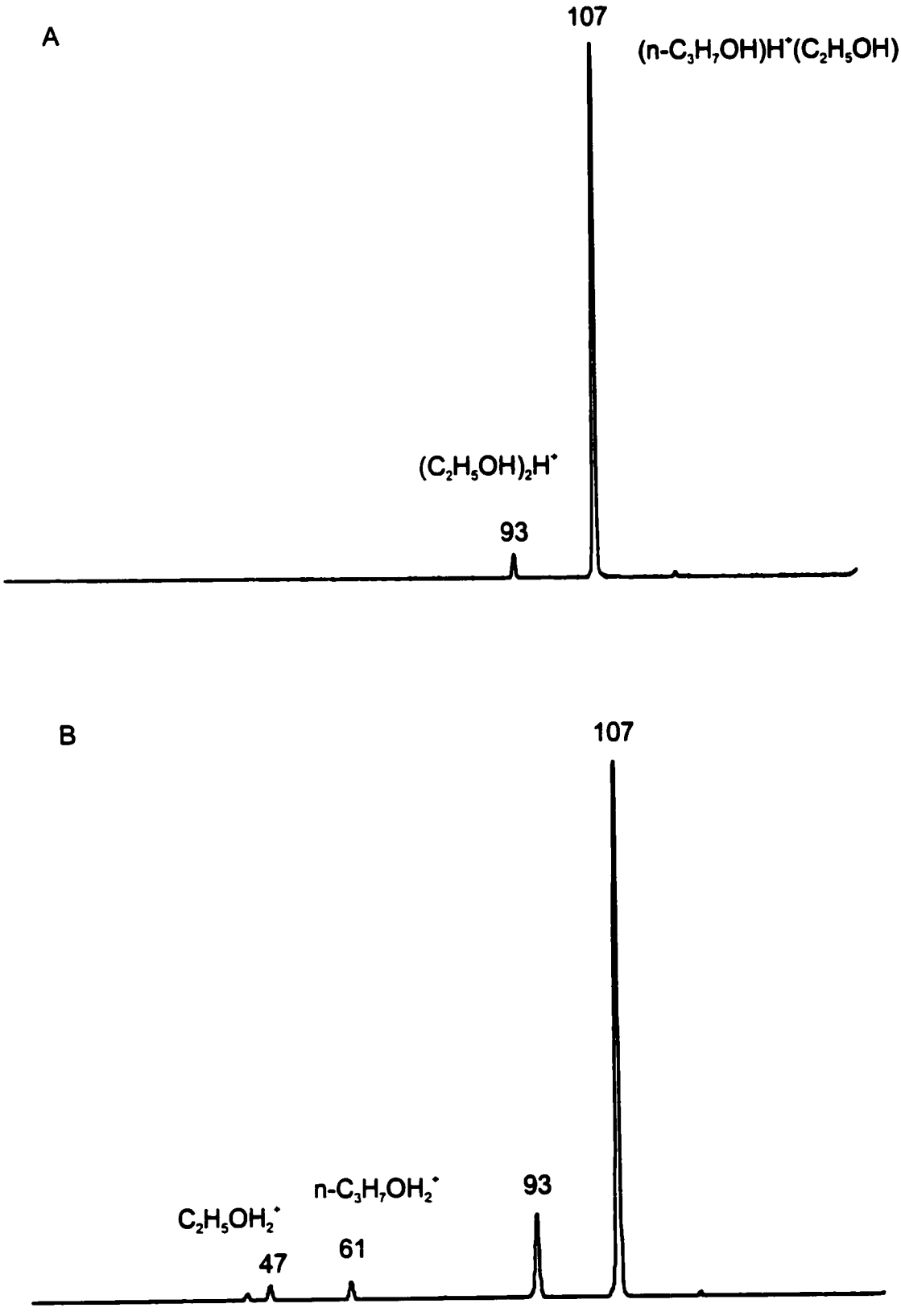

Figure 9.3 (A) MI mass spectrum and (B) CID mass spectrum of $(C_2H_5OH)_2H^+(n\text{-}C_3H_7OH)$

9.2.2.1 MPPA values for symmetric and unsymmetric dimers

MPPA values for symmetric and asymmetric dimers can be obtained using the thermochemical cycle shown in Scheme 9.1.

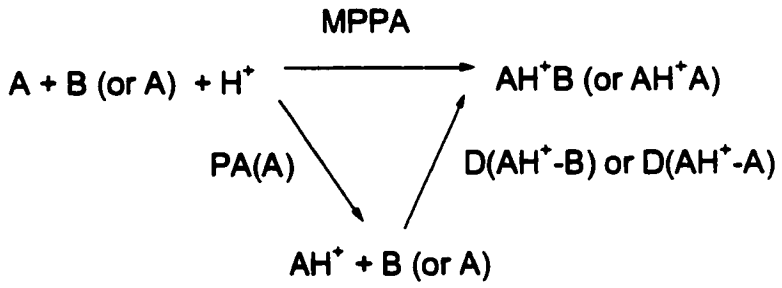

Scheme 9.1

$$MPPA(AB) = D(AH^+ - B) + PA(A) \qquad 9.9$$

$$MPPA(A_2) = D(AH^+ - A) + PA(A) \qquad 9.10$$

McMahon examined the solvent-exchange equilibra of nearly 30 oxygen n-donor bases including alkanols and ethers, aldehydes and ketones, carboxylic acids and esters and obtained a linear correlation (equation 9.11) between the strength of the hydrogen bond in unsymmetric proton-bound dimers and the difference in proton affinity of the two bases.[4]

$$D(AH^+-B) = 30.8 + 0.46\Delta PA \ (kcal\ mol^{-1}) \qquad 9.11$$

where $\Delta PA = PA(B) - PA(A)$. The value of 30.8 ± 2 kcal mol^{-1} is the average hydrogen bond energy in symmetric proton-bound dimers regardless of the functional group involved or the gas-phase basicity. The PA data were taken from references 5 and 6.[5,6]

However, if one uses the most recent PA values in the NIST database[2] and our experimental measurements[1], and rejecting the points giving the poorest correlation, a new relation (equation 9.12) is derived which is similar to Mautner's equation[7], $D(AH^+-B) = 30.4 + 0.30\Delta PA$,

$$D(AH^+-B) = 30.8 + 0.34\Delta PA \quad (\text{kcal mol}^{-1}) \qquad 9.12$$

The plot to give equation 9.12 is shown in Figure 9.4. Table 9.2 lists McMahon's data,[4] ΔH_1 and ΔH_2 obtained by measuring solvent-exchange equilibra (9.13 and 9.14), and PA values taken from the current NIST database[2] and our experimental measurements.[1] Tables 9.3 and 9.4 are the calculated results for $D(AH^+-B)$ and MPPA.

$$AHA^+ + B \overset{\Delta H_1}{\rightleftharpoons} AHB^+ + A \qquad 9.13$$

$$AHB^+ + B \overset{\Delta H_2}{\rightleftharpoons} BHB^+ + A \qquad 9.14$$

Table 9.2 Thermochemistry of proton-bound dimers of oxygen donor bases

A	B	ΔH_1[a] kcal mol^{-1}	ΔH_2[a] kcal mol^{-1}	ΔPA[b] kcal mol^{-1}
CH_3OH	C_2H_5OH	-2.3	-2.4	5.3
C_2H_5OH	n-C_3H_7OH	-0.8	-1.1	2.4
C_2H_5OH	n-C_4H_9OH	-1.1	-1.3	4.1
n-C_3H_7OH	n-C_4H_9OH	-0.1	-0.2	1.7
CH_3OH	CH_3CHO	-1.0	-1.6	3.4
n-C_3H_7OH	$(CH_3)_2O$	-0.3	-0.4	1.3
$(CH_3)_2CO$	$(CH_3)(C_2H_5)CO$	-1.2	-1.0	3.6
$(CH_3)_2CO$	$(C_2H_5)_2O$	-1.4	-1.0	3.9
$(CH_3)_2CO$	$(C_2H_5)_2CO$	-1.9	-1.7	5.9
$(CH_3)(C_2H_5)CO$	$(C_2H_5)_2CO$	-0.7	-0.7	2.3
$(C_2H_5)_2O$	$(C_2H_5)_2CO$	-0.5	-0.7	2.0
$(C_2H_5)_2O$	$(n\text{-}C_3H_7)_2O$	-1.1	-0.6	2.3

a) see ref.4; b) see ref. 1 and 2

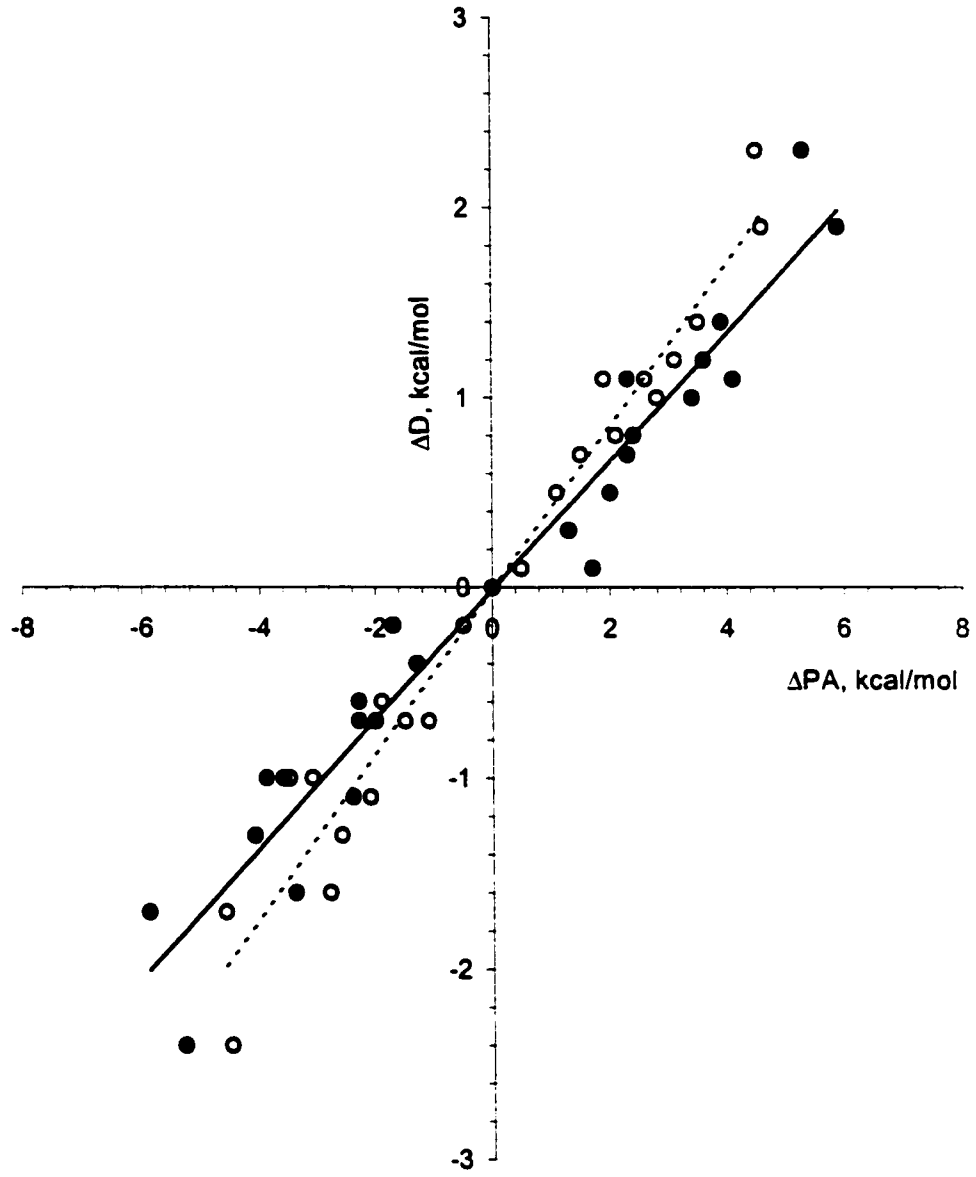

Figure 9.4 Plot of ΔD (D(AH^+-B) - D(AH^+-A)) vs. ΔPA (PA(B) -PA(A)). Points in the upper right quadrant are $-\Delta H_1$ values from Table 9.2; points in the lower left quadrant are ΔH_2 values from Table 9.2. Closed circles (solid line) use NIST PA data as x values; open circles (dashed line) use PA data from references 5 and 6 as x values.

Table 9.3 Thermochemistry of ethanol solvation of protonated alkanol ions

$AH^+ + C_2H_5OH \rightarrow AH^+C_2H_5OH$	
AH^+	$D(AH^+\text{-}C_2H_5OH)^a$ (kJ mol^{-1})
$CH_3OH_2^+$	136
$C_2H_5OH_2^+$	129
$n\text{-}C_3H_7OH_2^+$	125
$n\text{-}C_4H_9OH_2^+$	123
$n\text{-}C_5H_{11}OH_2^+$	122

a) calculated from equation 9.12

Table 9.4 MPPA data for symmetric and asymmetric alkanol pairs

A	$MPPA(A_2)^a$ (kJ mol^{-1})	B = C_2H_5OH A	$MPPA(AB)^a$ (kJ mol^{-1})
CH_3OH	883.3	CH_3OH	890.3
C_2H_5OH	905.4	$n\text{-}C_3H_7OH$	911.5
$n\text{-}C_3H_7OH$	915.5	$n\text{-}C_4H_9OH$	916.7
$n\text{-}C_4H_9OH$	922.7	$n\text{-}C_5H_{11}OH$	918.0
$n\text{-}C_5H_{11}OH$	925.0		

a) PA values are adopted from the NIST database[2] and our experimental measurements.[1]

The MPPA values generally parallel the PA values and MPPA(AB) data lie between MPPA(A_2) and MPPA(B_2). Like PA data, the MPPA for homologous series change smoothly with the alkyl chain length, becoming asymptotic at high molecular weight (see Figure 9.5). The slope for MPPA(AB) is less steep than MPPA(A_2). This plot can help to estimate the MPPA value for a missing member among the series.

9.2.2.2 Experimental data

Since secondary decompositions leading to the protonated monomer are normally observed as minor peaks under CID condition, when calculating $\ln[ABH^+]/[A_2H^+]$, the sum of the abundances $[ABH^+ + BH^+]$ and $[A_2H^+ + AH^+]$ were used. Results for MI and CID experiments are shown in Table 9.5.

Two series of trimers, AB_2H^+ and A_2BH^+ (where B = C_2H_5OH, A are homologous n-alkanols from CH_3OH to n-$C_5H_{11}OH$) were observed under MI and CID conditions. The corresponding plot is shown in Figure 9.6. The lines cross at MPPA = 906 kJ mol^{-1} corresponding to the MPPA $(C_2H_5OH)_2$.

Table 9.5 Ratios (R) in the metastable ion (MI) and collision induced dissociations (CID) of proton-bound allkanol trimers

B_2AH^+ B = C_2H_5OH	A	
R = $[B_2H^+]/[ABH^+]$	CH_3OH	249 (1.6)
R: MI (CID)	n-C_3H_7OH	19.1^{-1} (3^{-1})
	n-C_4H_9OH	87^{-1} (4.8^{-1})
	n-$C_5H_{11}OH$	198^{-1} (5.9^{-1})
A_2BH^+ B = C_2H_5OH	A	
R = $[A_2H^+]/[ABH^+]$	CH_3OH	241^{-1} (6.7^{-1})
R: MI (CID)	n-C_3H_7OH	3.8 (0.85)
	n-C_4H_9OH	9.7 (1)
	n-$C_5H_{11}OH$	16.2 (1.3)

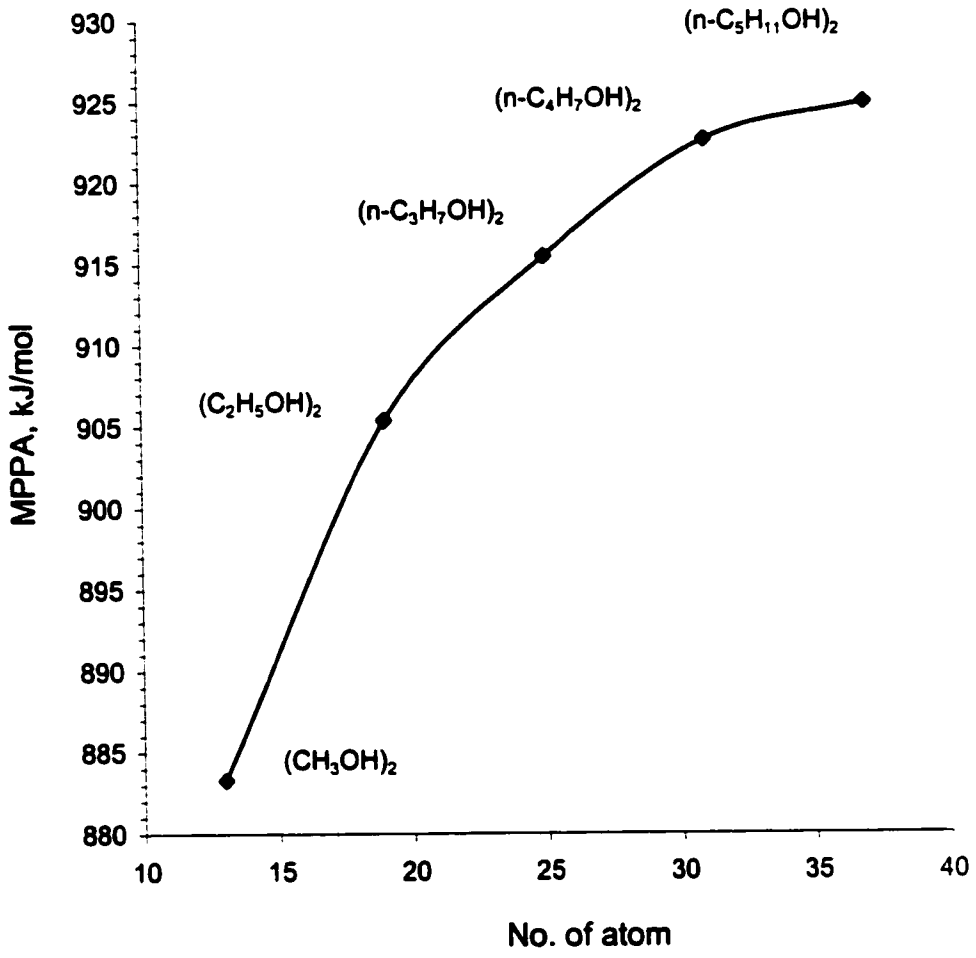

Figure 9.5 MPPA values as a function of size (No. of atoms)

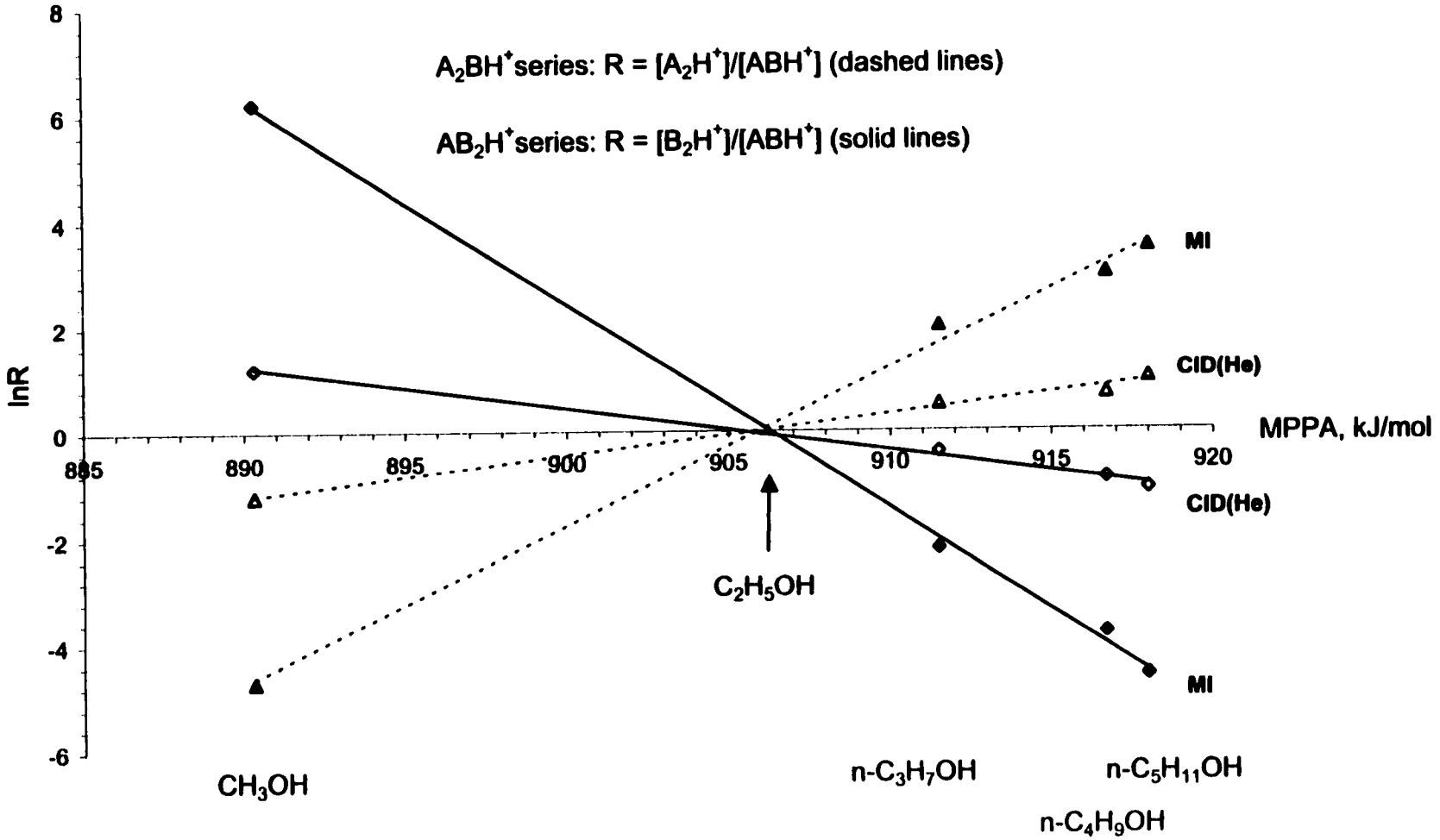

Figure 9.6 Plot of lnR as a function of MPPA(AB), where A = MeOH, n-PrOH, n-BuOH, n-PeOH; B= EtOH

9.2.3 *Potential diagram for the unimolecular dissociation of a proton-bound dimer, trimer and tetramer*

A simplified potential energy diagram is used to demonstrate the relationships between the various dissociation channels (Figure 9.7). Δ indicates the difference in bond dissociation energies between the two channels. Thus $\Delta_1 = D_1 - D_2 = PA(A) - PA(B)$, D_1 and D_2 are the bond dissociation energies of ABH^+, $\Delta_2 = D_3 - D_4 = MPPA(A_2) - MPPA(AB)$, D_3 and D_4 are the bond dissociation energies of A_2BH^+ and $\Delta_3 = D_5 - D_6 = MTPA(A_3) - MTPA(A_2B)$, D_5 and D_6 are the bond dissociation energies of A_3BH^+. MTPA represents Molecular Triplet Proton Affinity.

The order $\Delta_1 > \Delta_2 > \Delta_3$ is expected. This can be understood from the fact that as the number of ligands A bonded to H^+ increases, both $D(A_nH^+-A)$ and $D(A_{n-1}BH^+-A)$ decrease and the difference between them tends to zero. Note that molecule A has a higher PA than molecule B.

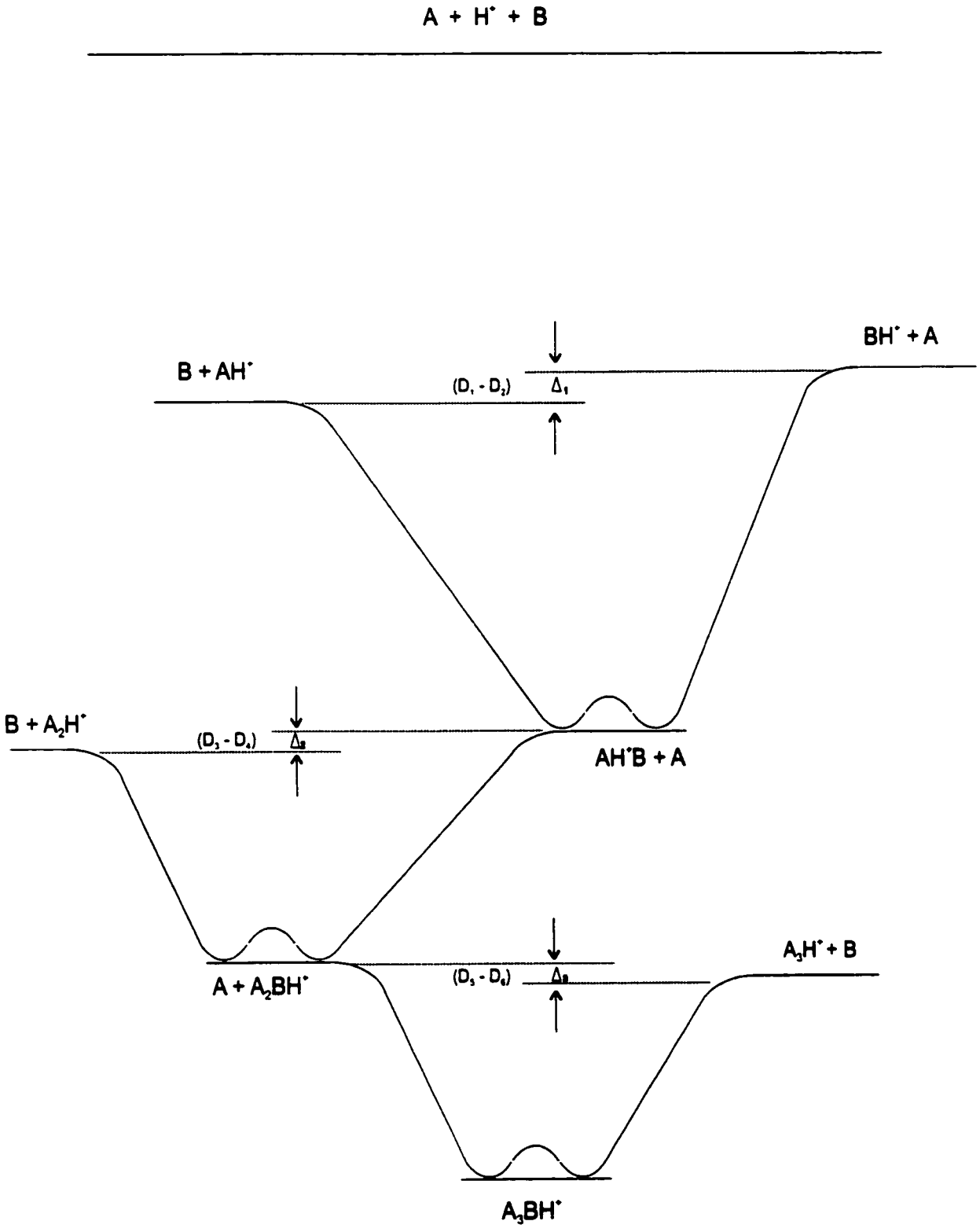

Figure 9.7 Potential energy diagram for a proton-bound dimer, trimer and tetramer

9.3 Thermodynamics of cluster reactions

The clustering of molecules around ions provides information on the strong (inner shell) solvation of ions.[8] The thermodynamic data, i.e., $\Delta G°_{n-1,n}$, $\Delta H°_{n-1,n}$ and $\Delta S°_{n-1,n}$, obtained from the measured temperature dependence of equilibrium constants $K_{n-1,n}$ are of interest to the field of ion solvation in condensed media[8] and theoretical attempts to describe this solvation by quantum mechanical calculation of the binding of a few solvent molecules to the ion.[9,10] Examples of equilibrium determinations are shown as reactions 9.15 and 9.16.

$$H_3O^+(H_2O)_{n-1} + H_2O \rightleftharpoons H_3O^+(H_2O)_n \qquad 9.15$$

$$NH_4^+(NH_3)_{n-1} + NH_3 \rightleftharpoons NH_4^+(NH_3)_n \qquad 9.16$$

Equilibrium constants $K_{n-1,n}$ were measured according to equation 9.17. P_n/P_{n-1} are observed ion intensities for $H_3O^+(H_2O)_{n-1}$ and $NH_4^+(NH_3)_{n-1}$. P_N are partial pressures of neutral molecules such as H_2O and NH_3. van't Hoff plots of $K_{n-1,n}$ against 1/T give $\Delta H°_{n-1,n}$ and $\Delta S°_{n-1,n}$ from which $\Delta G°_{n-1,n}$ can be derived.

$$K_{n-1,n} = \frac{P_n}{P_{n-1}P_N} \qquad 9.17$$

The plot of $-\Delta H°_{n-1,n}$ vs. (n-1, n) illustrates the energy changes for reactions (n-1,n) which are shown in Figure 9.8. For $H_3O^+(H_2O)_n$, there is a distinct break after

$-\Delta H°_{2,3}$, i.e., $-\Delta H°_{3,4}$ is significantly lower than $-\Delta H°_{2,3}$. There are two falloff points in the bonding energies: after the dimer $H_3O^+ \bullet H_2O$ and after $H_3O^+ \bullet (H_2O)_3$,[11] the Eigen structure which represents the complete inner shell. The pattern of changes for $NH_4^+(NH_3)_n$[11] is similar, but now the second falloff occurs after $NH_4^+(NH_3)_4$, i.e., the complete inner shell for the ammonium ion.

The bond dissociation energy of the nth neutral molecule to the core ion is remarkably constant irrespective of alkylation,[12] For example, $ROH_2^+(ROH)_n$ and $RNH_3^+(RNH_2)$ ($R = n\text{-}C_nH_{2n+1}$), $-\Delta H°_{1,2} = 21$ kcal mol^{-1} for the former and $-\Delta H°_{1,2} = 16$ kcal mol^{-1} for the latter, which correspond to the values for $H_3O^+(H_2O)_n$ and $NH_4^+(NH_3)_n$ clusters. These results show that the binding energy to the core ions is not affected by alkyl substitution. If hydrophobic interactions did occur, they could increase the binding energies but would also cause significant entropy loss. The absence of such effects suggests that the inner shell ligands are purely hydrogen bonded to the core ions and the alkyl groups are oriented away from the hydrogen-bonding centers and also do not interact with each other.

Bonding to the core ions in the protonated organics appears to be dominated by distinct ionic hydrogen bonds and alkyl group interactions do not contribute significantly. It would be of much interest to extend thermochemical studies on organic molecules to even larger clusters, but equilibrium studies are limited. New methods[13,14] applied to organic clusters should reveal rich and complex behavior.

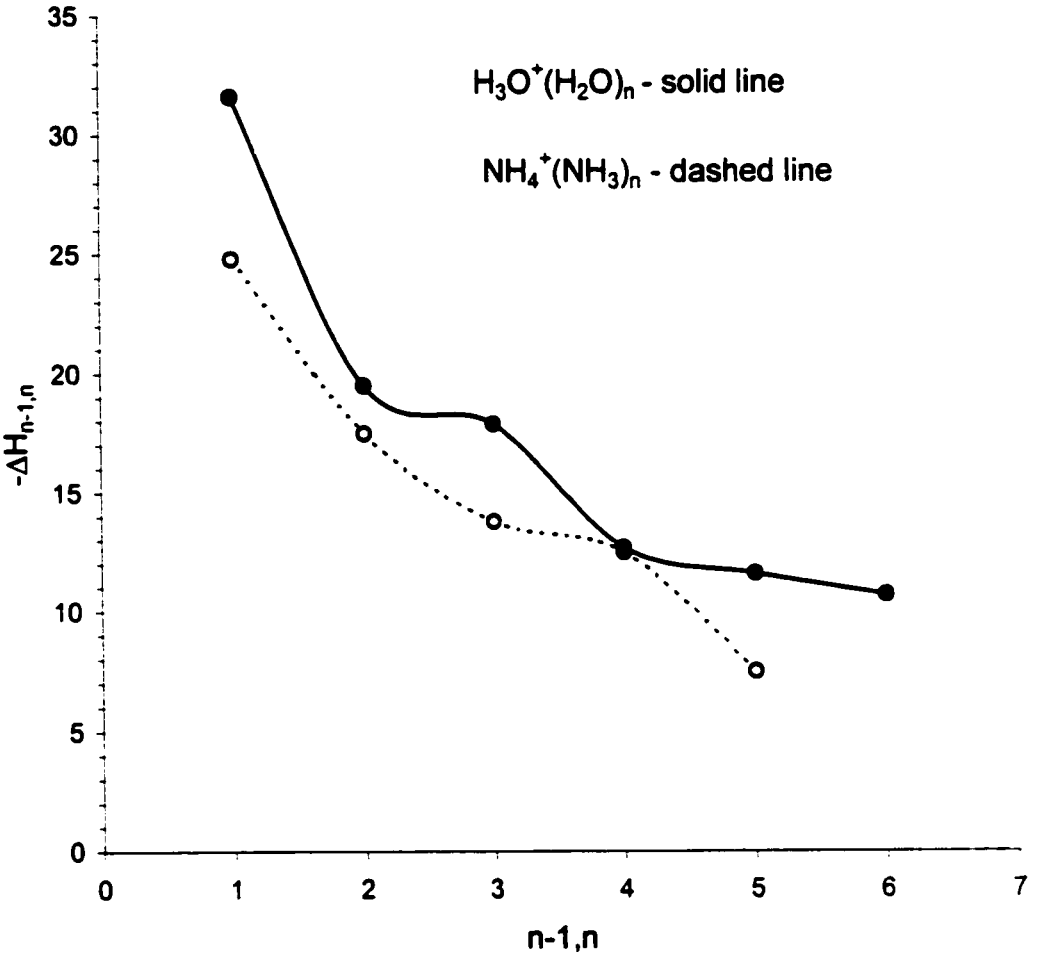

Figure 9.8 $-\Delta H^0_{n-1,n}$ vs. n-1,n for $H_3O^+(H_2O)_n$ and $NH_4^+(NH_3)_n$ cluster ions

9.4 References

(1) Holmes, J. L.; Aubry, C.; Mayer, P. M. *J. Phys. Chem. A* **1999**, *103*, 705.

(2) Hunter, E. P. L.; Lias, S. G. *J. Phys. Chem. Ref. Data* **1998**, *27*, 413.

(3) Vekey, K.; Czira, G. *Rapid Commun. Mass Spectrom.* **1995**, *9*, 783.

(4) Larson, J. W.; McMahon, T. B. *J. Am. Chem. Soc.* **1982**, *104*, 6255.

(5) Wolf, J. F.; Staley, R. H.; Koppel, I.; Taagepera, M.; McIver, R. T.; Beauchamp, J. L.; Taft, R. W. **1977**, *99*, 5417.

(6) Yamdagni, R.; Kebarle, P. *J. Am. Chem. Soc.* **1976**, *98*, 1320.

(7) Meot-Ner, M. *J. Am. Chem. Soc.* **1984**, *106*, 1257.

(8) Kebarle, P. . In *Modern Aspects of Electrochemistry*; Conway, B. E., Bockris, J. O. M., Eds.; Plenum Press: New York, 1974; Vol. 9.

(9) Clementi, E. . In *Lecture Notes in Chemistry*; Springer Verlag: New York, 1976; Vol. 2.

(10) Diercksen, G. H. F.; Kraemer, W. P. *Thoer. Chim. Acta* **1972**, *23*, 387.

(11) Lau, Y. K.; Ikuta, S.; Kebarle, P. *J. Am. Chem. Soc.* **1982**, *104*, 1462.

(12) Meot-Ner, M. *J. Am. Chem. Soc.* **1992**, *114*, 3312.

(13) Wei, S.; Tzeng, W. B.; Castleman, A. W. *J. Phys. Chem.* **1991**, *95*, 585.

(14) Magnera, T. F.; David, D. E.; Michl. *J. Chem. Phys. Lett.* **1991**, *182*, 363.

Appendix

S-1 The vibrational frequencies used for k(E) curves of Figure S-2

Species	Harmonic vibrational frequencies (cm^{-1})
Molecular ion (48) $(CH_3NH_2)H^+(C_2H_5NH_2)$	6, 58, 79, 112, 166, 248, 268, 439, 481, 510, 855, 916, 1047, 1062, 1086, 1100, 1105, 1118, 1322, 1351, 1358, 1476, 1481, 1539, 1581, 1608, 1632, 1633, 1646, 1652, 1662, 1757, 1832, 1846, 1895, 2984, 3219, 3227, 3283, 3285, 3297, 3310, 3311, 3344, 3677, 3705, 3747, 3778
TS[a] (47) $\Delta S^{\neq}$ = 0.4 J mol^{-1} K^{-1}	4, 35, 47, 67, 100, 268, 439, 481, 510, 855, 916, 1047, 1062, 1086, 1100, 1105, 1118, 1322, 1351, 1358, 1476, 1481, 1539, 1581, 1608, 1632, 1633, 1646, 1652, 1662, 1757, 1832, 1846, 1895, 2984, 3219, 3227, 3283, 3285, 3297, 3310, 3311, 3344, 3677, 3705, 3747, 3778

a) The scaling factor is 0.6 and the vibrational frequency that most closely matches the dissociation reaction (248 cm^{-1}) is rejected.

References

(1) Ab initio calculations were carried out with the GAUSSIAN 942 suite of programs, on an SGI Octane workstation, at the HF/6-31G(d) level of theory.

(2) Frisch, M. J.; Trucks, G. W.; Schlegel, H. B.; Gill, P. M. W.; Johnson, B. G.; Robb, M. A.; Cheesman, J. R.; Keith, T.; Peterson, A.; Montgomery, A.; Ragavachari, K.; Al-Laham, M. A.; Zadrzewski, V. G.; Ortiz, J. V.; Foresman, J. B.; Cioslowski, J.; Stefanov, B. B.; Nanayakkara, A.; Challacombe, M.; Peng, C. Y.; Ayala, P. Y.; Chen, W.; Wong, M. W.; Andres, J. L.; Replogle, E. S.; Gomperts, R.; Martin, R. L.; Fox, D. J.; Binkley, J. S.; Defrees, D. J.; Baker, J.; Stewart, J. P.; Head-Gordon, M.; Gonzalez, C.; Pople, J. A. ab initio. In *GAUSSIAN 94*; Gaussian Inc.: Pittsburgh, PA, 1995.

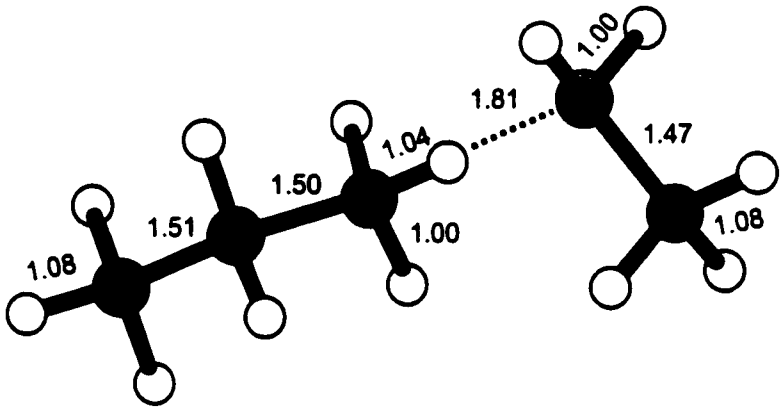

S-1 Seleted geometric parameters for the proton-bound dimer $(CH_3CH_2NH_2)H^+(CH_3NH_2)$. Bond lengths are in angstroms.

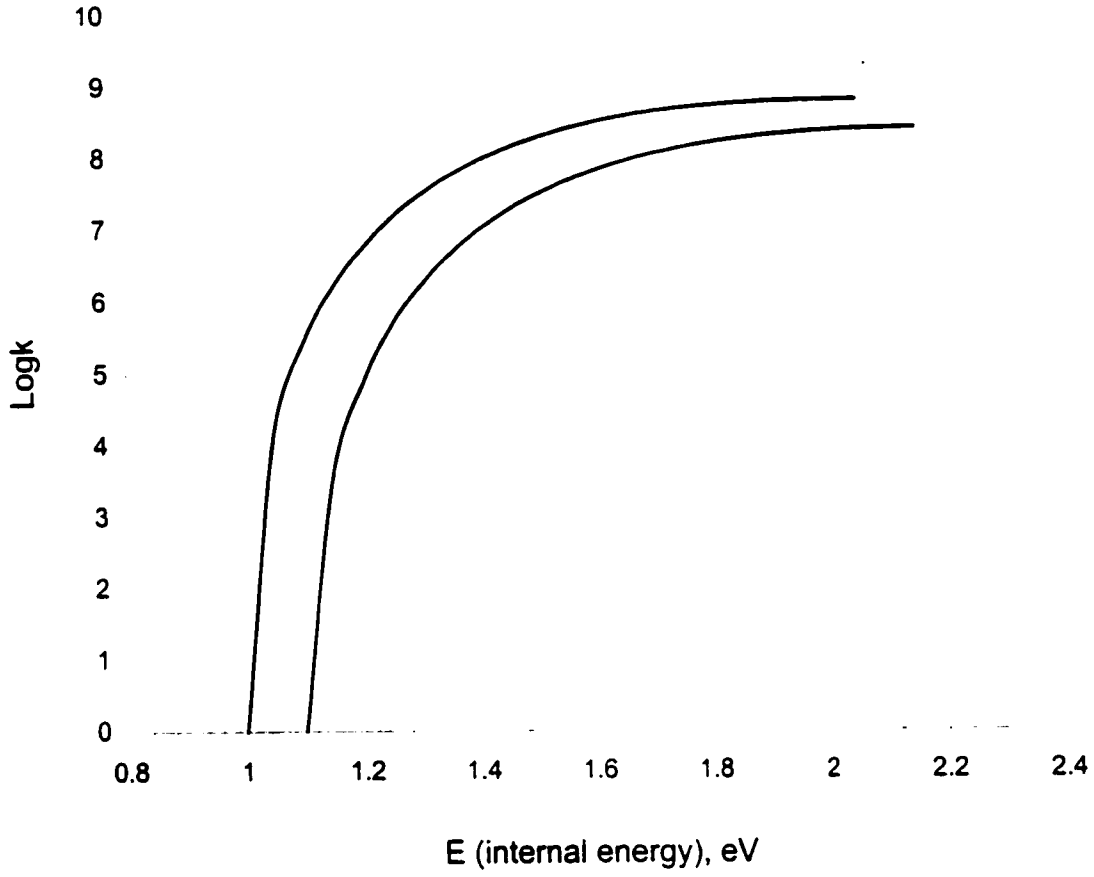

S-2 Logk vs. E curves for two simple bond cleavage reactions. The curves were generated using the standard RRKM expression. The model compound used to generate the curves was the proton -bound amine dimer and the vibrational frequencies were from *ab initio* calculations.[2]

Claims to original research

1. Appearance energy measurements were used to determine the $\Delta_f H°$ values for $(CH_3)_2C^+NH_2$, $CH_2=CHCH_2^+$ and $^+CH_2NH_2$ ions. The literature value for $(CH_3)_2C^+NH_2$ was too high and needed to be revised.[1]

2. A mass spectrometric study of immonium (or oxonium) ions showed that they interconvert freely at internal energies near their dissociation limit, on the basis of their having very closely similar fragmentation patterns and KER values but slightly different product ion abundances. The possible fragment ions' structures produced by these immonium (or oxonium) ions were assigned by observing their corresponding CID mass spectra.

3. Kinetic energy release (KER) values for the methyl loss from the ionized simple amines were used as a probe to elucidate their α-cleavage reaction mechanism. To account for the large KER value for t-butylamine, an ion-neutral complex was proposed as intermediate species which was separated from the molecular ion by a large energy barrier, as confirmed by *ab initio* calculations.[2] In contrast, the α-cleavage reaction for the ionized isopropylamine was found to be a simple bond cleavage process.

4. The systematic study of the kinetic method has been carried out by observing a wide variety of proton-bound pairs consisting of amines,[3,4] nitriles[5] and

alkanols[6] using tandem mass spectrometry. Results were obtained for other selected amines. New or revised PA values were given to the species whose PA value are either wrong or not reported in the current NIST database.[7]

5. The general effects expected from non-zero entropies of activation are described in terms of how they influence log k(rate constant) vs. E(internal energy) plots for such competing dissociations.[4] For these homologous series such effects were observed to be minimal and the kinetic method well reproduces most of the reference PA values. However, it is possible that small reverse energy barriers (ca. 5 kJ mol^{-1}) may in some cases be identifiable by the kinetic method, in particular for t-$C_4H_9NH_2$, the homologous di-n-alkylamines and possibly larger barriers for di-sec-alkylamines.

6. Results have also been obtained for some bidentate species such as 1,2-, 1,3- and 1,4-diaminoethane, propane and butane, respectively.[4] Particular attention was given to the effects of activation entropies, $\Delta S^{\neq}$, and the presence of reverse energy barriers, E_{rev}, both of which are here a significant problem for the kinetic method. The results indicate that similar difficulties may apply to biomolecules and that PA values for such species obtained by the kinetic method may be flawed.

7. The kinetic method was extended to determine molecular-pair proton affinities (MPPA), which were investigated through a study of proton-bound alkanol

trimers. Since these values were not available, it was necessary to establish a set of data for the reference bases.[8]

(1) Lias, S. G.; Bartmess, J. E.; Liebman, J. F.; Holmes, J. L.; Levin, R. D.; Mallard, W. G. *J. Phys. Chem. Ref. Data* **1988**, *17*, 1.

(2) Parker, J. E.; Johnson, C. A. F.; Smith, M. *Proceedings of 22nd British Mass Spectrometry Society Conference, Swansea* **1996**, 57.

(3) Cao, J.; Holmes, J. L. *Int. J. Mass Spectrom.* **2000**, *195/196*, 525.

(4) Cao, J.; Aubry, C.; Holmes, J. L. *J. Phys. Chem. A* **2000**, *104*, 10045.

(5) Cao, J.; Holmes, J. L. *Euro. Mass Spectrom.* **1999**, *5*, 19.

(6) Holmes, J. L.; Aubry, C.; Mayer, P. M. *J. Phys. Chem. A* **1999**, *103*, 705.

(7) Hunter, E. P. L.; Lias, S. G. *J. Phys. Chem. Ref. Data* **1998**, *27*, 413.

(8) Cao, J.; Holmes, J. *in preparation* .